POLYURETHANE AS A SUBSTRATE FOR CELL TRANSPLANTATION IN THE TREATMENT OF AGE RELATED MACULAR DEGENERATION (AMD)

Thesis submitted in accordance with the requirements of the University of Liverpool for the degree of Doctor in Philosophy

by

Eliesmaziah Alias

August 2011

Supervisors: Dr. R. Williams & Dr. C Sheridan.

Department of Eye and Vision Science,
Institute of Ageing and Chronic Disease
University of Liverpool, L69 3GA

PRELIMINARIES

ABSTRACT

Introduction: Age-related macular degeneration (AMD) results in the deterioration of the retinal pigment epithelial (RPE) layer under the macula. A potential surgical treatment involves the replacement of the diseased RPE cells with healthy cells. Clinically, this requires identification of the appropriate cells to use and the optimal substrate for use as a transplant vehicle. The material under investigation was polyurethane (PU) and ways to manufacture porous PU were explored. Iris pigment epithelium (IPE) is derived from the same embryonic origin as RPE and has been shown to have several of the same functions. IPE can be harvested more easily than RPE. The aim of this study was to compare the behaviour of primary bovine RPE (bRPE), IPE (bIPE) and human RPE (hRPE) cultured on PU membranes with the objective of optimising the cell/substrate combination for transplantation. Morphology and functionality of the cells attaching on the membranes were also evaluated.

Methods: The PU used in this study were Z3A1 and Z9A1 (b9™ Biomer Technology Ltd.) membranes with thickness <100µm. Several ways of producing porous PU were investigated. One of which was mixing Z3A1 with (dimethyl acetamide) DMAC in a concentration of 5% (vol/vol) and 5% icing sugar (by weight). The mixture was then dried in an oven at 75°C for 24 hours and then rinsed with distilled water. The surface topography was investigated using SEM. Properties of the membranes such as tensile strength, modulus of elasticity and wettability were examined. Freshly harvested bRPE, bIPE and hRPE cells were seeded on the b9 films, porous PU membrane and tissue culture polystyrene (TCPS) as control. The monolayer formation of the cells on the surfaces were controlled by optimising the correct harvesting technique, using the correct amount of seeding, controlling the amount of serum and the addition of retinoic acid. The cell morphology was assessed by phase contrast microscopy and stained for F-actin, zonula occludens-1 (ZO-1) tight junction marker and DAPI for nuclei distribution. Cytokeratin staining was used to confirm the epithelial phenotype. Phagocytosis assays, selectivity of phagocytosis assay and dextran transport studies were conducted to evaluate the functionalities of the cells on the membranes. An *In vitro* injury model of the cells attaching on the membranes was also investigated.

Results: The porous PU membranes produced were shown to have suitable properties as a replacement of a native Bruch's membrane with 5µm thickness and good porosities. All cell types demonstrated good epithelial phenotype, confirmed by cytokeratin expression when attached on the membrane. Nuclei were dispersed evenly, F-actin belt formation with ZO-1 at the cell borders were observed. Phagocytosis of photoreceptor outer segments (POS) demonstrated that the cells attaching on these surfaces were able to phagocytose in a time-dependant manner and show selectivity in phagocytosis when tested with polystyrene beads and blocking with the αVβ5-integrin. Dextran transport revealed a reduction in the transport of higher molecular weight dextran through the porous membrane-cells complex. The preliminary *In vitro* injury model study showed inconsistent cell integration.

Conclusion: This project has developed a porous PU with appropriate mechanical properties and porosities. The project has demonstrated that primary BRPE and BIPE were successfully harvested and differentiated into a functional monolayer *in vitro*. Primary bovine and human RPE and IPE were shown to grow as a differentiated monolayer on non-porous and porous PU substrates. The differentiated monolayer of primary cells on PU substrate displayed functional activities in the ability to phagocytose POS and transporting different sized dextran molecules.

CONTENTS

LIST OF FIGURES

ACKNOWLEDGMENTS

The author wishes to thank everyone in the Eye & Vision Science for their help, support and friendship. I would like to thank Mr. Daniel Brotchie for his technical help, preparing for posters and presentation, Miss Donna Gray for help with laboratory aspects and her patience in explaining difficult concepts.

Special thank goes to both of my supervisors: Dr. Rachel Williams and Dr. Carl Sheridan for all their guidance and continual support throughout my study.

I would like to acknowledge Mr. Ian Harrison, Mr. Fred Laws and Mr. Simon Dixon from Biomer Technology Ltd. for sponsoring and supplying materials. I would also like to thank Knowledge Transfer Network (KTN) and Engineering and Physical Sciences Research Council (EPSRC) for funding this project.

I am also grateful to Mr. Kyle Doherty for his help with DSA contact angle machine, Dr. Victoria Kearns with her wise words on the microscopes and laboratory techniques. Also, a special mention of Mrs. Ann Butler, for her help, in proof reading this thesis.

Finally, I would like to thank my family, my nanny (Hani) for her invaluable help throughout, my children (Adam, Adela and Adnan) and my husband (Badrul) for their constant patience, support, encouragements and love.

LIST OF TABLES

LIST OF ABBREVIATIONS AND SYMBOLS

ARPE-19. adult retinal pigment epithelium

AMD. Age-related macular degeneration

ANOVA. Analysis of variance

BIPE. Bovine iris pigment epithelium

BLamD. Basal laminar deposits

BLinD. Basal linear deposits

BM. Bruch's membrane

BRPE. Bovine retinal pigment epithelium

BSS. Balanced salt solution

CNV. Choroidal neovascularisation

DMSO. dimethyl sulphoxide

EDTA. Ethylenediaminetetraacetic acid

ePTFE. expanded polytetraflouroethylene

FBS. Foetal bovine serum

FDA. Food and Drug Administration (US)

FITC. Fluorescein isothiocyanate

HIPE. Human iris pigment epithelium

IHC. Immunohistochemistry

HRPE. Human retinal pigment epithelium

MRS. Macular relocation surgery

NBF. Neutral Buffered Formalin

NICE. National Institute for Health and Clinical Excellence (UK)

PBS. Phosphate buffered saline

PDMS. Polydimethlysiloxane

PVR. Proliferative vitroretinopathy

RA. Retinoic acid

SD. Standard deviation

SEM. Scanning electron microscope

TCPS. Tissue culture polystyrene

ZO-1. Zona occludens-1

LISTS OF SYMBOLS

C Carbon

CH_3 Methyl

F Fluorine

O Oxygen

Si Silicon

1 CHAPTER ONE: INTRODUCTION

1.1 Structure of the eye

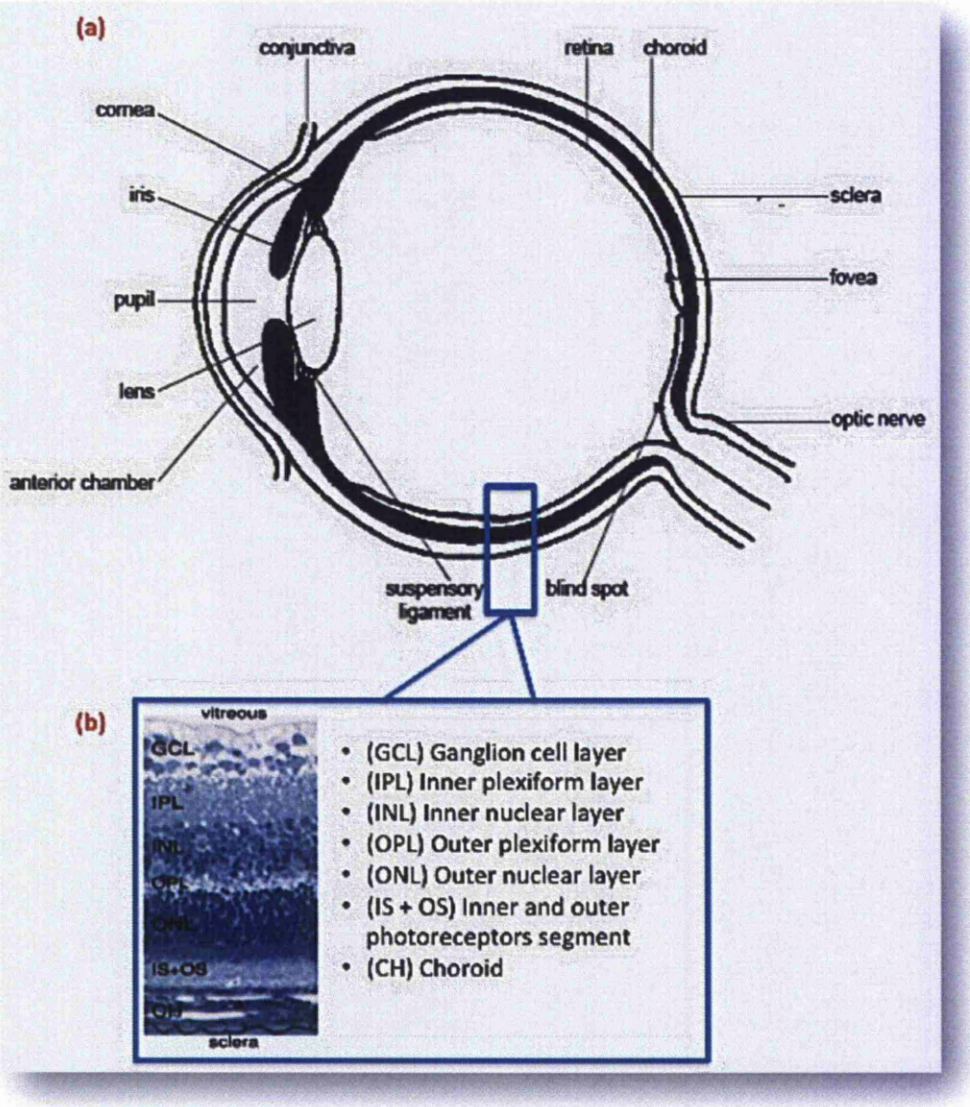

Figure 1-1: Illustrations of a human eye and its relation with the retina. (a) The eye consists of two fluid-filled chambers separated by the lens. (b) The retina is composed of complex layer of nerve cells, which leave the eye through the optic disc (blind spot). Pictures modified from Cheng et. al[1].

The human eye is spherical in shape about 24mm to 25 mm in diameter and consists of the anterior chamber (region between the cornea and the lens that contains aqueous humour) and the posterior chamber (region between the lens and retina that contains vitreous humour) see **Figure 1-1.** The eye is protected by a tough outer coat, the sclera, and is nourished by blood from the surrounding choroid. The cornea is about 0.52mm in axial thickness, more curved than the rest of the eye and is the most powerful refracting surface (refractive index, n=1.375) in the eye[2]; two-thirds of focusing is via the cornea. As light enters the eye through cornea, the pupil, which is controlled by the smooth muscle of the iris, acts as an aperture to control the amount of light that gets in. The lens adjusts its thickness so that the lights falls onto the macula area surrounding the fovea, the area of the retina which has the most abundant photoreceptors. The macula is about 5.5 mm in diameter. The fovea is about 4 mm temporally from the optic disc and its centre is the thinnest part of the retina and is free from capillaries[3]. The photoreceptors lie in a single row on a layer of retinal pigment epithelium, which is situated on a basal lamina called the Bruch's membrane. The Bruch's membrane maintains the integrity of the barrier between the choroid and the retina, acting as a blood-retinal barrier. The ciliary body continuously produces the aqueous humour, which flows out of the eye via the trabecular meshwork into the Schlemm's canal and in doing so maintaining the intra-ocular pressure (IOP) within the eye. The normal IOP of the human eye is between 1.4×10^3 Pa and 2.8×10^3 Pa. Therefore as well as functioning as a transparent visual tool, the eye must be tough enough to

withstand the pressure. The eye is richly supplied with blood vessels that enter via the optic disc. A blood vessel network radiates throughout the retina, allowing nutrient supply and wastes exchange and another network is spread out throughout the choroid providing supply to the pigment epithelium. However, both of these networks have a very limited supply to the outer retina.

1.1.1 The retina

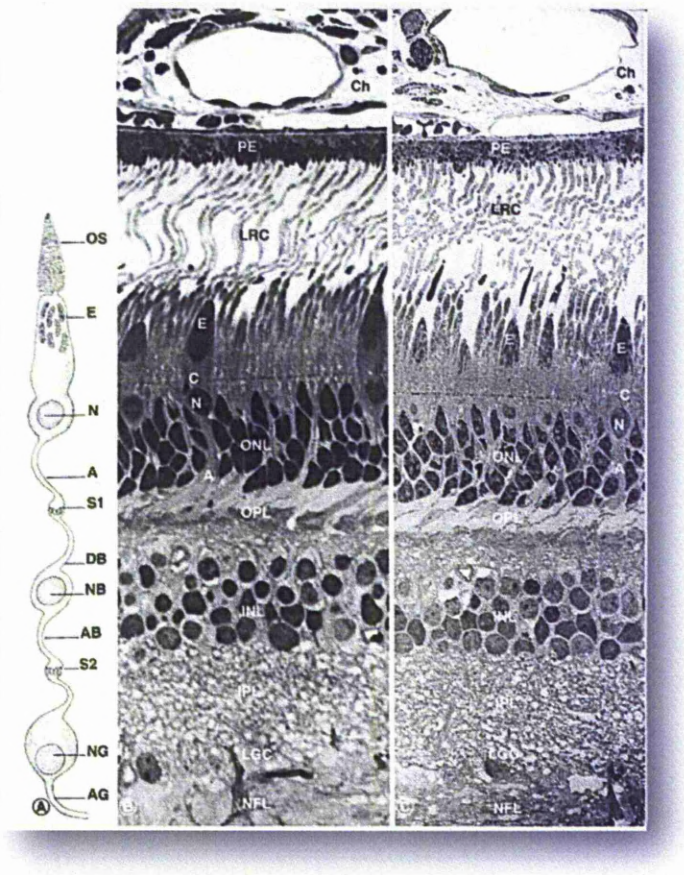

Figure 1-2: Cross sectional area of light micrograph through the human retina. Ch=choroid, PE=pigment epithelium, OS=outer segments, LRC=layers of rods & cones, E=ellipsoids (apical pole to the cell border), N=nucleus, ONL=outer nuclear layer, A=axons, OPL=outer plexiform layer, DB=dendrites of bipolar cells, NB=nuclei of bipolar cells, AB=axons of bipolar cells, INL=inner nuclear layer, IPL=inner plexiform layer, LGC= layer of ganglion cells, AG=axons of ganglion cells, NFL=nerve fibre layer. From Moran & Rowley[4].

The retina consists of complex layers of nerve cells (**Figure 1-2**) situated next to the retinal pigment epithelium (RPE) and choroid and leaves the eye via the optic nerve. Similar to the film in a camera, the retina detects the inverted image that falls on it, changing the light signal into a communicable chemical signal, in a process called photo-transduction, before sending the accurately ordered pattern to the brain. The light has to first pass through three layers of nerve cells (bipolar cells, horizontal cells and amacrine cells), before reaching the photoreceptors. The other two layers of cell bodies are called the outer and inner nuclear layers and the ganglion layer; the other two plexiform layers are where the synapses are located. The photoreceptors are situated just outside the outer limiting membrane.

The human photoreceptors (**Figure 1-3a**) consist of an outer segment with stacks of membranous sacks, containing four photopigment molecules (rhodopsin), one for rod and three for cones. The protein moieties on the rhodopsin (opsin and retinal) are sensitive to light. Each of the rhodopsin has a different maximal absortion wavelength; rod's rhodopsin has its peak absorption at 496nm, while the three cones have maximal absorption at 419nm (blue) 531nm (green) and 558nm (red). The rhodopsins are imbedded within the phospholipid bilayer of the disc's membranous sac of the photoreceptors (**Figure 1-3b**). Depending on the intensity of light projected onto the photoreceptor, rhodopsin will undergo structural changes (bleached), where the 11-cis-retinal changes to all-trans-retinal and these trigger action potential.

Once bleached, the retinal has to be restored and re-attaches itself to the opsin in an enzyme-driven process called regeneration. The regeneration process is quicker in the cones and takes place partly in the RPE[5].

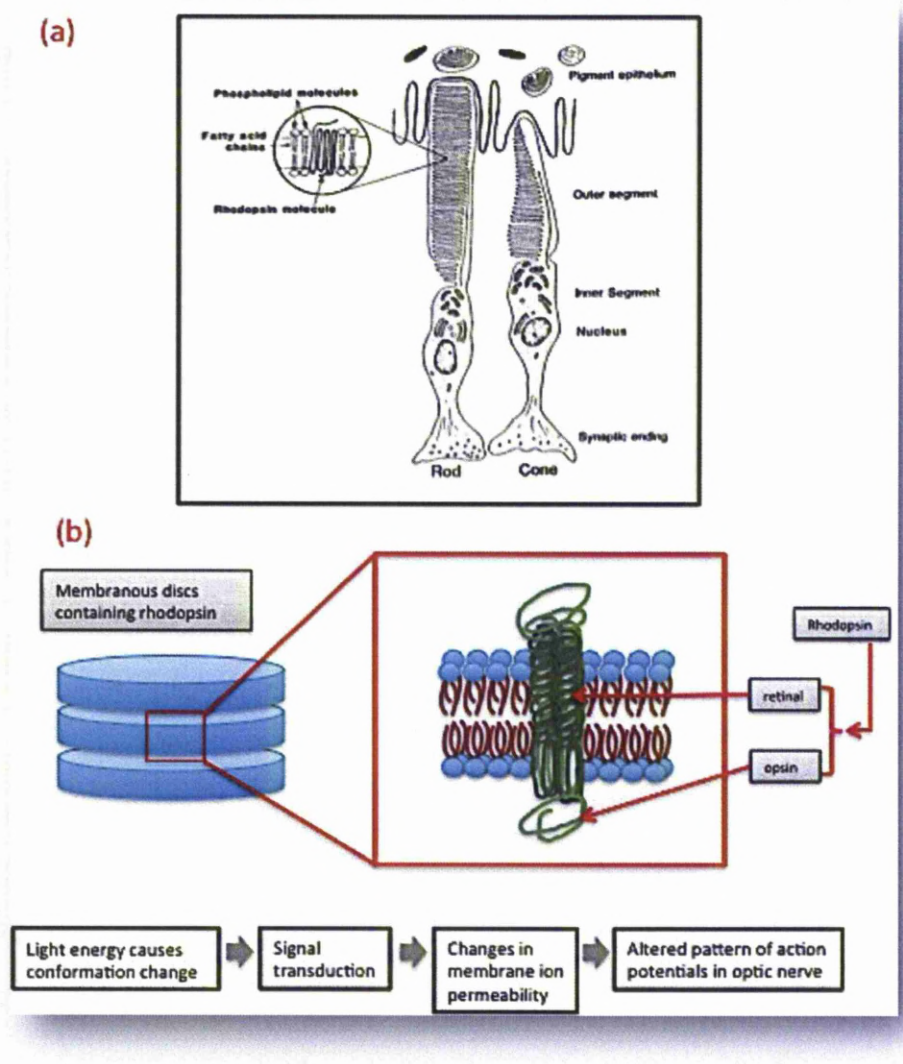

Figure 1-3: Morphology of the photoreceptors rods and cones (a)[6], and the schematic drawing of membranous discs containing rhodopsin photopigments (b). The rhodopsin itself was embedded within the lipid bilayer on the disc membrane and undergoes changes when hit by light.

The disc stacks are constantly renewed; the old stack is displaced up the outer segment and is phagocytosed by the RPE. They form phagosomes in the RPE and are broken down by lysis. This process will be significant when discussing one of the experiments in **section 2.12.1**.

1.1.2 The Retinal Pigment Epithelium

The RPE is a cuboidal hexagonal monolayer, which sits on Bruch's membrane and forms the barrier between the choriocapillaris (basolateral sides) and neurosensory retina (on its apical sides) (**Figure 1-4**). The subretinal space is the extracellular space at its apical sides, filled with inter photoreceptor matrix. The RPE surface has specialised microvilli (**Figure 1-5**) onto the retinal space. On the basal side, the RPE's infolded base sits on a pentalaminar (less than 4 μm thick) Bruch's Membrane[7]. The RPE cells in the macular region are generally smaller than the flatter and broader cells near the periphery. The cells in the macular are columnar shaped and tightly packed, thus giving the area its darker appearance[8].

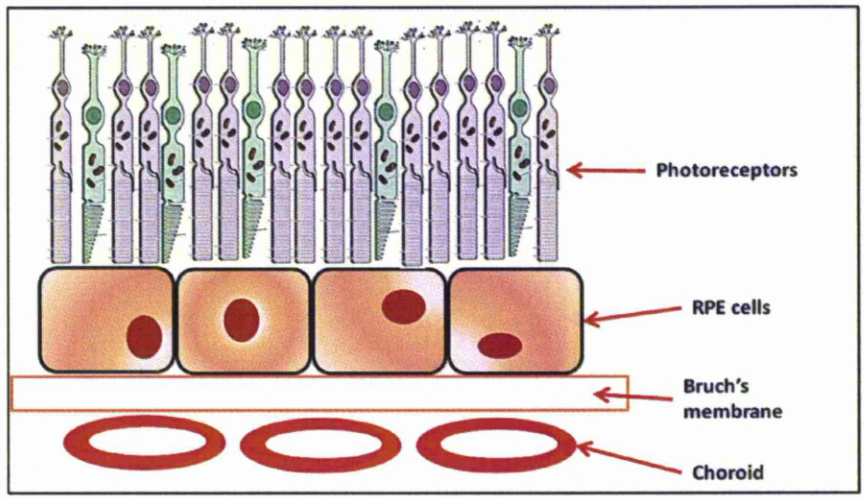

Figure 1-4: Drawing to show the relationship and the location of RPE cells to its surrounding. The RPE sits on Bruch's membranes, which separate it to the choroids. On its apical side, it was in close arrangement to the photoreceptors.

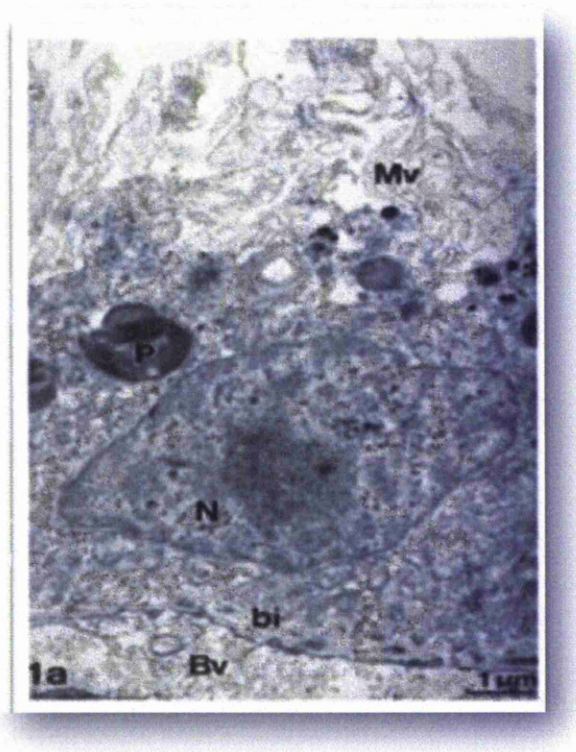

Figure 1-5: Transmission electron microscope of RPE cell. The cell has long projected microvilli (Mv) at the apical side and the phagocytosed outer segments are stored as dark dense phagosome (P). The RPE cell sits on the basal infolding bilayer (bi) indicated by the position of its nucleus (N), next to the blood vessel (Bv) of the choroid. Diagram obtained from: FrÖchlich et. al [9]

RPE acts as a physical barrier with its tight junctions (zona-occludens and zona adherens[10]), absorbs stray light[11], protects against photo-oxidation, maintains trans-epithelial transport (ions, amino acids, vitamin A), buffers ions in the subretinal space, acting as a key manager for phagocytosis of photoreceptors outer segments, which in turn regenerates rhodopsin molecules in the visual cycle of vitamin A and secretion of growth factors and other cytokines [12,13] . With advancing age, the cells decrease in numbers[14]. This will be discussed further in **section 1.2.1**.

1.1.3 The Iris Pigment Epithelium

The iris is a diaphragm that can constrict or dilate, thus controlling the amount of light entering the pupil. The iris is about 12 mm in diameter and consists of four layers: the anterior border layer, the stroma, the dilator papillae muscle and the posterior pigment epithelium. The iris is thickest at the collarets and thinnest at the root. The iris is dark in appearance, due to its high content of melanosome; the colour of the iris is dictated by the density and the pigment granules, contained in the melanocytes, within the superficial stroma[15]. The iris joins the ciliary epithelium posteriorly, where it continues with the retina. The anterior border layer of the iris contains a mixture of modified stroma and a dense collection of fibroblasts, melanocytes and collagen fibres. The posterior layer of the pigment epithelium consists of heavily pigmented iris pigment

epithelial (IPE) cells, which are embryologically derived from the neuroectodermal layer of the optic cup. It is here, at the posterior layer that the IPE cells can be found. The cuboidal IPE cells are stacked as two cells thickness layer behind the iris (**Figure 1-6**). The IPE cells are connected to each other via intercellular junctions, such as maculae occludentes and desmosomes[16]. The IPE are responsible for reducing reflected stray light in its path, and have been said to have some metabolic functions, due to their close association with the aqueous humour and the iris stroma.

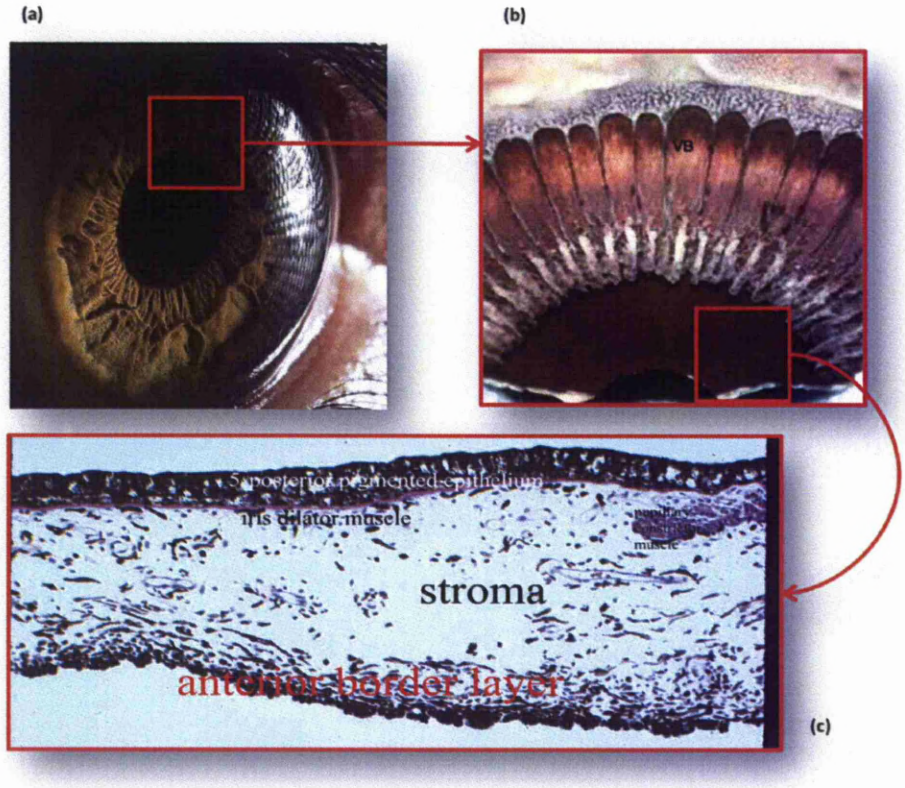

Figure 1-6: The location of the iris pigmented epithelium (IPE). The iris is the thin circular structure at the front of the eye (a), viewed from posterior side of the iris, which was connected to the ciliary body at its base and connected to the (VB) vitreous base and the retina. (c) Inset of the haematoxylin-eosin staining of the iris showing the anterior and the posterior layers of IPE. (b & c were obtained from www.missionforvisionusa.org)

1.1.4 The Bruch's Membrane

The Bruch's membrane (BM) which is a type of basement membrane, separating the choroid and the retinal epithelial cells, consists of 5 layers[17]: the basement membrane of the RPE, the inner collagen fibre layer, the elastic fibre sheet, the outer collagen fibre layer and the basement membrane of capillary endothelial cells of the choriocapillaris (**Figure 1-7**). The BM in the macula region is thinner and more porous than the surrounding area[18], with average thickness of around 2 to 5μm, average interspaces width of 25nm to 50nm and distances between connections of between 0.5 to 1.0μm. The thickness of the BM varies between individual, ages and between species, dictating the difference in elasticity and hydraulic conductivity. On average, the thickness of the BM increases with age[19]. It is suggested that the changes are attributed to the changes in calcification of the elastic fibres, cross-linking of the collagen fibres, increased production of glycosaminoglycans, advance glycation end products (AGEs) and accumulation of fat in the BM. These are said to be the major contributing factors to the development of Age-related macular degeneration (AMD)[20].

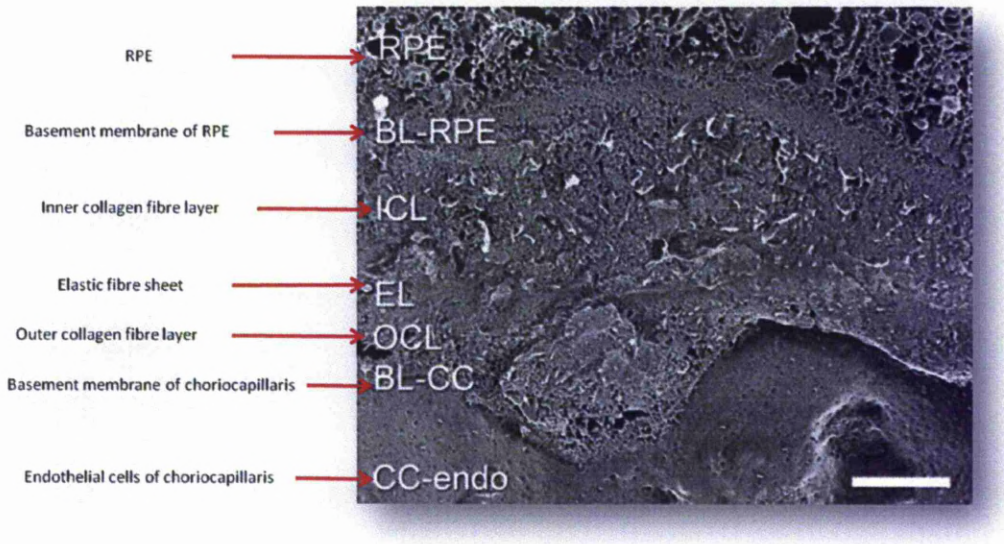

Figure 1-7: Electron micrograph showing the layers of the Bruch's membrane, 1) the basement layer of the RPE, 2) inner collagen fibre layer, 3) elastic fibre sheet, 4) outer collagen fibre layer and 5) basement membrane of choriocapillaris. Photo obtained from Huang et al[21].

Hydraulic conductivity of the BM was found to be between 110-2.5 x 10^{-10} $ms^{1}Pa^{-1}$. This decreases with increasing age and especially so at the central macula[20]. It was suggested that the values were much lower than the real value, because of the small diameter of samples used. There have been many studies conducted to find the values of the modulus of elasticity of the BM. This is difficult due to the fragile nature of the BM. Different measurement methods have been used; it was found that the value of the BM's modulus of elasticity, using a tonometer was between 3.5 MPa (at 20 years old) to 0.25 MPa (95 years old)[20]. Measurements using Atomic Force Microscopy (AFM) indentation by another group suggested a different value, between 2 to 4 MPa with stiffer central macula values[22], and later in their research found this value to be about

1 MPa[23]. Elasticity of the BM is important as its underlying choroid possesses high pulsatile blood flow, ranging from 444 μl/min to 803 μl/min[20]. Therefore, it is suggested that reduced elasticity will effectively reduce the choroidal blood flow and reduce transport capability. In terms of macromolecular permeability, it was found that the BM of a younger adult can transport protein with a molecular weight of 200 kDa, and this is reduced to 100 kDa in the elderly[24]. It was suggested that in patients with AMD, the protein trans-diffusional transport were even more impaired[25].

1.1.5 The Relations between RPE & IPE

1.1.5.1 Embryological relationship

From as early as the 22 days stage of development, the optic vesicle bulges out from the forebrain. By the end of the sixth week and at the early part of the seventh week, the optic cup differentiates to become two epithelial sheets, that turn into pigmented sheet and the sensory layers, the RPE and the neural retina posteriorly, and extends anteriorly to become the ciliary body and the iris (**Figure 1-8**). Both RPE and IPE are derived from the neoroectoderm (neural plate ectoderm) part of the optic cup, together with the ciliary body and the optic stalk, which later form into the optic nerve and the optic chiasma. The photomicrograph in **Figure 1-9** shows the close association between these two cells.

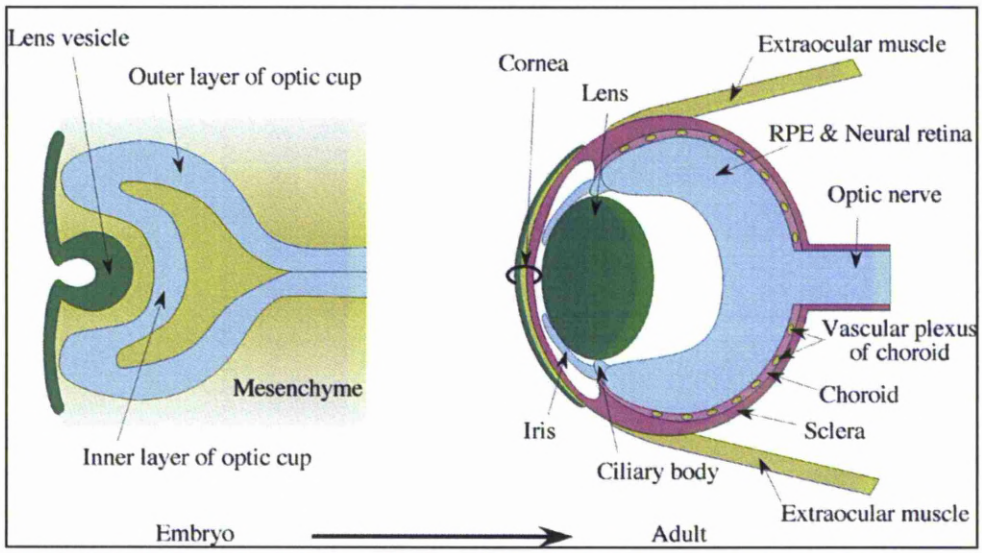

Figure 1-8: Schematic drawing of the embryological development of the eyes. (blue)=neuroectoderm, (green)=surface ectoderm, (pink)=neural crest, (yellow)=mesoderm. The layers of the optic cup fused and turned into RPE and the neural retina posteriorly, and continue anteriorly to become the ciliary body and the iris. Obtained from Harada et al.[26].

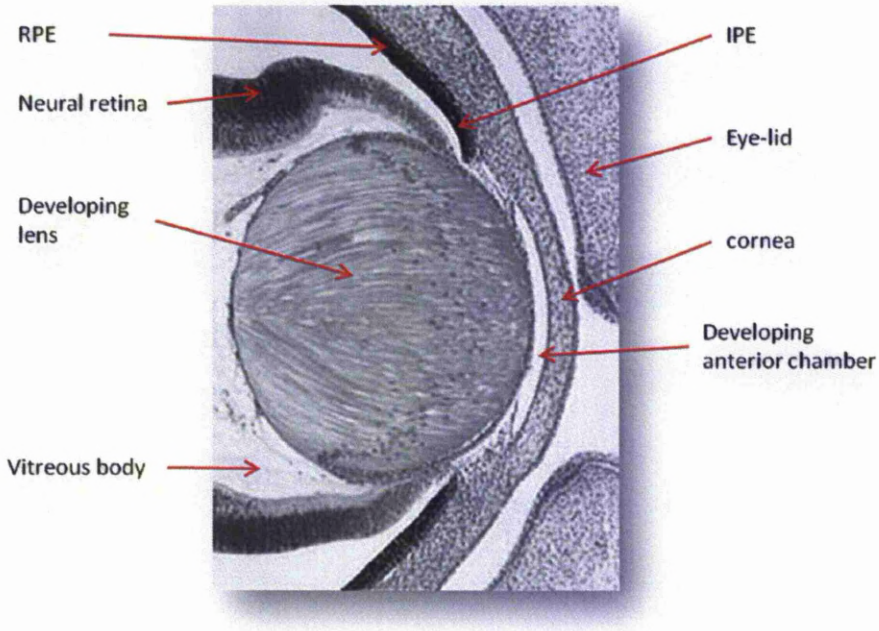

Figure 1-9: Photomicrograph showing saggital section of a developing eye at 56 days gestation showing the close relationship between the RPE and the IPE. Photo from Moore et al.[27]

1.1.5.2 Functional relationship

The RPE and IPE cell are both pigmented (dark in appearance) to reduce reflected light rays in its path. It has been shown in some experiments that IPE can behave like RPE in terms of retinol metabolism[28], consuming outer segments[29] and latex beads[30]. Cai et al. in analysing the gene expression between the two cells found that both of them share a large number of expressed genes[31]. This suggests the close resemblance of the two cell types. It was also hypothesised that the IPE might change its genes expression, once it is transplanted within the sub-retinal space.

1.2 Age-related Macular Degeneration (AMD)

Macular degeneration is a group of diseases characterised by break down of the macula (central portion of the retina). World Health Organisation (WHO) has reported that AMD is the primary source of visual impairment in industrialised countries and is in the third position for all causes of blindness (incidence of 8.7%[32]). In the UK, it is estimated that there are 500 000 people suffering from AMD, of these 40% are over the age of 75[33].

1.2.1 Histo-pathological changes in AMD

In a normal eye, retinal epithelial cells (RPE) phagocytose outer segments of photoreceptors cells. In a young individual, the Bruch's membrane (BM) is thin; the visual cells are regularly aligned and densely packed. Through the process of ageing, the thickness of BM increases, the cells become less efficient in carrying out their normal tasks, and so the retina cannot receive appropriate nourishment and the build-up waste material occurs. RPE gradually accumulate sacs of molecular debris, such as lipofuscin, which is the remnant of the incomplete degradation of abnormal molecules, which have been damaged within RPE cells or obtained from phagocytosed rod and cone membranes. These functionless residues become waste until the cell's normal metabolic activities begin to be compromised. The wastes accumulate on the Bruch's membrane and aggregate in the form of drusen, basal laminar deposits (BLamD) and basal linear deposits (BLinL) and thus cause further deterioration of the RPE. The Bruch's membrane, devoid of RPE attachment, is susceptible to invasion of new blood vessels from the choroid. The newly formed blood vessels are also weak and so leakage of blood to the surrounding area can occur.

Drusen can manifest themselves in two forms, hard and soft (**Figure 1-10**). In the early stage, drusen may be ophthalmoscopically visible as semi-translucent punctuate dots in retroillumination. As the overlying RPE thins, drusen become more noticeable as yellow-white deposits. Hard drusen are usually made of small pin-point, yellow-white solid deposits, typically less than 63μm in

diameter, which cause no harm in small quantities. Soft drusen are usually larger and have indistinctive borders with a tendency to become confluent. With rising age, drusen can become calcified or filled with cholesterol, appearing crystalline or polychromatic. Build-up of drusen in between RPE and Bruch's membrane can force the two layers apart and this typically happens in the central macula[34]. There is a suggestion that migration of apoptotic human RPE cells, from the periphery to the macula, trigger AMD from the centre and these apoptotic cells increase with age[35]. The increasing size of drusen, their confluence and numbers are also associated with rising rates of choroidal neovascularization (CNV).

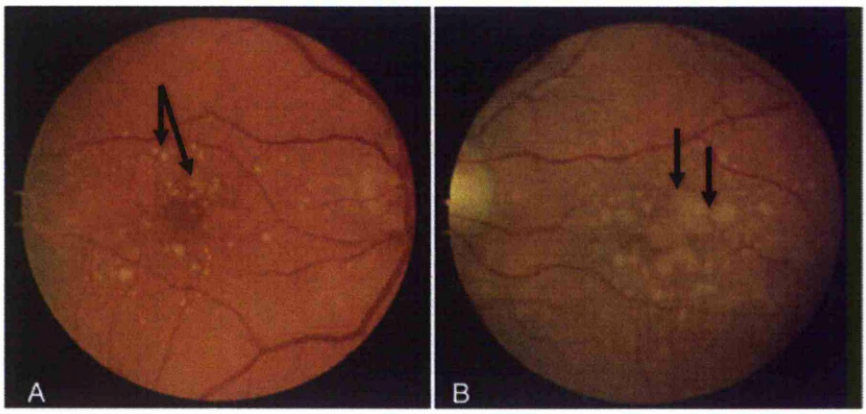

Figure 1-10: Gross appearance of the two major Drusen phenotype (arrows); (A) Hard Drusen (B) Soft Drusen. Hard drusen is usually formed in small deposits, in small quantities causing no complications. Soft drusen is bigger, can become comfluent and spreads over larger area along the BM, forcing the two layers apart, providing regions of geographic atrophy. Diagram from [43].

CNV refers to the growth of new blood vessels from the choroids, usually beneath the RPE (or sometimes entering the sub-retinal space) in the case of AMD. This often occurs in the late stage of wet AMD. Its earliest indicators are sub-retinal or sub-RPE haemorrhage. CNV can cause leakage of blood (and thus serum and lipid), which can lead to scar formation and RPE detachment, as described previously, as a result of drusen formation between RPE layer and Bruch's membrane (**Figure 1-11**).

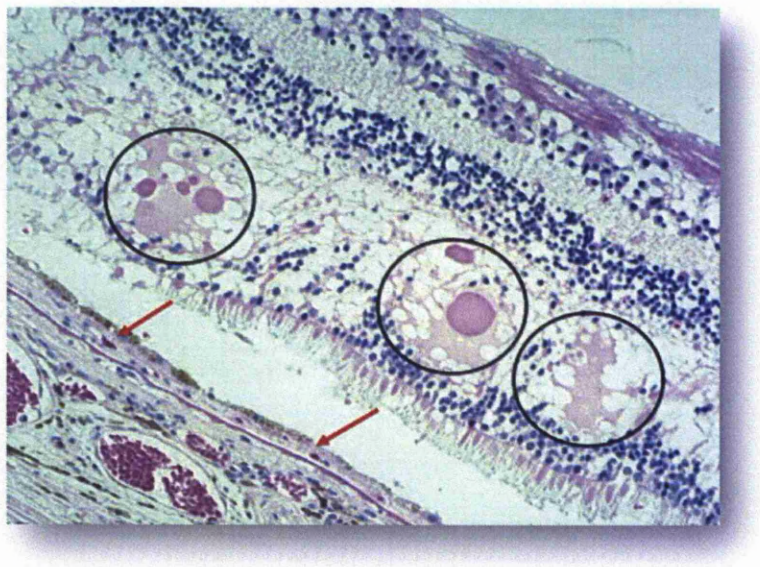

Figure 1-11: Choroidal neovascular (CNV) formation (arrows) in wet AMD creating a layer between the RPE and the Bruch's membrane. Leakage of blood (circles) can be seen at the surrounding area. Picture from [56].

Apart from drusen and CNV, other characteristics of AMD are the development of geographic atrophy (GA) and RPE detachment. This often occurs in the late stage of dry AMD. The development of GA is usually following the rising

numbers of lipofuscin granules in the RPE cells, and is a major cause for severe visual loss in AMD[36]. Following fading of drusen, especially in an area of RPE attenuation, after RPE detachment or involution of CNV, GA is usually accompanied by choriocapillaris atrophy. GA is also related to the significant decline of visual acuity (as photoreceptors overlying areas of RPE are metabolically dependent on the RPE cells) and continually enlarges with time[37]. The average rate of GA progression is 139µm per year and is lower in the over 75 compared to below 75 years age[38]. The area of GA can be seen as hypopigmentation (due to cell loss) and thinning of the retina (due to photoreceptors death) (**Figure 1-12**).

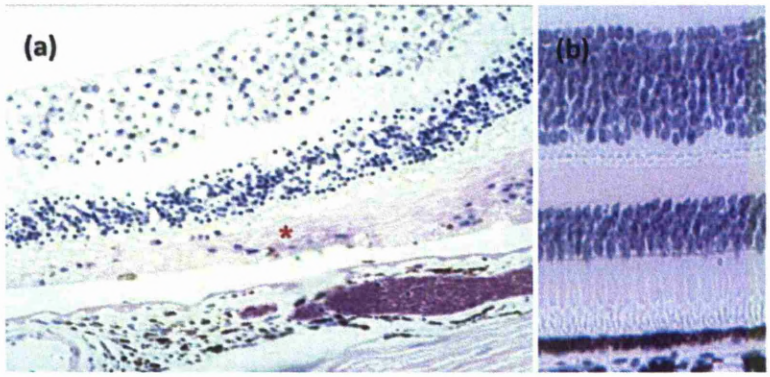

Figure 1-12: Geographic atrophy (GA), the development of the late stage of dry AMD (a) and the normal retina (b). GA was characterised by hypopigmentation due to loss of RPE cell loss and degeneration of photoreceptors (*). These cause thinning of the retina. Picture from Xiaoyan et al [56].

The molecular and cellular elements of drusen have been investigated in many studies. Complement components, inflammatory molecules, lipids, lipoproteins B and E, and glycoproteins have been suggested to be the main constituents of drusen. These were confirmed by immune-histochemical analyses, with the additions of other molecular components such as immunoglobulins, factor X, amyloid P component, amyloid β, some complement terminal complexes, fibrinogen and vitronectin among others were present in both hard and soft drusen[56].

There are several papers describing the morphology and physiological changes in AMD sufferers, including its relationship with age, the presence of pigmentary disturbances, drusen, thickening of Bruch's membrane and basal laminar deposits. All of these changes, however, are commonly associated in the eyes of all elderly individuals, but only in some individuals do the changes progress to cause cell death and functional loss. AMD is, therefore, said to be the accumulation of all the deleterious features, which takes place in the eye[39]. The summaries of the pathological development leading to the occurrence of AMD are arranged in Chart 1-1.

Chart 1-1: Summary of the pathological development leading to AMD (modified from[40])

- Accumulation of membranous debris on both sides of RPE's basement membrane.
- Clinical manifestations of drusen.
- Atrophy of the RPE/choriocapillaris.
- RPE detachment.
- CNV formation.

Pathological sequence of events (hypothetical)

- RPE dysfunction
- Accumulation of intracellular material (which is not enzymatically degraded and abnormal substrate) in the RPE.
- Abnormal accumulation of extracellular material (BLamD and BLinL deposits).
- Change in Bruch's membrane composition (increased lipid deposition and protein crosslinking).
- Change in Bruch's membrane permeability to nutrients (impaired diffusion of water soluble plasma solubility across the membrane).
- Response of the RPE to metabolic distress (either by atrophy or CNV growth)

1.2.2 Assessment of AMD

The first symptom of AMD is blurring of the central vision; most apparent when undertaking visually detailed tasks such as sewing or reading. As the disease progresses, it spreads from the central to the periphery. People affected with AMD may be very sensitive to lights. They can also have difficulties in seeing straight lines (which will appear wavy or fuzzy) and report seeing colours or shapes that are not there. An Amsler grid was usually used to detect signs of AMD (**Figure 1-13**). Advance AMD sufferers often notice a blank patch or a dark

spot in the centre of their sight. This painless symptom causes discomfort to the sufferers with difficulties in doing daily tasks such as reading, writing and recognising small objects. The incidence of depression is also found to be significantly high in AMD sufferer[41].

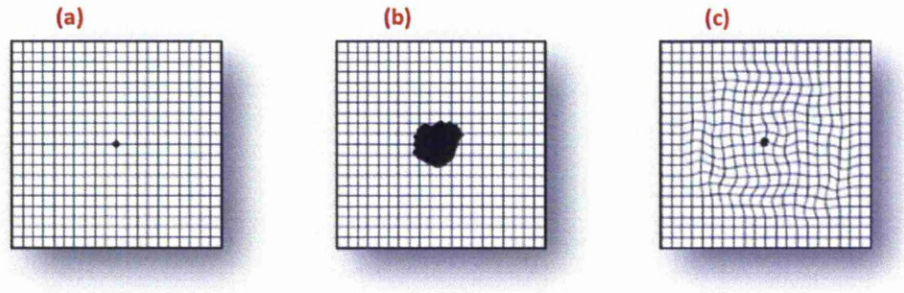

Figure 1-13: Amsler grid used to diagnose AMD: (a) vision of a normal person, (b) vision of a person with dry AMD, (c) vision of a person with wet AMD. Diagram obtained from http://www.brower.co.uk/opticians/maculardegeneration.html

The international age-related maculopathy (ARM) epidemiological study group has defined AMD as a degenerative disorder in persons over 50 years of age, characterized by colour fundus transparencies, with the presence of some abnormalities in the macula area, such as drusen content, pigmentation levels of the retinal pigment epithelium (RPE), RPE detachment, retinal haemorrhages, atrophy of RPE or retinal fibrous scarring in the absence of other retinal (vascular) disorders[42].

AMD is classified into two types: wet and dry. Dry AMD, the more common type develops slowly causing gradual loss of central vision. Wet AMD results from new blood vessels growing behind the retina causing bleeding and scarring. Wet

AMD accounts for 10% of all AMD and can develop quickly. AMD usually affects both eyes, although one may be affected long before the other, so the unaffected eye can sometimes be used to compensate for the loss of vision in the affected eye. The pathophysiology of AMD will be discussed later. The two types of the AMD can also be seen by the appearance of the patient's fundus (**Figure 1-14**). Leakage of blood can be seen in the macula area of the eye in a wet AMD case, whereas in the dry form of AMD, small yellow spots or large (softer) drusen formation can be seen in the macula and the surrounding area.

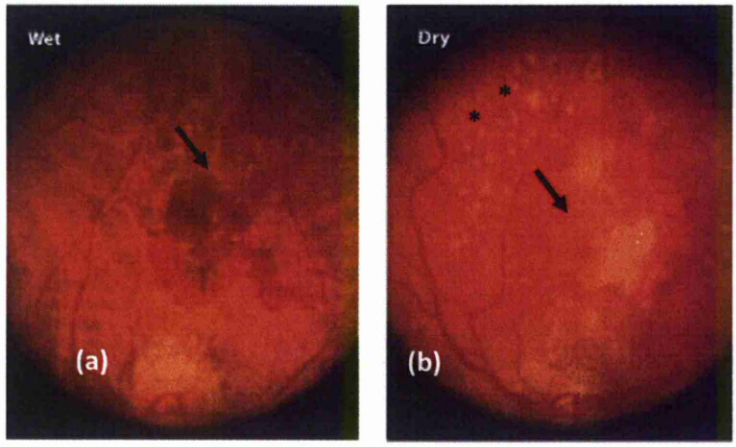

Figure 1-14: Photographs of the retinal images of a wet and dry AMD. (a) In the wet form of AMD, neovascularisation causes leakage of blood to the surrounding area (arrow). (b) In dry form of AMD, yellow deposits of hard (smaller dots *) or soft (bigger-arrow) drusens can be seen near the macula area. Diagram obtained from www.blindness.org

1.2.3 Epidemiology of AMD and Assessment of Health Risks

There are many conflicting conclusions in literature relating to the precise aetiology of AMD and it is still poorly understood. There are a number of risks

factors associated with AMD, including *age*[43] (older people are more likely to develop AMD and it was more prevalent in the over 50s) and *gender*[44] (females are more at risk from AMD) but others found that it is still inconclusive[45].

Some studies found that a *genetic* contribution is important[46] in the development of AMD such as apoliprotein P[47]. The incidence is also found to be more common in the white population than the black[48]. There have been large population-based studies within three continents: the Beaver Dam Eye study in Canada[49], the Blue Mountains Eye Study in Australia[50] and the Rotterdam Study in the Netherlands[51], which found that the prevalence of neovascular AMD was more frequent than geographic atrophy in whites than in the black population, even with similar amount of drusen size at an early stage. For this, it has been suggested that the 'melanin may have been acting as a free-radical scavenger' in protecting the pigment epithelium[52]. Many researchers believe there is a strong correlation between smoking and AMD[53]; a very large randomized study in the UK has proved this relationship[54] and others have strongly emphasised smoking as the only modifiable cause to AMD[55]. Smoking may increase the risk of AMD by reducing the production of antioxidants and reactive oxygen species, inducing hypoxia and inducing change in choroidal blood flow[56]. Other factors such as *total cholesterol level*[57] (i.e. people with higher total cholesterol level are more at risk from AMD) and *nutrition*[58] (some vitamins such as A, C & E can help protect against AMD) and *obesity*[59] (i.e. people with an obesity problem are more at risk of developing AMD) were important factors in determining the

occurrence of AMD. Another confounding factor such as *education level*[60] (reduced incidence of AMD in people with higher level of education) has also been suggested to be linked to the possible cause of risks to AMD.

There are some other factors that are still causing debate such as if sun-exposure causes a risk for AMD. Some research show positive correlation between light-induced AMD[61] and some studies deny this association[62]. Hypertension is also thought to contribute to AMD, especially neovascular AMD and even in those who are still receiving antihypertensive drugs[63].

1.3 Therapy for AMD

There are several types of treatment for AMD with different approaches for the wet and dry form of AMD.

In wet AMD, choroidal neovascular membranes invade Bruch's membrane; neovascularization occurs beneath the retina and causes blood and fluid leakage. Wet AMD is further subclassified into two forms: *classic* form and *occult*. Classic wet AMD is when the invading neovascularization grow in between RPE and the neurosensory retina; the angiogenesis and scarring has a very clear, delineated outline beneath the retina (CNV). Occult wet AMD is when the neovascularization grow underneath the RPE; angiogenesis beneath retina is not as obvious and there is less leakage[64]. Classic CNV is associated

with more severe vision loss compared to occult CNV. Therefore, it is thought, by tackling the angiogenesis, wet type of AMD can be brought to a halt.

Although the dry form of AMD makes up the majority of all cases of AMD, currently there is no FDA or NICE approved treatment available for this type of AMD. There are many studies taking place to find a suitable treatment for dry AMD. There is some research which suggests that taking vitamins[65] (C, E, zinc and beta carotene) and supplements[66] (such as Lutein and Zeaxanthin) can slow down the progression of dry AMD, but it will only play a part in prevention and will not restore the sight. The research claimed that free radicals are involved in pathogenesis and these antioxidant supplements can prevent damage to the retina[67].

1.3.1 Gene therapy

In recent years, there have been many studies carried out to identify the specific gene contributed to the development of AMD[68]. Genes such as CD36, complement factors H and B (CFH, CFB), C-reactive protein (CRP), C3 gene variant, Fibulin 5, interleukin 6 and 8 (IL6, IL8) amongst others have been suggested to have participated in the development of AMD. At present, there is a large clinical trial in progress with Leber's congenital amaurosis type 2 (LCA2), an abnormality associated with RPE65 gene, which is a protein required for photoreceptor cell function. The trials in humans, which started in 2007, utilising the sub-retinal route of administration, have demonstrated some

promising results, with some improvement in vision, increasing sensitivity to light in the legally blind. Another gene therapy undergoing in human trials include adeno-associated virus (AAV), with the possibility of intra-vitreal route of administration[69]. However, both of the therapies mentioned were targeted for wet AMD patient and currently no known gene therapy approach had been approved for the treatment of dry AMD.

1.3.2 Therapeutic Strategies

There is some evidence suggesting the contribution of an anti–vascular endothelial growth factor (VEGF-A); a protein that triggers abnormal blood vessel growth and leakage in the development of CNV. VEGF is said to be present in fibroblastic cells and in differentiated RPE cells in surgically excised CNV membranes. Furthermore, research found that VEGF-A secretion in the basolateral membrane is increased during hypoxia, and in the case of AMD[70].

There are several drugs currently developed for the wet type of AMD that inhibit angiogenesis. A drug used such as Pegabtanib, was found to be effective in the treatment of neovascular age-related macular degeneration[71] (**Figure 1-15**). Pegabtanib, also known as Macugen, is an anti-VEGF agent and applied by injection into the cavity of the eye of the patient (**Figure 1-16**). However, a newer drug such as bevacizumab (avastin), which works on a similar principle, was demonstrated to be better than pegabtanib (Macugen), when given via

intravitreal injection, especially in patients (losing vision secondary to macular CNV), who responded poorly to Macugen therapy. Normal or improved macular morphology was observed (for at least 4 weeks) and the patients had stable visual acuity[72]. Avastin was initially derived for anti-cancer treatment. Its AMD-version; Lucentis (ranibizumab) has been developed and was found to have excellent clinical value. When injected into a patient's eye in monthly intervals, research found that Lucentis maintained or improved vision by 95% in AMD sufferers[73]. However, Lucentis only benefited those with early vision loss in AMD. Both Macugen and Lucentis have FDA approvals but in the UK, only Lucentis has NICE approval for use in AMD treatment due to cost-effectiveness.

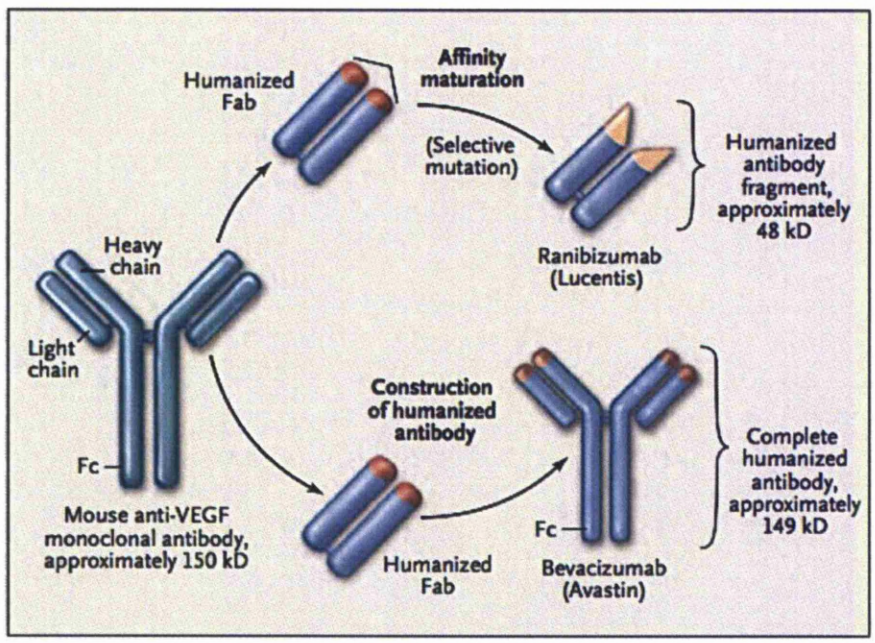

Figure 1-15: Relationship between Ranibizumab (Lucentis) and Becavizumab (Avastin), both antibodies bound to and inhibit all the biologically active forms of vascular endothelial growth factor (VEGF). Diagram from [73].

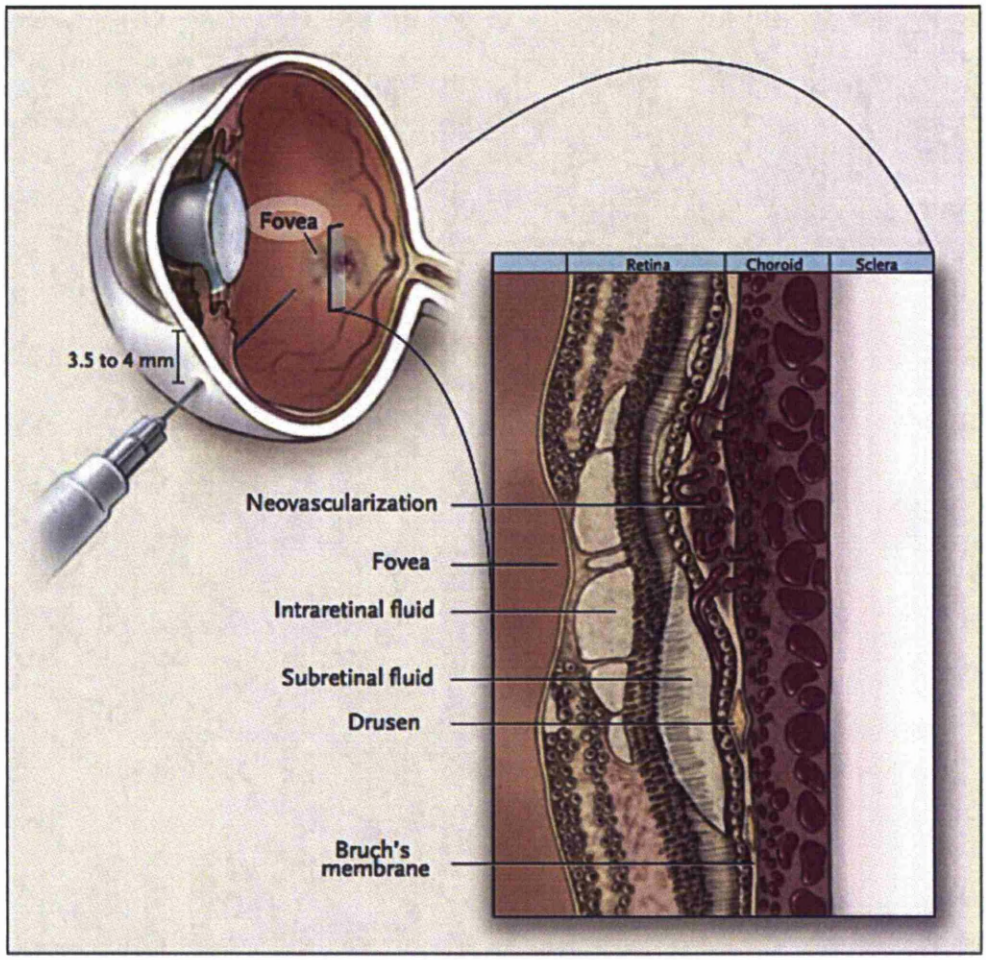

Figure 1-16: Intravitreal injection in AMD treatment. It is carried out under topical anaestatic, Macugen or Lucentis is injected behind the lens of the eye. Diagram from [73].

These drugs do not cure AMD completely, but do provide some relief in patients. Recently, drugs such as Mecamylamine (also known as AT003), which has similar properties as Macugen and Lucentis, and Combrestatin (an anti-tumour drug) have been developed with the advantage of application as eye-drops (instead of injection). But their uses are still under investigation. Another drug called Evizon (squalamine lactate), which was derived from dogfish shark, has been reported to disrupt the cells responsible for abnormal angiogenesis,

but it was later found to be inferior in effectiveness to Lucentis and Macugen. However, Evizon is believed to be more effective, if used in high doses for AMD treatment and is still under investigation.

1.3.3 Laser treatment

In *Photodynamic Therapy*, an injected dye accumulates around the leaking blood vessels and then a 'cold' (low powered) laser is directed onto the treatment area in the eye and by means of phototoxicity causes local thrombosis in the area of the neovascular membrane. The aim is to treat patients with new CNV in wet AMD, who still retain some visual acuity i.e. to stop further loss of vision rather than restore vision already lost.

Photocoagulation uses a similar principle as those of photodynamic therapy, but this time, the laser beam is used to destroy newly formed blood vessels. This therapy, however, will only be suitable to patients whose leaking blood vessels are located in the periphery, rather than at the macula. This is most useful when the neovascularisation has not yet encroached to the surrounding macula.

1.3.4 Surgical Approach

The surgical excision of the macula area is difficult due to the close association of RPE and its underlying choroids resulting in removal of both structures. There

are a few surgical strategies attempted for retinal transplantation[74], but they are very complex and generally lead to scarring.

1.3.5 Grafting

Histopathological findings of the non-exudative form of AMD show decrease in choroidal vessel densities and narrowing of vessel lumens, suggesting that there is a lower chance of immunological and inflammatory responses in the introduction of grafting. However, immuno-histochemical analyses show various molecular constituents, such as apoliproteins B and E, different immunoglobulins, factor X, amyloid P component and other acute-phase reactants to be participating in this region, suggesting the role of drusen in the pathogenesis[75].

There have been some experiments to investigate the use of RPE-patch grafts in dry-AMD patients. In a study, human foetal RPE grafts were transplanted subretinally in both dry and wet AMD patient groups without immunosuppression[76]. Another similar study by the same group was carried out but using RPE allograft[77]. Both studies found that there are signs of rejection in the case of neovascular AMD, but with non-exudative AMD, there were lower signs of rejection and the small extrafoveal transplant remained unchanged in shape, size and colour for more than two years. It is thought that the intact blood-retinal barrier is likely to protect against rejection and show a promising

result for transplanting human RPE into the submacular space, without adversely affecting long term visual function in the dry form of AMD. This has provided us with proof of principle for our current research.

1.3.6 Macular Relocation

Macular relocation surgery (MRS) is said to be capable of enhancing vision in some patients despite moderate and severe visual loss[78] and is currently undergoing research as an alternative to photodynamic therapy. It is described as 'relocating the central neurosensory retinal or fovea intraoperatively or postoperatively specifically for the management of macular disease'[79]. In the case of AMD, neuroretina of the fovea is relocated away from the underlying CNV to an area of healthy RPE and choroids. In addition, patients can be selected to see if they are likely to experience an improvement in vision following MRS[80]. There are various techniques involved in the procedure including subtotal vitrectomy, followed by a partial or total retinal detachment. Then, the retina is moved relative to the underlying RPE by either rotation, displacement or by scleral shortening and then is reattached to a new position (away from the CNV). The CNV is being surgically removed and its feeder vessel cauterised.

Results from some studies show encouraging results. In a study following 12 months postoperatively, visual acuity increased by 15 or more letters (in a

Snellen chart) in 27% of patients, remained stable for 41% and deteriorated in 32% of patients[81]. However, this is a difficult procedure and has complications such as proliferative vitreoretinopathy, macular pucker, macular hole and retinal detachment that can lead to loss of both central and peripheral vision[82]. There are some prospects of improved skills and success rate however, as the experience increases[83]. MRS has the capability to treat dry AMD and advance disease, such as subfoveal haemorrhage, which cannot be compliant to any anti-angiogenic strategy[84]. Further randomised, controlled studies are needed to identify who will benefit most from this surgical procedure.

1.4 Tissue Engineering approach

In a tissue engineering approach, healthy cells derived from humans such as RPE cells, could be cultivated in the lab and then delivered under the macula. Using donor cells might impose problems such as tissue rejection[85] even with the immuno-privileged site like in the eyes, thus patients have to be supplied with immuno-suppressive drugs for the rest of their lives. This problem can be reduced by using the patient's own cell (autologous implants), as demonstrated by some research[86], but since those patients have depleted RPE cells in the first instance, maybe a different solution is required. Some studies have suggested the use of iris pigment epithelial (IPE) cells from the back of iris, as both IPE and RPE are derived from a single stem cell embryologically[12]. A pilot study has

provided promising results for this approach, where autologous IPE cells were transplanted into a subretinal space following removal of choroidal neovascular membranes. The resulting transplanted cells were well tolerated and did not affect the function of the photoreceptors[87]. In the same year, autologous IPE transplantation, used to treat AMD, demonstrated no significant improvement of macular function, but showed no rejection or deterioration in visual acuity[88]. Another finding reported that the IPE layer formed did not remodel itself as a smooth monolayer after transplantation, i.e. IPE cells formed a compound layer with the native cells[89]. It is also reported that IPE, in culture, have some of the functions of RPE, such as specific phagocytosis of rod outer segments and retinol metabolism[28]. Therefore, we hypothesise that IPE cells could be made to behave like RPE and cultured to form a viable monolayer on our chosen substrate, before the insertion underneath the macula (Figure 1-17).

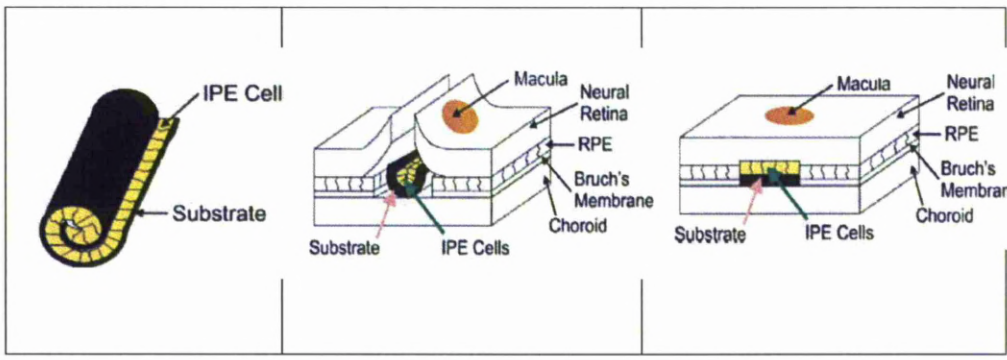

Figure 1-17: How IPE cells are proposed to be transplanted below the macula. IPE cells are going to be cultured on a chosen substrate, forming a viable monolayer and transplanted underneath the affected macula. Diagram reproduced with kind permission from[90]

In this research, we opted for surgical/tissue engineering approach for the treatment of AMD. Looking at the transplantation procedures of AMD, there are several methodologies: autografts versus allografts, loose cells versus sheets or patches, RPE or IPE cells (**Table 1-1**).

Table 1-1: Methods used in cells transplantations; modified from data obtained from Meurs[91]

Types of Transplantation	Types of seed layer	Types of Cells	Research Group
Allograft	Loose	RPE	Engelmann 2002
Allograft	Patch	RPE	Peyman 1991, Algvere 1994, 1997, del Priore 2001
Autograft	Loose	RPE	Binder 2002, van Meurs 2003
Autograft	Patch	RPE	Peyman 1991, Aylward 2002, van Meurs 2003
Autograft	Loose	IPE	Thumann 2000, Lappas 2000
Autograft	Patch	IPE	Navea 1998

Autologous cell transplantation, while reducing the risk of rejection, may have the disadvantage of carrying the same genetic impairment that led to the development of AMD. This calls for using cells from the same patient but of

different cell types, IPE for example. And there is also a question of seeding the cells either as a suspension (loose) or as an intact monolayer (patch).

There have been many types of donor cells involved in transplantation for AMD. They include fresh, cryopreserved, cultured or immortalized RPE cells of both animal and human origin. Additionally, the use of IPE cells, stem cells, photoreceptors and Schwann cells have also been experimented. However, the results from these experiments pointed to a similar conclusion. The cell interaction with its surrounding substrate determines the success of the operation. Another important consideration was the number of cells seeded/transplanted. It has been shown that too large a number of cells produce rejection, but too little a number of cells, although do not show rejection, did not show any improvement in vision[92].

1.4.1 Choice of cells

As the preliminary objective is to restore vision, any cells that are transplanted under the retina must form a polarized monolayer and cover the exposed photoreceptor outer segments. It must also be integrated with the Bruch's membrane complex. Both IPE and RPE cells have similar functions such as phagocytosis and retinol metabolism, although this is a bit slower in IPE[93]. Furthermore, if IPE are used instead of RPE, the IPE must attain the RPE cellular functions, such as providing the survival and trophic signals for the

photoreceptors, to phagocytose outer segments, to form a reliable blood-retinal barrier and to hinder choroidal new vessel formation[94].

There has been a review conducted by Crafoord in 2001, regarding experiments with both RPE and IPE cells[89]. Results show that a fresh suspension of autologous-pigmented RPE cells, implanted in subretinal space in rabbits, produced an undesirable outcome. After a six-month period, the transplant consisted of a multilayered form of RPE and macrophage, and changes to adjacent photoreceptors. In another experiment, Crafoord et al. used both RPE and IPE autograft, delivered to the subretinal space by injections. After a six-month period, there was remodelling of the IPE cellular layer at which they join with the native RPE layers. RPE transplantation however, displayed pathological changes, whereas IPE transplant showed normal outer segment length and outer nuclear layer above the grafted IPE cells. They concluded that experiments using an autologous IPE graft, exhibited non-immunogenic (less immune rejection) mechanism compared to RPE cells.

Transplanted pigmented cells in suspensions, although well tolerated immunologically, do not improve patients' visual acuity, due to failure to maintain its phenotype. A functioning cell must be able to be organised as a monolayer, with differentiated apical and basal domain. Therefore, it is of extreme importance, that the transplanted cells are properly oriented and transplanted as a preformed monolayer.

1.4.2 Choice of substrates

Another consideration to bear in mind is the substrate membrane (support layer), which will also serve as a replacement for the damage Bruch's membrane (BM). The substrate must be able to integrate into the BM-retinal complex.

As the substrate is needed to replace damaged BM, it should replicate as closely as possible its physical and chemical properties. Such a substrate must be able to support a monolayer of functional RPE cells. It must also be potentially bio-stable so that it can remain functional in the patient for their lifetime, to support and protect the cell. Since it will be used for implantation, flexibility is an essential requirement, so that it can be easily manipulated to minimise implantation trauma. Studies have shown that the native BM thickness is about 2.0 to 5.0 μm[95] and so ideally the substrate should be made into thin films to minimise distortion and at the same time be sufficiently robust for handling. The material is required to be porous to maintain transport of nutrients and waste, as in the native BM.

1.4.3 Current Research in cell transplantation under the retina

There have been some experiments carried out to find out a suitable material to be used to support a viable layer of epithelial cell growth underneath the retina. The basic concept of the scaffold is that it must be biocompatible (to meet both

nutritional and biological needs for the specific cell population), when it is used to provide an architecture on which seeded cells can organize and develop prior to implantation. The scaffold will also provide an initial biochemical profile for the replacement tissue, until the cells produce an adequate extracellular matrix.

There are some challenges that need to be faced upon transplantation. One of which is the host response to transplantation i.e. rejection failure. Immunological responses pose a threat in the eye as even small distortion in the axis can cause visual impairment; light has to fall accurately and precisely on the retina[96]. The retina is known to be immunologically privileged, i.e. down regulation of response resembling those of the anterior chamber associated immune deviation (ACAID). It has been documented that transplantation in the posterior part of the eye shows detectable rejections, (i.e. it is not absolutely immunologically privileged) and that rejection is a serious problem in human retinal transplantation. Rejection remains the main cause of retinal transplantation failure[97]. Some studies have suggested the use of immuno-suppressant to reduce the risk of rejection, but this is not very well tolerated by the elderly. It is thought the use of autologous cell implants can reduce the rejection failure rate but transplanted cells might not survive in the subretinal space initially, irrespective of immune rejection[98]. Therefore, it is more important to establish cell adhesion prior to differentiation.

Another problem one could encounter is following the surgical removal of CNV. Although submacular surgery with CNV excision offers the possibility of

removing larger CNV, whilst preserving the overlying retina, it increases the risk of more subretinal bleeding and scarring, therefore potentially damaging more photoreceptors. Visual recovery subsequent to CNV excision is usually poor in patients with AMD[99].

As explained previously, it is possible that a successful transplantation is determined by the strength of adhesion between the transplant and the BM. Nevertheless, BM varies between individuals and thus its properties are difficult to predict. This will have an effect on adhesion. A study has also demonstrated that different thickness of BM has different effects on the cell population. Cell attachment is better on the more superficial level than the deeper level[100] of the BM. The cell's donor age is also important in calculating the outcome of a procedure. Results have shown that foetal cells are more likely to survive than an aged cell, when repopulating the BM[77].

The fate of the cells, their phenotype and their differentiated state are also dependent on the nature of the substrate[101]. It has been documented in an experiment that the molecular content of the macular is different than those in the periphery. The elastic lamina, which comprises of elastin and collagen laminae, is six times thinner and two to five times more abundant in the macula than in the periphery[102]. These structural properties of the macula elastic lamina correspond spatially to the distribution of macular lesions associated with AMD and thus may help to explain why the macula is more susceptible to degenerative events that occur in this disease.

As described previously, several studies show that injected RPE and IPE in suspension fail to fully differentiate into the required phenotype. They tend to dedifferentiate: losing their cuboidal shape and becoming more fibroblast-like in appearance, disperse and migrate resulting in contraction and distortion of the macular. This condition is known as proliferative vitreoretinopathy (PVR) and poses a challenge in transplantation. PVR may cause overwhelming visual loss. It is imperative to understand the state of dedifferentiation. It is because the RPE cells are transplanted into a non-immunological privileged site in the eye, which then adopts a fibroblast-like morphology. To obtain viable cells as a monolayer on BM, the establishment and maintenance of differentiated cell is crucial [75]. Many factors such as adhesive proteins produced by the extracellular matrix (collagen, laminin, fibronectin), anti-adhesive proteins such as thrombospondin I and osteonectin and some growth factors, tend to be distributed equally within the dedifferentiated cells in the PVR membrane.

A study [75] has been carried out and demonstrated that a particular cell will express their phenotype differently, depending on where it was implanted. This is probably because of the interaction of the cell and surface receptors, such as integrins or matrix metalloproteinases, which differ in different tissues.

1.4.3.1 Growing cells on biological tissues

Some groups used biological tissues as substrates for BM. Biological tissue is said to be an ideal choice of material as they have the mechanical properties of the tissue they are replacing. Biological tissue, especially obtained from the same patient (autologous graft) can reduce the risk of immunological responses such as rejections as well as viral infections[103]. Examples of biological substrates used in the treatment of AMD are collagen[104], Descemet membrane[105], anterior lens capsule[106] and amniotic membrane[107].

Collagen has the added benefit of low antigenicity (thus low immunological reactions), being easily degradable *in vivo* (so acting as a temporary scaffold for cells), easily manufactured as a very thin sheet (so will not disturb the anatomy of the subretinal space), commercially available (type 1 collagen are available in foam, sheet and gel template) and has been extensively investigated and obtained approval for clinical and biomedical uses. However, collagen has limitations such as contraction, which reduces gel permeability and thus can have the ability to limit the size of tissue-engineering construct. A study carried out by Thumann et al.[104] found that RPE and IPE derived from porcine tissue formed an intact monolayer when they were cultured on the collagen.

Nevertheless, most biological material poses problems, such as being difficult to handle, degradable, causing tissue response (such as inflammation) or causing

dispersion of RPE monolayer. Potentially, there could also be a problem with the commercial availability and having a limited shelf life.

1.4.3.2 Growing cells on artificial membranes

Synthetic membranes, as the name implies can be manufactured to have the desired properties. As current trends in technologies change, developments of biomaterials move from finding a bio-inert material (so as to cause minimal interaction or reaction in the body), to finding a material with bio-activity (a material with biologically interactive components to elicit a controlled reaction in tissues). The current trend is bio-interactive i.e. to regenerate functional tissue that is integrated and which can stimulate a specific cell response at a molecular level[108].

Polymers have some advantages as a choice for an artificial membrane compared to biological tissue. The chemical properties of polymers can be tailored for a specific requirement. The chemical properties can be designed so they will influence cell adhesion and growth, whereas their physical properties can dictate their method of transplantation.

1.4.3.2.1 Degradable polymers

There are many types of polymer membranes currently under investigation to be used as a basement membrane in the therapy of AMD. Some use degradable polymers in gel-form, as a method of cellular delivery, which is completely degradable between 3 to 6 months. A biodegradable scaffold will degrade or be metabolized, leaving eventually a desired vital organ or tissue. However, we hypothesised, that using biodegradable material in patients, whose BM is already damaged by AMD, will leave cells without protection, after the polymer has degraded.

Examples of degradable polymers used included Poly(lactic-co-glycolic acid) PLGA and Poly-L-Lactide Acid (PLLA) polymers, which found epithelial cellular growth[109]. Another group chose a method called in situ gelation of polymer, in which the polymer is applied as a suspension, in the hope that it will self-assemble to a monolayer. Polymers used included PEO (polyethylene oxide), PVA (polyvinyl alcohol), PDLLA (polyDLlactide), PAAc (polyacrylic acid), and PHPMA (polyhydroxy propyl methacrylamide), which were modified to include RGD sequence modification to enhance cell growth. The RGD peptide were included as part of the repeat unit in the polymeric backbone[110].

Problems with this approach are the cellular viability of the cells that sit on the substrate, especially when the original BM that is already damaged in AMD. In addition, degradable polymer will produce degradative products, which tend to

induce an inflammatory response[111] that may eventually lead to damage. The rate of degradation is also difficult to control, as demonstrated in an *in vitro* experiment using PLGA[112].

1.4.3.2.2 Non-degradable polymers

Another approach is by pre-culturing cellular monolayers on stable non-degradable polymer membranes. Mechanical strength and strong anchoring of the polymer membrane to the surface of the BM might be important, so that it will not fold during later processing. Non-degradable polymers have the advantage over the degradable polymers, in that they will act as a permanent BM's prosthesis, reducing the risk of accumulated degradable wastes, which contribute to the disease in the first instance. The non-degradable substrate will hopefully remain functional throughout the life of the patient.

Examples of these are Polydimethyl siloxane (PDMS)[113], expanded polytetrafluroethylene (ePTFE)[114] and polyurethane (PU)[115]. On some of these, the surfaces were treated to increase their wettability to improve cell adhesion and spreading.

Polydimethyl siloxane (PDMS) or silicone rubber has been widely used for implantation in the eye as in intra-ocular lens. This is due to its hydrophobic character. Methyl groups attached to the polymer backbone limit cell adhesion

and will reduce the incidence of opacification. However, to be used in this application, a different surface property of the material is needed, therefore it needs to be modified. Simple gas plasma treatments followed by a post-treatment storage in distilled water, results in a reduction in the surface concentration of methyl groups and the integration of surface polar groups, and this improved the hydrophilicity of the surface. Krishna et al have carried out an investigation regarding the use of PDMS as a candidate material for membrane substrate[113]. The PDMS surfaces were modified (by air and ammonia gas plasma) to increase the wettability. This enhances cell growth and results in a monolayer of healthy differentiated RPE cells on PDMS substrate.

Another example of non-degradable polymer used in cell transplantation for AMD was ePTFE (or commonly known as Goretex®). It has been widely used in medical applications such as vascular grafts, stent covering material and as cardiovascular patches. ePTFE is however a hydrophobic material, and so does not support cell attachment and spreading. Several studies have been carried out with surface modified ePTFE, such as pre-treatment with RGD sequence peptide[116] or plasma treated with amine or amides[117], which were demonstrated to improve cell adhesion.

1.4.4 Methods of transplantation

It is important to deliver the substrate-cells complex as an intact monolayer into the sub-retina area. For this reason, many studies have been carried out to find a suitable transplant method. Injuring the RPE-choroid complex could result in PVR[118] and the delicate procedure needs a very experienced vitreoretinal surgeon. However, the feasibility of RPE transplantation has been demonstrated by a full thickness RPE-choroid patch graft transplant, either by removal from the periphery, or on the macula itself[119, 120, 121].

Transplantation of cells, as a suspension, appears to be the easiest route, but without the extracellular matrix as a scaffold for the cells, they may fail to adhere, survive or function[122]. Previous investigations have demonstrated that cells, preformed as a monolayer are essential, as RPE cells will not expand once *in vivo*[123]. Others have attempted to transplant a sheet of RPE, but this proved to be a difficult process due to the fragile nature of RPE[124]. Because of this, we are planning to expand cells *in vitro* pre-cultured on our chosen substrate.

The trans-scleral approach has been investigated by many[125-126]. It has been suggested that with some modification, the method could be the answer to deliver the intact cell-monolayer-substrate complex underneath the macula, thus reducing the risk of bleeding from the choroid. Detachment of the neural retina can be controlled by Ca- and Mg-free balanced salt solution (BSS) infusion or temporarily held in place by gas or silicone tamponade[127].

The aim of the proposed research is to create a substrate on which cells can be cultured and expanded *in vitro*. The substrate will be designed such that the cells cultured will form a viable differentiated monolayer, prior to insertion under the macula. In the proposed project, the substrate used will be pliable polyurethane membranes (B9®, produced by Biomer Technology Ltd.) and the growth condition of both RPE and IPE cells will be optimised. This will lead to a surgical procedure to transplant a monolayer of epithelial cells under the macula.

1.5 Polyurethanes

1.5.1 Structures, chemical and physical properties

Polyurethane (PU) is a generic name of any polymers, which are joined by a urethane link — **NH-(C=O)-O** in the chain. This urethane group may only be in a small quantity in a large urethane copolymers. The linear chain can be produced by either reacting a bischloroformate with a diamine or by reacting diisocyanate with a diol.

1.5.2 Urethane copolymers

Polyurethane polymers are formed via a step-growth polymerization by reacting diisocyanate (hard segment) and macroglycol (soft segment) in the presence of a catalyst. The hard segment, is highly polar is formed by reaction of diisocyanate with a low molecular weight diol or diamine chain extenders. With a high glass transition temperature (T_g), the hard segments are rigid and glassy. The soft segment is derived from a hydroxyl-terminated aliphatic polyester, polyether or polyalkene. It is flexible and rubbery due to the low T_g.

The property of a PU can be greatly varied by choosing a different group of the monomers or by adding chain extenders during the synthesis. In addition, varying the proportion of the two components will alter the PU's mechanical property: strain, initial modulus and tensile strength. PU with a high elastomeric behaviour demonstrated hysteresis when subjected to stretching, due to the

restructuring between the hard and the soft segment regions. It was reported that the hard segment crystallisation caused increased hysteresis and tensile strength[128]. It was also claimed that under ultimate tensile stress, PU undergo heterogeneous fracture as the macroscopic stress concentration sites accumulates. At the same time, the high-modulus hard segment can reduce this by undergoing deformation or internal structural reorganization[129]. The required properties of PU were usually controlled by the introduction of additives (antioxidants, stabilizers, plasticizers and opacifiers) or by having a different polymer orientation.

1.5.3 Biomedical PU

PU has been used in medicine since the early 1960s in bone fixation and as coatings to cardiovascular implants. However, in the early days, PU has been associated with a poor outcome, mainly due to premature degradation, which was sometimes accompanied by an infection and scarring. Recent developments of PU research have changed this. PU was implanted successfully as blood sacs in humans in the early 1980s. Current medical applications of PU include cardiovascular devices, artificial organs, tissue replacement and augmentation and performance enhancing coatings. Some PUs were used for short term implants (less than 30 days)[130].

The wide possibilities of modifying its bulk or surface properties have made it feasible for the attachment of desirable biologically active species or bio-

recognizable groups. Many attempts have been made to increase its wettability to improve cell adhesion on its surface. *In situ* polymerized, cross-linked systems could extend this biodurability even further[131].

Surface structure of an implant is an important criterion for dictating cells' response. A rough textured surface enhanced cell adhesion. Medical PU in textured forms has performed positively, when in contact with soft tissue and blood. Porous structures have been used by a different application: pore sizes less than 1μm will allow collagen in growth but not fibroblast, less than 5μm show little fibrous in growth, porosities of above 200μm will promote vascularisation. However, too large a pore not filled with tissues can lead to infection[128].

Surface charge is known to affect cell adhesion. Cell will be attracted to a positively charged surface. The surface charge of PU can be changed by grafting with either RGD sequence[132], treated with gas plasma[133], modified with carbonate linkage (polycarbonate)[134] or with silicones[135]. Hydrophilic wettable surface, pre-coating PU with extracellular matrix (ECM) proteins, binding prostaglandins or heparin-like materials on the PU surfaces will also increase cell adhesion[128].

PU, used as a biomedical implant, must then fulfil a certain criteria: the ability to be reproducibly manufactured as pure materials, the ability to withstand changes and degradations, to have the appropriate chemical, physical and

mechanical properties and can withstand sterilisation without changes in the properties. PU has been often associated with properties such as elasticity, durability, resistance to fatigue stress and does not elicit known immune response when implanted *in vivo*.

1.5.4 Commercially manufactured PU

There were some medical grade commercially available PUs. *Biomer®* (Ethicon Inc.) produced various blood-contacting devices such as bladders, catheters, heart valves and ventricular assist pumps. Biomer® was produced by either dip-coating, solution casting, spraying or by precipitation from a dilute solution. *Cardiothane-51®* (Kontron Inc.) is used in intra-aortic balloons, catheters, artificial hearts and tubings. Cardiothane® was processed by solution casting, dip-coating, spraying or glueing. *Pellethane®* (Dow Chemical) was used as insulation in placing leads in heart pacemakers' connectors, blood bags and endotracheal tubings. Pellethane® is supplied in a granular form in injection moulding and as extrusion grades.

1.6 PU production by Biomer Technology Ltd.: B9™

B9™ (series A) produced by Biomer Technology Ltd. has a wide variety of properties[136]. By altering the proportion of hard and soft segments, B9™ series ranging from Z1A1 (softest) to Z11A1 (stiffest) and generally have high

durability. The B9™ series has low temperature flexibility, wide range of hardness numbers, hydrolytic stability, solvent resistant, low extractables and are compatible with a wide range of fillers. The manufacturer claimed that B9™ is compliant with USP Class VI (FDA approval standard for compounds made from ingredients with clear histories of biocompatibility) and ISO 10993 for biocompatibility (i.e. international standards used to evaluate biocompatibility of a medical device prior to a clinical study).

The hard segments:

$$\{O\text{-}[\text{-}CH_2\text{-}CH_2\text{-}CH_2\text{-}CH_2\text{-}O\ \text{–}CO\text{-}NH\text{-}R\text{-}NH\text{-}CO\text{-}O\text{-}CH_2\text{-}CH_2\text{-}CH_2\text{-}CH_2\text{-}]\text{-}O\}B$$

The soft segments:

$$\{\sim CO\text{-}NH\text{-}R\text{-}NH\text{-}CO\text{-}[\text{-}O\text{-}CH_2\text{-}CH_2\text{-}CH_2\text{-}CH_2\text{-}O\text{-}]n\text{-}\ CO\text{-}NH\text{-}R\text{-}NH\text{-}CO\sim\}A$$

The polymer properties can be adjusted by controlling the value of n, the nature of R and the ratio of A to B.

1.7 Research Questions and Aims

The aim of the proposed research is to create a substrate on which cells can be cultured (*in vitro*). The substrate will be designed to a certain thickness with required porosities. In the case of the proposed project, the substrate used will be pliable polyurethane membranes (B9™, produced by Biomer Technology Ltd.).

This raises specific research questions:

1. Can polyurethane (PU) support attachment, proliferation and growth of epithelial cells?
2. Can PU be manufactured into a porous substrate? Can the structure be made to closely resemble the native Bruch's membrane?
3. Can the primary pigmented epithelial cells (RPE and IPE) be harvested and expanded *in vitro*? Can their growth be controlled?
4. Can IPE behave similarly to RPE in its morphologies and functions?
5. Can the primary pigmented epithelial cells (RPE and IPE) be grown on the porous PU? Can they then maintain their phenotype, cellular expressions and normal functions when grown on these surfaces?

Primary RPE and IPE cells will be grown onto the substrate. Techniques of harvesting primary RPE and IPE cells obtained from bovine eyes will be explored and their optimum growth conditions will be investigated. They will also be tested to see if they would exercise similar functions as the replaced RPE. The

cells cultured will form a viable monolayer prior to insertion under the macula for use in a novel surgical procedure to treat AMD.

2 CHAPTER TWO: MATERIALS AND METHODS

2.1 Substrates

The Polyurethanes (PU) supplied by Biomer Technology Ltd. was either in pellet, granules or already made into thin films. They can be dissolved into solution form by mixing it with di-methyl-acetamide (DMAC) or di-methyl-formamide (DMF).

2.1.1 Manufacturing PU as a film

PU as a film was supplied by Biomer. It was made by adding a thin layer of the solution into a small glass of Petri dish and placed into an oven. The films were used in many of the preliminary experiments to assess their properties and behaviour with cells, as they were easy to handle and worked well with fluorescent staining.

2.1.2 Manufacturing porous PU

It is important for the substrate to be porous. There were several methods used to manufacture porous PU.

2.1.2.1 Freeze drying

The freeze drying process was carried out in the department of Chemistry, University of Liverpool. It is a technique used to remove residual solvent from a material, thus leaving voids, which created porosity in the material. The solvent

used with the PU was dimethylacetamide (DMAC); an organic compound with the formula $CH_3C(O)N(CH_3)_2$. It is a colourless, water miscible liquid with a high boiling point. It was used to dissolve PU at different at concentrations (weight/weight).

In the first part of the experiment, different concentrations of PU solution; 5%, 10%, 15% and 20% were used and 11%, 12%, 13% and 14% concentrations were used in the second part of the experiment. The mixtures were poured onto the surface of a small glass beaker, just enough to cover all the beaker's surface, and quickly immersed into liquid nitrogen as in **Figure 2-1** before being transferred into a freeze dryer.

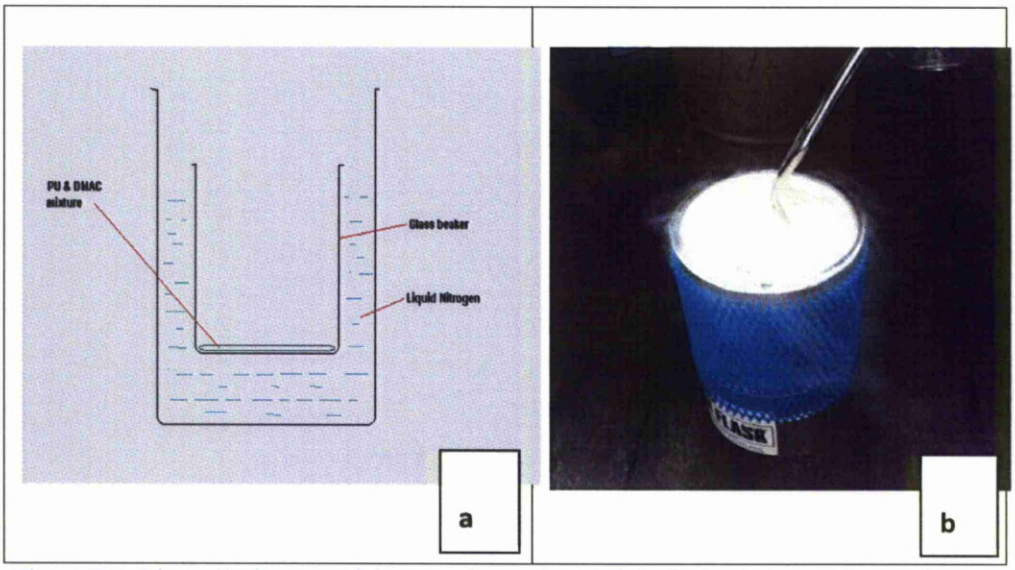

Figure 2-1: Schematic diagram of the experimental setup (a). The beaker was immersed in liquid nitrogen before being transferred into the freeze-drying machine (b).

Next, the beaker was transferred into a freeze-drying machine and the temperature was set at -22.4 °C (the melting point of DMAC is -20 °C). The samples were left in the freeze-dryer for approximately 48 hours to completely dry. The samples were then examined with light microscopy and SEM.

2.1.2.2 Electro-spinning

The PU formed via the electrospinning (Z3A1) procedure was supplied by our collaborator in the University of Strathclyde. In this procedure, Z3A1 in liquid form was drawn from a gauge of 22 needle at 0.2ml/hour and using electrical charge of 18kV, the fluid was charged, stretched and became a very thin thread, which was formed on a surface. The threads developed in a very thin mesh, creating crypts and holes, to provide the required porosities.

2.1.2.3 Oven drying

Similar to the process described in **section 2.1.1,** but this time the PU (Z3A1) in solvent mixture was dissolved at different concentration (5% and 10%) in DMAC (weight/weight). Confectioner's icing sugar (Silver Spoon) was sieved through a 70µm nylon cell strainer (BD Bioscience) and added to the solution at 2%, 5% and 10% by weight and stirred using a magnetic stirrer. After 5 minutes when there were no traces of sugar granules to be seen, the solutions were poured

into small glass bottles of 3.5cm diameter with just enough to cover the surface. In the second part of this experiment, 5% PU in DMAC plus 5% icing sugar were used but the effect of containers used to cast them was investigated. After mixing of sugar and stirring, the mixtures were poured into 3 different types of containers, a crystallising dish of 9.5 cm diameter, a small glass bottle of 3.5 cm diameter and a conical flask of 7.5 cm diameter to see which produced the best substrates. A tissue paper was secured on top of each container to control the rate of evaporation. The containers were left for 24 hours in a 70°C oven to dry. After the substrates formed, they were washed with distilled water 3 times and left to dry in a 50°C oven for 30 minutes.

2.1.2.4 Water precipitation

The PU in DMAC solution with icing sugar described in **section 2.1.2.3** was also tested using the water precipitation method. In this method, the solution was poured so that just enough was added to cover the container's surface and cold distilled water was slowly added to it. A substrate could be seen forming on the surface of the water.

2.2 Investigation of substrates' properties

2.2.1 Contact angle measurement

Contact angle measurement was carried out for investigation of surface adhesion property and wettability. It is the angle at which a liquid interface meets a solid surface and is an important indicator of how well the surface is likely to interact with live cells **(Figure 2-2).** Static contact angles of the samples (both film and porous) were measured using a DSA100 Krüss Drop Shape Analyser (Krüss GmbH). The sample was placed on a stage; 10µl water droplets were carefully dispensed on the sample whilst a video of the droplet was recorded at 25 frames per second for 20 seconds. The contact angle for each frame was calculated and the mean and standard deviation value was calculated using DSA3 software. For a non-porous PU, average readings were taken from the video recordings, but for a porous PU, 20 different sessions were measured and only the first 5 readings (the first 0.16 seconds) were taken as the water was absorbed and the mean values obtained.

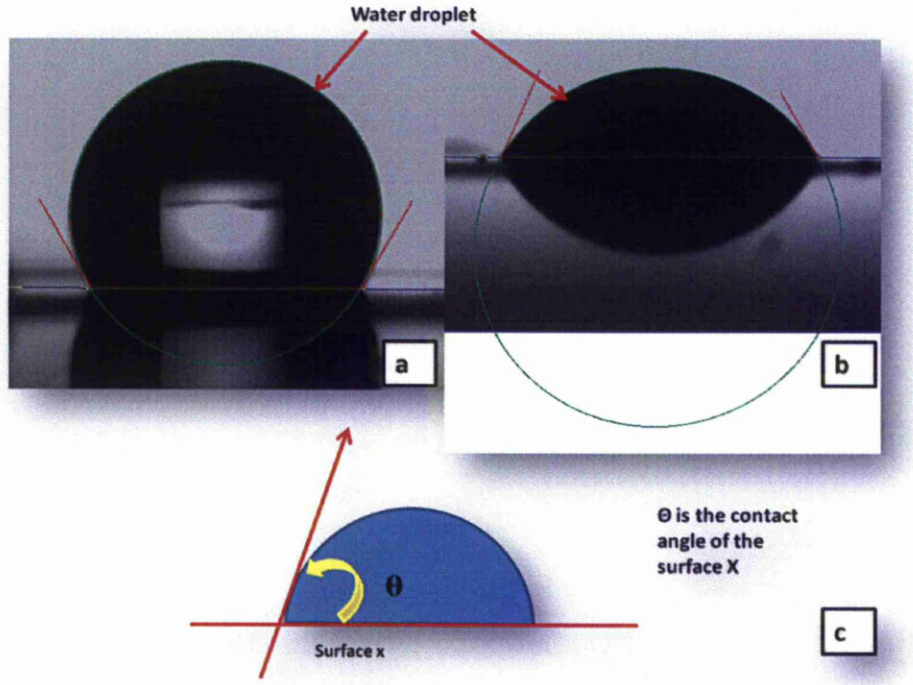

Figure 2-2: Measurement of a contact angle. It is the angle formed between the tangent of the water droplets; angle θ in (c) and the surface (substrate) it meets. The angle indicates the surface wettability, smaller angle as in (b) means higher wettability and vice versa.

2.2.2 Tensile testing

TST350 Tensile Stress testing system (Linkam Scientific Instrument Ltd.) was used to measure the tensile strength of the substrates. Average measurements of sample width of 5mm were taken before being loaded onto the 'jaws' of the tester. The jaws moved in opposite directions at constant speed of 50μms^{-1} (**Figure 2-3**) using a 20N load cell. Force measurements were automatically detected. The tester was stopped when the sample broke. All the readings were processed by Linksys32X-DV software. The tests were repeated 5 times with

Z3A1 film samples, 6 times with Z9A1 samples and 9 times with porous Z3A1 samples.

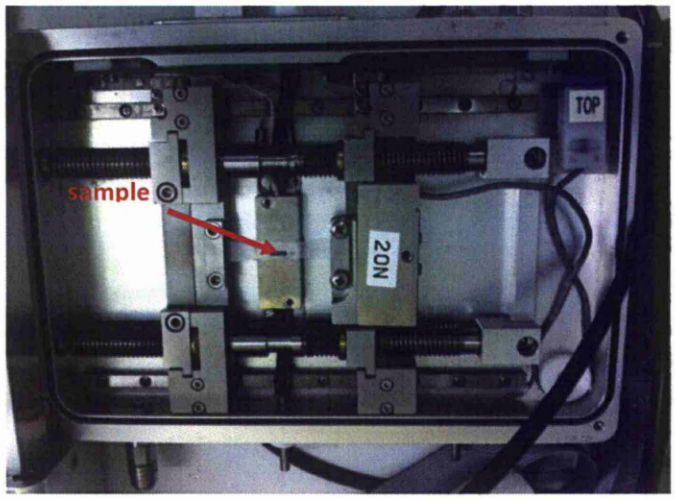

Figure 2-3: The tensile experimental set-up. The sample was held by two 'jaws' and the force were applied to stretch. The percentage strains were measured automatically by computer software.

2.3 Evaluation of the influence of ageing on the PU properties

This experiment was carried out to investigate the effect of ageing on the properties of PU. This is important for the material's shelf life. Different ages of Z3A1 (manufactured from the year 2005 to 2007) were evaluated in terms of their properties and effect on the cell growth. They were supplied in either pellets or granules form and were cast as films as in **section 2.1.1**. Cells were

grown onto the substrates and were investigated after they reached full confluence.

2.4 Cell cultures

All work with cell cultures was carried out in the sterile hood (class II microbiological hood) cleaned with 70% ethanol. Aseptic techniques were routinely in practise throughout the experiment. All the cells were cultured in the incubator at 37°C with 5% CO_2.

2.4.1 Media preparation

These are the solutions used throughout the experiments unless otherwise stated.

Table 2-1: Solutions used in media preparations.

Name	Abbrev.	Company	Cat. number
Dulbecco's Modified Eagle Medium	DMEM	Sigma-Aldrich	D5671
Minimum Essential Medium Eagle	MEM	Sigma-Aldrich	M2279
Nutrient Mixture F-10 Ham	F10	Sigma-Aldrich	N6013
Nutrient Mixture F-12 Ham	F12	Sigma-Aldrich	N4888
Penicillin Streptomycin *10 mg streptomycin per mL in 0.9% NaCl*	Pen-Strep	Sigma-Aldrich	P0781
L-Glutamine 200 mM	L-Glut	Sigma-Aldrich	G7513
Amphotericin B *250 µg/mL in deionized water*	Fungizone	Sigma-Aldrich	A2942
Trypsin-EDTA *10 ×, 5.0 g porcine trypsin and 2 g Ethylenediaminetetraacetic acid (EDTA)*	Trypsin	Sigma-Aldrich	T4174
Foetal Calf Serum	FCS	BioSera	S1900

2.4.1.1 Media preparation for ARPE-19

A mixture of 50:50 DMEM and F12 plus 1% L-glutamine, 1% Pen-Strep and 1% Amphotericin B supplemented with different percentages of FCS was used to culture ARPE-19 cells.

2.4.1.2 Media preparation for BRPE and BIPE

Culture media for both BRPE and BIPE was made from MEM with the addition of 1% L-glutamine, 1% Pen-Strep and 1% Amphotericin B supplemented with different percentages of FCS.

2.4.1.3 Media preparation for HIPE

The culture media was made of F-12 along with 1% L-glutamine, 1% Pen-Strep and 1% Amphotericin B supplemented with different percentages of FCS for HIPE cultures.

2.4.1.4 Media preparation for HRPE

The media was made of F-10 with the addition of 1% L-Glutamine, 1% Pen-Strep, 1% Amphotericin B supplemented different percentages of FCS for HRPE cultures.

2.4.2 Cell sources

Cells were obtained from frozen stock, stored in liquid nitrogen, or harvested freshly from cow's eyes from a local abattoir. Primary bovine cells were harvested from the eyes within 24 hours of death. Primary human cells were obtained from donor eyes within 72 hours of death. Human cell line (ARPE-19) was obtained from frozen and was previously purchased from American Type Culture Collection, Manassas, VA, USA.

2.4.3 Cell harvesting

Bovine eyes were transported on ice and stored in a transport medium; CO_2-independent medium (Gibco, Invitrogen) containing 1% Penicillin, 1% Streotomycin, 1% Amphotericin B and supplemented with 5% FBS.

Tissue dissection and processing were carried out under sterile conditions, in a laminar airflow hood. The method used for isolation of RPE and IPE cells is a combination of mechanical dissection and enzyme digestion. Eyes were washed in cold solution, containing 2% Pen-Strep and 2% Amphotericin B, excess muscles were cleaned-off, and then transferred into Dulbeccos Phosphate Buffered Saline (DPBS, Invitrogen) with antibiotic solution for 15 minutes at 4°C. They were cut circumferentially 1 to 2 mm posterior of the ora serrata. The two parts were used for harvest of different cell types. The anterior section of the eye was used to harvest BIPE and the posterior section was used to harvest BRPE as in **Figure 2-4.**

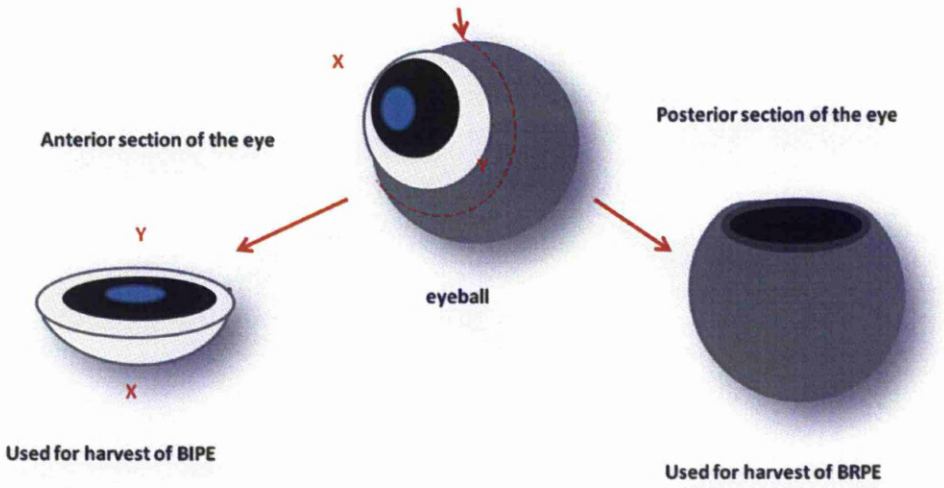

Figure 2-4: The eyeball was cut 1 to 2 mm posterior of the orra serrata, the anterior section is used for harvest of BIPE and the posterior section is used for harvest of BRPE.

2.4.3.1 Methods of harvesting BRPE

There were several methods used for the harvest of BRPE.

2.4.3.1.1 BRPE: Method I

After anterior segment detachment, the vitreous and neural retinas were carefully removed, without touching the RPE surface. The area of the retina over the optic nerve stump was cut-off (to minimise contamination from the neuroretina). The explant pieces were placed apical side downwards and a brass cloning ring was placed on their basal side. 20% Trypsin-EDTA were placed inside the cloning rings and was left to incubate at 37°C for 20 minutes (see **Figure 2-5**). After that, the solutions containing enzyme and loose cells were

collected by pipette, proliferation media as in **2.4.1.2** containing 20% FCS was added to reverse the enzyme reaction. The mixtures were centrifuged (1000 rpm/180g for 5 minutes), re-suspended in proliferation media and seeded on the desired surface.

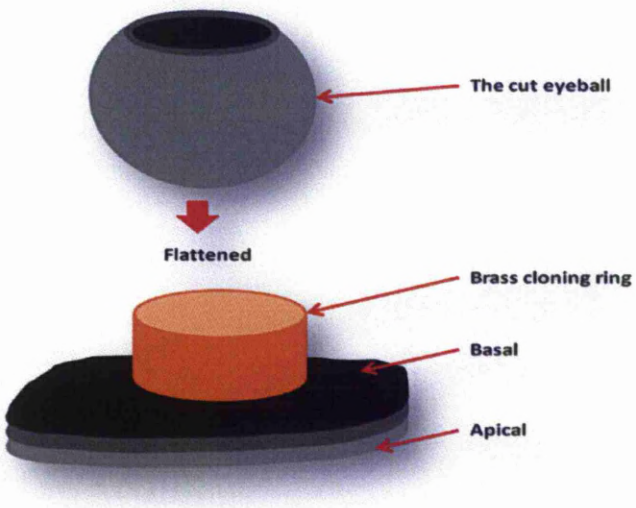

Figure 2-5: One of the methods used to harvest BRPE. After the eyeball has been cut, it was flattened and placed apical side down; cloning ring was placed on its basal surface and filled with trypsin to loosen-up the RPE cells.

2.4.3.1.2 BRPE: Method II

The second method is adapted from Zhu et al.[137]. After the separation from the anterior segments, the RPE layer was gently peeled and stuck to the bottom of the culture dish with apical surface downwards. A layer of cells would grow

from the explants, by culturing the cells in culturing medium as in section **2.4.1.2**.

2.4.3.1.3 BRPE: Method III

This method was adapted from Tezel[138] and Ho[139]. After the separation of the anterior segments, the eyecup was flattened in a tissue culture dish with the apical surface facing up. 0.25% of EDTA (Sigma-Aldrich) was added to cover the apical surface of the RPE and this was incubated for 12 minutes. The EDTA was carefully pipetted off without touching the surface of the eye. 12% gelatine solution was prepared by heating (40°C) gelatine powder (Sigma-Aldrich) in distilled water. This gelatine solution was then coated thinly on the apical surface and allowed to solidify at 4°C for 10 minutes. A microsurgical blade was later used to cut off a circular piece of the RPE layer up to, but not through the Bruch's membrane-choroid and with the help of a micro-spatula the layer was peeled off. The layer was transferred into a culture dish, media as in **section 2.4.1.2** was added and culturing process resumed.

2.4.3.1.4 BRPE: Method IV

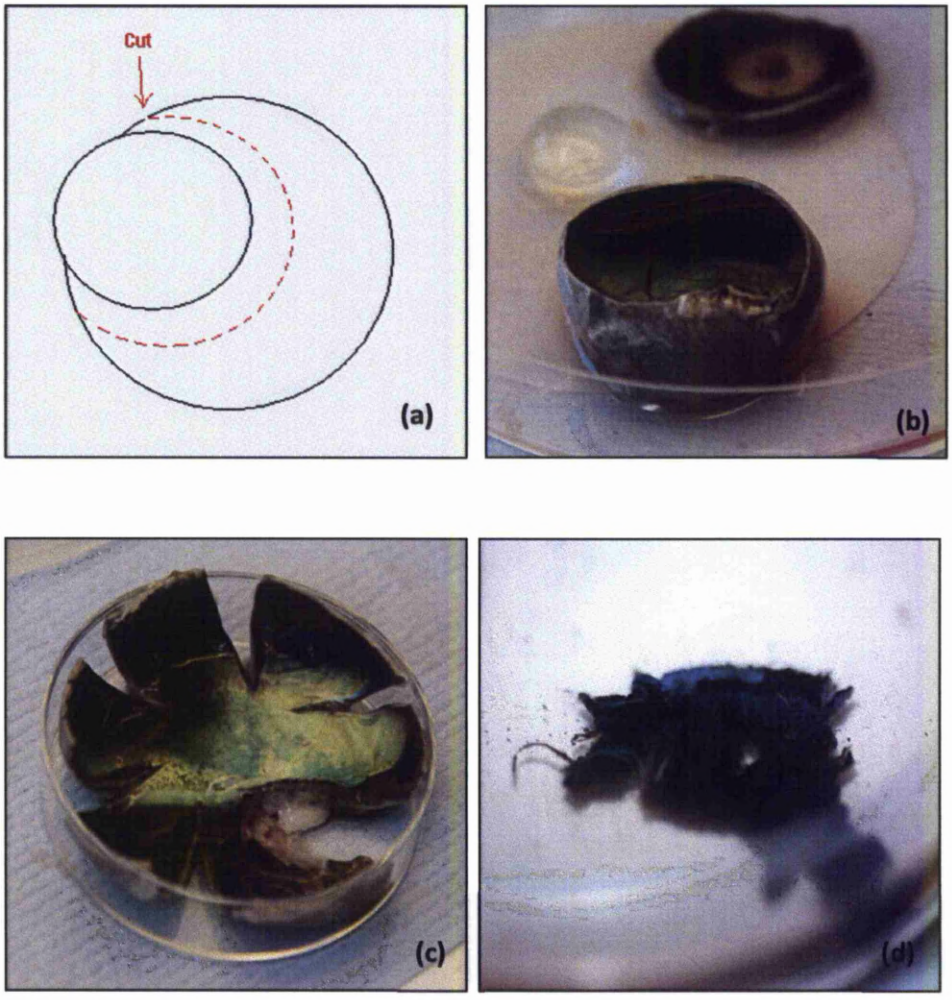

Figure 2-6: After the separation from the anterior segment (a & b), the eye-cup was cut into a 'flower' shape in a *petri dish* (c). Collagenase type IV was used to separate BRPE cells from its matrix (d).

In this method, after anterior segment detachment, see **Figure 2-6 (a)**, the vitreous and neural retinas were carefully removed without touching the RPE surface **(b)**. The remaining eyecup was cut open into a 'flower' shape and

transferred into a small *petri dish* **(c)**. The eye was then immersed in 0.5 mg/mL Collagenase type IV (Worthington Biochemical) for 15 minutes at 37°C. The enzyme reaction was reversed by rinsing the eye in serum-free MEM followed by incubation in the same media for 20 minutes at 37°C. Afterwards, the eye was completely immersed into a *petri dish* containing pre-warmed CO_2-independent media. The RPE-choroid complexes were separated from the sclera and were moved into a new dish containing CO_2-independent medium **(d)**. Large continuous sheets of RPE can be harvested by scraping the surface of the tissue using a silicone instrument **Figure 2-7**. The loose sheet and cells were aspirated using a fire-polished Pasteur pipette into a 15mL tubes containing proliferation medium as in **2.4.1.2**.

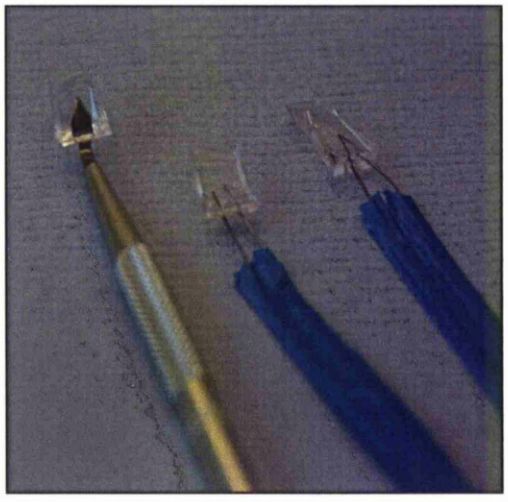

Figure 2-7: Tools used to scrape the RPE off the retinal surface.

The collected cells were then centrifuged (1000rpm/180g for 5 minutes), re-suspended in the culture media and seeded onto the desired surface.

2.4.3.2 Method of harvesting BIPE

After the detachment from the posterior section of the eye as in **Figure 2-4,** the anterior parts of the eye were placed posterior side up and placed in a *Petri* dish. One of the methods below was used to harvest BIPE.

2.4.3.2.1 BIPE: Method I

This method was obtained from Hu et al.[140]. The iris was grasped at its root with forceps and excised with scissors. It was then placed in a culture dish with its posterior surface upward and washed with the antibiotic solution. The iris was immersed in Trypsin-EDTA and placed inside an incubator at 37°C. After 1 hour, the IPE was gently separated from its stroma by micro-dissection using a pair of fine forceps and a fire-polished pasture pipette tip. The collected IPE was centrifuged (1000rpm/180g for 5 minutes) before being re-suspended in culture medium as in **section 2.4.1.2** and seeded onto the required surface.

2.4.3.2.2 BIPE: Method II

After the removal of the posterior part of the retina, the eye was placed posterior side up as in **Figure 2-8**. The lens and the aqueous humour were carefully removed **(a)**. The iris was carefully cut using iris scissors and placed in a

culture dish with its posterior side facing upwards. Small plastic cloning rings immersed in sterile medical grease (Dow Corning® High Vacuum Grease, Belgium) were placed on the posterior side of the iris, paying particular attention to avoid touching the outer side of the iris. 20% Trypsin-EDTA was placed inside the cloning rings and was left to incubate at 37°C for 10 minutes **(b)**.

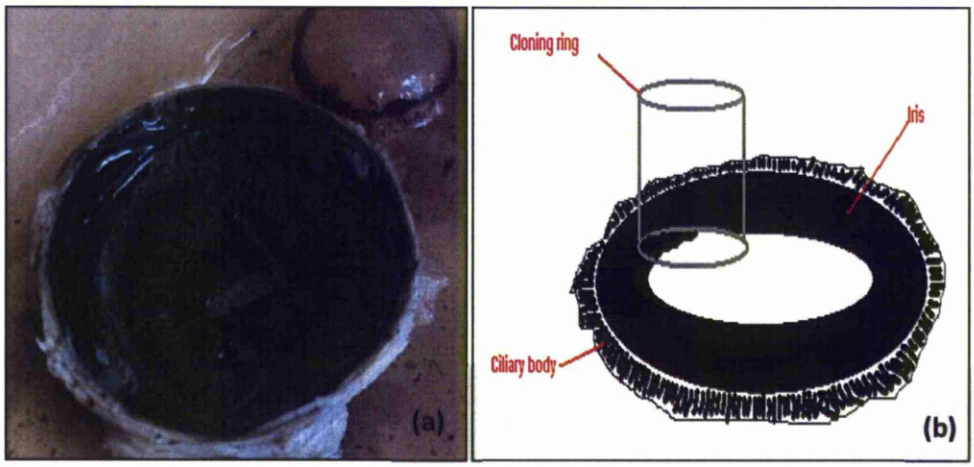

Figure 2-8: a method of harvesting IPE. After anterior segment separation, the iris was positioned posterior side up (a), a cloning ring was previously dipped in grease and placed on top on the iris. Trypsin was inserted into the cloning ring and the IPE-containing liquid was then harvested.

After the incubation, isolated cells were collected by pipette. The cell suspensions were centrifuged (1000rpm/180g for 5 minutes), re-suspended in culture medium as in **section 2.4.1.2** and seeded onto the required surface.

2.4.4 Cell Feeding

The cells were fed twice weekly by removing approximately 70% of the media by pipette and replacing it with pre-warmed (at 37°C) fresh media solution. The other remaining media left was important, as it might have contained vital products such as growth factors produced by the cells. The flasks or plates were frequently inspected under a light microscope to check for any abnormal growth or infections.

2.4.5 Cell Passage

When the cells reached near confluency, they were split in a ratio of 1:3. To do this, all the media in the flasks was discarded by pipette into bleach solution. The flasks were gently washed with phosphate buffered saline (PBS) twice, after which, a mixture of 10% Trypsin-EDTA in PBS (vol:vol) was added to loosen cells from the culture flask and stored in the incubator at 37°C for 5 minutes. The flasks were then checked under the microscope to ensure most cells were loosened. Next, 10ml of serum-containing medium was added to the cells to quench the trypsin reaction and the mixture was transferred into a universal tube, which was centrifuged at 1000 RPM for 5 minutes. The supernatant was discarded and the cell pellet broken by a continuous drawing and dispensing action, by mixing it in 1ml of media with micropipette. If needed, cell counting or freezing procedure was carried out at this stage. Then, another 8ml was

added to the cell mixtures, which were then divided equally into three flasks with 22ml of fresh media solution (make-up total 25ml in a flask). Primary cells are cell passage 0 as they were harvested directly from fresh tissues.

2.4.6 Cell storage/freezing

Surplus cells (especially ARPE-19) were frequently stored by freezing them in liquid nitrogen as stock. To store cells, the procedures as in cell splitting **2.4.5** were carried out as above. The cell pellet suspended in 900μL of their medium was transferred into 1ml cryo-tubes positioned on ice. 100 μL of Cryopreservation medium, Dimethyl Sulphoxide (DMSO, Sigma) were gradually added to the mixture, whilst simultaneously swirling the cryo-tube, to ensure an even dispersal by inversion, after the addition of each aliquot. Afterwards, the cryo-tubes were placed in a freezer wheel and wound to the top. Every 45 minutes, the wheel is lowered, until by about 6 hours, the vial is completely immersed in the liquid nitrogen; they were subsequently removed from the wheel and placed in the liquid nitrogen. An alternative technique is via Mr Frosty isopropanol containers (Nalgene; Nalge Nunc International, Rochester, NY) and stored at -80°C (freezing rate -1°C/min) for 12 hours. These vials were then transferred into liquid nitrogen for the long-term storage of cryopreserved cells at -196°C.

2.4.7 Cell recovery/retrieval

DMSO had to be removed as soon as cells were thawed and this was carried out as outlined below. A universal tube containing 15ml media was kept warm, ready for the content of the cryo-vial, after it had defrosted. Defrosting of the cryo-tube was achieved by carefully inserting it in a water bath at 37°C, as the tube could explode, if nitrogen was trapped in them. Next, the content of the cryo-vial was emptied into the universal tube and centrifuged at 1000RPM for about 5 minutes. The supernatant was then discarded and the pellet was re-suspended in 2ml media mixture. The now newly suspended cells were transferred into a new flask and topped-up with an appropriate volume of media.

2.4.8 Trypan blue viability counting

Trypan blue was used to test the viability of the cells. This is based on the fact that the chromopore is negatively charged and does not interact with cell unless the membrane is damaged[141]. Thus, all the cells, which exclude the dye, are viable. This staining was usually carried out after the cells were re-suspended, after centrifugation, just before seeding of the cells on substrates or control surfaces. 0.4% Trypan blue (Sigma-Aldrich, T8154) stain (vol/vol in PBS) was prepared and added to the same amount of cells suspended in complete medium without serum to an approximate concentration of 1 x 10^5 cells per ml.

They were allowed to stand for 5 minutes at room temperature. The mixtures were pipetted into a haemocytometer for cell counting. They were later observed underneath a light microscope; non-viable cells were stained blue. The number of live cells was indicated by non-stained cells and used to adjust the cell seeding calculation.

2.5 Cell culture experiments on artificial substrates

2.5.1 Substrate preparation

There were several approaches for preparing substrates for the experiments depending on the investigations.

2.5.1.1 Holding substrates by adhesive technique

Substrates were first cut into the desired size, using scissors or a hole-punch. They were then attached to the surface of the well, using silicone adhesive produced by NuSil® (MED-1137, Silicone Technology Buckinghamshire). The surfaces were either a glass slide surrounded by reusable cell culture insert made of silicone; flexiPERM® micro12 (Greiner Bio-one Ltd.) as in **Figure 2-9 (a)**, 8-well polystryrene labteks (Lab-Tek® Chamber Slide System, Nalge Nunc

International), 24-well plates (Cellstar Greiner Bio-one) or 6-well plates (Cellstar Greiner Bio-one). The sizes of B9 were a circular shape of 6mm diameter for flexiPERM and labteks, circular shape of diameter of 16mm for 24-well plates and a circular shape of 26 mm diameter for 6-well plates. These sizes were determined for maximum coverage, so that the cells would be forced to grow on the substrates, rather than on the base of the well (both glass and polystyrene).

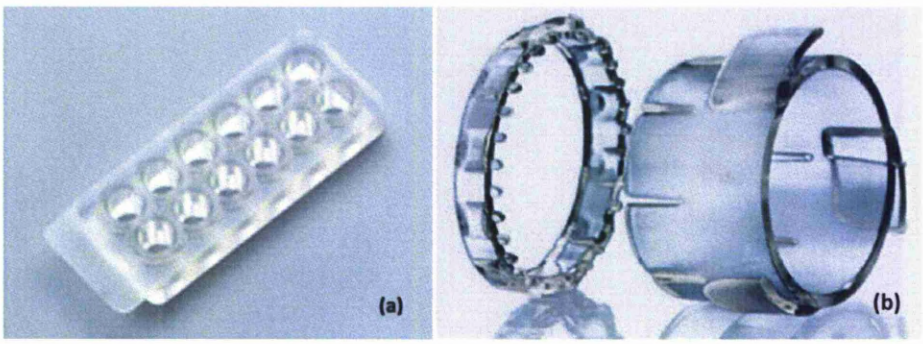

Figure 2-9: flexiPERM® (a) and CellCrown™ (b). The flexiPERM® was used as a cell culture chamber when stuck to a glass slide. The CellCrown™ holds the substrate in its place and is used in conjunction with a well-plate.

As the substrate material was very delicate to handle, the circular shape was cut by placing it between sheets of paper and acetate to be separated only when ready to be used. To stick it to the glass slide, a template of the flexiPERM® was used underneath so that it was placed exactly in the middle of flexiPERM®, to ensure no leakage. The polyurethane substrate was stuck down, so that the cells grew on the top surface of the substrate and not underneath it.

2.5.1.2 Holding material with culture inserts

In some experiments, substrates were held by using a cell culture insert made of medical grade polycarbonate polymer; CellCrown™ (Scaffdex Oy, Finland) as in **Figure 2-9 (b)**. The inserts ensured that the substrate would not float in the well plate at the same time holding it taut in its place. It was used with a 24-well plate.

After the substrates were fixed on the surface, they were sterilised using ultraviolet cross-linker (UVP CL1000, Ultra-Violet_Products Ltd.) at energy of 1500 watts for 5 minutes. Some chambers of the well were left without substrate to act as control.

2.5.2 Seeding of cells onto substrate

A seeding density experiment (see section **2.9.1**) suggested that seeding densities of $1x10^4$ cells per substrate in a 24-well plate (or $3.33x\ 10^3$ cells per mL) to be the most favourable for both substrates and controls for this experimental set-up. After the cells reached full confluency, procedures as in cell splitting/passage were performed and the cell count was recorded.

In these experimental settings, the maximum volume used for flexiPERM® was 100μl, for Lab-Tek® was 300μl, for 24-well plates was 1500μl and for 6-well plates was 3000μl. After performing a cell count, using a haemocytometer

(improved Neubauer haemocytometer), calculations were made, so that each well contained the required seeding densities. Cells were also seeded in the control well (i.e. without any substrate). Samples were maintained in the prescribed volume of culture media and incubated at 37°C with 5% CO_2. They were fed with fresh complete media twice a week and were regularly inspected for signs of cell death or infections. These procedures were performed until a specified time interval and staining methods as outlined below being executed.

2.6 Microscopy and staining methods

2.6.1 Cell or tissue fixing

Cells or tissues needed to be fixed, before any staining procedures were carried out. They were washed thrice with PBS, before the addition of fixative. The fixative used was 10% Neutral Buffered Formalin (NBF, 3.7% formaldehyde, Sigma) by immersing the cells or tissue for 10 minutes. After this, excess PBS was added to quench the NBF.

2.6.2 Staining tissues

Tissue staining was undertaken to compare with the staining of the cells *in vitro* and as a positive control. Tissue explants were fixed in 10% NBF and stained in a similar manner to the cells *in vitro*.

2.6.3 Methylene Blue

This staining is particularly useful to observe the morphology of the cells. For methylene blue staining preparation, cell culture media was removed. Afterwards, 100% (vol/vol) methanol was added to the sample for 5 minutes and the sample was covered to prevent evaporation of the alcohol. Then the methanol was discarded and 0.04% (vol/vol) methylene blue was added to cover the sample for approximately 1 minute. Subsequently, the sample was rinsed in copious amounts of distilled H_2O, until the water ran clear. The sample was then left to dry at room temperature.

2.6.4 Haemotoxylin Meyer

This staining is beneficial to demonstrate the nuclear and cytoplasmic structures within the cells. After fixation, enough haematoxylin Mayer's solution was pipetted into the well to cover the sample. The solution was left for 5 minutes,

before being removed, after which the sample was washed with distilled water, until the water ran clear. The samples were left to dry at room temperature.

2.6.5 F-actin staining

This staining is used for investigation of the distribution of cellular F-actin. Alexa Fluor® 488 Phalloidin solution (Invitrogen, A12379) was obtained by dissolving 1mg of the powder in 1.5ml Methanol (working concentration 1μg/ml). After fixation, the Phalloidin solution was diluted 1 in 40 (in fresh PBS) and used to cover the sample for 30 minutes at room temperature in total darkness (tin foil was used to cover the samples). This procedure can be coupled with other staining, before the samples are mounted.

2.6.6 Propidium Iodide (PI)

This nuclear staining is usually carried out in combination with Phalloidin antibody staining. After the procedure for Phalloidin staining was performed, the sample was again rinsed three times with PBS. Propidium Iodide (Sigma-Aldrich) solution was obtained by dissolving PI in water (1.0mg/ml). PI solution was added to a mixture of RNAse and PBS at the concentration of 1%: 10%: 89% respectively. RNAse (Sigma) comes in 100mg powder and was prepared as

10mg/ml in sterile ELGA water. The samples were covered in the solution at room temperature in darkness for 10 minutes.

2.6.7 Antibody staining

All antibodies staining in this study used a similar technique described below. The name of the primary and secondary antibodies are summarised in **Table 2-2**. After the fixing process, the samples were permabilised with 0.01% Triton X-100 (Sigma) for 5 minutes at 4°C, and were rinsed with PBS. After that, the samples were blocked with goat serum (10% in PBS) for 30 minutes to block non-specific binding sites. Next, the samples were treated with diluted (in 1% bovine serum albumin, BSA) primary antibody (see table) and left overnight at 4°C. After this, the samples were washed with wash buffer (99.9 ml PBS: 100 μl Tween 20, ICN Biomedicals) 3 times and left for 5 minutes at room temperature.

Diluted secondary antibody (see table) in 1% BSA was added to the samples and incubated at 37 °C for 1 hour. The samples were washed again with the wash buffer and permabilised with Triton. If needed, Phalloidin staining (diluted in 40 parts PBS) was added to the sample at this stage for 30 minutes before mounting. After washing with PBS, the samples were mounted in mounting medium to enable examination underneath fluorescent microscopy.

Table 2-2: Summary of primary and secondary antibodies used in the immunohistochemical staining with their respective dilutions.

Staining	Primary antibody	Secondary antibody	Negative control
Cytokeratin	Mouse anti-cytokeratin monoclonal IgG Sigma (1:100) F-2012	Rhodamine-conjugated goat to mouse IgG Sigma (1:500)	Mouse IgG 2a Dako (1:1000) X0943
Zona-Occluden-1 (ZO-1)	Rabbit anti-ZO1 monoclonal IgG Sigma (1:100) F-0511	Rhodamine-conjugated goat anti-rabbit IgG Sigma (1:500)	Rabbit IgG Dako (1:1000)
Rhodopsin	Mouse anti-Rhodopsin monoclonal IgG clone 1D4 (1:1000) Abcam5417	Goat anti-mouse IgG Alexa Fluor 488 (1:2000) A11029	Mouse IgG 2a Dako (1:1000) X0943

Cytokeratin staining was carried out to see if the cells express cytokeratin markers, to verify that all cells were of epithelial origin. Zona-Occluden-1 (ZO-1) staining was carried out to explore the formation of junctional protein at the borders of the pigmented cells. Rhodopsin is a marker to photoreceptor outer segments (POS); its staining was carried out to verify phagocytosis of POS.

2.6.8 DAPI nucleic acid staining

DAPI (4'-6-Diamidino-2-phenylindole) staining is usually performed after all other staining has been carried out and is placed on the substrates, just before mounting. DAPI binds with natural double-stranded DNA to form fluorescent complexes and so represent the nuclei of the cells on the substrate. DAPI used in our lab is incorporated with mounting medium from Vector Vectashield mounting medium for fluorescence.

2.6.9 Mounting

To mount the samples, there were two types of mountants used, DakoCytomation Fluorescent mounting medium (DakoCytomation). Coverslip was placed on top of the sample, clearing out any trapped air bubbles and sealed with nail varnish. Another type of mountant used was Vector (Vectashield) and it was incorporated with DAPI stains (**2.6.8**).

2.7 Microscopies

2.7.1 Phase contrast light microscopy

Phase contrast in light microscopy uses the principle of variations in phase and amplitude, when light travels through living tissues or cells. Cells or tissues examined using this method has the advantage of observing them without fixing or staining, which is usually carried out in a tissue culture environment. The microscope used was Nikon Diaphot microscope (Nikon Instruments, UK) and captured using Nikon D40 digital single lense reflex camera. Images were processed using CameraControl software (Nikon Inc.).

2.7.2 Fluorescence microscopy

This is similar in principle to the normal phase contrast microscopy above, but is specialised to capture fluorescent images. The fluorescent microscope used in the experiment was Reichert-Jung Polyvar (Vienna, Austria) using filter sets allowing the fluorophores' excitation/emission wavelengths of 488/525nm and 535/580nm. The microscope was attached to Roper Scientific Photometrics camera control systems. Images were processed via IomegaPro Plus ver4.5 software. The lens used for the experiments was a 25x objective lens with 1.2x zoom factor. The field of view was 255µm making the area imaged 48 769µm^2.

2.7.3 Scanning electron microscopy (SEM)

There were no pre-treatment needed for samples sent for SEM. Samples were placed on a stub and coated with a metal conductor (chromium) to allow electrical conductivity using Emitech K575X. SEM images were then obtained by placing the samples in the vacuum chamber of ZEISS 1550VP Field Emission SEM (Leo Electron Microscopy Ltd. Cambridge). The settings for the SEM: using secondary detector (SE2), which was situated underneath the objective lens. The working distance (WD) was between 4-30mm and operated at the working EHT of between 300V to 30kV. The images were scanned at scan speed 7 at 1024x768 pixels.

2.7.4 Confocal laser scanning microscopy

Confocal microscopy offers the advantage of controlling depth of field and the ability to gather serial optical sections from a thick or uneven specimen. Mounted specimens, investigated under the technique, were scanned using AxioPlan2 Zeiss LSM 510 (Carl Zeiss GmbH). Images were processed using Zeiss LSM Image browser ver3.4 software. Images were usually stacked images, unless otherwise stated. The laser beam from the microscope scans the image at any single plane, line-by-line and pixel-by-pixel. The usual settings for the microscope were frame size X512 Y512 with line step 1 and scan speed 8, dynamic range of 12 bit, using line mode and taking mean readings of 4

readings per line. There was several laser beams with different excitement of wavelengths: UV enterprise 402nm (for violet/blue excitation such as DAPI), Argon 488, 514nm (for green excitation such as FITC and 488 Alexa Fluor®), HeNe1 543nm (for red excitation such as Rhodamine or Propidium Iodide) or HeNe2 633nm (for far-red excitation such as Alexa Fluor® 633). The microscope was used in conjunction with 10X Plan Neo/0.3 NA objectives, 20X Plan-Apo/0.75 NA, 40X Plan-Neo NA Oil with DIC or 63X Plan-Apo/1.4 NA Oil with DIC.

2.8 Preliminary studies

2.8.1 Preliminary studies: Growing ARPE-19 on film membrane

Several sets of experiments were set up to determine if B9 supported growth of ARPE-19 cells. ARPE-19 were grown until reaching sub-confluence (as described in **section 2.4**) and were seeded onto substrates, which were stuck down into 8-well polystyrene labteks (as described in **section 2.5.1.1**). Cell numbers and cell cytoskeletal morphology were assessed at intervals of 1, 4 and 7 days by counting nuclei (stained with PI as in **2.6.6**) and F-actin staining by means of Phalloidin staining (as in **2.6.5**). Data from nuclei counts was used to construct a comparison graph.

2.8.2 Preliminary studies: Growing Bovine pigmented epithelial cells (BIPE, BRPE) on film membrane

Both BRPE and BIPE cells were grown and seeded onto the substrates and control (as outlined in **section 2.5.2**). They were fixed and stained (as described in **section 2.6**), using Phalloidin and PI staining at days 1, 4, 7 and 10. Nuclei counts were performed and the data was used to construct a comparison graph.

2.9 Optimisation of cell growth

2.9.1 Seeding densities experiment

In this experiment, optimum seeding densities for both primary cultures of BRPE and BIPE were investigated. Z3A1 and Z9A1 were cut out into a circular shape of diameter 6 mm across and were stuck down into 8-well Lab-teks® (Nalgene Nunc International), using tissue culture grade silicone adhesive (Nusil Silicone Technology) and some of the surface of the wells (permanox/polystyrene plastic) were left without any substrate as control. Both BRPE and BIPE cells were seeded polyurethanes (Z3A1 and Z9A1) surfaces and on the controls. Each well of Lab-teks® had a working surface of 0.8 cm^2 per well.

The numbers of cells used in seeding were $1x10^4$, $5x10^4$ and $1x10^5$; each well was topped-up with 300µl of media (making the seeding densities of $3.33x10^3$

cells/ml, $1.67x10^4$ cells/ml and $3.33x10^4$ cells/ml respectively). They were incubated at 37°C at 5% CO_2 and were fed once every three days (as described in **section 2.4**). They were then fixed and stained using Phalloidin and PI at day 1, 4 and 7.

2.9.2 Effect of varying serum concentrations and Retinoic Acid on BRPE and BIPE

In this experiment, both BRPE and BIPE cells were grown onto tissue culture base with varying serum concentration, so as to study the effect of serum concentration on their growth. To these, different amount of RA was added to evaluate the effect on their morphology.

Different amount of foetal calf serum (FCS) was added to the culture media (**2.4.1.2**) at concentration of 1%, 5%, 10% and 20%. The BRPE and BIPE cells were seeded at a density of $1x10^5$ cells per well in a 24-well plate, topped-up to 1.5 mL of the media. At day 4, a different amount of RA was added to the medium (as shown in **Figure 2-10**). Plates were incubated at 37°C at 5% CO_2 and were fed twice weekly. Cellular attachment and growth was observed using a contrast-phase microscope at days 4, 7 and 11, after which they reached confluence.

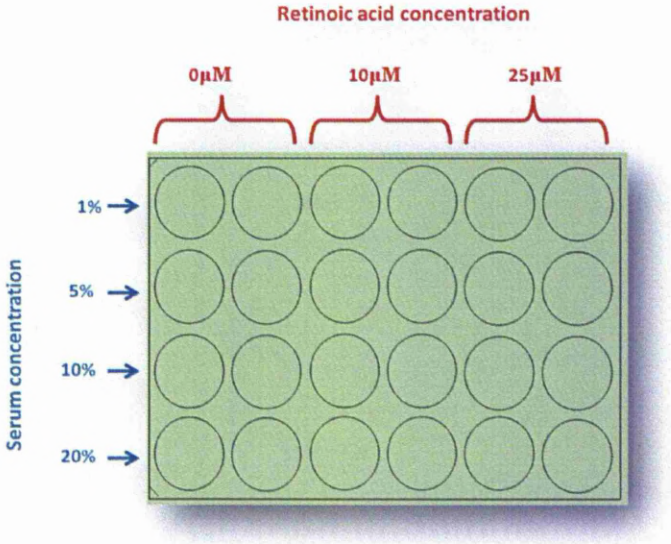

Figure 2-10: Experimental setup for serum concentration experiment. Different serum concentrations; 1%, 5%, 10% and 20%, and different amount of RA; 0µM, 10µM, and 25µM were initially used.

2.9.3 Effect of coating on material-adhesion assays with fibronectin and laminin

It has been suggested that the use of fibronectin and laminin enhances the adhesion of cells on a tissue culture surface *in vitro*[142]. 24-well tissue culture plates were used in this experiment to test out the effect of coating with fibronectin and laminin on cell adhesion. To coat the plate with fibronectin: a stock solution of bovine fibronectin (1030-FN, R&D Systems, Minneapolis, USA) was thawed on ice for several hours. Plates and tips were pre-chilled before use. 1mg/ml of fibronectin was made-up in PBS buffer and was added to the plates. They were incubated overnight in the fridge. Afterwards, the solution was aspirated and the plates were rinsed once with PBS. It was then blocked with 2% BSA for 1 hour at 37°C. Cells were then added to the plate as described in **section 2.5.2**.

To coat the plate with laminin: a stock solution of mouse laminin I (3400-010-01, R&D Systems, Minneapolis, USA) was thawed on ice for several hours, tips and plates were pre-chilled before use. 1mg/ml of laminin was prepared using cold serum-free medium and this was then transferred to the plates with just enough to cover the surface. The plates were stored in the fridge until needed. Just before use, the plates were left in the incubator at 37°C for 1 hour. Excess fluid was removed and culture media was used to rinse once, before seeding of cells. BRPE

and BIPE cells were seeded on well plates coated with fibronectin, laminin and control surfaces, and their morphologies and attachment were investigated using phase contrast microscopy.

2.9.4 Comparing effect of trypsin and collagenase IV enzyme

By applying method of harvesting BRPE cells (as described in **2.4.3.1.4**), the effect of using different enzymes was investigated. The cells were incubated with either 20% Trypsin-EDTA or in 0.5 mg/mL collagenase IV for 15 minutes at 37°C to loosen the cells. After that, the procedure of harvesting BRPE cells (as described in the same section) followed. Cells were seeded on the tissue culture polystyrene surface (TCPS) and their morphologies were investigated after one week.

2.9.5 Determination of optimised growth conditions for HIPE

This experiment was designed to explore which serum concentration and retinoic acid would produce the best morphology of the cells. In this experiment, HIPE cells were grown on tissue culture base, with varying serum concentration, without PU substrate, so as to study the effect of serum concentration on HIPE growth.

Different amount of foetal calf serum (FCS) were added to culture media as described in **2.4.1.3**. FCS was added to media mixture at concentration of 0%, 1%, 2%, 3%, 5%, 10%, 15% and 20%. HIPE cells were seeded at a density of $1x10^5$ cells per well in a 24-well plate, topped-up to 1.5ml of mentioned media. They were incubated at 37°C at 5% CO_2 and were fed twice weekly. Cellular attachment and growth was observed using phase-contrast microscope at days 5, 7 and 11, after which they reached confluence.

2.10 Growing Cells on Polyurethane Films

Using the data and growth conditions available from previous sections, primary pigmented epithelial cells obtained from bovine (BIPE and BRPE) and also obtained from human (HRPE) were grown on the PU film membrane (Z3A1 and Z9A1).

2.10.1 Growing BRPE and BIPE on polyurethane films

Cells were harvested via a method described in **section 2.4.3.1.4** for BRPE and a method described in **section 2.4.3.2.2** for BIPE. The cells were seeded directly on the PU films and on TCPS, which acts as control at a seeding density of 1×10^4 cells

per substrate and cultured (as described in **section 2.5**). Retinoic acid was added just before the cells reached full confluent and maintained up to 33 days (i.e. about four weeks after cells were maintained at full confluence). They were frequently investigated using phase contrast microscopy for signs of growth or infections. At the end of the experiment, cells were fixed and stained accordingly using methods described in **section 2.6**.

2.10.2 Growing HRPE on polyurethane films

The aim of the experiment was to investigate the growth of human retinal pigment epithelial (HRPE) cells on polyurethane (B9) and to study their morphology (monolayer formation) and functionality (junctional protein). HRPE cells were cultured from human donors according to **section 2.4**. The HRPE cells were grown on control (TCPS) and polyurethane films (Z3A1 and Z9A1) surfaces according to **section 2.5** and RA was added just before they reached full confluence and maintained for over a period of 20 days (i.e. they were maintained at full confluence for about 2 weeks). At the end of 20 days, the cells were fixed and stained using Tro-pro-3, ZO-1, Phalloidin and Cytokeratin stains according to procedures described in **section 2.6**.

2.11 Growing cells on porous PU

Porous PU made (as described in **section 2.1.2.3),** was used in this experiment. Several experiments were conducted on porous PU: testing out attachment, growth and morphologies of ARPE-19, BRPE and BIPE on porous PU, phagocytosis assays of cells on porous PU and dextran transport through the porous PU.

2.11.1 Investigation of morphology of cells on porous PU

ARPE-19, BRPE, BIPE and HRPE cells were grown on the porous PU. Substrates were held in a 24-well plate, using cell-culture inserts (as described in **section 2.5.1.2)**. The cells were seeded onto the substrates and control surfaces at 1 x 10^4 cells per well and cultured according to their optimum conditions (as described in **section 2.9**). Initially, 20% serum concentration was used. When the cells were approximately 80% confluent, the serum concentration was reduced to 5% and retinoic acid was added at 0.5µl/ml. These growth conditions were maintained for 5 weeks with primary cells, and up to 2 weeks with the cell-line to ensure formation of junctional proteins. At the end of the experiments, cells were fixed and stained according to **2.6** for investigations of ZO-1 formations, F-actin staining, nuclei distributions and cytokeratin expressions.

2.12 Functionality tests

It was important to test if the cells were able to perform, at least to some of their *in vivo* function when they were cultured *in vitro*. Some of their major functions are their phagocytic capability, as a blood/retina barrier and to allow trans-epithelial transport.

2.12.1 Phagocytic activity of cells

2.12.1.1Retrieval of Photoreceptor outer segments (POS)

20 bovine eyes were obtained from a local slaughterhouse, placed on ice and used within 24 hours. All the procedures in this method were carried out under dim red light to reduce conversion of rhodopsin to opsin. Excised retinas were homogenized in 0.73M sucrose solution in 0.1M phosphate buffer (Na2HPO4/KH2PO4; pH 6.8) using a method modified from (Godchaux[143] and Higgins[144]). The mixtures were placed in a 30ml homogenizing tube and were gently homogenized using 6 strokes of mechanical homogenizer; Potter S homogenizer (Sartorius) operating at 300rev/min. The homogenates were filtered through 100 µm nylon cell strainer (BD Biosciences) and layered onto a discontinuous sucrose density layer (2.5ml each) of

gradients 0.8M, 1.0M and 1.2M in the phosphate buffer made using 16G cannula and syringed into 12mL Beckman Polyallomer centrifuge tubes, creating 4 sucrose gradients. They were then balanced and centrifuged, using a swing-out rotor (Beckman Coulter – SW40Ti) at 60,000g (217,000 rpm) for 60 minutes at 4°C. A distinct orange band containing POS was seen between the layer of 1.0M and 1.2M interface. These were pipetted off and re-suspended in the phosphate buffer. They were spun again at 27,000g (12,000 rpm) for 20 minutes at 4°C. This was repeated twice more. Finally, all the pellets were re-suspended in 1ml phosphate buffer. The protein content of the POS was analysed using bicinchoninic acid (BCA) protein assay see **2.12.1.2**. The POS were then stored at -80°C until the phagocytosis experiments.

2.12.1.2 The bicinchoninic acid assay (BCA) protein assay

The concentration of protein in a solution is estimated using the BCA protein assay based method, developed by Lowry[145] and Smith[146], exhibited by colour change when Cu^{1+} is being reduced to Cu^{2+}. The reduction in colour is in proportion to protein concentration, which can then be measured using colorimetric techniques

and compared to protein solutions with known concentrations. In this case, the concentration of POS was analysed using this technique.

First, the working reagent was made up using 50 parts of BCA (Sigma-Aldrich B9643) and 1 part of copper sulphate (Sigma-Aldrich C2284). Standards containing known concentration of water and protein (bovine serum albumin; BSA, Sigma-Aldrich P0914) were made up in serial dilutions. The working solution was added to the protein standards and a standard curve was generated from the reading using a plate reader (μQuant Biotek Instrument. Inc) and KC4 v3.1 Biotek software. The protein content of the sample was then calculated from the curve.

2.12.1.3 Outer segments labelling with SNARF®-1

The POS obtained from **2.12.1.1** were labelled according to manufacturer's instructions. 5-(and-6) Carboxy SNARF®-1 (Invitrogen, C1270) is a fluorescent pH indicator, which undergoes changes in its emission's wavelengths (580/640nm) in different pHs. Therefore, when phagocytosed by the cell, it will be surrounded by acidic condition, changes its emission's colour from red (basic), when attached to cells, to yellow-orange (acidic). The POS were labelled by adding 100μg of the Carboxy SNARF®-1 in 10μl of dimethyl sulphoxide (DMSO) per 1mg of POS. The

Carboxy SNARF®-1 was slowly added to the POS, which was placed in a rotating vortex, to ensure even distribution of the label. It was rotated in the dark at room temperature for 1 hour. It was then centrifuged (Fresco17 Heraeus, Thermo electron corporation) at 5000rpm/2.4g for 7 minutes. The supernatant was removed and the labelled POS pellet was re-suspended in phosphate buffer (pH 6.8) before being centrifuged. This process was repeated and finally, it was re-suspended in 1.0ml phosphate buffer (ph 6.8) and stored at -80°C.

Before being used with cells in an experiment, the labelled POS were placed in three well plates, one with pH 9 buffer (basic), another with pH 6 buffer (acidic) and another in a well with mixtures of labelled POS, which were previously immersed in the two different pHs (pH 9 and pH 6). They were then examined underneath fluorescent microscope to observe the difference in colour changes with the different pH.

2.12.1.4 Investigation of anti-Rhodopsin antibody

To confirm that the anti-Rhodopsin antibody was working, the antibody staining was carried out on fixed retinal tissue (fixed according to the procedure in **2.6.1**)

and on extracted POS from **2.12.1.1**. After labelled secondary antibodies were attached, they were imaged using laser confocal scanning microscope (**2.7.4**).

2.12.2 Phagocytic activity of cells: Phagocytosis of photoreceptor outer segments

Extracted POS was suspended in the normal feeding media (as in 2.4.1) supplemented with 5% sucrose. It was suggested that the amount of POS needed to challange the cells was at 10mg/ml of media[147]. After the cells reached full confluence, cells were cultured with the POS-containing media and incubated at 37°C in the dark. After the ends of the culturing period (in this case 2 hours and 24 hours), cells were rinsed free of unattached POS, by supporting the dishes at an angle and gently washing with a PBS. Cells were then fixed for 10 minutes in 10% NBF as in **2.6.1** before immunochemistry. Samples were treated with trypan blue (1mg/ml, Sigma-Aldrich, T8154) in PBS for 15 minutes to remove bound uningested POS according to method described in [144] and some were left without the treatment as negative control. A primary antibody (anti-Rhodopsin antibody see **Table 2-2**) was used to attach to the ingested POS, which was then labelled with a secondary fluorescent antibody using the method described in **2.6.7** before being mounted and imaged. All procedures were carried out in the dark.

2.12.3 Phagocytic activity of cells: Phagocytosis of polystyrene beads (PB)

The cells attached on the PU were also investigated for their ability to ingest polystyrene beads (PB). They were challenged with 1 x 10^7 beads/ml of Fluospheres® Polystyrene Microspheres (1.0µm, blue-green fluorescent, Invitrogen F13080) for 3 and 24 hours. They were washed with trypan blue in PBS (1mg/ml) for 15 minutes to remove bound but un-ingested beads, before fixing and being imaged. All procedures were carried out in the dark.

2.12.4 Phacogytic activity of cells: Exclusivity of phagocytic activity of epithelial cells

In this experiment, the cells were examined on their ability to selectively reduce their ability to ingest POS, by blocking their αVβ5-integrin receptors. Cells were cultured on substrates and control surfaces until full confluence. Referring to **Figure 2-11**, some of the wells were pre-incubated with anti-αVβ5 antibody (Covance, clone P1F6, MMS-474R) or with mouse IgG (Dako, X0943) both at 1:1000 dilution at 37°C for 1 hour. POS or PB was then challenged to the cells, according to the

procedures in **2.12.2** and **2.12.3**. They were incubated in the dark for 3 or 24 hours at 37°C before fixing, treatment with trypan blue and immunochemistry.

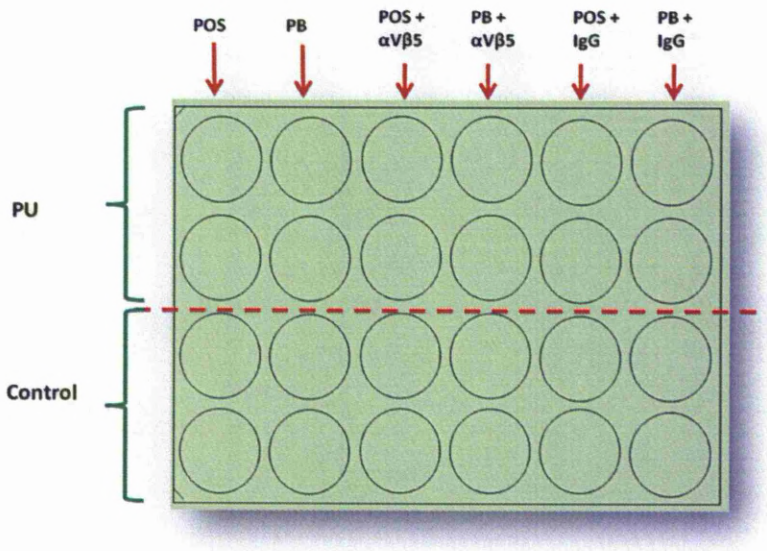

Figure 2-11: The configurations of the 24-well plates for selectivity of phagocytosis experiment. Some of the wells were pre-incubated with αVβ5 antibodies or IgG (as control) before feeding with either POS or PB.

2.13 Dextran transport studies

This was an experiment to investigate the role of epithelial cells in controlling trans-epithelial transport, using fluorescently labelled dextran of different molecular weights. PU film (non-porous, as control) and porous PU were attached to a

cylindrical shaped polystyrene cloning ring (Bel-Art Scienceware, USA) with the aid of silicone glue (NuSil Silicone Technology, USA) as in **Figure 2-12**(a). The samples were tested, initially, to determine if there were any leaks. Three different types of dextrans were used in this experiment: Blue 10kD (Cascade Blue® lysine-fixable dextran, Invitrogen, D1976), Green 70kD (Fluorescein isothiocyanate-dextran, Sigma, FD70) and Red 155kD (Tetramethylrhodamine isothiocyanate–Dextran, Sigma, T1287). Several serial dilutions of the dextrans were carried out to find the optimum concentrations to be used in the experiment. The readings of dextran concentrations were performed in a black 96-well plate (Nunc®FluoroNunc™, Sigma, P8741) via FLx800 Microplate Reader (BioTek software KC4). They were also mixed with each other in culture media and fluorescence readings were taken to determine the effect of phenol red in culture medium and if they could be used together in one single plate. The dextrans were also incubated with cells in wells to check their effects on cell growth. A serum-free medium was used to suspend a suitable concentration of dextran as found previously.

After the cells were known to reach full confluency, 100µg/ml of the different coloured dextran in serum-free medium was added into the cloning ring (as in **Figure 2-12(b)**). 500µl of normal medium was left outside the ring. The amount of media used in (100µl) and outside (500µl) of the cloning ring was chosen to allow

the cloning ring to be raised slightly inside the well (due to buoyancy), but enough to maintain the same level of the media. At the same time, the cloning ring was maintained horizontally without tipping over. At certain time points (1h, 2h, 3h, 4h and 24h), 50µl of the outside medium was collected and placed into a well of the black 96-well plate. The reading of the fluorescence was taken with the microplate reader. The same amount of normal medium was replaced outside the well each time. Readings for red wavelength were carried out at 530nm absorption/590nm emission; green wavelength was at 485nm absorption/528nm emission and blue at 360nm absorption/460nm emission.

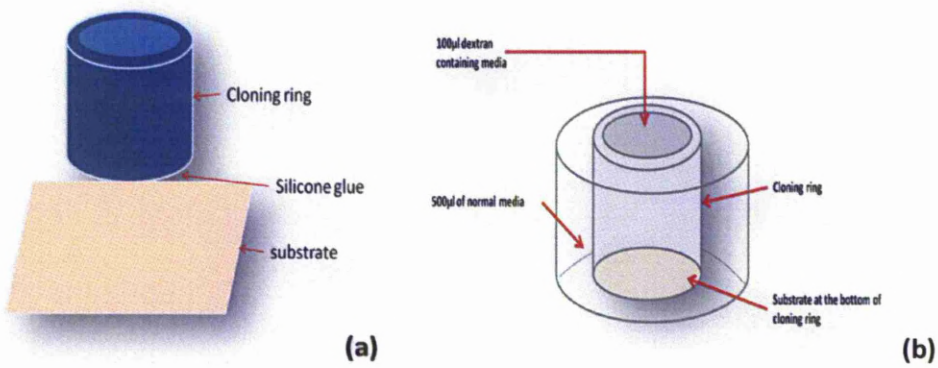

Figure 2-12: Pictorial representation of the set-up for dextran transport experiment. Substrate was joined to the cloning ring using a medical grade silicone glue (a). Figure in (b) shows the administration of dextran and media in the cloning ring, the cloning ring was slightly raised due to buoyancy of the fluid.

2.14 *In vitro* injury model experiment

In this experiment, BRPE and BIPE were grown on the porous PU substrates and on plastic cover-slips, until full confluency (as described in **2.4**). At the same time, BRPE were also grown in a 6-well plate under the same culture conditions. Cell-dyes were used to label the cells on the two different surfaces (as in **Figure 2-13**); Green (Vybrant® DiO cell-labelling solution, Invitrogen, V-22886) was used to label BRPE cells in tissue-culture dish, Red (Vybrant® DiL cell-labelling solution, Invitrogen, V-22885) was used to label BRPE or BIPE cells on substrates (a). To do this, the dye was added to the normal medium at 5µl/ml, and just enough was added to cover the surface. They were then incubated at 37°C for 20 minutes followed by removal of the staining medium. Normal medium was added back to the well and standard culture condition resumed overnight. Next, substrates (with monolayer of cells) were carefully cut (b) and placed onto the BRPE (c) in the 6 well-plate, secured by stainless steel needles (Watkins & Doncaster pins, 0.25mm x 10mm). They were grown together in normal tissue culture conditions for 3 days before fixing and imaging. Particular attention was given to the edges between the substrate and cells in 6-well plates. Any signs of integrations of cells were also noted.

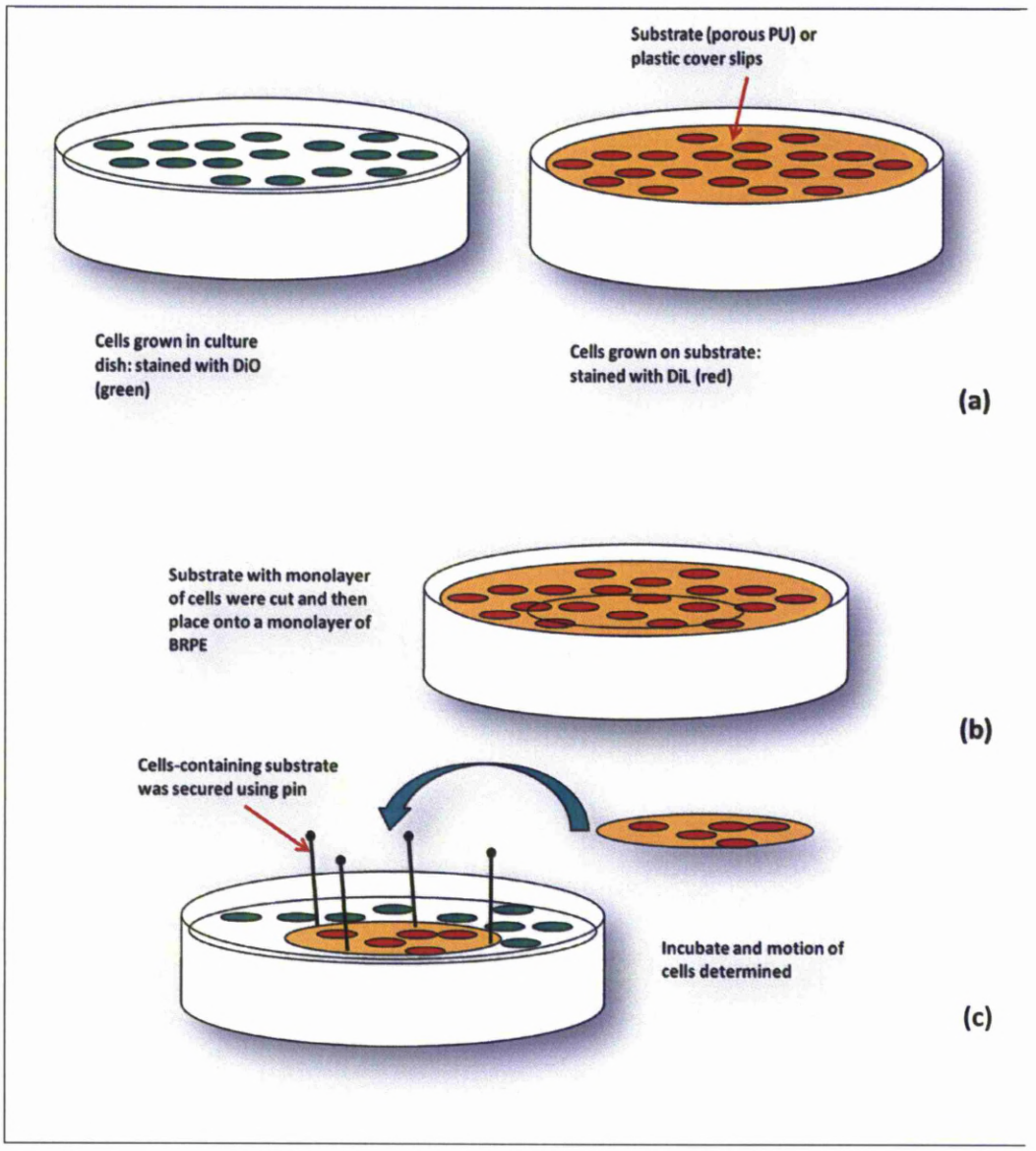

Figure 2-13 show schematic of tracker dyes experiment. Different coloured dyes were attached to different surfaces. Their movements could be detected, after they were grown together for 3 days.

3 CHAPTER THREE: RESULTS

3.1 Substrates

3.2 Manufacturing of PU as film membrane

The PU membrane constructed by casting (**section 2.1.1**) produced a smooth surface and these could be seen when investigated with the SEM (Figure 3-1) at 100X magnification (a, b and c). An investigation at higher magnifications (1000X) proves that the surfaces are still smooth with no discernible feature on all samples (d, e and f).

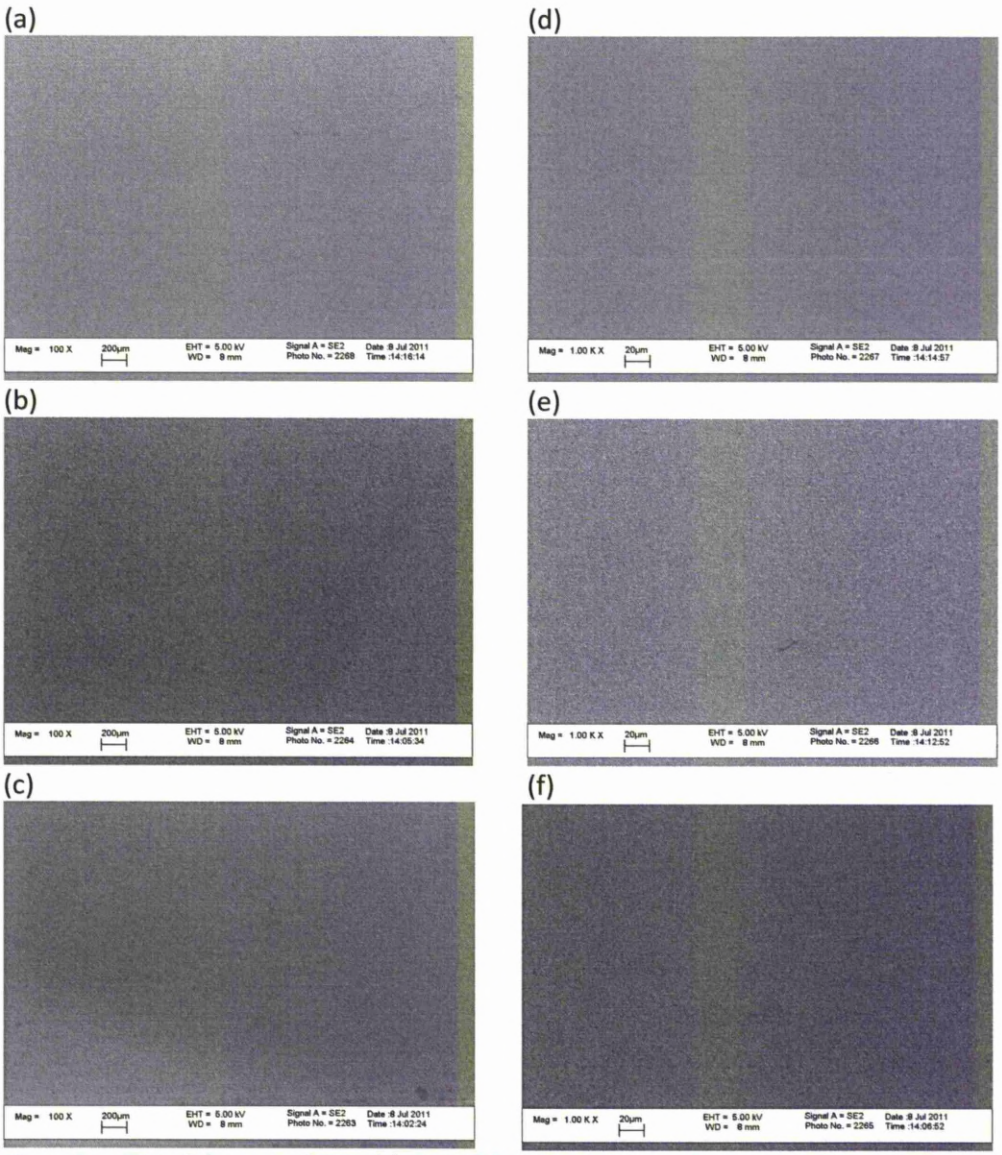

Figure 3-1: SEM of the control TCPS (a), Z3A1 (b) and Z9A1 (c) membranes at x100 magnification demonstrated smooth surfaces. At higher magnification (x1000), the control TCPS (d), Z3A1 (e) and Z9A1 (f) confirmed the smooth surfaces. Scale bar 200µm.

3.3 Manufacturing porous PU

Throughout this chapter, a material or a substrate was described as porous, when the holes formed on its surface, penetrated all the way through. Holes, which were formed as crates and did not penetrate through, are described as holes. The porosities of the substrates were confirmed by traces of water on the other side, when droplets were left on the surface.

3.3.1 Freeze drying

The substrates produced by the PU in DMAC (in 20%, 15%, 10% and 5%) were examined by an SEM. The substrate produced at 20% PU in DMAC (**Figure 3-2 (a)-(b)**) was more than 100μm thick and had a poor handling property. There was no sign of any porosity, when examined using SEM. At 15%, there was an uneven distribution of holes in linear arrangements (see **Figure 3-2 (c)-(d) arrow**). At 10%, and on closer examination there were uniform distributions of pores approximately 10μm in width with some irregular surface features with lines and ridges (see **Figure 3-2 (e)-(f)**). At 5%, the substrate produced was very thin (less than 5μm), easily broken and there was no sign of any pores (see **Figure 3-2 (g)-(h)**).

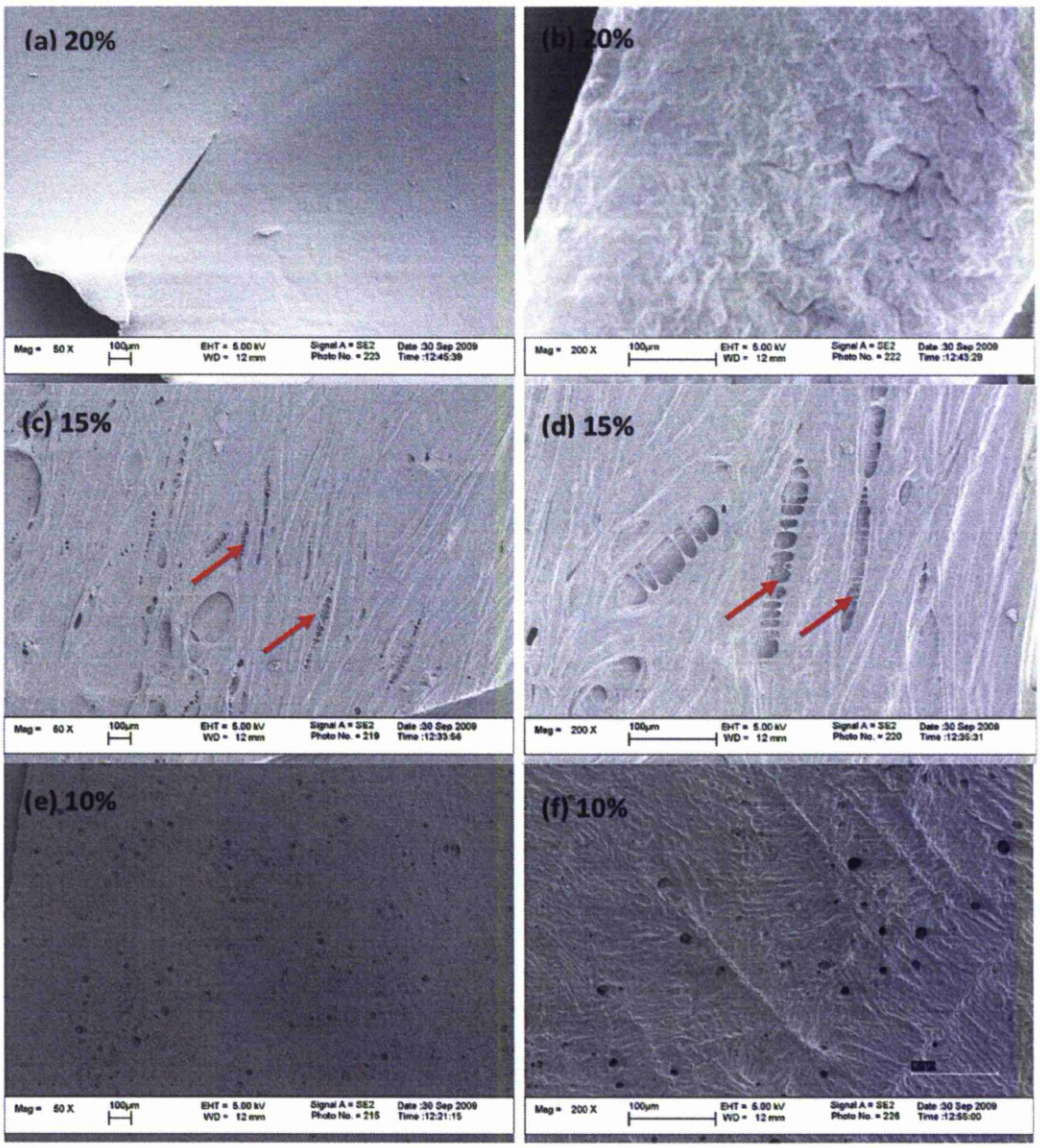
(a) 20%
(b) 20%
(c) 15%
(d) 15%
(e) 10%
(f) 10%

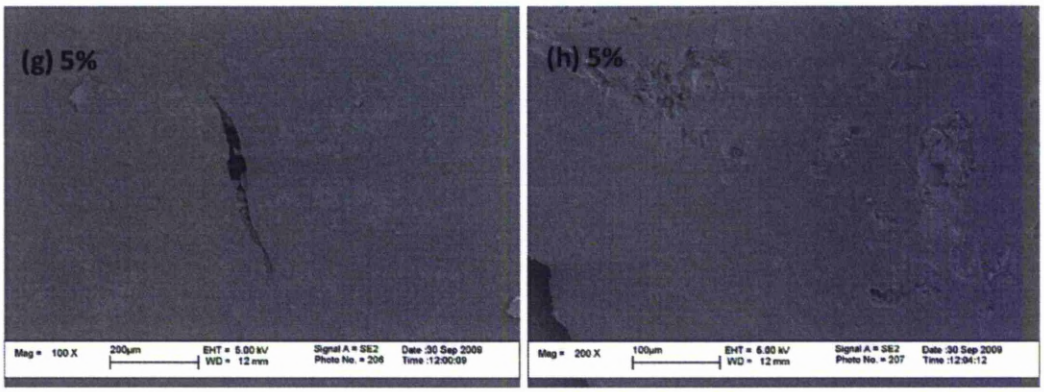

Figure 3-2: SEM micrographs show the substrates formed by freeze drying process on lower magnification on the left panels (a)-(g) and on higher magnification on the right (b)-(h). The substrates were formed by dissolving PU in DMAC in certain percentages (weight/weight); (a)-(b) 20%, (c)-(d) 15%, (e)-(f) 10% and (g)-(h) 5%. There were no signs of porosities in the 20% and 5% materials. At 15%, there were porous holes formed in linear arrangements (arrows). Formation of ridges and crease-like lines with some irregular surface formation can be seen with 10% substrate.

Following the results from the previous experiment, the concentration of PU in DMAC of between 10% and 15% were used (i.e. 14%, 13%, 12% and 11%), for further investigations of pores formations. Under SEM investigation, substrate formed by 14% PU in DMAC **(**Figure 3-3 **(a)-(b))** appeared to have larger indentations and undulations compared to the 13% substrate (Figure 3-3 **(c)-(d)**), but neither of them appeared to have any pores. Substrates formed by 12% (Figure 3-3 **(e)-(f)** and 11% (Figure 3-3 **(g)-(h)**), showed smaller indentations and undulations with some pores visible. The pores were more evenly distributed in 11% than in 12%. There were some random rough surfaces with fibrous-like

features seen throughout the surface, as the concentrations were reduced from 13% to 11% (**see** Figure 3-2**).**

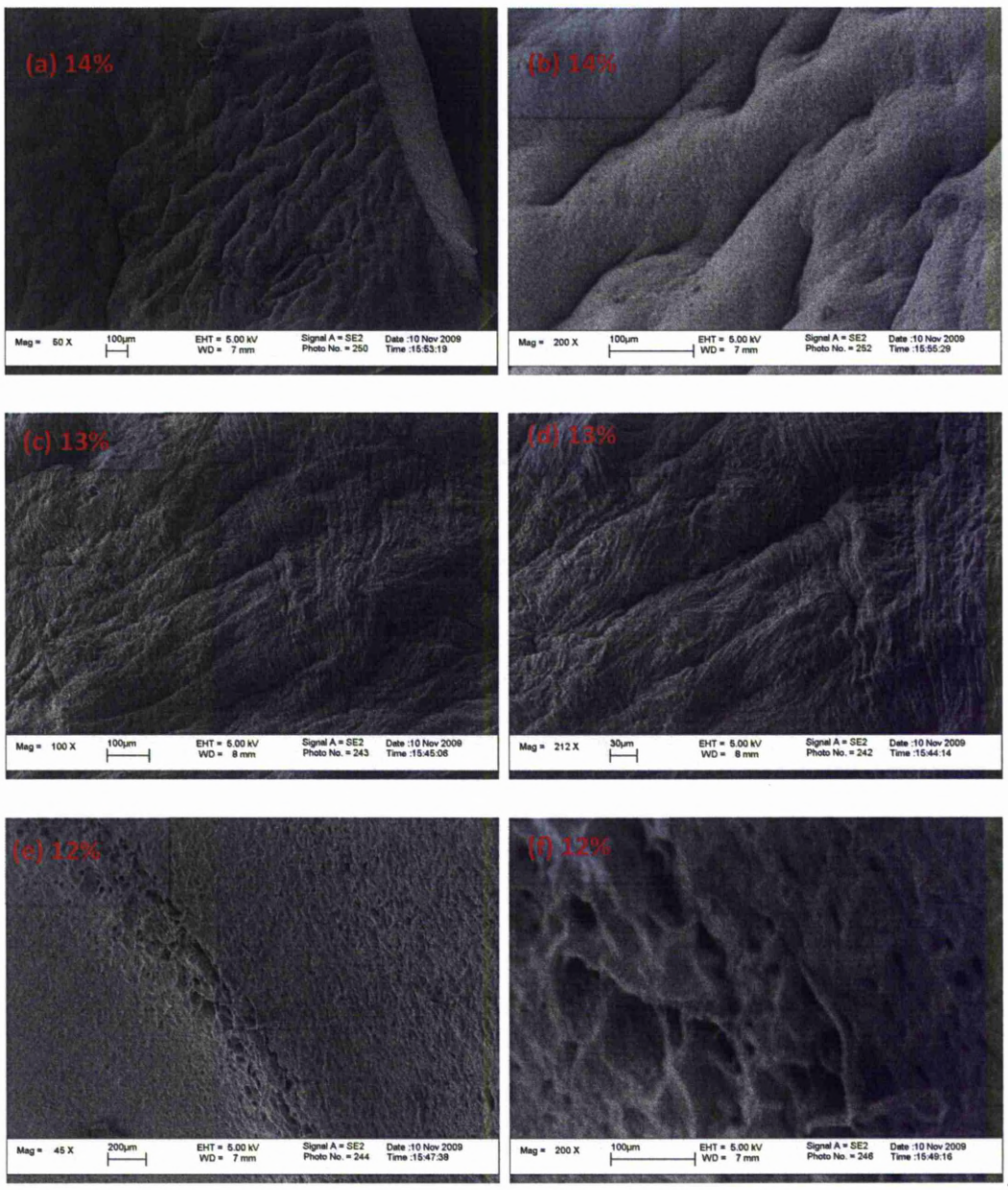

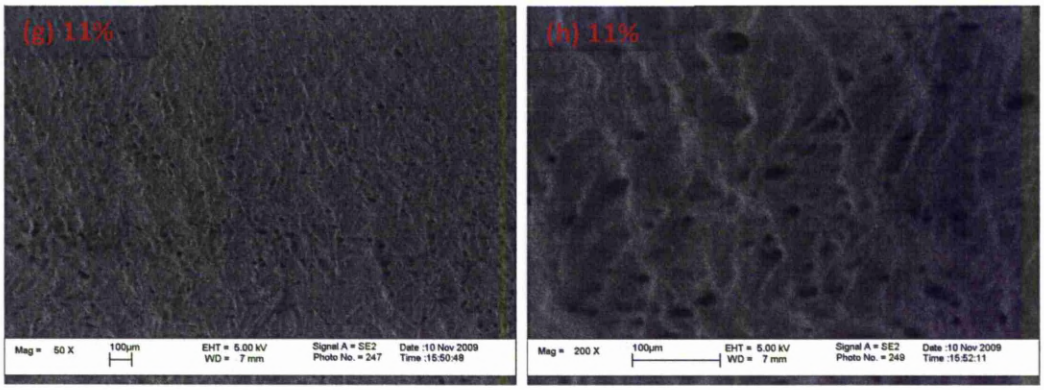

Figure 3-3: SEM of substrates formed by freeze-drying. Lower magnification on the left (a)-(g) and higher magnification on the right (b)-(h). The substrates were dissolved in DMAC at certain percentages (weight/weight). (a)-(b) 14%, (c)-(d) 13%, (e)-(f) 12% and (g)-(h) 11%. The formation of indentations, undulations and surface roughness could be seen on all surfaces, but the pores were more evenly distributed in 11% substrate (g, h).

3.3.2 Electrospinning

Our collaborator from the University of Strathclyde supplied the substrates, produced by electrospinning. Under closer examination using SEM, fibrous thread of PU can be seen as randomly oriented fine fibres (between 500nm to 800nm in diameters), throughout the material, at the same time producing inter-connecting three-dimensional pores (**Figure 3-4 (a)-(b)**). The material has a strong adhesive property at one surface making it difficult to handle.

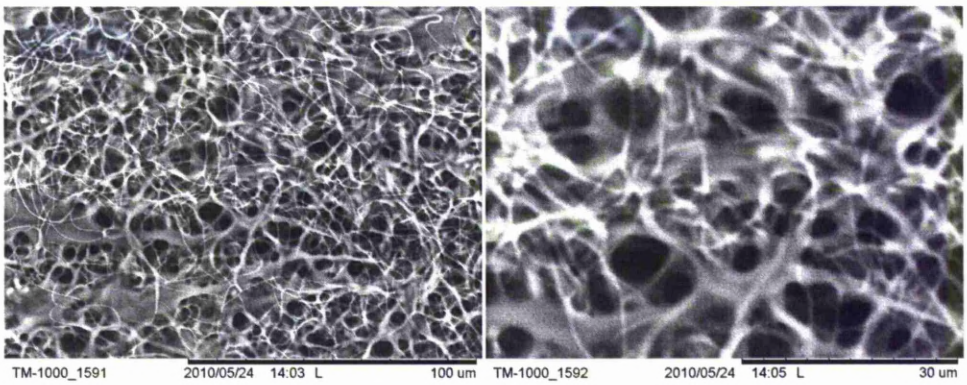

Figure 3-4: SEM of PU fibres formed via electro-spinning process. The fibres formed were randomly oriented and composed of ultra-fine fibres between 500nm to 800nm in diameters with interconnected three-dimensional pores distributed throughout the structures.

3.3.3 Oven drying

Comparisons of substrates, produced by small 3.2 cm diameter glass bottle, demonstrated that: The material produced by higher concentration of PU in DMAC (10%) exhibited uneven distributions of pores, whereas the higher concentration of sugar displayed holes that were not perforated through the material (Figure 3-5).

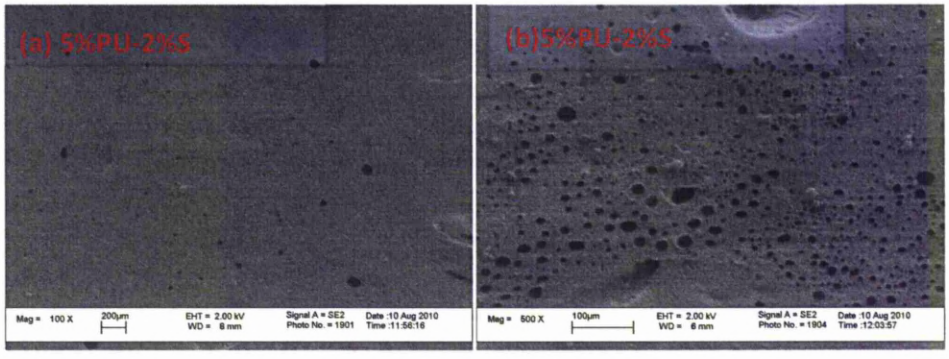

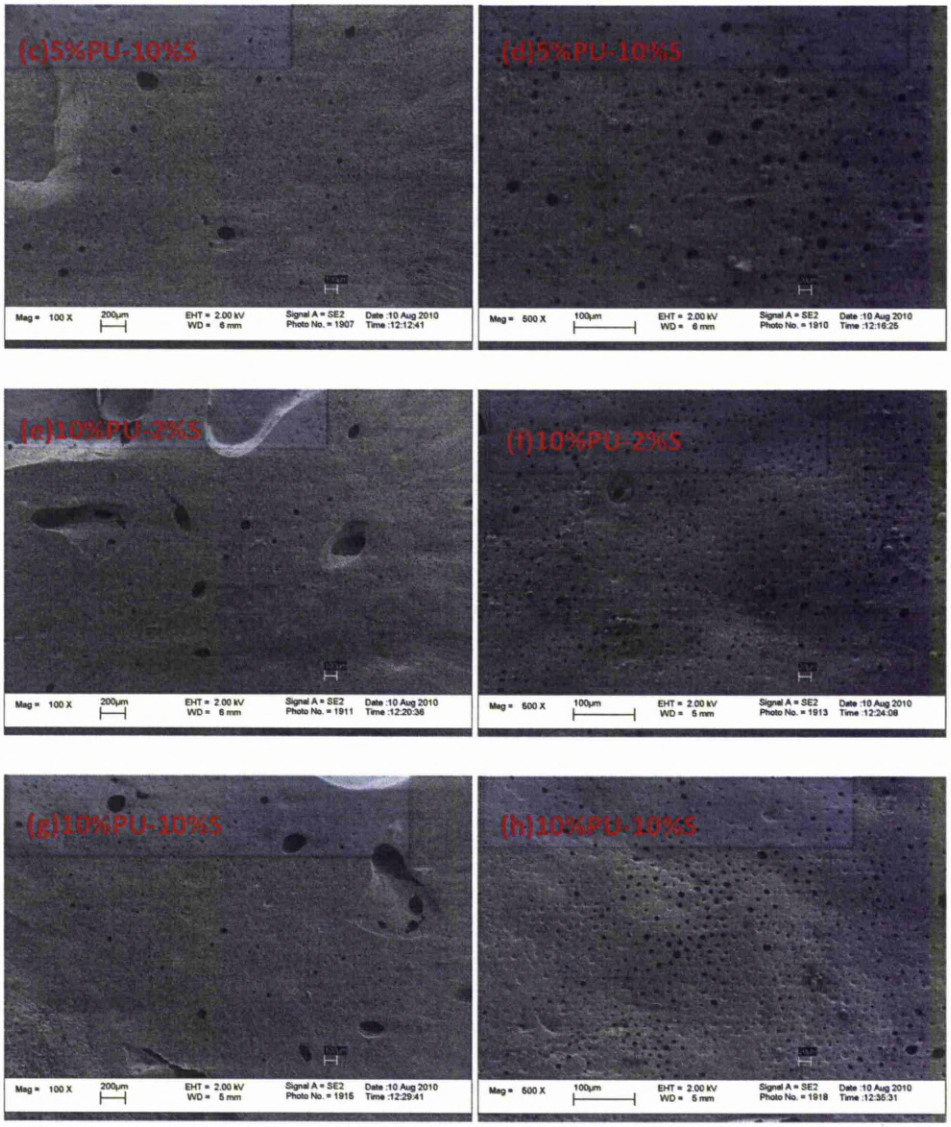

Figure 3-5: SEM of the substrates produced by mixing different concentration of PU in DMAC and different percentages of icing sugar, then dried using oven at 70°C. Lower magnification on the left (x100) as opposed to higher magnification on the right (x500). 5% PU in DMAC plus 2% icing sugar in (a) and (b) and 10% icing sugar in (c) and (d). 10% PU in DMAC plus 2% icing sugar in (e) and (f) and 10% icing sugar in (g) and (h). The distribution of pores were not consistent throughout the substrates, especially at higher percentages of PU in DMAC (10%) and the holes created were not perforated through the material, especially at higher percentages of sugar (10%).

Following the experiment, 5% PU in DMAC were used, but this time the effect of the different casting shapes were investigated. Under macro examination, the material produced using the small bottle was more than 200μm in thickness, the crystallising dish produced thin fragile materials and the materials produced by the conical flask were quite difficult to take out of the flask and easily torn. Examination using SEM found that the material produced, using the bottle, had elongated pores (arrows) **(**Figure 3-6**(a)-(b)),** the materials produced by the flask had mixtures of big and small pores (Figure 3-6 **(c)-(d)**) and the ones by the crystallising dish, produced the most homogenous pores throughout the substrate (Figure 3-6 **(e)-(f)**).

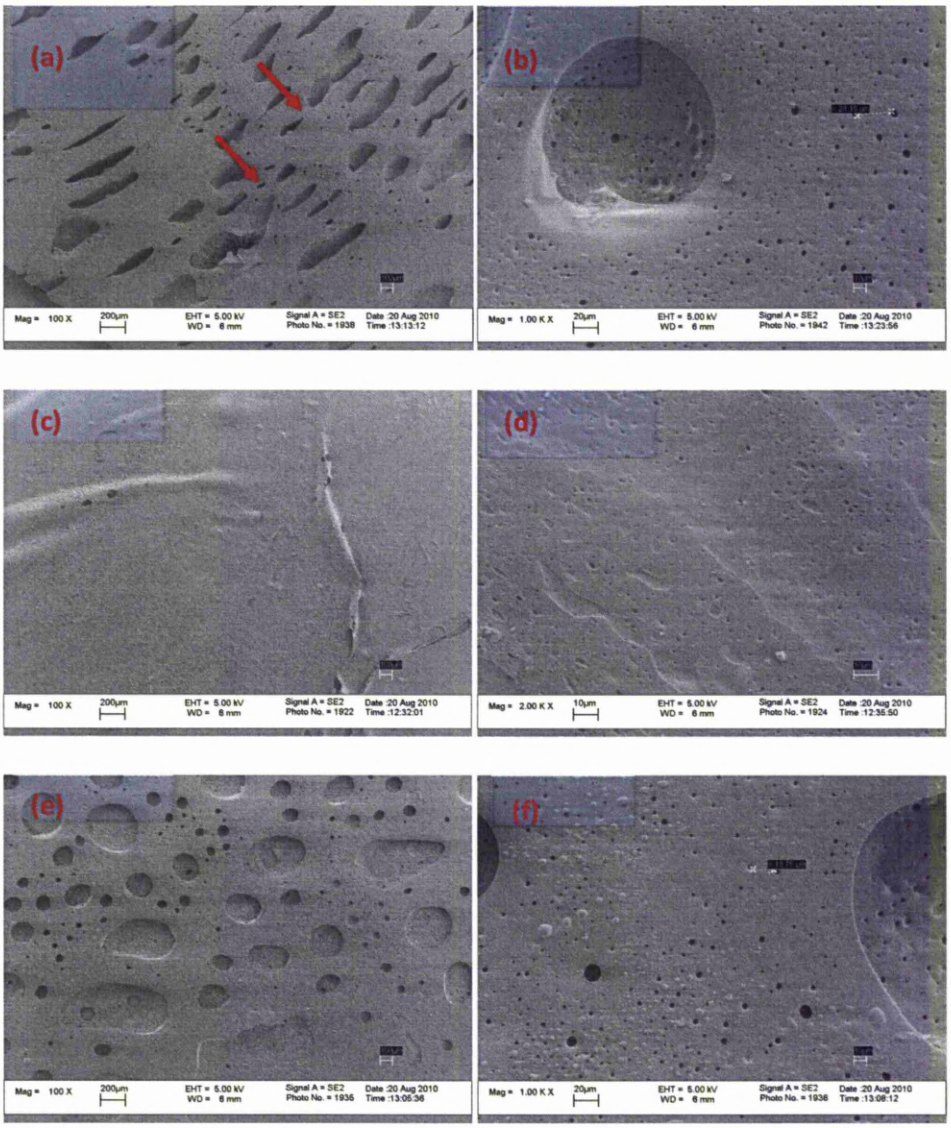

Figure 3-6: SEM images of the substrates formed using different containers; (a)-(b) small bottle, (c)-(d) crystallising dish and (e)-(f) conical flask. Low magnification SEM (x100) on the left and higher magnification (x1000) on the right. Although they were formed from the same mixtures (5% PU in DMAC plus 5% icing sugar), the containers did have some effect on the substrates produced. The small bottle yielded the thickest material with elongated holes (arrow), the conical flask produced mixtures of large and small pores. The crystallising dish produced homogeneous pores throughout the surface.

Under closer inspection with SEM (**Figure 3-7**) the substrate produced by the crystallising dish was found to have thickness of about 5μm and to have pores of approximately at 1μm in diameter with typical distance of about 10μm apart.

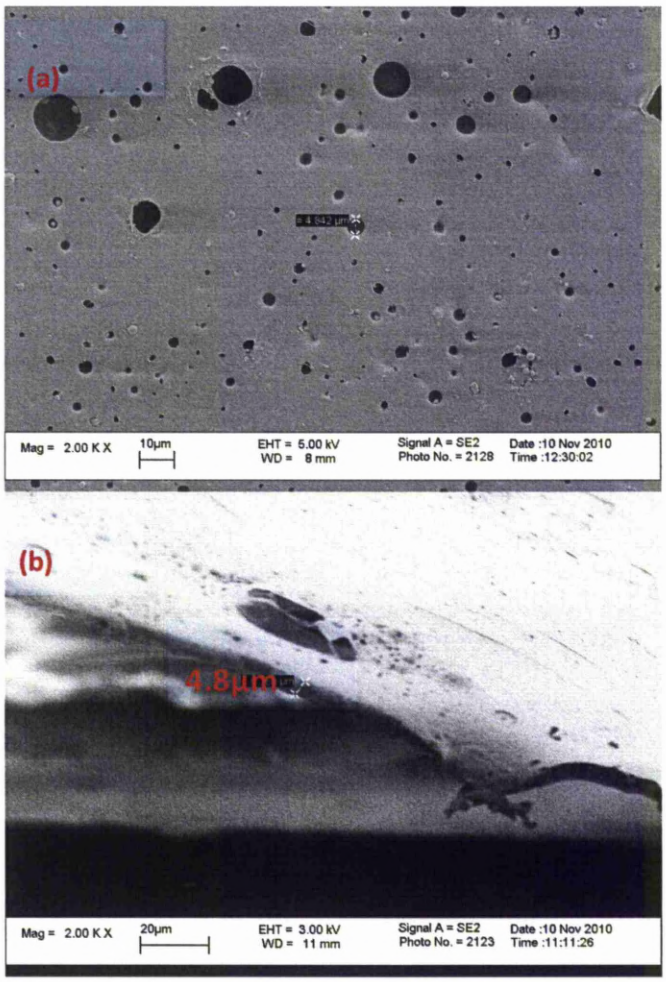

Figure 3-7: SEM photographs of the PU produced by mixing DMAC (5%) with icing sugar (5%) then oven dried demonstrated the (a) surface topography of the substrate, uniform pore distributions averaging at 1μm pore sizes and distances of around 10μm from each other. (b) Lateral view of the substrate. The thickness of the substrate measured was approximately less than 5μm. Both pictures were at 2000x magnification.

Repeated experiments of 5% PU in DMAC, plus 5% sugar dried in the crystallising dish using the oven technique, produced similar results every time.

3.3.4 Water precipitation

Precipitation in water technique was performed to attempt to make the substrate porous. Macro examinations showed that the substrates formed via this method were thick and have rubber-like textures. Under closer examination using SEM (Figure 3-8 **(a)**), the topography of the surface demonstrated randomly aligned fibrous matrices with irregular pores, formation of wrinkles and folds with some projections. The thickness of the substrate was approximately 100µm (Figure 3-8 **(b)**).

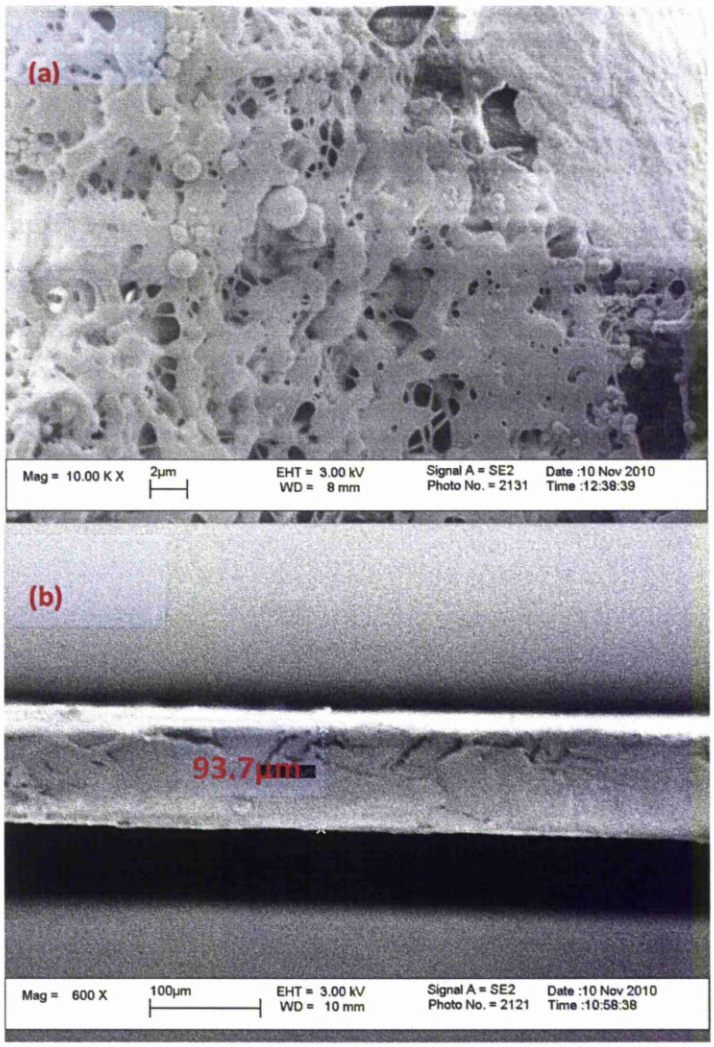

Figure 3-8: SEM photograph of PU produced by water precipitation technique. (a) The surface topography was irregular random fibres with pores, wrinkles and folds with some projections (x10 000 magnification). (b) The lateral view of the substrate showing the thickness of approximately 100µm (x600 magnification).

3.4 Measurements of substrate's properties

3.4.1 Contact angle measurement

For the non-porous substrate, 10µl of distilled water was dropped onto the substrate; video recordings were taken for 20 seconds at 25 frames per second and the contact angle measurements were taken. Contact angle for Z3A1 was 70° (± 3.4° std. dev.), Z9A1 was at 65° (± 3.6° std. dev.) n=30 for each sample.

For porous substrates, as the water droplets would not stay long on the material, only the first 5 readings were taken from each session (i.e. the first 0.16 seconds). Results from 20 different readings were obtained. The mean value of contact angle for porous PU was 43° (± 5.5° std. dev.), n=100. Results were shown in **Table 3-1**.

Table 3-1: The values of contact angle measurement of the film (Z3A1 and Z9A1) and porous Z3A1.

Film (non porous)	Z3A1 71° (±3.4° std. dev.) n=30	Z9A1 65° (± 3.6° std. dev.) n=30
Porous Z3A1	43° (± 5.5° std. dev.), n=100	

3.4.2 Tensile test of the substrates

The samples were randomly cut into different orientations. Uni-axial tensile stresses were applied to the samples. The stress was expressed by the force (F, unit N) acting per cross-sectional area (A, unit mm^2). The strain measured was expressed by the percentage deformation (elongation), when the force was applied per unit length. Throughout the experiment, the ambient temperatures and pressures were kept constant. The tensile test results were presented in the form of scatter graph of stress against strain (see **Figure 3-9**). From the general patterns of the graphs, Z3A1 films demonstrated an elastomeric behaviour (see **Figure 3-9(a)**), Z9A1 films show plastic deformation patterns **Figure 3-9(b)** whilst porous Z3A1 demonstrated some strengthening effect, as compared to its film form, while maintaining its elastomeric behaviour **Figure 3-9(c)**.

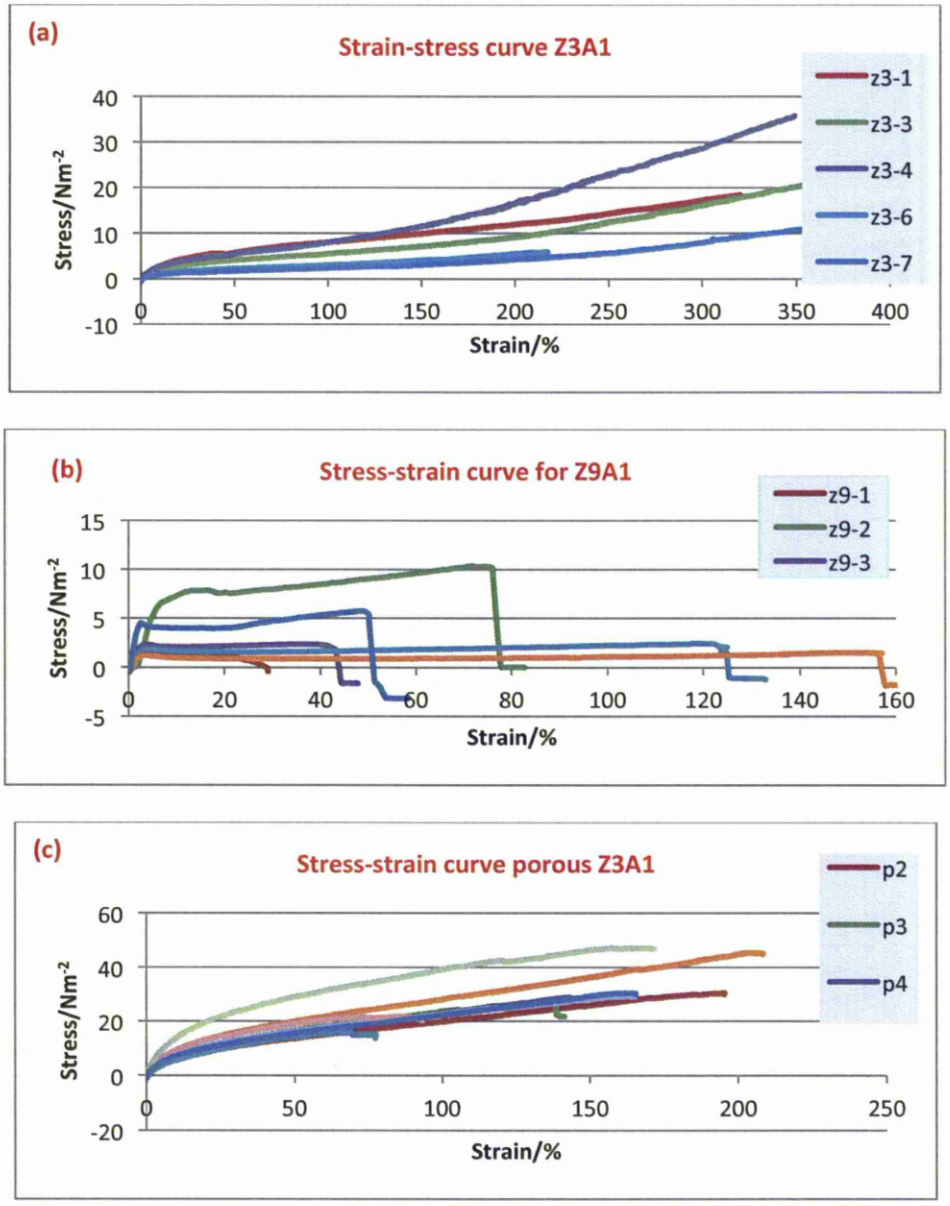

Figure 3-9: Scatter graphs demonstrated stress against strain of (a) Z3A1 film, (b) Z9A1 film and (c) porous Z3A1. Note the differences in the magnitude of the axes. The Z3A1 films demonstrated elastomer behaviour, Z9A1 film showed plastic deformation patterns, whereas the porous Z3A1 showed some strengthening effect while still retaining its elastomeric behaviour.

The slope of a stress-strain graph was used to obtain modulus of elasticity (Young's Modulus). These slopes were measured at the first part of the graph, which is known as their elastic region. This is where substrates will revert to their original length, shape and form, when the force was removed. It was revealed that Z9A1 in film form had the highest modulus of elasticity. Z3A1 in porous form had higher modulus of elasticity than its film form (see **Table 3-2**). It was also found that there were two populations of the porous Z3A1 (see **Figure 3-10**).

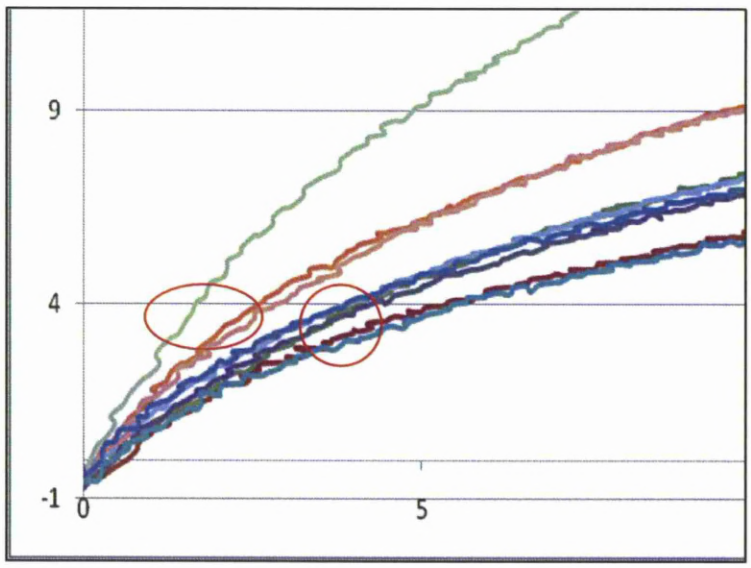

Figure 3-10: Closer examination of the Figure 3-9(c) graph showing the two populations of the porous PU.

Table 3-2: Modulus of elasticity calculation. The values were taken from the slope of the graph, Z3A1 n=5, Z9A1 n=6, porous Z3A1 n=9. All of the modulus of elasticity values were obtained at less than 5% tensile strain.

	Average/Nmm^{-2}(MPa)	Std. dev/ (MPa)
Z3A1 film	0.092	±0.035
Z9A1 film	1.24	±1.08
Z3A1 porous	0.56	±0.23

Stresses at fractures were calculated from the graphs, at the point at which the material started to rupture. Porous Z3A1 presented with the highest fracture stress: about a third stronger than its film form but around half of its percentage strain at fracture to the film form. Z9A1 film shows the lowest fracture stress with the lowest strain at fracture (see **Table 3-3**).

Table 3-3: The values of stress fracture and the percentage strain at fracture. Z3A1 n=6, Z9A1 n=6, porous Z3A1 n=9. Numbers in the brackets are the standard deviation for the sample.

Substrate	Stress Fracture (Nmm^{-2} or MPa)	% strain at fracture
Z3A1 film	18.9 (± 11.2)	326 (± 64.4)
Z9A1 film	4.52 (± 3.7)	87.5 (± 49.1)
Porous Z3A1	31.2 (± 10.7)	150.7 (± 43.6)

3.5 Evaluation of ages of the PU on their properties

The numbers of primary BRPE cells attached did not vary between substrates. Experiment showed that there was no difference in terms of attachment and growth of cells on all substrates, which were produced from varying ages and initial forms (pellets or granules) and these were confirmed by fluorescent morphological staining. These show that the ages of the PU have no effect on their properties.

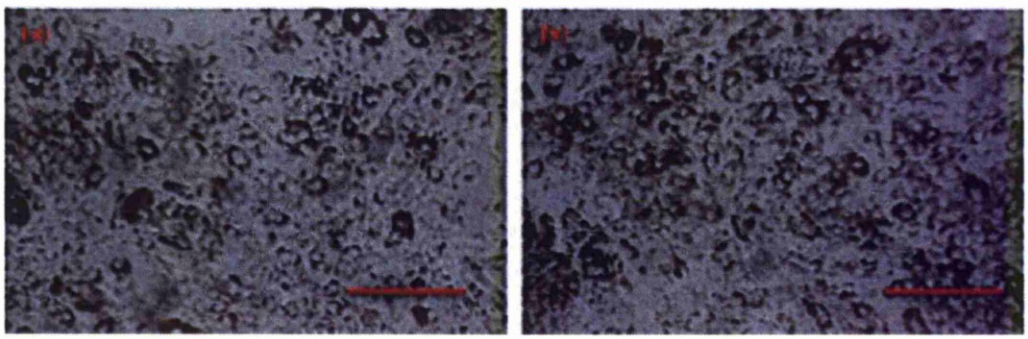

Figure 3-11: Investigation demonstrated that there were no significant difference on the growth of cells on the different ages of the PU produced, as represented by the phase contrast microscopy of the BIPE cells above. The PU in (a) was produced in 2005 and (b) was produced in 2007. Scale bar= 100μm.

3.6 Cell cultures

3.6.1 Mounting of tissues

Fluorescently labelled Phalloidin staining on BRPE and BIPE tissues revealed that the F-actin belt formations of the BRPE were bigger and were more uniformly distributed (Figure 3-12**a**) compared to the smaller and irregularly shaped BIPE cells (Figure 3-12**b**). The cells demonstrated the typical hexagonal epithelial cells morphologies, often described as 'cobble-stone' shape. The epithelial cells were in contact with each other, densely packed and were composed of flattened monolayer of cells in a continuous sheet, usually associated with the simple epithelium. The whole tissue mount staining served as a morphological guide for later experiments with the epithelial cells *in vitro*.

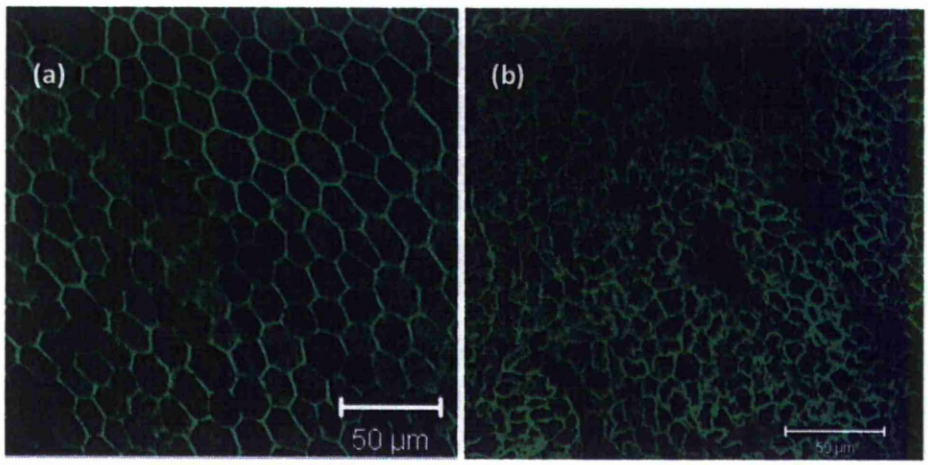

Figure 3-12: Laser confocal microscope showed the fluorescent Phalloidin staining on BRPE (a) and on BIPE (b) whole tissue mount. The shape of the F-actin belt of the BRPE on the retina displayed a bigger and more uniformly distributed hexagonal morphology as compared to the BIPE on the iris. Scale bar: 50µm.

3.6.2 Results of harvesting BRPE by different methods

Small colonies of BRPE cells could be seen to initially attach and proliferate with time with all methods I (**Section 2.4.3.1.1**), method II (**section 2.4.3.1.2**) and method III (**section 2.4.3.1.3**) of harvesting BRPE. However, with all these methods, their morphologies were different from one culture to another. There were some elongated fibroblastic-like appearances (Figure 3-13**(a))** or some multilayer and overgrowth (Figure 3-13**(b)),** whilst some had good cobblestone shape type appearances (Figure 3-13**(c)**) and good pre-confluent cells **Figure 3-13(d)**).

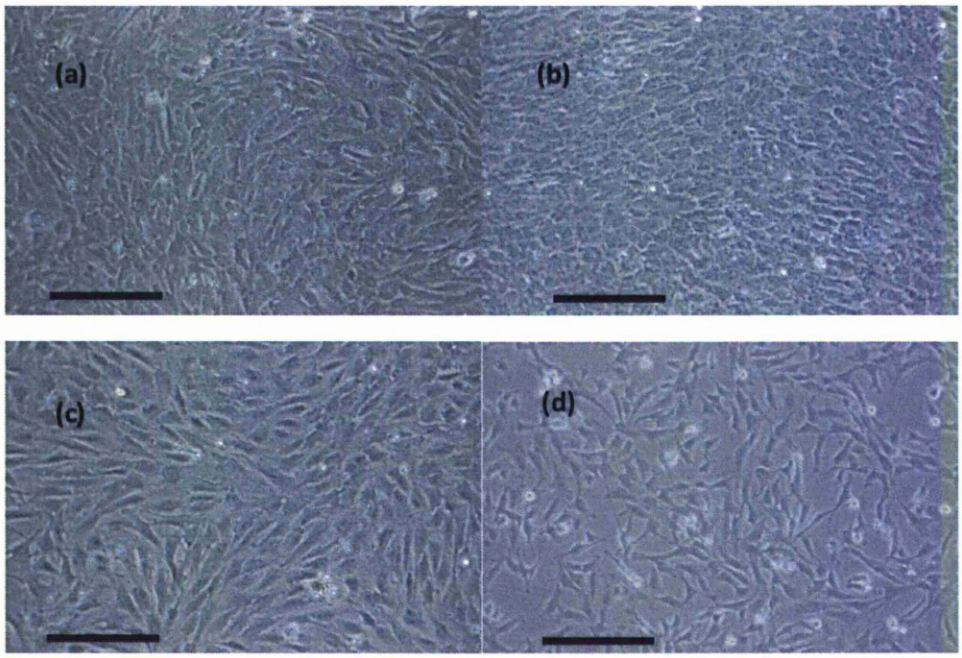

Figure 3-13: Phase contrast photomicrographs show variety in the outcome of growth of BRPE with methods I, II and II of harvest. (a) Fibroblastic-like contamination (b) overgrowth (c) and (d) example of good pre-confluent BRPE, which do not repeat the same shape after trypsinization. Scale bar: 100µm.

Harvest method IV (**section 2.4.3.1.4**), however, produces better morphology (**Figure 3-14**); Sheets of BRPE attached and formed small colonies initially. With time, the cells increased in size by approximately four-fold, continued to proliferate and were flattened when in contact with the adjacent cells. As they grew, their overall pigmentation diminished. When the cells reached full confluence, they developed into a sheet of hexagonal cobblestone-shape cells, a typical morphology of the RPE cells *in vivo*. There were also mixtures of larger heavily pigmented cells

and smaller less pigmented cells that appeared to proliferate quicker. The large pigmented cells were often bi-nucleated, rounded, had wedge-like features and seldom in numbers, intermingled between the smaller mostly single nucleated cells.

This harvest method proved to be reliable and repeatable in producing epitheloid morphology.

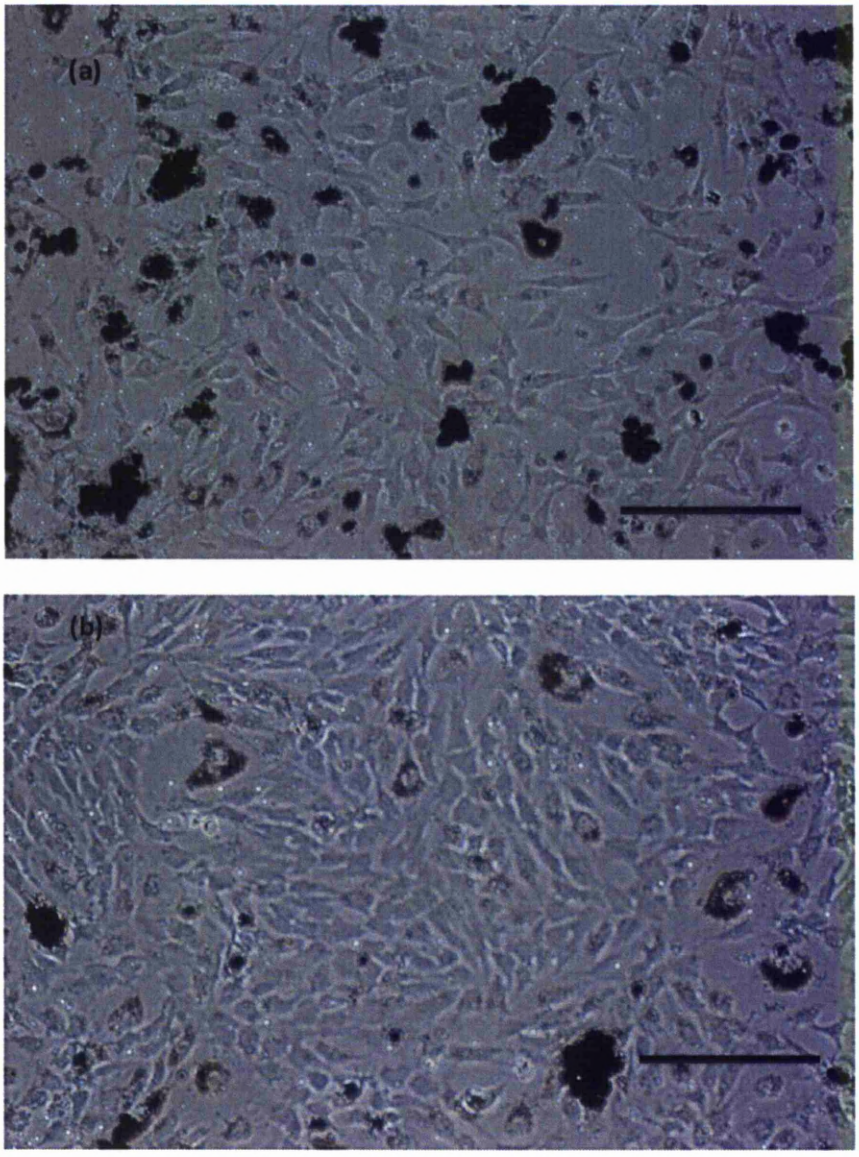

Figure 3-14: Phase contrast of BRPE harvested by method IV; BRPE cells grew from sheets of BRPE, which was gently removed by collagenase IV (a) at day 4 and (b) at day 7. With time, the cells increased in sizes, and become flattened, when in contact with neighbouring cells. Note that there were mixtures of larger heavily pigmented cells and smaller less pigmented RPE cells. The overall pigmentation reduced with time. Scale bar: 100µm.

3.6.3 Results of harvesting BIPE by different methods

Both of the harvest methods yielded small colonies of cells at early time points (within the first week). However, method I (**section 2.4.3.2.1**) of harvesting BIPE, generated cells, which were elongated, spindle-shaped and were fibroblastic-like in appearance (**Figure 3-15**). The amount of overlapping cells could also be seen in abundance. However, when the cells were stained with cytokeratin antibody, it was stained positively confirming its epithelial origin (**Figure 3-16**).

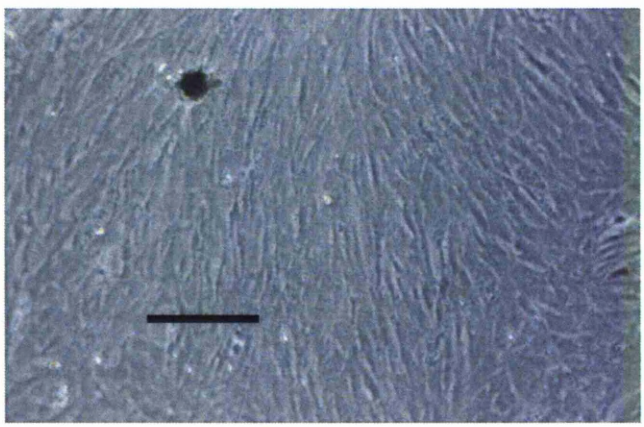

Figure 3-15: Phase contrast microscope image of BIPE produced by method I of harvest. The cells were elongated and had fibroblastic-like appearance. Scale bar: 100µm.

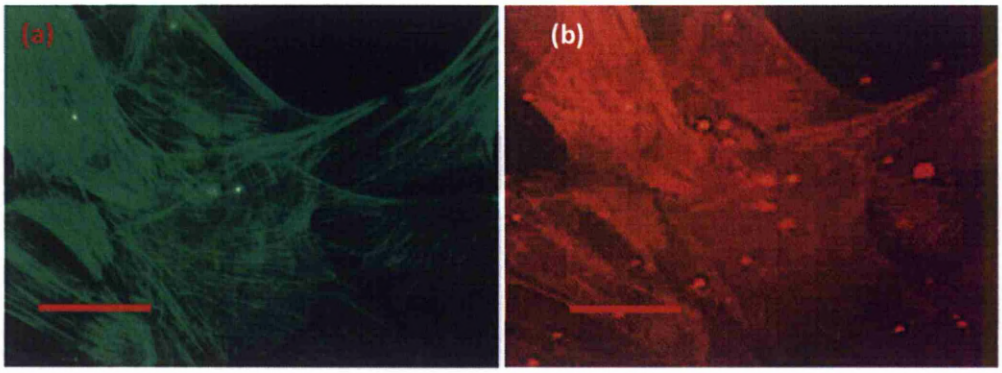

Figure 3-16: Fluorescent microscopy demonstrated the phalloidin (a) and cytokeratin (b) staining for the fibroblastic-like BIPE cells in Figure 3-15. Positive cytokeratin staining comfirmed the cells were of epithelial type. Scale bar: 100μm.

Method II (**section 2.4.3.2.2**) of harvesting BIPE demonstrated that small colonies of heavily pigmented BIPE attached, forming micro-aggregates (Figure 3-17**(a)**). At this stage, the cells appeared to be spindle-like and elongated. Once they encountered neighbouring cells, their shape became flatter and more rounded (Figure 3-17**(b)**) As the cells proliferated, their pigmentation was reduced and they became smaller and more polygonal (Figure 3-17**(c)).** When the cells reached full confluence, they formed into hexagonal cobblestone-shape like morphology (Figure 3-17**(d)**). There were various degrees of pigmentation in the confluent monolayer. Epithelial cell borders were seen surrounding each individual cell.

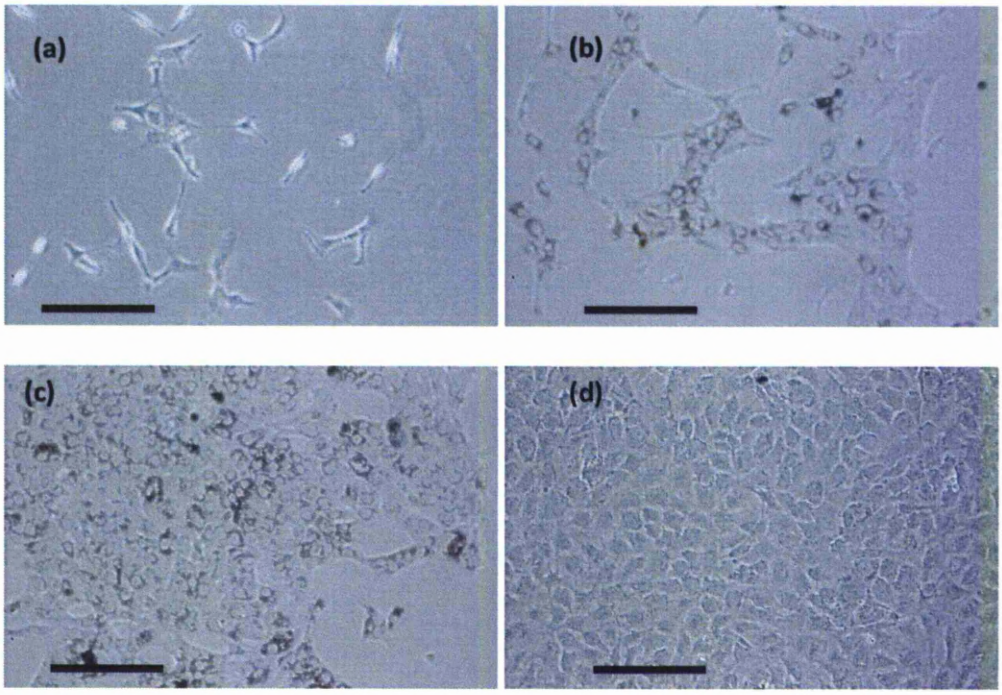

Figure 3-17: Phase contrast micrograph showed the growth and spread of BIPE. Growing from small colonies, the heavily pigmented BIPE started to proliferate from (a) day 1 to (b) day 7 (c) day 11 and (d) day 20. Initially, cells were elongated (a) and as they proliferated, they came into contact with neighbouring cells and changed their appearance to a flat and more rounded (b) to a polygonal shape (c). When the cells reached full confluence, their pigmentation was reduced and they took up a more hexagonal shape. The borders of the cells were evident (d)., Scale bar: 100μm.

The second method of harvesting IPE demonstrated a high yield of pure IPE, which was consistently replicated (data not shown).

3.7 Preliminary studies with ARPE-19:

Attachment numbers and cell morphologies on the surfaces were investigated with fluorescent green Phalloidin staining and fluorescent red propidium iodide (PI) staining. The green F-actin stress fibres were seen surrounding each individual nucleus (red) and they were evenly distributed throughout the surfaces (Figure 3-18). The ARPE-19 cell numbers attached on the control, Z3A1 and Z9A1 surfaces were evaluated (as described in **section 2.8.1**). Nuclear counts per field of view (area of 27,600μm^2 or 27.6 x 10^7 μ mm^2) were obtained for each of the surface. 4 fields were counted for each surfaces for each time point (day 1, day 4 and day 7) making n=12 for each surfaces. These were used to compute a graph. Results were shown in **Figure 3-19**. The data was tested for its variance (var=0.014) and statistical analysis by means of one-way ANOVA was performed. Cell counts showed a gradual increase in cell numbers on both substrates, with significant increase on cells attachment on Z9A1 at day 1 than Z3A1. Cell numbers on control surfaces showed rapid increase from day 1 to day 4, but at day 7 the numbers of cells decreased, with signs of cellular overgrowth and detachments in the tissue culture. It can be said that at this seeding density and at this seeding period, the substrates (Z3A1 and Z9A1 films) promotes growth and proliferation of ARPE-19 cells, with a good sign of attachment ($p<0.05$). While it was evident that the substrates support

proliferation and growth of ARPE-19 cells, they did not form the desired cobblestone epithelial morphology with these growth conditions.

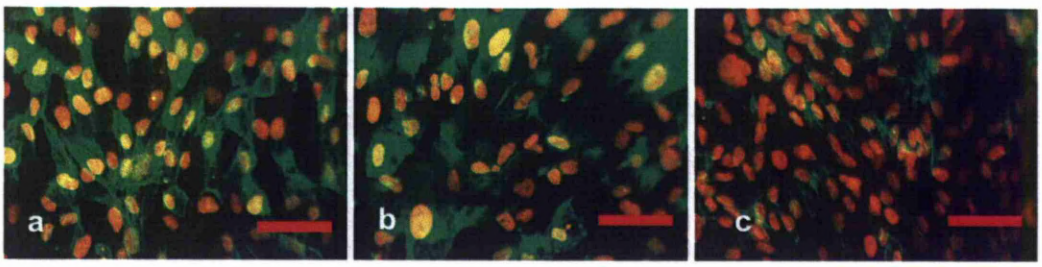

Figure 3-18: Fluorescent photograph of ARPE-19 cells on control and substrates shows nuclear distribution of ARPE-19 cells (red staining) and actin cytoskeletal (green staining), on control surface (a) Z3A1 (b) and Z9A1 (c) at day 7 indicating that the substrate does support cellular growth. Scale bar 100μm.

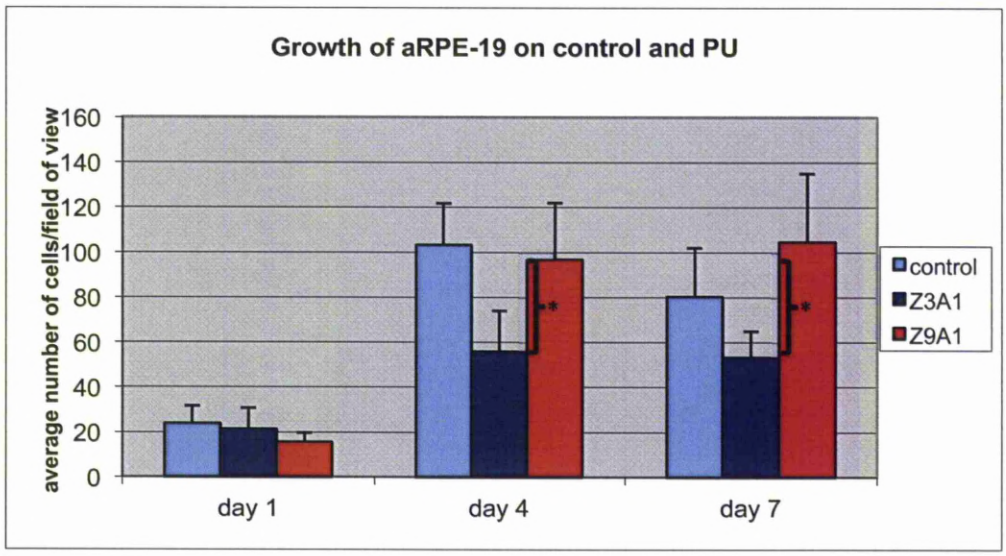

Figure 3-19: Histogram denotes numbers of nuclei on all surfaces; on control, Z3A1 film and Z9A1 film. The numbers of cells increased significantly (*) on Z9A1 compared to Z3A1 ($p<0.05$), but were lower than control from day 1 to day 4. The numbers of cells dropped by day 7. Statistical analysis using one way ANOVA, n=12 for each surface, error bar=standard deviation.

3.8 Preliminary study: Experiments with primary BRPE & BIPE

Other preliminary experiments were carried out with primary bovine RPE and IPE cells to evaluate the growth of the primary cells on the substrates (as described in **section 2.8.2**). Assessments of cell counts were performed at specific time points (day 1, day 4, day 7 and day 10).

Morphological examination as represented by **Figure 3-20:** and **Figure 3-21.** Under closer examination of both substrates, all the cells showed good signs of attachment and proliferation with time. The morphology of the cells and the F-actin staining indicated good monolayer formation on some surfaces, especially BRPE on Z9A1 at days 7 and 10, comparable to those on the control surfaces. The uniformity in the cell shape and formation was more prominent on Z9A1. However, the BRPE cells did not form the typical epithelial hexagonal morphology at the end of day 10. It was found that, with both BRPE and BIPE, on days 7 and 10, there was cell detachment on Z3A1 substrates and this was more prominent with BRPE (marked with * in **Figure 3-20**). On closer examination, it was also observed that there were some nuclear contents leakages of cells on Z3A1 following enlarged cells indicating signs of cell apoptosis. This phenomenon was not seen with Z9A1 substrates on which, after forming a layer of cells at day 7, the number of cells did not show increase in numbers at day 10. Similar observation with both substrates can also be

seen with BIPE cells (see **Figure 3-22** and the *). Cell counting demonstrated by nuclei staining were used to construct comparison graphs. Data was analysed using one-way ANOVA and tested for variance, n=48 for each cell types. For BRPE (var=0.693), the numbers of cells increased on all surfaces up to day 7, after which the cell numbers did not show any further increase (on Z9A1 and on control) or declined (on Z3A1), indicating cell detachment and death (**see** Figure 3-22**a**). There was no significant difference of numbers of BRPE cells on all of the surfaces at 95% confidence interval ($p>0.05$). Compared to BRPE, BIPE on the other hand (Figure 3-22**b**), demonstrated slower increase in cell numbers on all surfaces, despite the similarities in the initial seeding numbers. There were little differences between the growth and proliferations of BIPE on Z3A1, Z9A1 and control ($p=0.068$).

The data implies that B9 does provide a suitable surface for cell growth. However, ARPE-19, BRPE and BIPE did not grow in a desired morphological form. Since all of them behave similarly on substrates and on control surfaces, the next logical way is to optimise the cell's growth conditions to obtain the desired morphology.

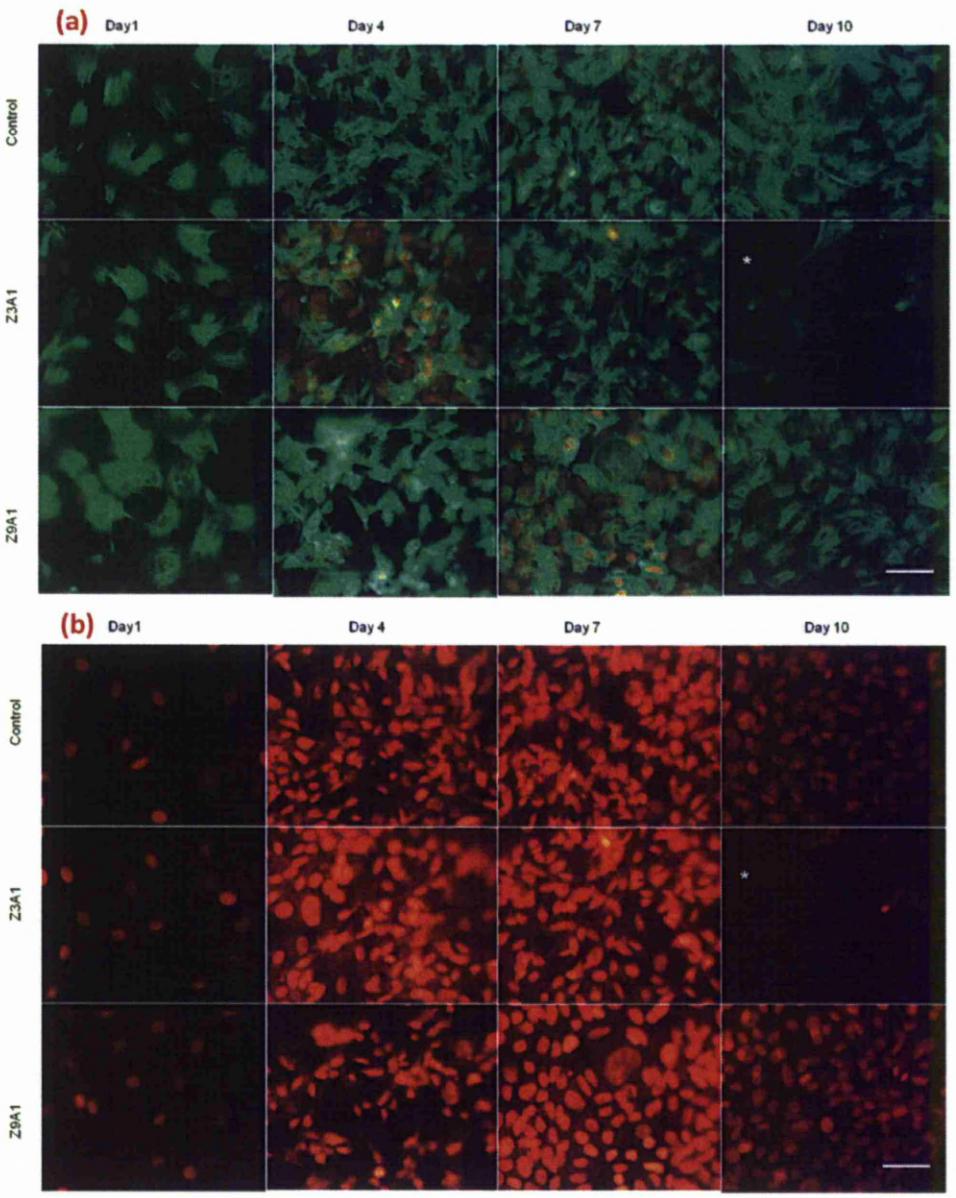

Figure 3-20: Representative image capture of green Phalloidin F-actin cytoskeletal staining (a) and red Propidium Iodide nuclear staining (b) of BRPE cells growing on control, Z3A1 film and Z9A1 film. It can be seen that the PU support growth of primary cells. Cells attach, grow and proliferate with time. At day 7 however, the cells become overgrown with some overlapping nuclei and then detached at day 10 (*). Confocal microscope, scale bar: 50µm. Brightness to some of the images was due to substrate's auto-fluorescence.

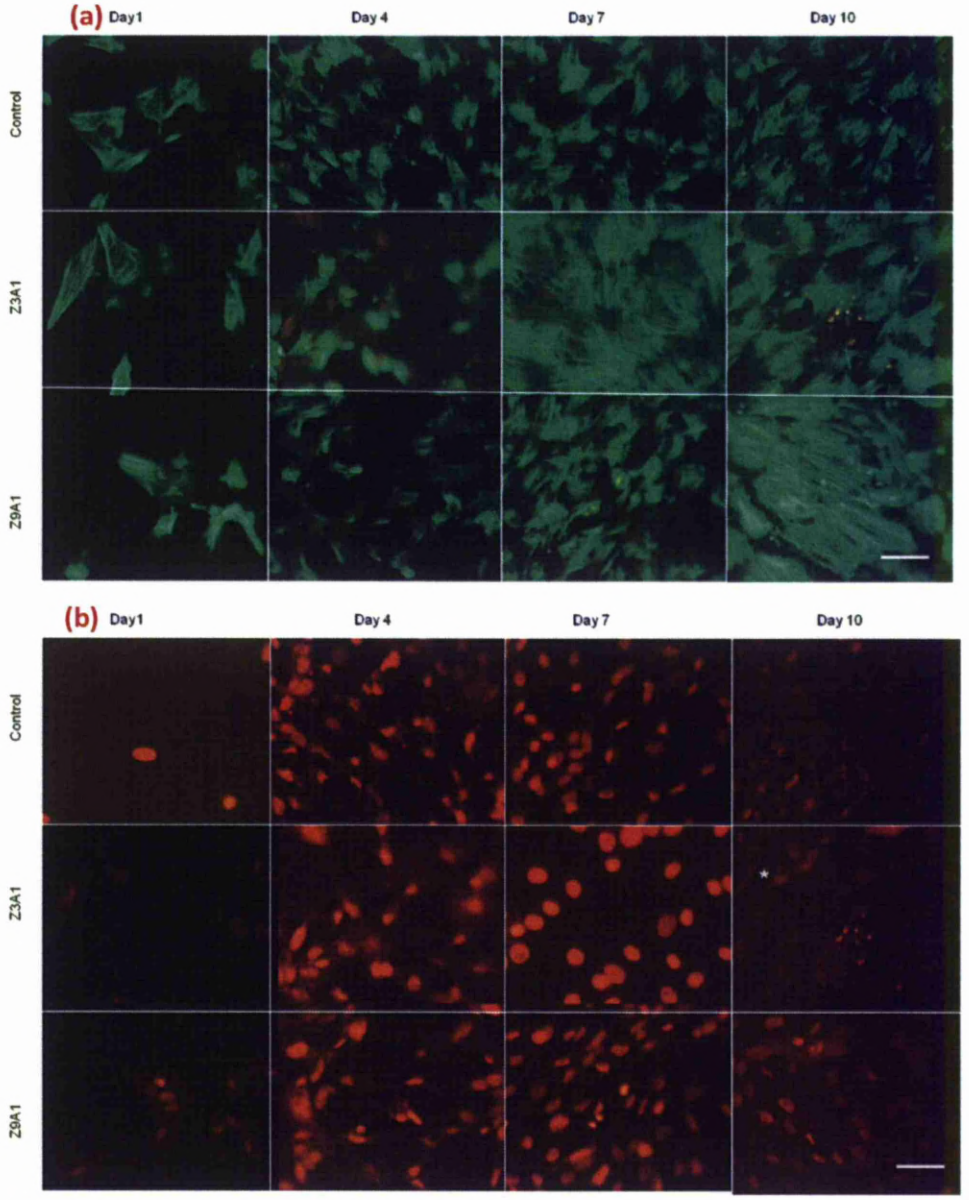

Figure 3-21: Showing representative image capture of BIPE cells growing on control (TCPS), Z3A1 film and Z9A1 film. Cells were stained with cytoskeletal F-actin Phalloidin staining (a) and PI nuclei staining (b). The increase in numbers suggested that the PU does support growth and proliferation of BIPE, but after day 10 overpopulation of cells (indicated by nuclei overlapped) lead to cell detachment and signs of apoptosis (* nuclear content scatter following nuclei enlargement on day 7). Confocal microscope, scale bar: 50μm. Brightness to some of the images was due to substrate's auto-fluorescence.

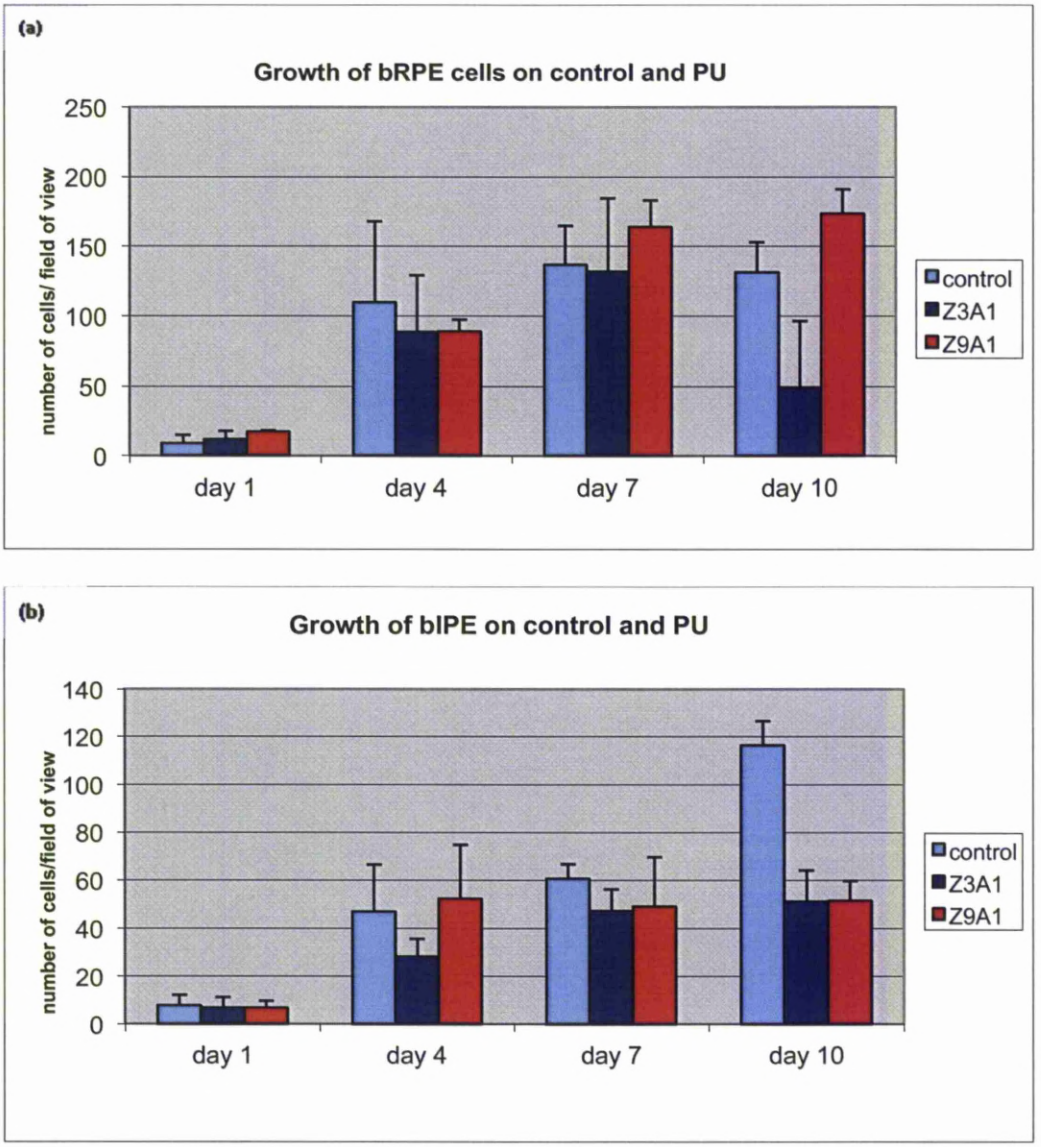

Figure 3-22: Histograms showing the numbers of BRPE (a) and BIPE (b) cells on control (TCPS), Z3A1 film and Z9A1 film, calculated using nuclei number correspond to the observation in Figure 3-20: and Figure 3-21. Statistical analysis using one way ANOVA, n=16, error bar=standard deviation. The graphs suggest that both substrates provide a suitable surface for cell growth. The number of cells decreased by day 10 was due to the fact that cells became overgrown and detached after day 7. There were no significant differences of cell growth on all the surfaces ($p>0.05$).

3.9 Optimisation of cell growth

3.9.1 Seeding density experiments

The experiments were carried out as described in **section 2.9.1**, to determine the optimal seeding densities for the epithelial cells. Different seeding numbers were used on the tissue culture polystyrene (TCPS) 24-well plate. Quantification of cells, by means of counting the nuclear contents of the cells (coloured red in the representative pictures), per field of views was carried out by staining with PI. Both **Figure 3-23** and **Figure 3-24** were representative photographs of nuclear PI staining for BRPE and BIPE at various seeding densities. Crowding and overlapping of nuclei were seen at seeding densities of 5×10^4 and 1×10^5 with signs of apoptosis indicated by arrows (nuclear content leakage with bright pigmented nuclei in the cells). With 1×10^4, homogeneous coverage was seen throughout the surface.

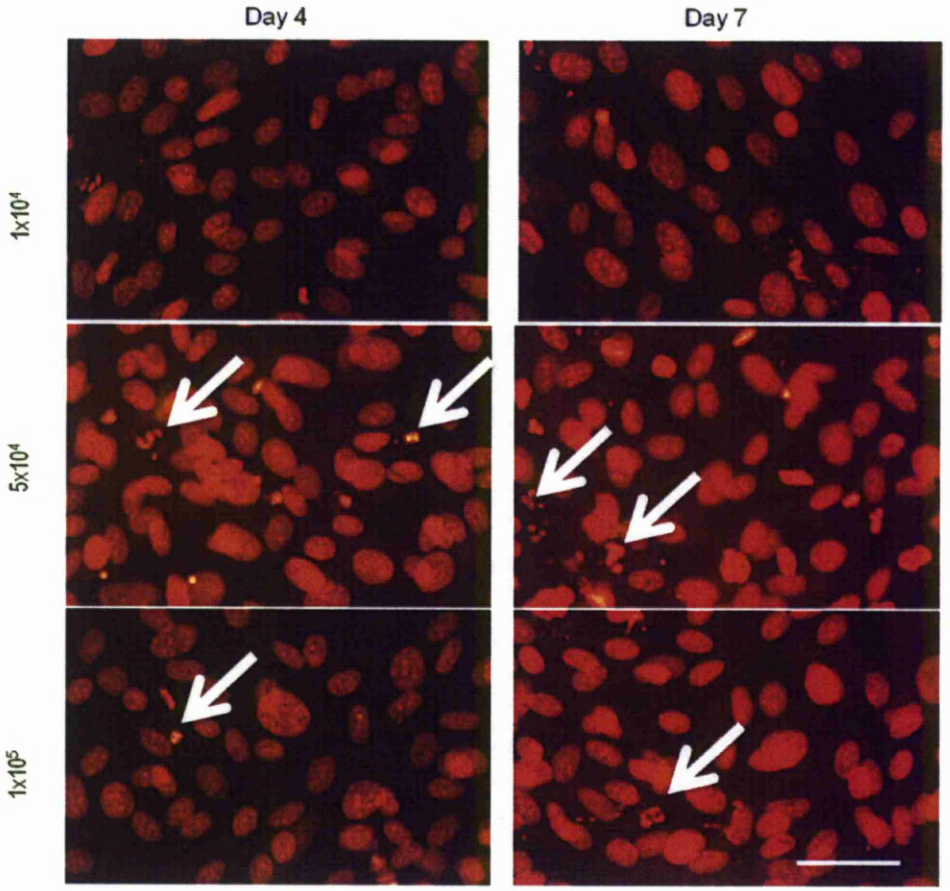

Figure 3-23: Seeding density experiment: Images show BRPE cells on TCPS surface stained with PI nuclei staining, indicating the numbers of cells. Different numbers of seeding per substrate were used on each surface and surfaces were fixed and stained at day 4 and day 7. There were signs of cells overlapping and apoptosis (arrows) with both 5 x 10^4 and 1 x 10^5. Scale bar: 50µm. Brightness to some of the images was due to substrate's auto-fluorescence.

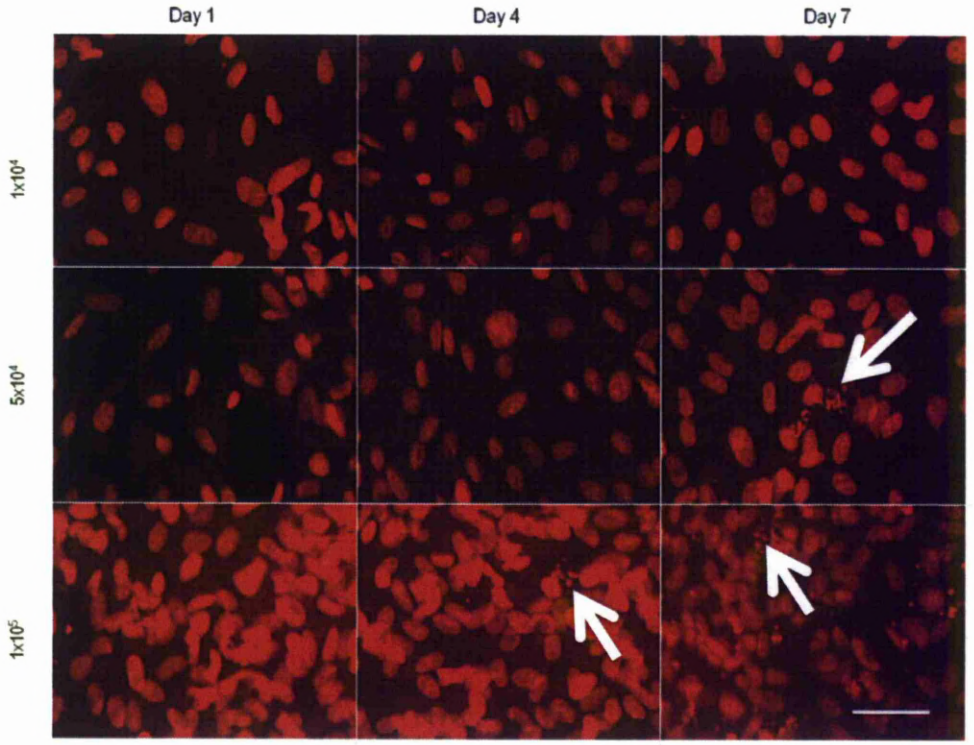

Figure 3-24: Seeding density experiment: Figure show PI nuclei staining of BIPE cells on TCPS surface. Numbers of cells seeding per substrate indicated on the left. Cells were fixed and stained at day 1, 4 and 7. There were signs of cells overgrowth and apoptosis (arrows) with both 5 x 10^4 and 1 x 10^5. Scale bar: 50µm. Brightness to some of the images was due to substrate's auto-fluorescence.

3.9.2 Effect of varying serum concentrations and Retinoic Acid on BRPE and BIPE

Another optimising experiment was to investigate the effect of serum and retinoic acid (RA) addition to the growth condition (as described in **section 2.9.2**). From the experiment, it was found that both BRPE and BIPE showed a limited growth pattern at low serum concentration (1% and 5%) without RA, as represented in **Figure 3-25 (a-b)**. There was little cell attachment plus no growth in low serum concentration with RA supplement (**Figure 3-25c**) and high cell attachment, but with fragmented-looking nuclear content at high serum concentration (20%) with high RA supplement (**Figure 3-25d**). It was found that the best growth and morphology was at higher serum concentration (10% and 20%) and at low serum, as represented in **Figure 3-26**. Some patches showed formation of 'cobble-stone' morphology in cultures with the addition of RA and there were signs of overgrowth at the higher concentration, without the addition of RA. Summaries of the results are shown in **Table 3-4**. These optimised growth conditions (i.e. 20% serum plus 5µM RA) were used to control the monolayer formation of epithelial cells in culture in the subsequent experiments. Patches of good epithelial morphology show that at these optimised growth condition, more investigations needed in terms of harvesting techniques.

Table 3-4: Summary of serum and RA concentration experiment

	Low serum	High serum
No RA	Little cell attachment	Cell overgrowth
Low RA	Little cell attachment	'Cobble-stone' formation
High RA	No growth	Fragmented-looking nuclear

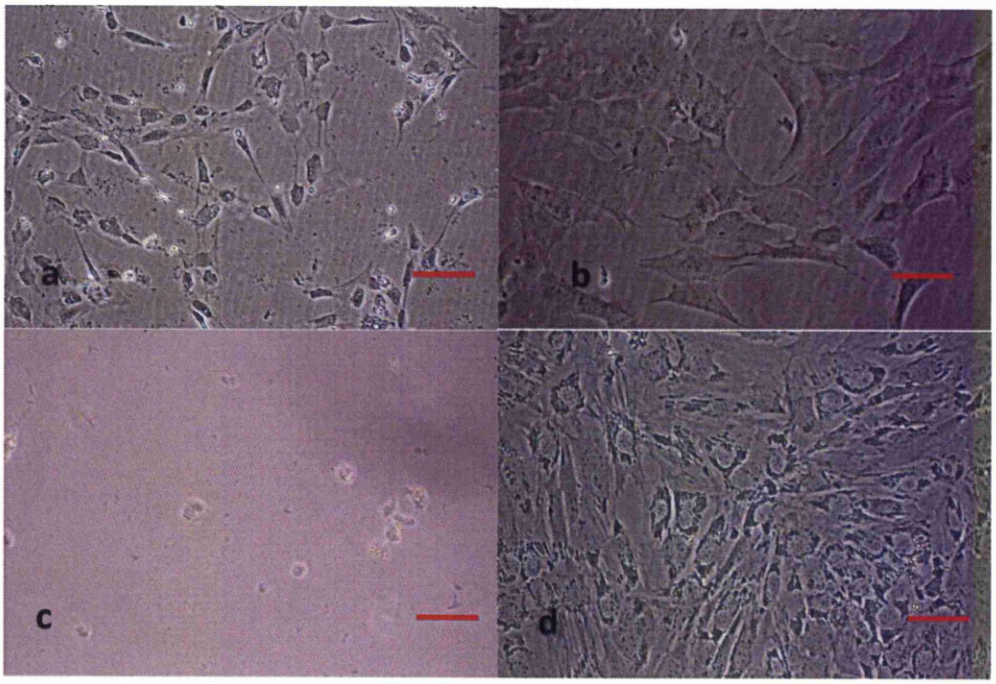

Figure 3-25: Representative pictures of morphology and growth of primary cells at various serum and RA concentration. There was little attachment and growth of BRPE cells (a) and BIPE cells (b) at low serum (1%) and without any addition of retinoic acid. Figures show no growth and very little attachment of BRPE cells at low serum (1%) with RA (10μM) in (c) and show shattered-looking nuclear content of BRPE cells at high serum (20%) and high RA (25μM) (d). All of the pictures were taken at 7 days after seeding. RA was added at day 4. Scale bar 100μm.

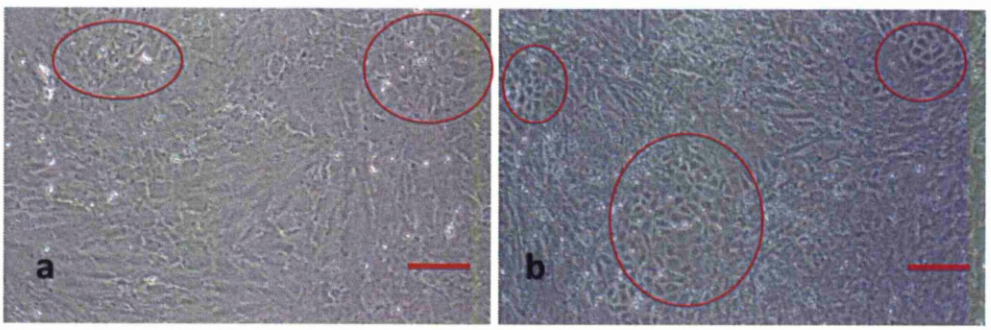

Figure 3-26: Phase contrast micrograph showing primary BRPE (a) and BIPE (b) on control surface with 20% serum concentration with the addition of 5µM RA as seen at day 10. There were some areas of good epithelial morphology (circled). Scale bar 100µm.

3.9.3 Optimising growth of human pigmented epithelial cells

3.9.3.1 Optimisation of growth condition for human IPE (HIPE)

Optimising growth experiments were repeated with HIPE as described in **section 2.9.5**. At day 5, it was found that there were no significant differences observed at all serum concentration, although clumping of cells was seen at 3% serum conc. At day 7, HIPE cells at serum concentrations of 0%, 1%, 2% and 5% became elongated, thin and started to show a reduction in numbers. At 3%, cells demonstrated clumping, overgrowth and did not attach properly to the tissue culture polystyrene (TCPS) base. Cells at 10% and 15%, although showing signs of proliferations, clumped together and did not attach to the base. Cells at 20% showed good signs of

growth and attachment. At day 11, cells showed signs of detachment at 0%, 1%, 2%, 3%, 5% and 10% of serum concentrations. At 15% serum concentration, although cells appear thinner and elongated, they showed good sign of attachment. At 20% serum concentration, although cells showed the 'best' growth, attachment and proliferation, HIPE cells did not resemble the normal morphology of the epithelial cells (see **Figure 3-27**).

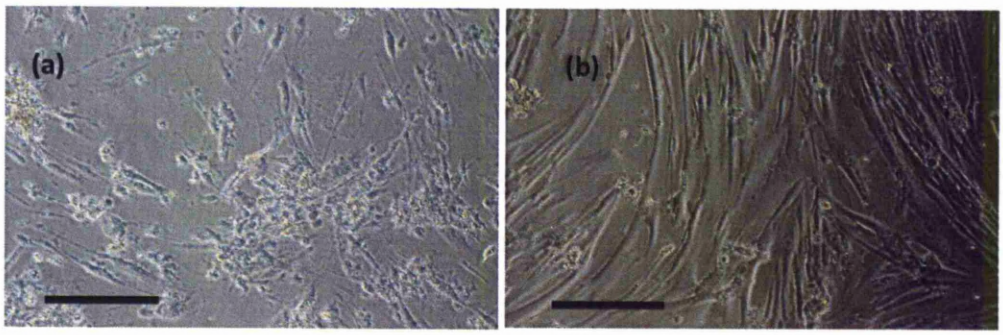

Figure 3-27: Phase contrast showing the difference in morphology between primary HIPE in 0% serum (a) and 20% serum (b) at day 11. HIPE cells clumped together and did not spread in 0% serum but showing thin, elongated morphology in 20% serum. Scale bar: 100µm.

3.9.3.2 Optimising growth condition for HRPE

Using the information obtained from experiments of primary bovine epithelial cells, the same conditions were repeated using HRPE, as in a method described in **section 2.10.2**. RA was added at day 4 as an anti-proliferative agent. Results showed that

HRPE demonstrated good epithelial morphology on all surfaces (control-TCPS, Z3A1 film and Z9A1 film) by phase contrast (**Figure 3-28**). There was good spreading of hexagonally shaped cells with individual borders surrounding each cell.

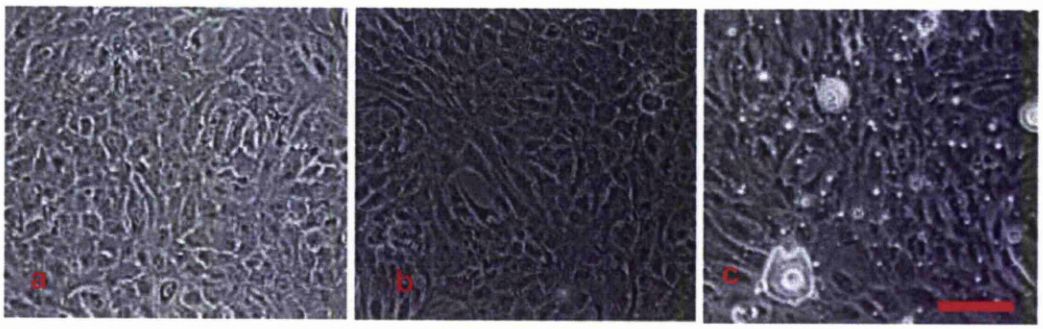

Figure 3-28: Phase contrast micrograph showing the primary HRPE on control (a), Z3A1 (b) and Z9A1 (c) on day 15. The HRPE showed typical cobblestone shape morphology on all surfaces. The white marks on (c) were air bubbles trapped underneath the film substrate. Scale bar 100 µm.

3.9.4 Effect of coating material with fibronectin and laminin

Experiments to investigate the effects of coating the surface with fibronectin and laminin were carried out over the period of 20 days (as described in **section 2.9.3**). The cells morphologies and numbers on the coated surfaces were then examined by phase contrast microscope, at specific time intervals. The initial observation found that the TCPS surface, coated with fibronectin, had a greater number of cells attached in comparison to the non-coated surface and laminin-coated, but these

differences were less apparent with time, from day 5 onwards (see **Figure 3-29**). By the time the cells reached full confluence, there were no apparent differences in terms of morphology of the cells on all surfaces (**Figure 3-30**).

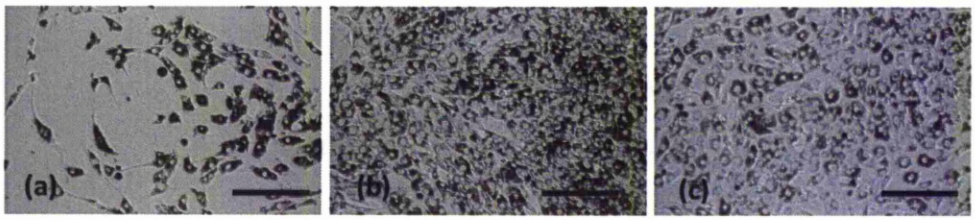

Figure 3-29: Phase contrast demonstrated pictures of primary BIPE grown on normal TCPS on day 5, (a) non-coated, (b) fibronectin-coated and (c) laminin-coated. There was more cell attachment on fibronectin-coated surface at this time point. Scale bar: 100μm.

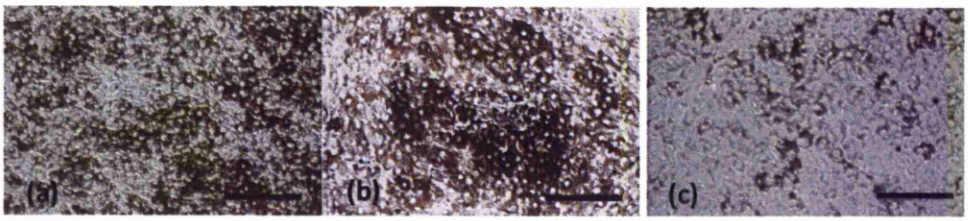

Figure 3-30: Phase contrast showing representative picture of primary BIPE grown on normal TCPS on day 13, (a) non-coated, (b) fibronectin-coated and (c) laminin-coated. The differences in morphologies and cell attachment on all surfaces were less apparent at this time. Scale bar: 100μm.

Another equivalent experiment was conducted for substrates (Z3A1 and Z9A1 films) surfaces. Similar observations were also detected with the non-coated, the fibronectin-coated and the laminin-coated of both substrates; Z3A1 film and Z9A1 film (**Figure 3-31**). The cells grew on all the surfaces at a different speed, i.e. initially quicker on the fibronectin coated but show no apparent difference in morphologies and cell numbers on all of the surfaces when the BIPE cells reached full confluence. Similar patterns of growth and observations were found when the experiments were repeated with BRPE cells.

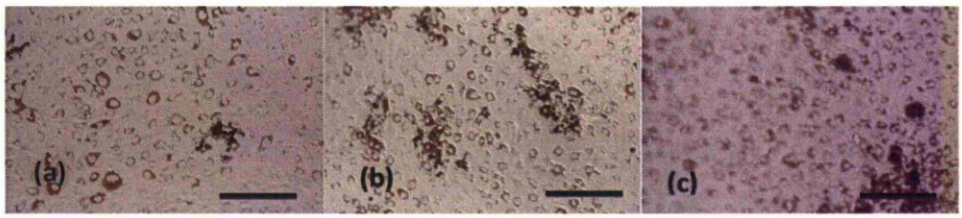

Figure 3-31: Phase contrast micrograph showing representative picture of primary BIPE grown on Z3A1 on day 19, (a) non-coated, (b) fibronectin-coated and (c) laminin-coated. There were no marked differences between all of the surfaces. Some surfaces were out of focus due to the unevenness of the substrates. Scale bar: 100µm.

The substrates were further analysed for their morphologies, using phalloidin and DAPI staining. The findings were in agreement with the phase contrast observations; there were no marked differences in the morphologies of cells in the fluorescent staining. The nuclei were distributed evenly throughout the surfaces, confirmed by the blue DAPI staining. The green-labelled F-actin stress fibre belts

were seen surrounding the nuclei showing typical epithelial cobblestone shape morphology (**Figure 3-32**).

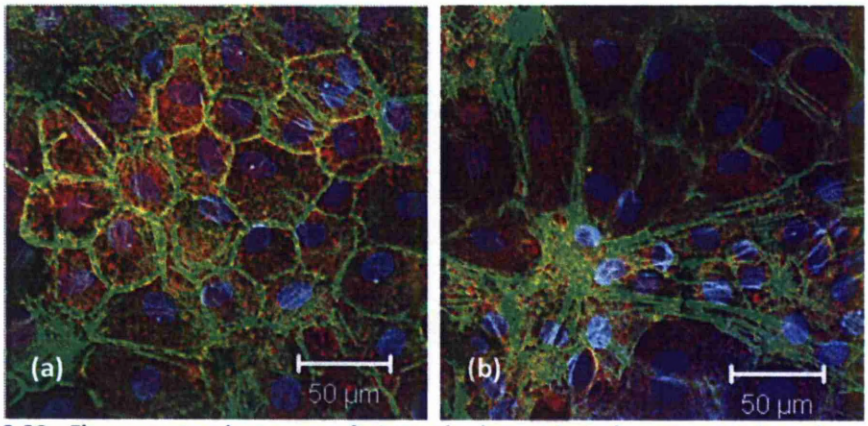

Figure 3-32: Fluorescent microscopy photograph demonstrated representative picture of staining of primary BIPE cells on fibronectin-coated surfaces; (a) on control and (b) on Z9A1. F-actin stress fibres surrounding the DAPI-stained nuclei. The BIPE cells presented as the typical hexagonal 'cobblestone' shape epithelial morphology. Scale bar: 50µm.

3.9.5 Comparing effect of trypsin and collagenase IV enzymes

The effects of trypsin and collagenase type IV enzymes on newly harvested BRPE were investigated by means of the method described in **section 2.9.4**. Results show that with collagenase type IV, more cells attached initially and the cells demonstrated better morphology than the cells harvested using trypsin. Nevertheless, when the cells were fully confluent, there was no significant difference in morphology between the two methods. The cells conformed to the

hexagonal epithelial type morphology, with borders of cells clearly shown under phase contrast microscopy (**Figure 3-33**).

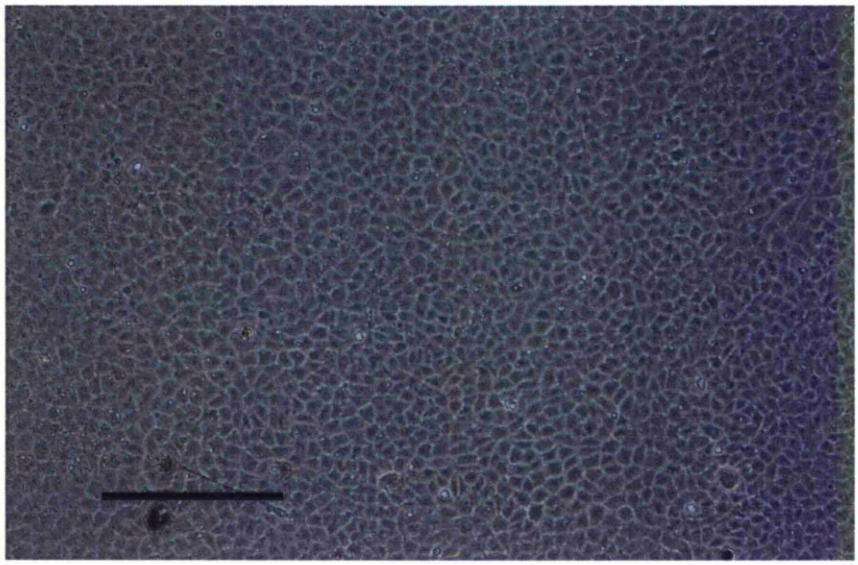

Figure 3-33: Phase contrast image shows a nice formation of hexagonal morphology of BRPE when harvested using Collagenase type IV at full confluence (Passage 0). Scale bar: 100µm.

3.10 Growing cells on polyurethanes films

3.10.1 Growing BRPE and BIPE on polyurethane films

BRPE and BIPE cells were grown on control (TCPS) and on substrate (Z3A1 and Z9A1 films) and as described in **section 2.10.1**, demonstrated uniform distribution of nuclei, as indicated by DAPI blue stains, hexagonal formation of F-actin stress fibres, as indicated by green phalloidin staining and the expression of Zona-Occuden-1 junctional protein at the borders of the epithelial BRPE cells (**Figure 3-34**) and BIPE cells (**Figure 3-35**). IgG control were carried out as negative staining and confirmed these findings.

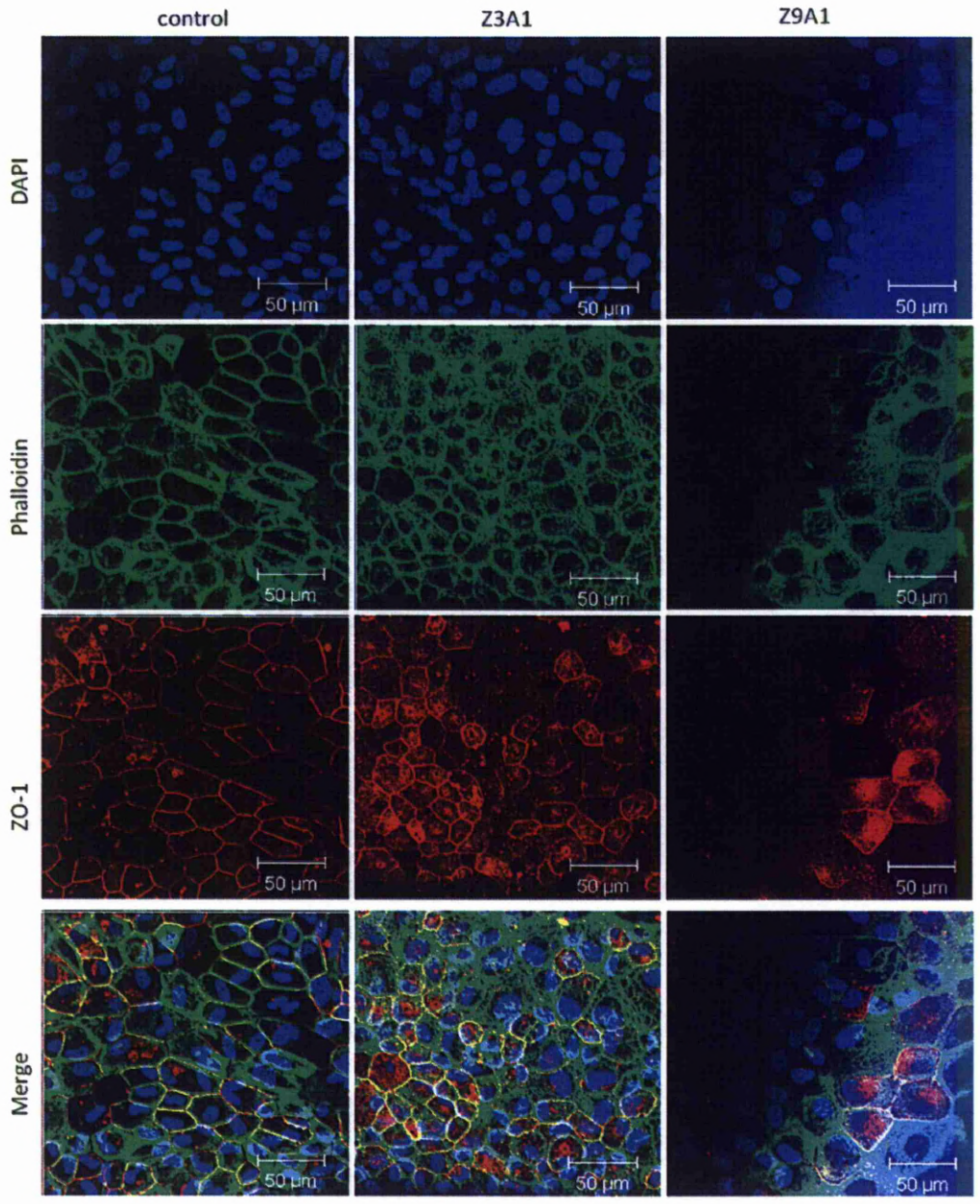

Figure 3-34: Laser confocal microscopy of representative pictures of BRPE grown on control and on film substrates at day 33. Figures show uniform nuclei distributions stained by blue DAPI, typical cobblestone-shaped green F-actin staining and red ZO-1 tight protein junctions. For Z9A1, only parts of the substrate are shown because of the surface irregular depth. Scale bar: 50µm.

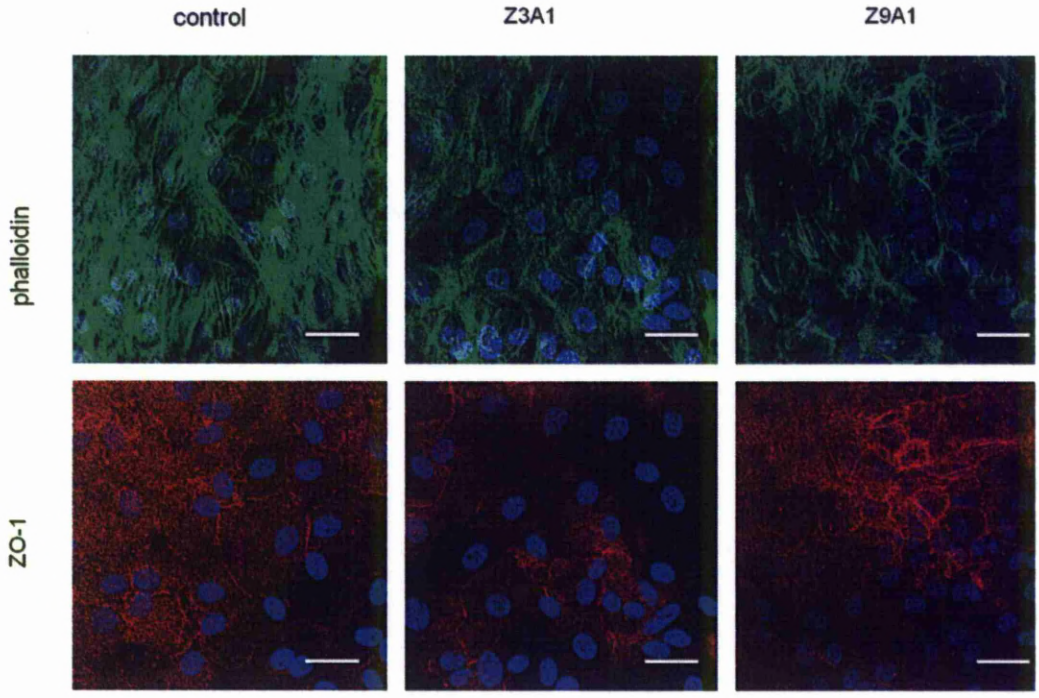

Figure 3-35: Laser confocal microscopy of representative pictures to show growth of BIPE cells on control and film substrate at day 33. Blue DAPI show uniform distributions of nuclei, green F-actin staining around the border of cells and formation of junctional protein ZO-1 indicated by red staining. Scale bar 50μm.

3.10.2 Growing HRPE on polyurethane films

The HRPE cells were plated and maintained on the PU films and TCPS control (as described in **section 2.10.2**). After Day 20, the cells were fixed and stained according to the procedures in **section 2.6**. Results show that HRPE express their normal morphology and characteristic epithelial behaviour when attached to the

PU films and TCPS control. A good monolayer formation could be seen in some areas on all surfaces. Staining procedures on the samples demonstrated good spreading of HRPE on all surfaces, as indicated by blue DAPI staining, with evidence of formation of Zona-occluden-1 junctional proteins on the cell borders with circumferential F-actin distributions (**Figure 3-36**). Cytokeratin examination confirmed their epithelial phenotype on both control and substrates (Figure 3-37).

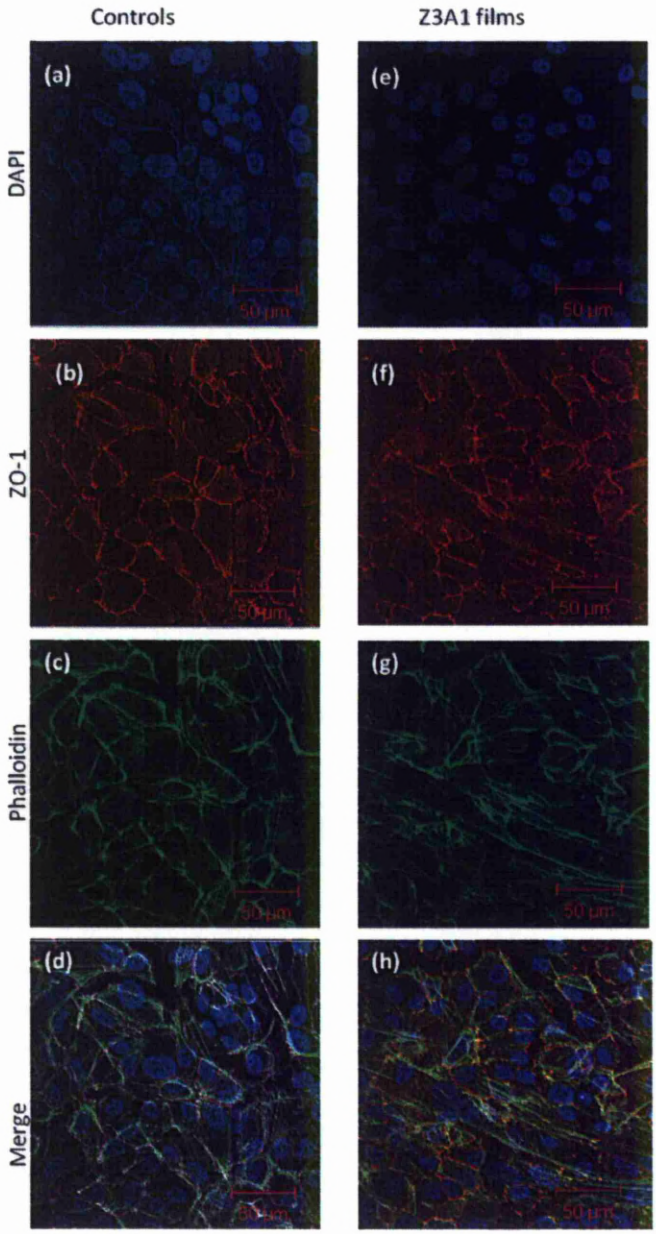

Figure 3-36: Laser confocal microscopy of representative pictures of HRPE on (a-d) tissue culture polystyrene (control surface) and (e-h) Z3A1 film, at day 20 shows cell nuclei distribution (blue staining: a & e), formation of junctional protein (Zona-occludin-1 stained red: b & f), actin distribution surrounding at the border (green staining: c & g) and all images merged (d & h). Scale bar 50 µm.

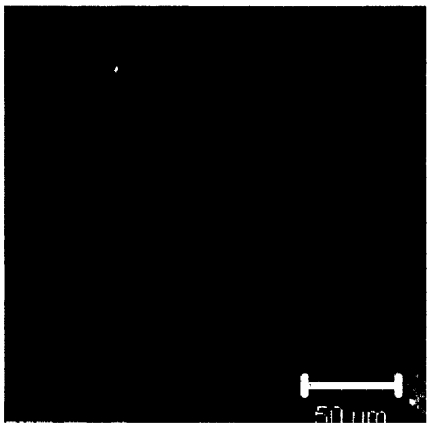

Figure 3-37 Laser confocal microscope shows Cytokeratin (red) expression and nuclei (blue) on Z3A1 at day 20 suggest that the cells do not change in their phenotype when attached to Z3A1. Scale bar: 50µm.

3.11 Growing cells on porous PU

3.11.1 On PU formed by freeze drying

Primary BRPE and BIPE cells were grown on porous PU (Z3A1) and were regularly checked using the phase contrast microscope for determination of growth or signs of infections. The opacity of the porous PU rendered it difficult to observe the growth of cells. Growth of neighbouring cells on TCPS control surface was used as a guide to ascertain the proliferation of cells. Nevertheless, some cells could be seen

by the phase contrast microscopy to a certain degree, although it was not sure if the cells were on the top or underneath the substrate (**Figure 3-38**).

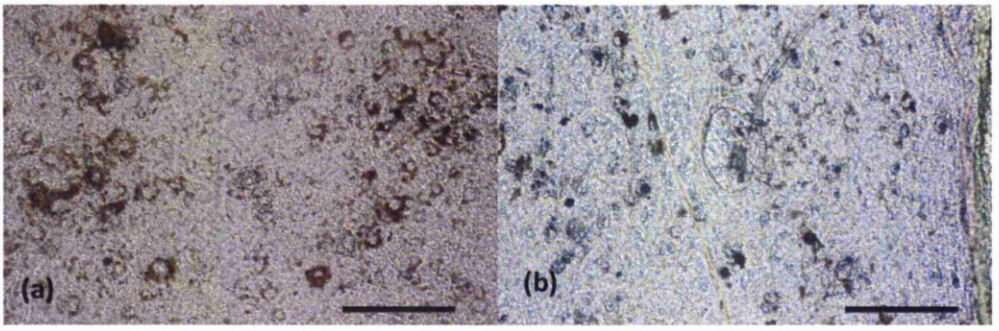

Figure 3-38: Phase contrast photographs of primary BRPE (a) and BIPE (b) grown on porous PU formed by freeze drying at day 33. At this stage, it could not be confirmed if the cells grew on the material or behind them. Scale bar: 100μm.

When the cells reached full confluence, they were fixed and stained. Fluorescent antibody staining revealed that the cells did not grow on the porous PU formed by freeze-drying, as the pore sizes were too large (**Figure 3-39**). When the microscope changed its focus distances, nuclei were seen underneath the substrate (**Figure 3-40**). Some of the cells had crescent shapes, suggesting that they might have been growing within the pores.

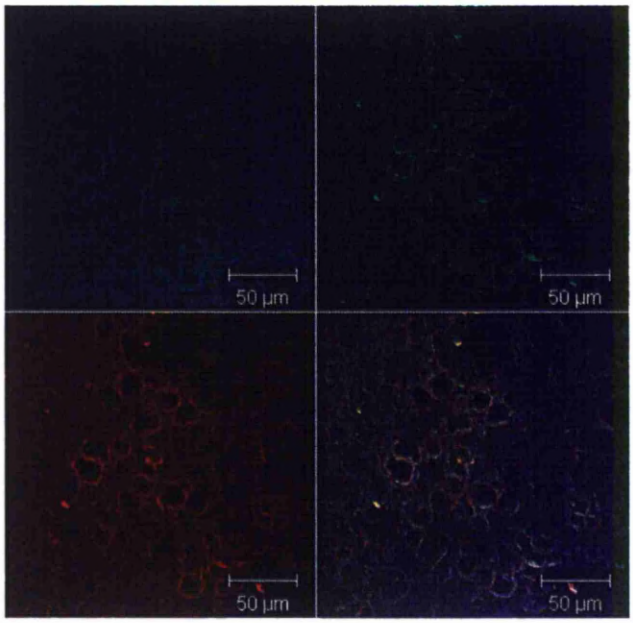

Figure 3-39: Results of the antibody staining via a laser confocal microscopy. No cells can be seen growing on the substrate. The pores of the substrate can be seen clearly in the picture, some with sizes bigger than 10µm. Scale bar: 50µm.

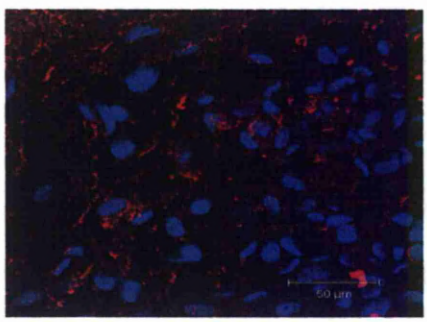

Figure 3-40: Fluorescent microscopy showing the distribution of cells (as indicated by DAPI nuclear stains) can be seen underneath the substrate when the focusing distance of the microscope was changed. Note that the shape of some of the nuclei as crescent, suggesting that they had grown within the pores. Scale bar: 50µm.

3.11.2 On electrospun PU

ARPE-19 cells were grown onto the porous PU (Z3A1) formed by electro-spinning (as described in **section 2.11.1**). They were fixed and stained when they reached full confluence at day 13. The fluorescent antibody staining demonstrated that the cells were grown successfully on all surfaces with the correct epithelial morphologies. Uniform distribution of cells was seen throughout the control (TCPS) and PU surfaces specified by blue DAPI nuclei staining, formation of F-actin belt surrounding the cells shown by green phalloidin and some very faint expression of ZO-1 junctional protein at the cell borders (**Figure 3-41**) at 13 days. However, when the cells were allowed to grow longer, i.e. up to 38 days, the ZO-1 expressions were seen more evidently (**Figure 3-42**). Cytokeratin antibody staining confirmed that the cells did not change their epithelial phenotype when attached to control and PU surfaces throughout the experiment (**Figure 3-43**). Similar experiments conducted with primary BRPE and BIPE cells on electrospun PU resulted in similar findings (**Figure 3-44**). No positive immunohistochemistry (IHC) was observed with IgG controls.

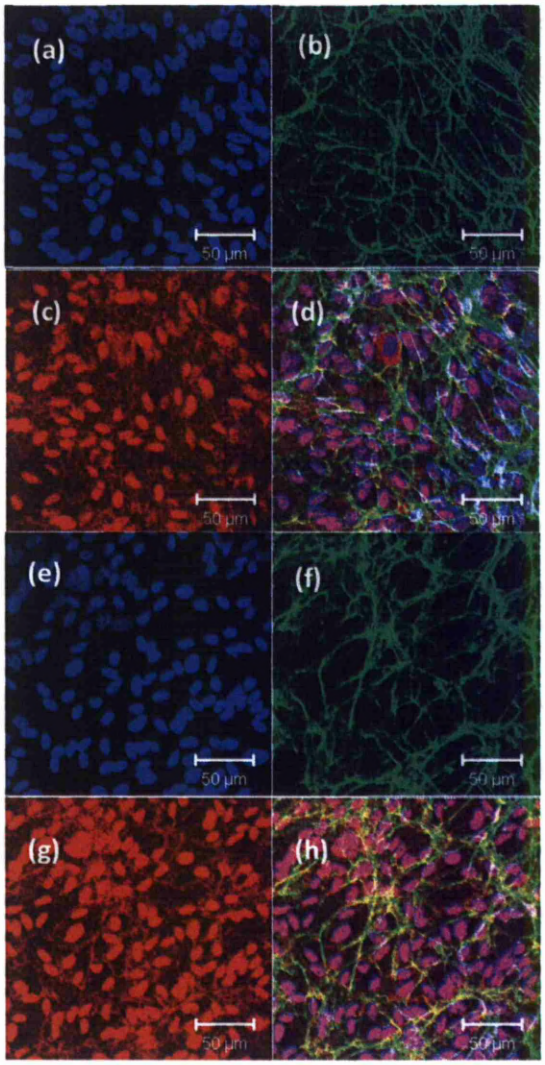

Figure 3-41: Representative picture of fluorescent antibody staining of ARPE-19 grown on TCPS control surface (a to d) and on porous electrospun PU (e to h) fixed on day 13. Uniform cells distribution can be seen on all surfaces (blue DAPI, a & e) and formation of F-actin stress fibre belt (green phalloidin, b & f). Notice the faint expression of the ZO-1 junctional protein surrounding the nuclei (c & g). The combinations of all images are on the far right (d & h). Laser confocal microscope, scale bar: 50µm.

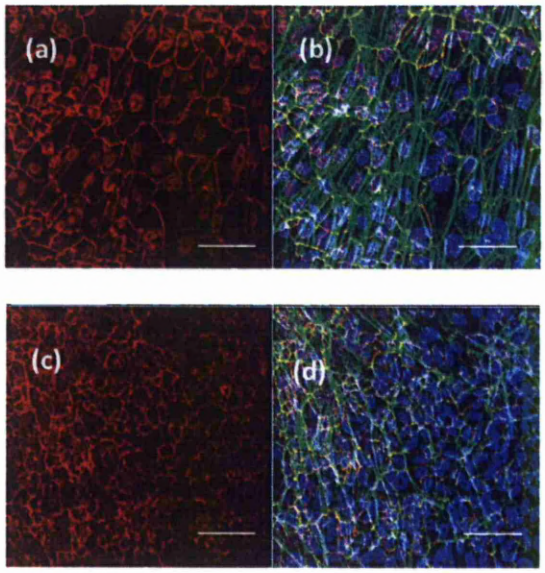

Figure 3-42: Laser confocal microscopy showing ARPE-19 cells grown in the same condition as in Figure 3-41 but left to grow longer, i.e. until 38 days. (a) and (b) ZO-1 expression on TCPS control surface, (c) and (d) on electrospun PU. The ZO-1 expressions were more prominent at this stage of growth. Scale bar: 50µm.

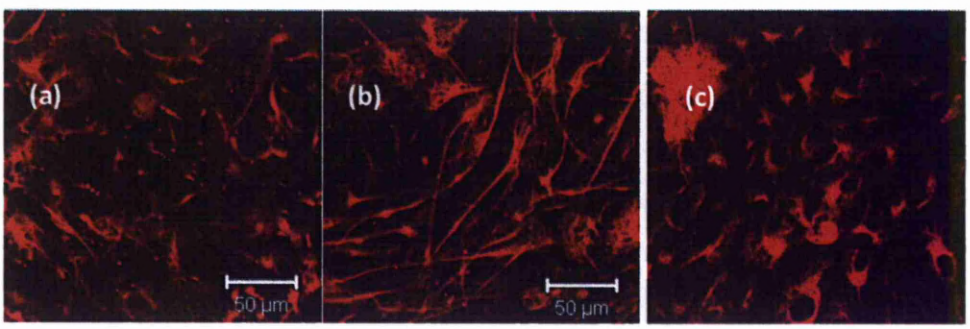

Figure 3-43: Laser confocal microscopy showing representative image of cytokeratin expression of ARPE-19 cells on TCPS control surface (a), on porous electrospun PU (b), at 13 days and on porous electrospun PU at 38 days (c). Scale bar: 50µm.

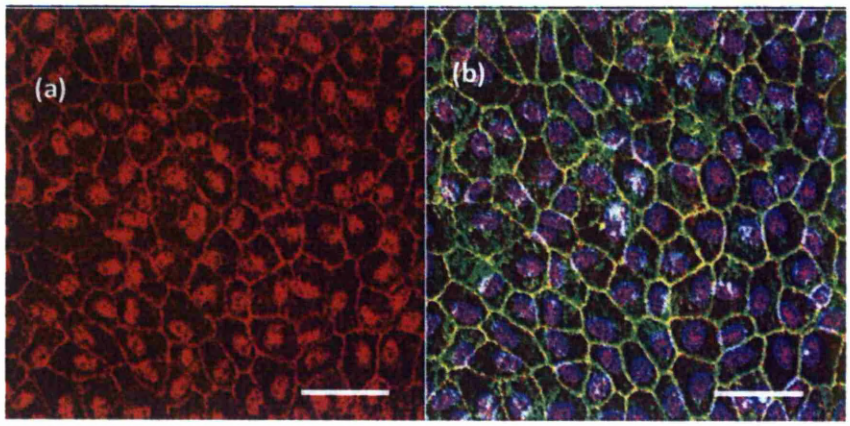

Figure 3-44: Laser confocal microscopy of representative picture of BRPE grown on porous electrospun PU, fixed at day 38, demonstrating ZO-1 junctional protein around the cells border (a), blue DAPI nuclei staining and its surrounding green actin belt (b). Scale bar: 50μm.

3.11.3 On PU formed with icing sugar

Porous Z3A1s formed by oven and icing sugar method (as described in **section 2.1.2.3**) were used as a substrate to grow primary HRPE cells. They were fixed and antibody-stained at day 33. The HRPE cells displayed typical epithelial hexagonal 'cobble-stone' shape morphology on both TCPS control and porous PU surfaces (**Figure 3-45**). There were even distributions of nuclei, as indicated by blue DAPI, with the formation of the f-actin belt surrounding. The formation of ZO-1 junctional proteins was evident at the border of the cells. The number of cells per field of view was lower on the porous PU than on control. The cells also expressed positive

cytokeratin epithelial markers on all surfaces (**Figure 3-46**). The control IgG was negative.

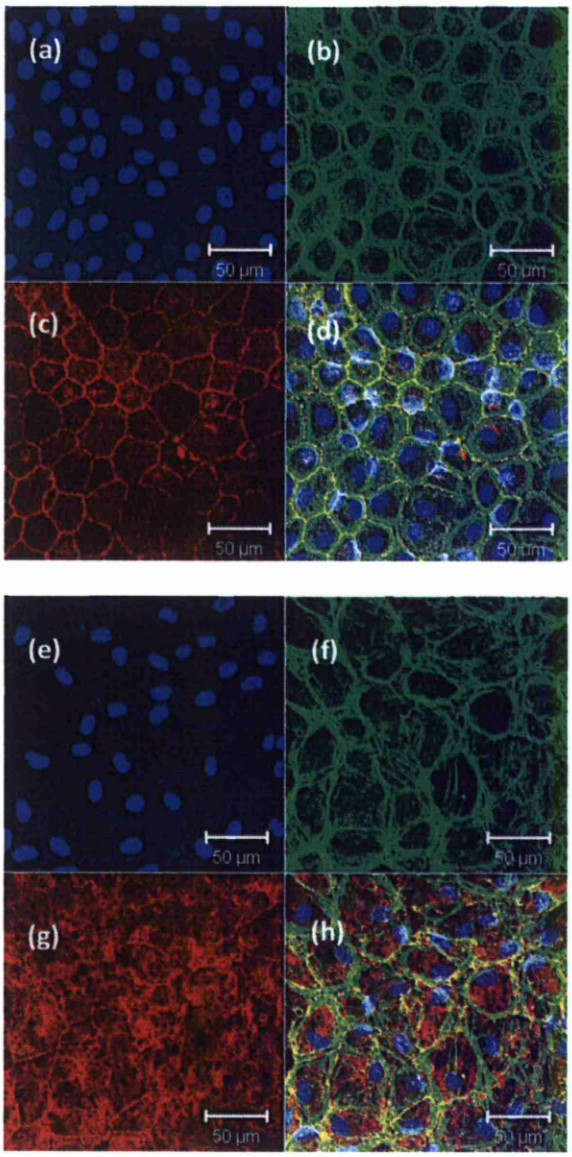

Figure 3-45: Photomicrograph demonstrated representative images of primary HRPE grown on TCPS control (a to d) and on PU formed with icing sugar (e to h) fixed at day 33. Cells showed uniform nuclei distribution (blue DAPI, a & e), F-actin fibres in typical hexagonal cobble-stone epithelial morphology (green phalloidin, b & f), evidence of ZO-1 junctional protein at cell border (red, c & g) and the merge of all staining in (d) and (h). Note that the nuclei number per area is lower on the porous PU. Scale bar: 50µm.

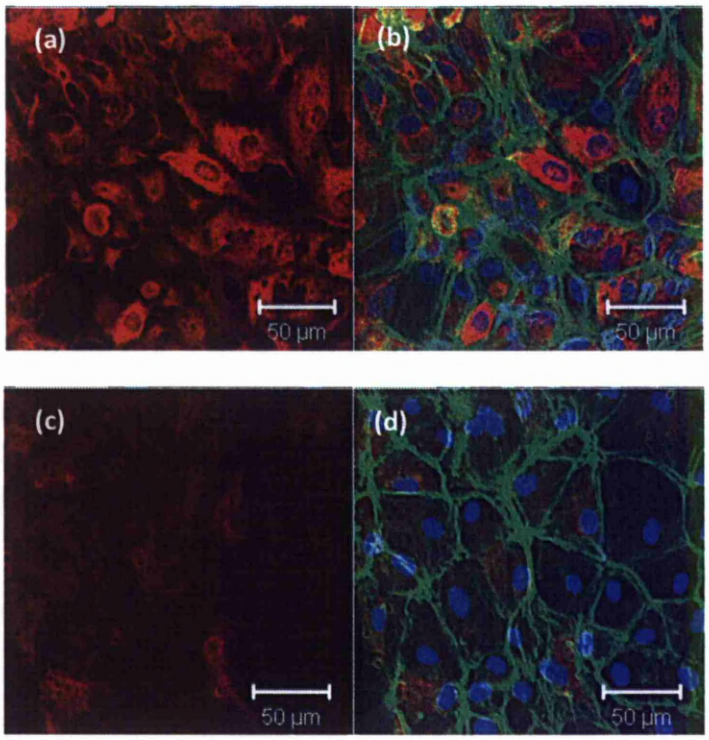

Figure 3-46: Representative images of primary HRPE's expression of cytokeratin markers when they attached on control surfaces (a & b) and on porous icing sugar PU (c & d) at day 33. Blue DAPI nuclei staining, green phalloidin actin fibres. Scale bar: 50µm.

3.12 Functionality test

3.12.1 Phagocytic activity of cells: Retrieval of photoreceptor outer segments (POS)

The orange band formed between the 1.0M and 1.2M sucrose layer (Figure 3-47**a**) as in the retrieval of POS methods (**2.12.1.1**) were collected, suspended in phosphate buffer and viewed underneath a phase contrast microscope (Figure 3-47**b**). Small broken particles could be seen throughout the liquid suspension. Investigations from SNARF-1-labelled POS in different media (as described in **section 2.12.1.3**) showed that there were no colour changes as viewed underneath a fluorescent confocal microscope, when the POS were placed in an acidic or in a basic buffer. Therefore, this labelling technique was abandoned. The isolated POS were then tested with anti-Rhodopsin antibody, conjugated to Fluorescein isothiocyanate (FITC), to confirm their presence (as in explained in **section 2.12.1.4**). The antibody bound to the rhodopsin portion of the POS, thus the fluorescence could be used to mark the presence of the POS. Underneath the fluorescent microscope, the existence of POS could be seen throughout the excised retina (tissue) and in the isolated POS (**Figure 3-48**).

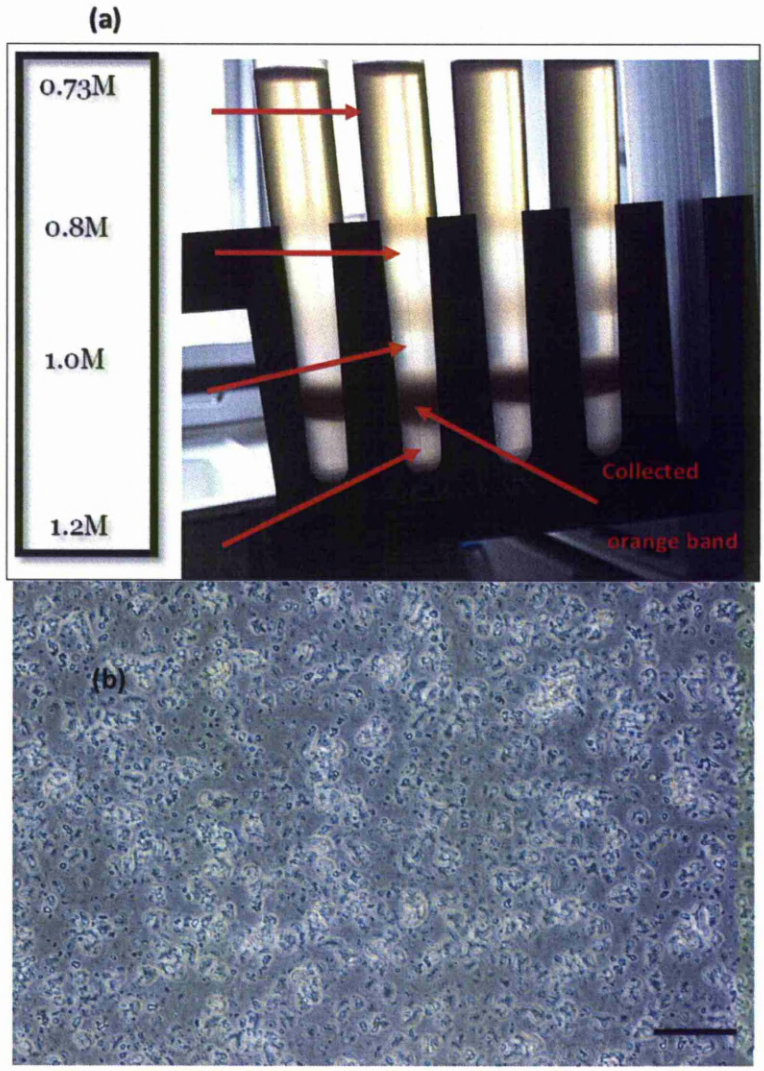

Figure 3-47: The location of the orange band where the POS were collected (a). The POS was pipetted off from sucrose density layer of 1.0M and 1.2M. The isolated POS suspended in phosphate buffer, viewed underneath a phase contrast microscope (b). They were seen as small broken particles. Scale bar: 100μm.

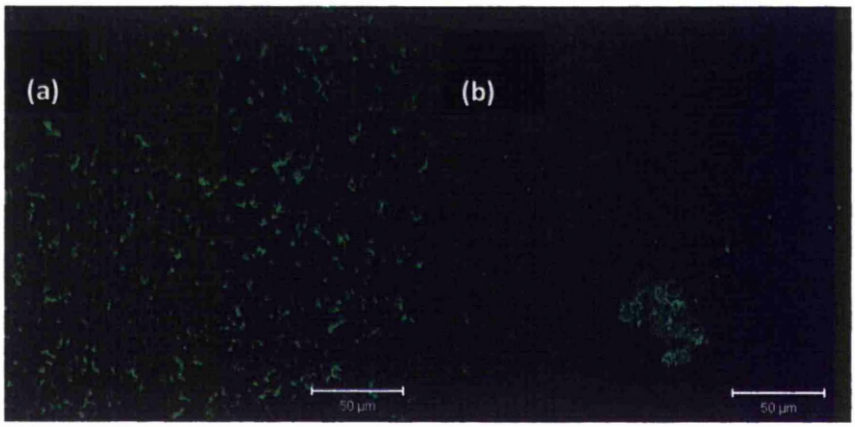

Figure 3-48: Confirmation of the presence of Rhodopsin in the retina (a) and in the isolated POS (b). The FITC-labelled anti-rhodopsin antibody bound to the rhodopsin portion of the POS. Therefore, the fluorescence was used to mark the presence of POS. Laser confocal microscope, scale bar: 50µm.

3.12.2 Phagocytic activity of cells: Phagocytosis of POS

The experiment was conducted to investigate the phagocytosis behaviour of the cells. The HRPE cells were grown on TCPS control and on the porous PU surfaces until they reached full confluence by day 11. They were then challenged with POS and fixed at 3 hours and 24 hours as described in **section 2.12.2**. The nuclei were stained with blue DAPI, and the fluorescently labelled POS, green (**Figure 3-49**). The effects of bound un-ingested POS have been removed by trypan blue and so the green label indicated the ingested POS. The number of 'green particles' per field of view were quantified and represented graphically in **Figure 3-50**. Data was tested for normality and investigated for statistical significance using the Student's t test.

Numbers of sample, n=16, error bar=standard deviation, p<0.001. The numbers of POS ingested increases with time on both control (TCPS) and on porous PU. More numbers of POS were ingested by the HRPE on the porous PU than by the HRPE on TCPS. Notice that the numbers of cells on the porous PU were less than on control; an observation repeatedly recorded in the studies. IgG staining was negative.

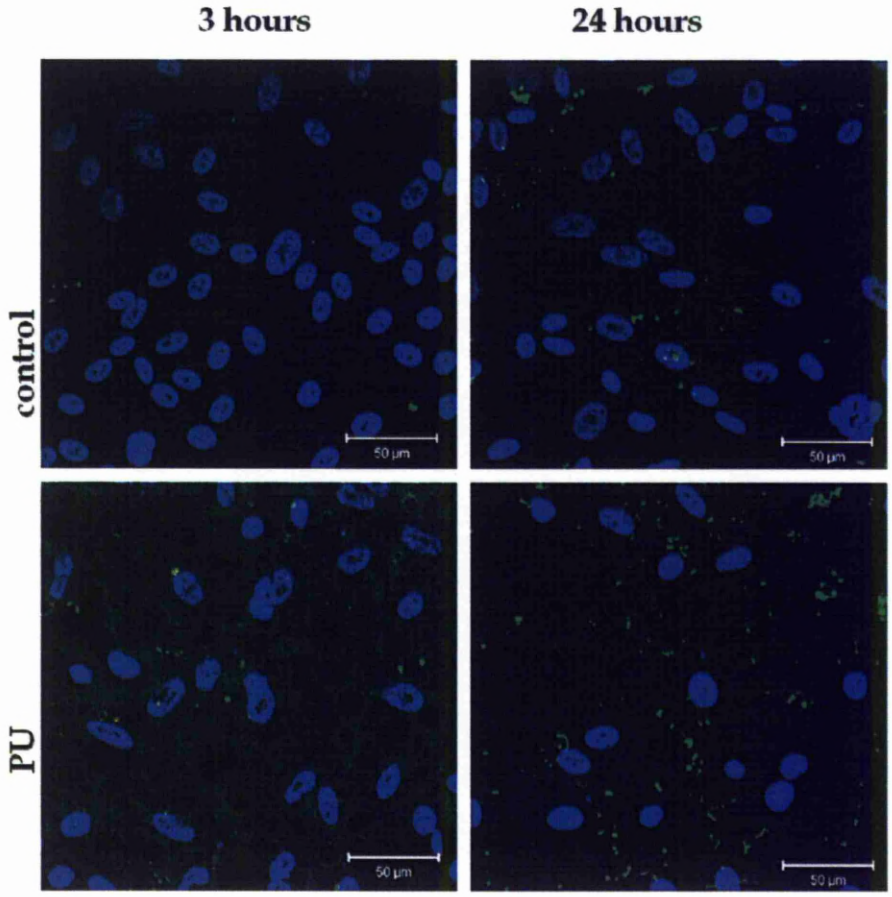

Figure 3-49: Representative images of phagocytosis of POS experiment using laser confocal microscopy. HRPE cells were grown on control and porous PU surfaces, challenged with POS and fixed at 3 hours and 24 hours. The numbers of POS (green particles) increased on both surfaces with more ingested cells on the porous PU. Scale bar: 50µm.

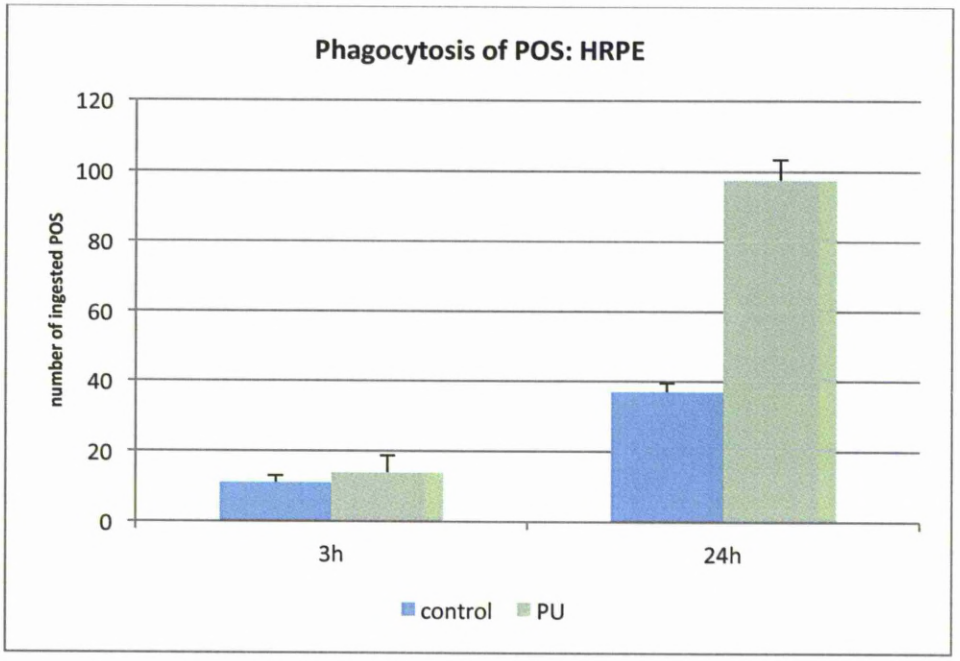

Figure 3-50: Phagocytosis of POS graph. The graph was created from numbers obtained from the captured images, as the numbers of POS ingested per field of view. Data was tested for normality and investigated for statistical significance using the Student's t test. n=16, error bar=+1 standard deviation, $p<0.001$. The graphs demonstrated that the numbers of ingested POS increased with time on both surfaces. Note that the numbers of ingested POS were significantly higher with HRPE grown on porous PU.

3.12.3 Phagocytic activity of cells: Exclusivity of phagocytic activity of epithelial cells

In this experiment, HRPE cells were grown on TCPS control and porous PU, until they reached full confluence and challenged with either fluorescently labelled POS or polystyrene beads (PB). They were then treated with either αVβ5 antibody to block αVβ5-integrin or with IgG as control. The methods were described in **section**

2.12.4. The numbers of ingested POS or PB, which were calculated per field of view, were represented in **Figure 3-51** and a graph was constructed (Figure 3-53). Data was tested for normality and investigated for statistical significance using a one-way analysis of variance (ANOVA) and were reported as mean value + standard deviation (SD). A p-value of less than 0.001 ($p<0.001$) was considered to be significant. The nuclei distributions were indicated by the blue DAPI staining. From the graph, it was demonstrated that the numbers of ingested POS increased after 24 hours on both control and porous PU surfaces, but the uptake was significantly reduced, when blocked with αVβ5 antibody ($p<0.001$). This suggests that αVβ5 demonstrated inhibitory effect on POS ingestion and this effect was more prominent on the porous PU than on control surface. As for the PB (represented by **Figure 3-52**), it was shown that the numbers of PB were increased on both surfaces after 24 hours, but there were no significant reduction in the ingestion, when the surface was blocked with αVβ5 antibody ($p>0.001$). The numbers of ingested PB did not show much difference on porous PU between 3 hours and 24 hours. This suggested that it might have reached its maximum ingestion by 3 hours. Note the scale differences between the two graphs (POS ingestion and PB ingestion graphs) and the reduced numbers of nuclei per field of view for porous PU surfaces. These findings implied the selective inhibitory effect of αVβ5 on POS ingestion. Negative staining was carried out throughout the experiment as control to justify the results.

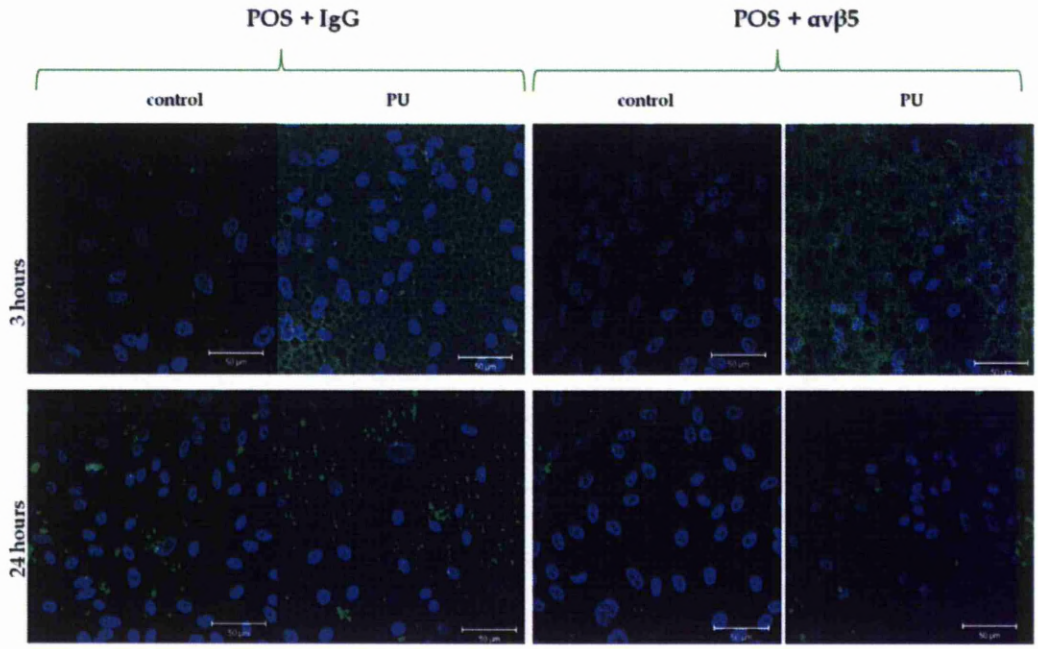

Figure 3-51: Representative images of selectivity of phagocytosis experiment by laser confocal microscope. The numbers of green POS ingested, increased with time for both control and porous PU surfaces, but there was a significant reduction of ingested POS for both surfaces when blocked with αVβ5 antibody. Note that the number of cells per field of view was less on the porous PU than on control. Scale bar: 50μm.

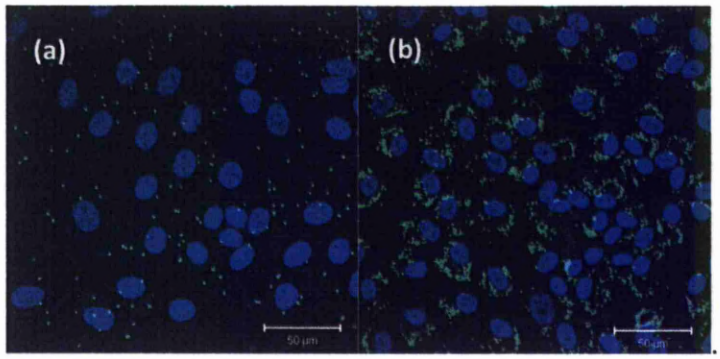

Figure 3-52: Representative images of HRPE cells fed with PB on control surfaces at 3 hours (a) and at 24 hours (b). Scale bar: 50μm

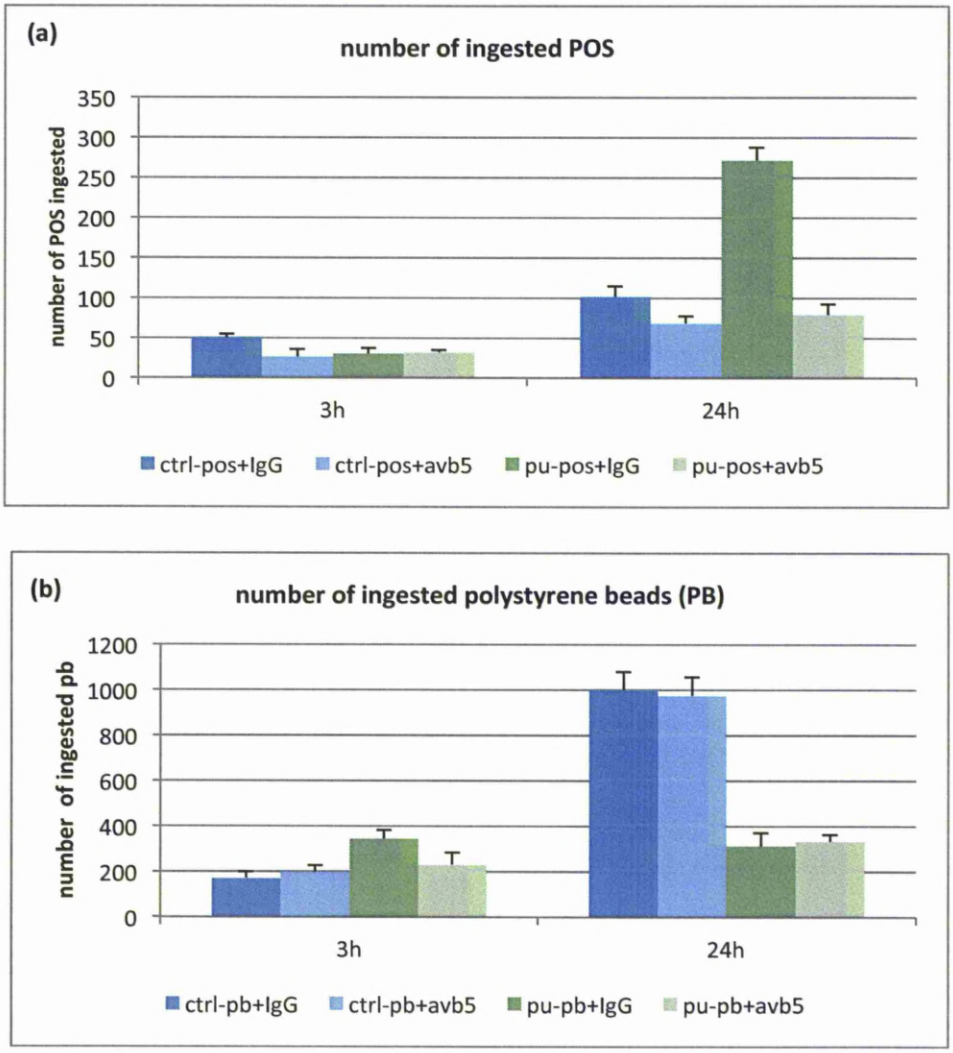

Figure 3-53: Histograms of selectivity of phagocytosis experiment. Data was tested for normality and tested for significance, using one-way analysis of variance (ANOVA). From graph (a), the number of ingested POS increased for both surfaces, but the uptake was significantly reduced when blocked with αVβ5 antibody ($p<0.001$). This reduction was more prominent on porous PU. Graph (b) showed that the number of ingested PB increased for both surfaces (but a small increment on porous PU) but their ingestions were not affected by blocking with αVβ5 antibody ($p>0.001$). Note the difference in scale between the two graphs a and b. n=32 for each graph, data was presented as mean value + 1SD.

3.12.4 Dextran transport studies

3 dextrans with different sizes were used in this experiment, blue 10kDa, green 70kDa and red 155kDa. The methods for this experiment were described in **section 2.13**.

3.12.4.1 Optimising dextran

Several experiments were carried out to optimise the concentration of dextran to be used with our cell culture. After establishing the linear range of dextran (**Figure 3-54**), the differently coloured dextrans were mixed together to ascertain that they would not be affected in readings under different wavelengths (Figure 3-55). Standard curves were calculated for each of the dextrans.

Results of standard curves for each dextran:

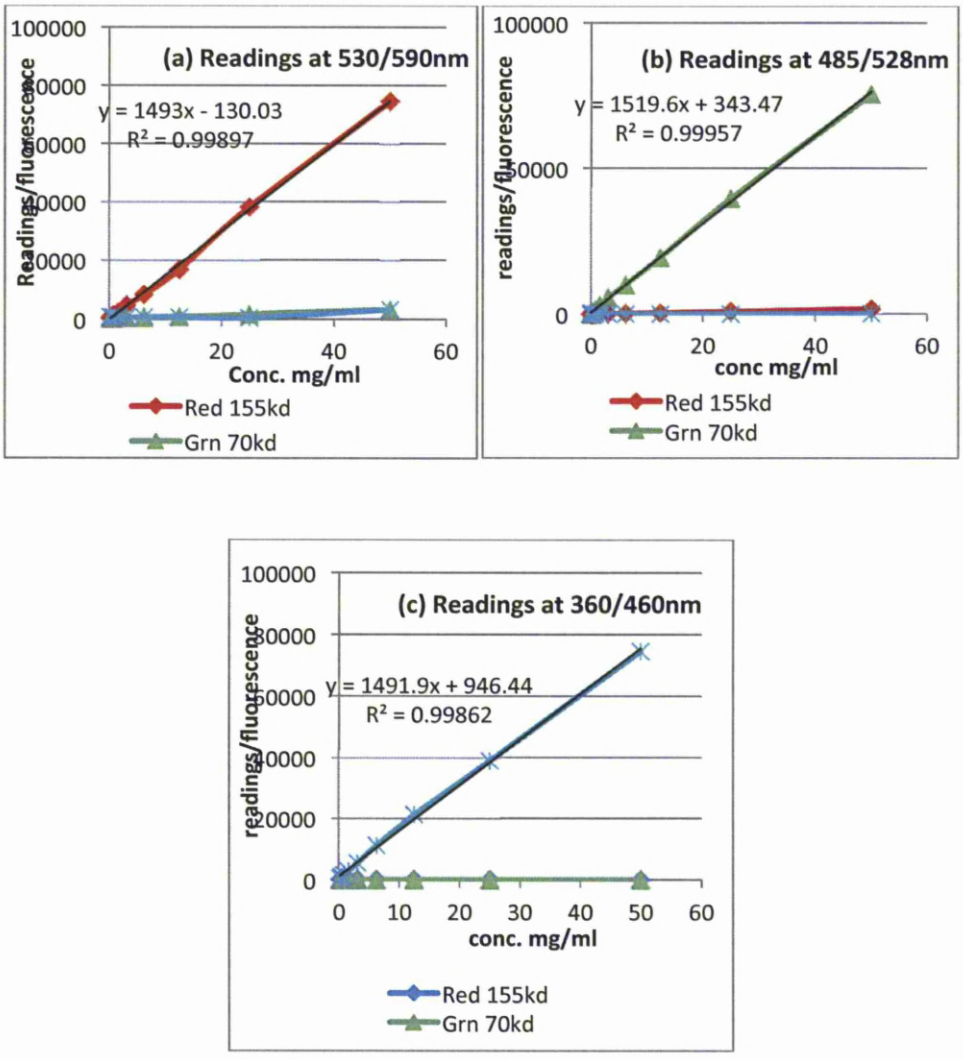

Figure 3-54: Scatter graphs of experimental results of finding the linear range of each dextran; (a) red 155kDa dextran under 530/590nm, (b) green 70kDa under 485/528nm and (c) blue 10kDa under 360/460nm wavelength. The linear range for all the dextrans to be used in this experiment was confirmed to be between 0 to 50 mg/ml.

Results of standard curves for mixtures of dextrans:

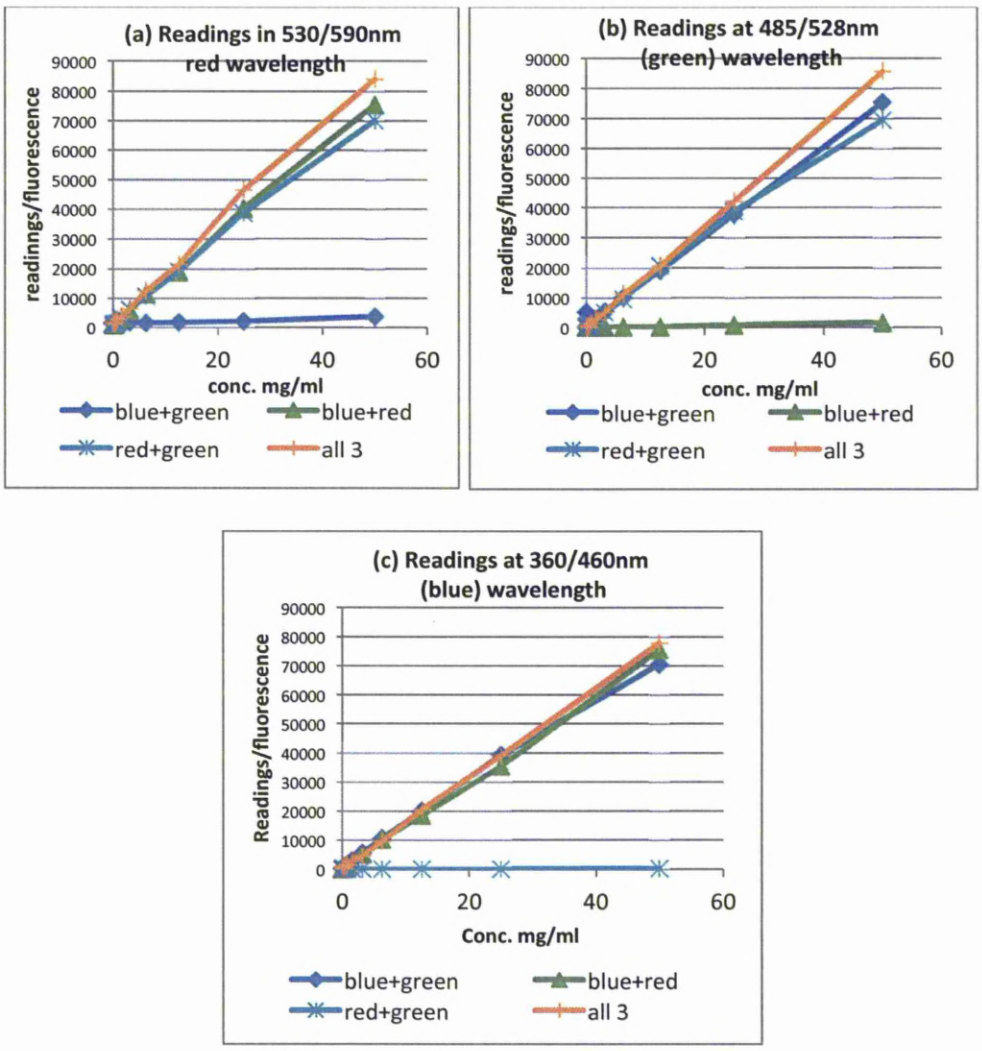

Figure 3-55: Scatter graphs of the dextrans when they were mixed with each other and their readings under different wavelengths; (a) under 530/590nm, (b) under 485/528nm and (c) under 360/460nm. The data shows that the readings of each individual dextran would not be affected when they were mixed with each other.

BIPE cells were cultured on porous and non-porous substrates, adhered to a cloning ring as explained in the method section **2.13**. After the labelled dextrans were added into the sample, diffusion of dextrans was measured by drawing 50µl sample from outside the cloning rings, at set time intervals, and the fluorescence readings were taken. Results were presented as a scatter line graph showing the cumulative amount of dextran collected as a percentage of the initial concentration vs time as displayed in **Figure 3-56**.

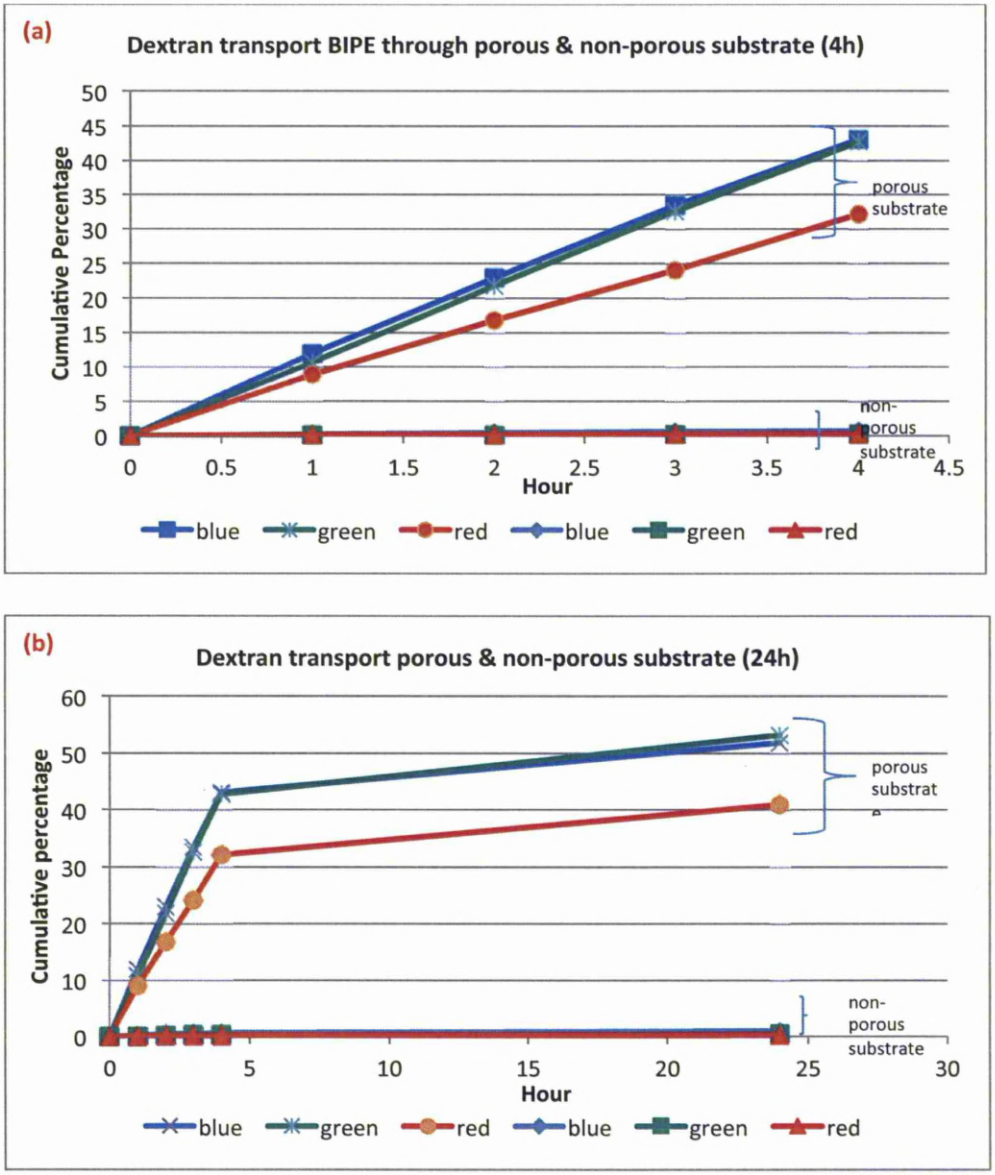

Figure 3-56: Scatter graphs showing dextran transport assay of BIPE grown on porous and non-porous substrates for 48 days. Different sizes of dextrans were used, blue 10kDa, green 70kDa and red 155kDa. The graphs show cumulative amount of dextran collected as a percentage of the initial concentration vs time, 4 hours in (a) and 24 hours in (b). Non-porous substrates act as control. It can be seen from the graphs that the smaller sizes dextran passed through the membrane quite easily compared to the 155kDa dextran.

The graphs illustrated that the transport of dextran across the epithelial cell containing monolayer, was size dependent. There were no significant differences between the readings of 10kDa and 70kDa dextran, suggesting that the gap junctions might have been bigger than both of the dextrans. The values for dextran crossing the monolayer decreased as the molecular weight increased from 10kDa and 70kDa to 155kDa. The 24-hour time-course studies also demonstrated the similar findings. The ability to transport high-molecular dextran (155kDa) was substantially reduced by 1.3 fold. The presence of the non-porous substrates as control surfaces were to justify that there was no leaks existing between the substrates and the cloning rings.

3.13 *In vitro* injury model experiment

BIPE and BRPE cells were grown until full confluence on TCPS control, Z3A1 and Z9A1 films and were dyed with red cell tracking dye as described in **section 2.14**. They (acting as an implant) were then fused and grown for 3 days onto BRPE cells in a well plate (acting as an implantee), which was dyed green. Results were represented in **Figure 3-57**. There were some mixed outcomes of the result. Some of the cells from the implant were seen to migrate onto the implantee surface (as

seen in **Figure 3-57** (a, b and f)), but in other situations (c, d and e), they remained non-integrated. They were also signs of extra activities or growth at the implantation borders of (a).

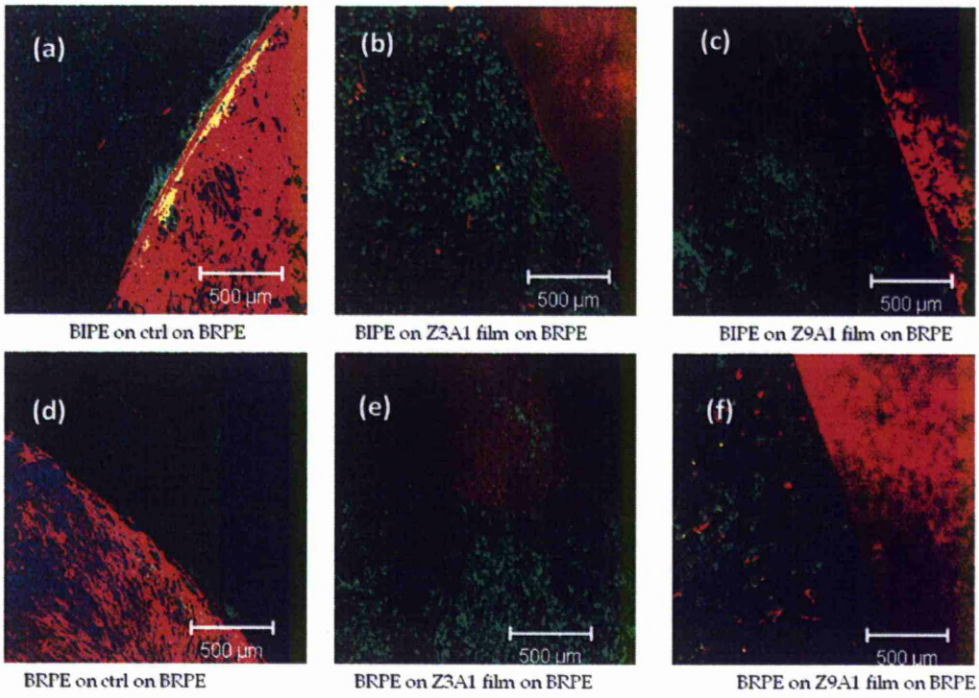

Figure 3-57: Fluorescent microscopy showing *in vitro* injury model experiment of both BIPE and BRPE on films, fused on BRPE in well plates. Cells were grown to 27 days on a separate surface; BIPE or BRPE were grown on TCPS control, Z3A1 and Z9A1 films (as implant) and dyed red, BRPE were grown on TCPS well plate (as implantee) and dyed green. They were fused and cultured together for a further 3 days. There were some signs of cell migrations as in (a), (b) and (f). No sign of integrations could be seen in (c), (d) and (e). There were also sign of activities at the implantation border as in (a). Laser confocal microscope, scale bar: 500µm. Some of the surfaces were out-of-focus due to the different depth of field.

Another similar experiment was repeated using porous PU formed by oven drying & icing sugar (**section 2.1.2.3**). BRPE and BIPE cells were grown onto porous PU for 35 days and were dyed red (as an implant). BRPE cells on the other hand were grown onto TCPS well plates and dyed green (as an implantee). They were then fused and cultured together for a further 3 days as described in **section 2.14**. Results were represented in **Figure 3-58**. The images demonstrated that there were no signs of cell migration or integration on all of the surfaces.

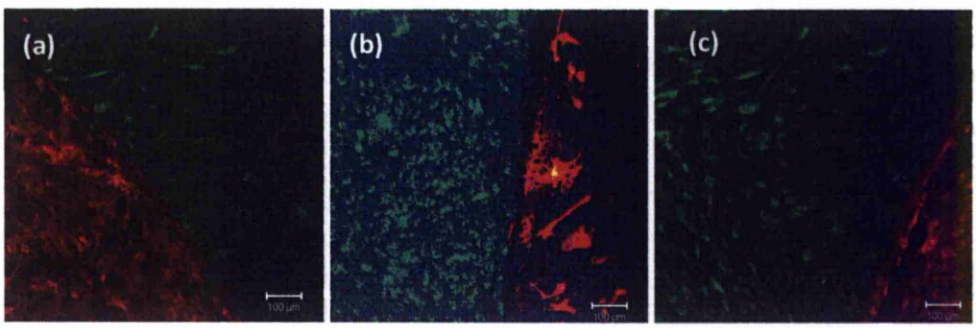

Figure 3-58: Photos of *In vitro* injury model with porous PU. (a) BIPE on TCPS control, (b) BIPE on porous PU, and (c) BRPE on TCPS control. The implants, were dyed red, the implantees were dyed green. Results showed that there were no signs of cell migration or integration. Laser confocal microscope, scale bar: 100μm. Some of the surfaces were out-of-focus due to the different depth of field.

4 CHAPTER FOUR: DISCUSSION

AMD is the main cause of age-related vision loss in the western world[148-149]. Despite this, there are currently no available effective treatments for the majority (90%) of the sufferers, the dry form of AMD.

AMD is characterised by a group of diseases that affects the macula, the central part of the retina, which is responsible for the acute vision. Whilst the disease itself was painless, there was higher incidence of depression within the group as well as a reduction in patients' quality of life, affecting their social health and independence. It was also a burden to the nations at an alarming estimated cost of £16.4 billion (for 10 years projection 2010 to 2020)[150].

The wet AMD is characterised by choroidal neovascularisation (CNV), the formation of blood vessels underneath the macula. Despite the fact that this can be stopped by anti-VEGF (vascular endothelial growth factor) drug, laser photocoagulation, photodynamic therapy or a combination of both, there are limited numbers of positive responses in patients receiving these treatments[151].

The dry form of AMD occurs gradually with the presence of basal laminar deposits, such as drusen, which in large quantities force the layers of the Bruch's membrane (BM) and retinal pigmented epithelium (RPE) apart, causing retinal detachment and

subsequently retinal death. To date, there have been some attempts at a surgical approach for treating patients with dry AMD, such as RPE patch grafting and macula relocation, but these are very delicate and complicated surgery that often leads patients to lose both central and peripheral vision[82]. However, studies have shown that transplantation of RPE allograft resulted in no signs of rejection in the non-exudative AMD. This has provided us with proof of principle for our current research, that replacing diseased RPE with a healthy RPE under the macula could restore some vision.

Some studies have demonstrated that the risk of rejection is greatly reduced, when the patient's own cells were implanted sub-retinally without immuno-suppresence, but the patient's vision did not improved in this case because the cells were in suspension. The cells were shown to form multi-layers and lead to RPE atrophy[152]. Transplantation of cells in suspension has the drawback of poor cell attachment with a low number of cells surviving over a large area of damaged Bruch's membrane. Transplantation of a monolayer of cells organised on a sheet can reduce this risk. Some other researchers have proposed the use of temporary (biodegradable) substrates as a scaffold but this raises a question that in patients whose BM is already damaged by AMD, degrading substrate on which cells sit will not allow enough time for a proper growth, and also the questions of the removal

of the biodegradable waste products. The cells will also not be protected over a long term.

Because of these concerns, this study proposes the use of a suitable non-degradable porous substrate as a supporting membrane. The membrane should allow the growth of a suitable cell, as an intact monolayer, before a sub-retinal transplant. The study asked the following research questions:

1. Can the membrane support attachment, proliferation and growth of epithelial cells?
2. Can the membrane be manufactured into a porous substrate, and can the structure be modified to closely resemble the native BM, so that it can perform the normal BM's function?
3. Can the harvest and expansion of primary pigmented epithelial cells (RPE and IPE*) in vitro* be optimised, and can their growth be controlled?
4. Can IPE behave similar to RPE in its morphologies and functions *in vitro*?
5. Can the primary pigmented epithelial cells (RPE and IPE) be grown onto the porous membrane, while at the same time maintaining their phenotype, cellular expressions and normal functions?

In this section; these questions will be discussed.

There were two main objectives of the research: (1) to prepare a suitable substrate to support the replaced cell and (2) to find a suitable cell source to replace the diseased RPE cells in AMD. In doing so, this study needed to indentify a reliable technique to harvest primary cell source, optimise its growth condition and finally investigate if the cell would carry out normal RPE tasks. As for the case of the substrate, this study investigated how to manufacture it to be the closest match to the native Bruch's membrane in its physical and surface properties, as well as to be able to support the cells with their intended functions.

4.1 The Bruch's membrane properties

The main role of the substrate is to replace the damaged Bruch's membrane (BM). BM is the thin porous membrane that supports RPE cells, separating the RPE cells from the underlying choroid and at the same time allowing exchange of nutrients and waste through passive diffusion (**Figure 4-1**). The BM's extracellular matrix is rich in elastin and collagen. With advancing age, the thickness, the elastic property and the hydraulic permeability of the BM changes, causing it to be ineffective in its role of permitting diffusion of nutrients and waste. These cause accumulations of basal laminar deposits, such as lipofuscin and drusens, which can aggregate

underneath the RPE cells and force the layers between the RPE and BM apart. The RPE cells devoid of nutrients became susceptible to invading neovascularisation, which often causes blood leakage (CNV). An accumulation of several other factors plus these then causes the development of the AMD.

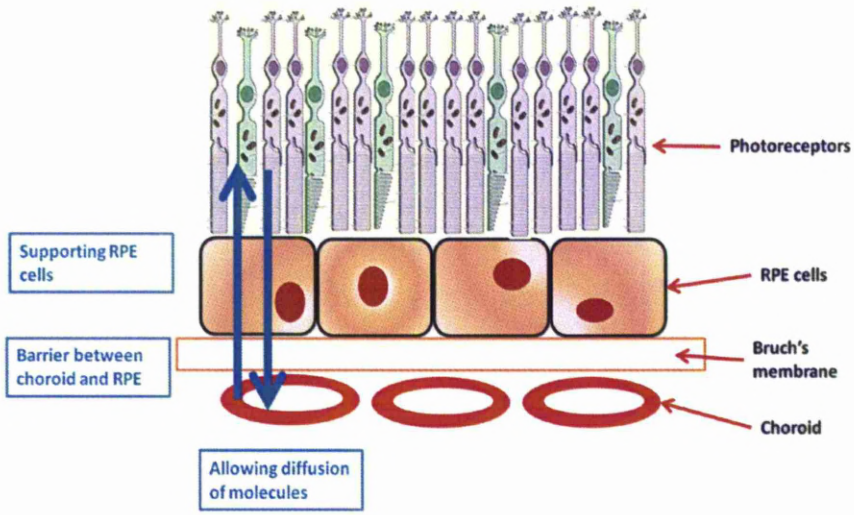

Figure 4-1 Schematic drawing of the main function of the Bruch's membrane, supporting the RPE cells, as barrier between the RPE cells and the underlying choroid and allowing passive diffusions of molecules.

Because of all these functions, it is paramount that the BM's substrate replacement is porous with suitable hydraulic permeability, has similar elastic properties, and similarities in thickness as the native BM. This would act as a scaffold to maintain

attachment and growth of replacement cells. It has also been demonstrated that cells transplanted onto aged BM do not maintain their functional phenotype[153-154].

There are many substrates used in AMD research that may fit into the required criteria for delivering cells into the sub-retinal space. Examples are poly-(L-lactic) acid (PLLA), poly-(D,L-lactic) glycolic acid (PLGA), poly-methyl methacrylate (PMMA), poly-glycerol sebacate (PGS) and poly-caprolactone (PCL). However, they need to be surface modified by either hydrolysis, coating with adhesion protein or pre-treated with air, plasma or ammonia to promote cell attachment[155]. The PU supplied to us by Biomer Technology Ltd. has the advantage that it can be used as received, without any surface modification.

PU has many useful properties such as elasticity, durability, resistance to fatigue stress and does not elicit known immune response, when implanted *in vivo*. The mechanical and the surface properties of the PU can be tailored by varying the proportion of its soft and hard segments.

PU as thin films has been used in another study as a possible support for ARPE-19 cell growth, with similar immuno-histological findings[156]. It was however, based on poly(caprolactone) and poly(ethylene glycol) for its soft segments, and isophorone diisocyanate and hydrazine, as its hard segments, and so was biodegradable. This

brought us back to the question of removal of biodegradable waste sub-retinally and the need of a proper long-term support of the transplanted RPE/IPE cells. Nevertheless, this study has demonstrated the possibility to manufacture PU with vast array of physical and mechanical properties, by adjusting its soft and hard segments. Nevertheless, the PU supplied was in pellets or granules form, and a way to manufacture PU in a suitable porous form was needed.

4.2 Optimising the substrate

4.2.1 PU as thin film

Most of the initial experiments and optimising studies were carried out on the substrate casts as films. There were two types of PU films supplied by Biomer Technology Ltd., Z3A1 and Z9A1. Whilst they were easy to handle, they did not emulate the porosity of the native Bruch's membrane. It is well published in many literatures that PU can be affected by light due to the changes in the chromophores in the aromatic isocyanate section in the PU[157]. With exposure to visible light, the PU can turn 'yellow' in its appearances and this is made worse with higher light intensities[158]. This is especially crucial if the PU is to be used commercially, so that it

will have a long shelf life. It is important to note that there is no difference in terms of cellular attachments and growth between different ages of the substrates.

4.2.2 Manufacturing porous PU

To date, there has been a limited number of studies investigating porous membranes for RPE transplantation. This is due to the difficulties faced in manufacturing membrane with micro-scale porosities with a suitable thickness. An example of a porous membrane studied for this application, was a non-degradable hydrogel[159]. However, with the thickness of over 25μm, it may disturb the surrounding the transplantation area.

When manufacturing porous PU, only one type of the PU; Z3A1 was chosen. This was to make it easier to compare the outcome between all the different techniques. Several methods have been tried and tested to manufacture the 'ideal' porous PU.

In an attempt to produce porous PU, a freeze-drying technique was employed. Freeze drying removes the residual solvent from the mixtures by cooling it below its triple point (the lowest temperature at which the solid and liquid phases of material

co-exist), thus sublimation from liquid to gas phase. This will leave voids in the material (PU) when the solvent sublimes. The rate of temperature change in the process can be controlled to produce the desired pore size, i.e. a higher rate of freezing will produce a smaller crystal size[160]. During the freeze drying process involved in this thesis, the mixtures were quickly immersed in liquid nitrogen (temperature at between -196°C to -210°C), before being left to dry at a constant -22.4°C in a freeze dryer. It was found that the 11% of PU in DMAC mixture produced the most uniform pore distributions with ridges and lines. These kinds of surface topographies were usually preferred for cell attachment[161]. But problems faced by producing the substrate by this technique were that the substrate was still too thick and reproducibility. Another problem was that the pores were too big for the size of the cells, such that it was difficult to control cells migrating through the pores and could not form a monolayer. Theoretically, it should be possible to construct a smaller pore size by increasing the rate of freezing. But due to the limited resources available and practicality, this method of producing pores was abandoned.

Our collaborator from the University of Strathclyde supplied Electrospun PU to us, using Z3A1 supplied by Biomer Technology Ltd. The ARPE-19 and BRPE cells demonstrated good epithelial phenotype and morphology, when cultivated on this

surface with occludin expression (**section 3.11.2**). However, this substrate as supplied, was sticky and difficult to handle. With thickness of more than 100μm, it was unsuitable for sub-retinal implantations. Nevertheless, the electrospun PU closely resembled the architecture of a native BM.

Another attempt was to use water precipitation technique to produce porous PU, but the substrate formed was really thick, more than 100μm and the pores did not pierce all the way through. So this approach was abandoned.

It was thought that further manipulation could be performed to the PU/DMAC mixtures (as found in freeze drying technique) to find the correct porosity and thickness. It was hypothesised, that if small (micro-sized) water-soluble crystals/particles were mixed into the PU/DMAC solution, were cast in an oven and the crystals washed out, perhaps holes with desirable sizes could be achieved. From the initial PU/DMAC mixtures experiment, it was found that the solution of 5% PU in DMAC vol/vol produced the thinnest cast. It was also proposed that fine confectioner's sugar (icing sugar) could be added to the mixtures, as they measured at between 2μm to 100μm in diameter (average 24μm)[162]. After several modification and improvements, it was found that 5% PU/DMAC mixtures with 5% by weight of sugar, produced the thinnest casts, but the thickness and pore distribution within the substrates produced were highly dependent of the

glassware in which they were contained. It was discovered that a type of glassware, crystallising dish produced the best thin substrate (5μm in thickness) with uniform pores distribution of 10μm from one hole to another. This had good repeatable results too. It was thought that the width of the beaker and its shallowness allowed maximum evaporation. The procedures of drying material in a crystallizing dish have been practiced in many studies, such as producing colloidal crystal[163] or macro-porous polymers[164].

The porosities of this PU were thought to be adequate to support an intact monolayer of cells, as average pore sizes (1μm) were much smaller than the average size of a cell, but to allow transport of wastes or nutrients. The distance from one hole to another averaging at 10μm, the average size of a cell was about 6μm, so it was hypothesised that each hole could provide for each cell. Transport of nutrients through the pores will be discussed later in the dextran transport experiments (**section 4.6.2**). The average thickness of the porous PU was 5μm, suggesting it to be a suitable candidate to replace a native Bruch's membrane as it would not cause too much distortion anatomically.

4.2.3 Properties of PU as a substrate to replace Bruch's membrane

The Z3A1 film, Z9A1 film and porous PU (produced by icing sugar) were tested in terms of their wettability and strengths. The contact angle measurement is important as it indicates the wettability of a material; a smaller contact angle denotes a more hydrophilic material and so is likely to promote a better cell attachment. In our measurements, it was found that the porous Z3A1 had the smallest contact angle of 43°, nearly half of the Z3A1 in film form (71°), Z9A1 film had the average contact angle of 65°. When measuring their tensile strengths, it was interesting to see that the strengths of porous Z3A1 (0.56MPa) were bigger than Z3A1 (0.092MPa) in film. Z9A1 (1.24MPa) films were the strongest amongst them but demonstrated a plastic deformation. It was hypothesised that the observed increase in hydrophilicities and strengths in porous Z3A1 compared to its film form might have been due to the change in its molecular structure, when it was mixed with sugar. Some sugar might have still been trapped within the structures, acting like a composite that might have strengthened the material. Sugar was positively charged and so would probably increase the wettability of a material. It was thought that the rinsing process with water should be longer to make sure all of the sugar was properly removed. After that, the process of identifying each element, as in Fourier transform infrared spectroscopy (FTIR) or mass spectroscopy could be performed to identify any traces of sugar or other additives left in the

substrate. Hypothetically, traces of sugar in the blood should not have a significant effect in the body, but in the production of domestic icing sugar, some mixtures of corn-starch, wheat flour, or calcium phosphate were used to improve its flowing ability. The effect of these substances if any, in the sub-retinal area is unknown clinically. Thus, it was suggested that an industrial grade icing sugar without any additives, should be utilised in the future.

From the tensile strength graphs, two populations of the graphs could be observed in the porous Z3A1. It was suggested that maybe there was some kind of alignment effect of the sugar, when it was used as porogens in the substrate. However, these data were a preliminary and were obtained from a low level of repeatability. Further investigations with more samples should be used in the future to confirm this observation.

It is interesting to note however, that the values of the tensile strengths of the substrates were in the same magnitude of the native Bruch's. A study found that choroid-Bruch's-RPE complex had the value of elasticity of between 0.22MPa to 0.72MPa[165]. Candiello et al. found that the value of Bruch's modulus of elasticity to be around 2 to 4 MPa[22] (measured using AFM) and later after perfecting their technique, the same group found that this value to be at around 1MPa in adult human[23]. The value would be higher in an aged human[95] (due to BM thickening,

increased collagen cross-linking and calcification)[166] and this was confirmed in findings of different stages of development in embryonic to neonatal chick and mouse[23]. The elasticity of our substrates fell within a similar magnitude and more experiments should be performed to modify our substrate to have the correct elasticity (and thus mechanical property). It is important to have a similar mechanical property to the native BM, because this will have an effect on the permeability and filtration capabilities, which leads to the development of AMD.

4.3 Sources of cells

There have been various types of cells investigated in the studies of AMD namely ARPE-19, Schwann cells, mouse 3T3 fibroblasts, dermal fibroblasts, glial cells and vascular smooth muscle cells[155]. While these cells can be easily grown and expanded in culture, they do not represent the real clinical practice. Recent advancement in research shows the tendency to investigate the retinal progenitor cells (RPC)[167], induced pluripotent stem cells (iPSC)[168] and embryonic stem cells (ESC)[169] as a potential source of cells. However, stem cells technologies are still new and there are still problems in isolating stem cells. Because of the ability of stem

cells to differentiate, there are also problems with maintaining the cells differentiated state[155].

4.3.1 Using cell lines

ARPE-19 cells are an established and immortalised human RPE cell-line. They demonstrate the normal phenotype of primary RPE cells *in vivo* and express RPE-specific markers, do not transform into a different phenotype and form differentiated polarised monolayers, and so they are useful model for assessing RPE growth and function. In this study, ARPE-19 cells were used as a preliminary study to see if the substrate supports cellular growth. Experiments with ARPE-19 showed that the substrates (b9™) support growth of cells.

In comparison to establish cell lines, BRPE and BIPE tend to change their phenotype as the passage number is increased and so, will lose their ability to behave as RPE and IPE cells. There are also differences between batches of primary cells harvested, and this could be due to a number of reasons such as post mortem, age and health of individual cow. This makes them harder and less reproducible to use experimentally, however, they are a better model for the clinical situation, in which biopsies of IPE or RPE will be collected from a patient's eye and grown on the

substrate for transplantation back into the same patient. These cells, therefore, will enable better understanding of the use of human's pigment epithelial cells than that of the ARPE-19 cells.

Another important finding to point out, when comparing between cell line and primary cells, is the difficulty in comparing their seeding densities and thus proliferation rate. This is because, the primary cells are heavily pigmented, and using trypan blue exclusion method as viability counting might not be the best estimate of dead cells. This technique tends to overestimate cell viability, especially following treatment with trypsinization, EDTA treatment and serum containing media. Furthermore, the cell exclusion counting needs to be carried out in a very short time period (less than 5 minutes)[170]. Therefore it was suggested that a different viability technique (such as fluorometric assays) could be employed in the future.

Generally, preliminary experiments in these studies were carried out using ARPE-19 because of their predictability. Once it had been established that the substrate tested supported the growth of cells, primary cells were used instead.

4.3.2 The potential of using IPE as an alternative to RPE

To treat patients with damaged RPE, the next logical way is to replace them with new healthy layer of RPE. However, in patients whose RPE has already depleted, this is not always the easiest route. RPE removal in exudative AMD patients increases risk of complication on the retina. The removal of CNV causes additional removal of surrounding healthy RPE and leads to a further choriocapillaris atrophy and photoreceptor loss[171]. However, there were some initial improvements in vision shown after RPE transplantation in both exudative and nonexudative AMD[172] and autologous transplantation of RPE cells show no signs of rejection[173] with some promising results.

It is thought that IPE is an ideal candidate to replace diseased or damaged RPE because both IPE and RPE are derived from the same embryonic origin[174]. RPE and IPE have also demonstrated very little difference in gene expression profiles[31]. IPE has been also demonstrated to perform similar functions as RPE, capability to metabolise retinol[28] and ingestion of outer segments[93]. IPE can be easily obtained from patients undergoing surgery, where iridectomy is performed with cataract surgery. IPE can then be expanded in culture, before being implanted sub-retinally in the patient. Using patient's own cells can also eliminate concerns about immune rejections. A trial in humans show that the transplanted IPE were well tolerated

after several years in patients with wet AMD[175] showing that further investigation is needed for their use in the dry form of AMD. Currently, it is uncertain if the IPE placed under the neural retina will acquire a similar expression profile to retina, because this has not been adequately studied.

Next is about the question of either growing the cells in suspension or as patch graft. There has been some debate over the rejections in the immune-privileged site, such as in the sub-retinal space being due to the delivery of cells (i.e. because the cells were in suspensions) or because the blood-brain-barrier has been compromised such as in wet form of AMD[176]. This is because some studies have shown that autologous suspension of cells in the wet form of AMD has signs of immune rejection compared to the dry form of AMD[77]. It has also been suggested that the cells injected as suspension, fail to regain a fully differentiated phenotype[98]. These demonstrate the importance of growing cells as an intact sheet before transplantation and we are proposing to use autologous IPE as an intact monolayer on a substrate for the sub-retinal transplantation.

4.4 Optimising cells

4.4.1 The importance of correct procedure during harvesting

Reliable methods were necessary for the culture of the epithelial cells for subsequent functional studies. For this project, several methods of isolating pure RPE from other studies were investigated. RPE harvest were tested using gelatine sheets[177,178], adhesion to agarose[179], isolation using filter papers[180] and growing from an explants[181] were investigated. Cells were found to grow from small colonies. In some instances, hexagonal cobblestone type morphology was seen in some patches, known as blister dome, a phenomenon also found in a different study[182]. But in many incidences, pure cultures of RPE could not be achieved. Method of harvest of RPE by mechanical dissection and enzymatic digestion using collagenase type IV (as described in methods **section 2.4.3.1.4**) yielded the most reproducible result with high cell numbers. The existence of contamination from other cell types was also reduced.

Technique for isolating pure IPE using enzyme-assisted micro-dissection[183] was also tested. However, there was nearly always an incidence of contamination with other cell types like fibroblasts, indicated by elongated spindle shape cells. Although a

study by Hu et al.[140] found that this method produced the best IPE isolation technique, it was found that some of the IPE harvested were mixtures of anterior and posterior IPE, which have different properties and functions. The current method of isolating IPE, using cloning rings ensured that the IPE obtained were purely from the posterior IPE. This method has also shown to deliver pure IPE with good reproducible results. The IPE cells produced were polygonal or cuboidal in morphology with circular nuclei and pigmentation, similar to those found *in vivo*.

4.4.2 The effect of seeding density

Earlier work in tissue culture with primary bovine cultures suggested that they were slow to grow and to reach full confluence. Optimum seeding density was therefore required, so as to produce confluent monolayer with optimal utilization of cells as quickly as possible in clinical situation. It was suggested that the seeding densities would determine the shape of the cultured cells[184]. RPE cells were also proposed to exhibit contact inhibition[185]. Previous work with ARPE-19 cells had been carried-out and was found to be of 1 x 10^4 cells per substrate[115] (per well in a 24-well plate). It is therefore a useful indication that investigation of seeding densities should start at this similar concentration if not higher. In this experiment, optimum seeding

densities for both primary cultures of bovine retinal pigmented epithelial (BRPE) and bovine iris pigmented epithelial (BIPE) were investigated. Both BRPE and BIPE demonstrated good spreading at $1x10^4$ cells per substrate and they started to reach confluence. However, both $5x10^4$ and $1x10^5$ cells per substrate, by day 4 showed signs of overcrowding and started to show multilayer (i.e. overlapping of nuclei) at day 7.

It is important to have a compromise between having a sheet of cells quickly (i.e. by having higher cell densities at plating) and to have them growing slowly but in a correct epitheloid morphology. Higher growth rate has been associated with fibroblastic-like morphology, overgrowth and detachment as seen with the preliminary studies with the primary bovine RPE and IPE cells. But too low a plating density will result in low reattachment values as the limited interactions and signalling pathways between adjacent cells[186]. Clinically, it is more practical to obtain a small sample of the patient's own cells for culture then transplantation and therefore, using a lower seeding density seems more sensible. Therefore, it was suggested that the optimal seeding densities for both BRPE and BIPE should be about $1x10^4$ cells per substrate (per well in a 24-well plate) making it to be equivalent to a seeding density of 3.33×10^3 cells/ml.

However, primary BRPE and BIPE used in this study were obtained from young bovine (less than two years old). Cells from a younger donor were easier to culture than from an older donor and this is not the true clinical representation. A limited numbers of primary HRPE and HIPE were obtained from aged human donors in the studies and hopefully more aged human cells can be used in future studies.

4.4.3 The effect of modifying serum concentration and retinoic acid

Following observation from previous experiments, epithelial cells cultured *in vitro* became overgrown and floated as fragments inside the culture dish after they reached full confluence. A possible explanation for the lack of evidence of their normal 'cobble-stone' morphology and the suggestion of the presence of apoptotic behaviour could be that the cells were continuing to proliferate rather than stopping proliferation when they came into contact with each other.

It was suggested in some studies that low serum concentration plus retinoic acid promotes growth arrest in these types of cultures[187]. The studies demonstrated that serum causes rapid depletion of the large retinoid stores within the RPE cells *in vitro*. It was also suggested that tight junction formation was inhibited in retinal epithelial cell culture model for the blood-brain-barrier by affecting zona occludens-

1 (ZO-1) protein expression[188]. Previous experiments show arrest of cellular overgrowth and maintenance of monolayer formation can be achieved by reducing the amount of serum in the culture media. This will also reflect the situation when substrates are being implanted sub-retinally in patients.

In this study, retinoic Acid (RA) was found to promote the RPE cell growth until they reach confluence. RA is a differentiating agent that is present in the eye to arrest RPE cells in their differentiated state and thus inhibit over proliferation[189]. Cells grown in the presence of RA were found not to exhibit cellular overgrowth and maintain characteristics associated with the morphologic appearance of mature RPE cells *in vivo*[190]. Some studies suggested that retinoic acid inhibition of epithelial cell adhesion is associated with a reduction in the synthesis of fibronectin and thrombospondin, components of extra-cellular matrix that serve as epithelial cell adhesion factors[191, 192, 193]. This will be discussed further in **section 4.4.4.**

Modifying the serum concentration and adding RA saw some patches of monolayer formation with both BRPE and BIPE. Therefore, it was decided that higher levels of serum should be used to promote cells attachment and proliferation. The addition of lower concentration of RA commenced before the cells were fully confluent and the amount of serum was then reduced when the cell reached confluency. Therefore, by the time the cells were ready for transplantation, the amount of

serum needed to maintain the monolayer in culture was already very low (5%) and it was hoped that no more serum would be needed *in vivo* after transplantation due to patient's own serum (therefore reducing risk of negative reaction by introduction of 'foreign' protein). In summary, the serum and RA were only used in culture to control cells monolayer, and were be discarded once implantation had started. RA acid is a form of retinoid, found in small quantities naturally throughout the body and so a small trace of RA found on the substrate would hopefully have no significant effect on the patient. There were no negative effects of RA found in cell cultures[194] and when used in transplantation in an animal model[195], but more studies are required in the future to study the effect of RA traces *in vivo*.

4.4.4 The effect of pre-coating the surface with extracellular matrix (ECM) protein

There have been many publications about the use of extracellular matrix ligands such as fibronectin, laminin, vitronectin and collagen IV to enhance the attachments of cells on plating surface[196, 197, 198]. Adhesion assay experiments were carried out to investigate if the use of fibronectin and/or laminin would enhance the growth of cells on the control and substrate. It was then proposed that if the adhesion assay turned out to be positive, the use of serum could be reduced and so

by identifying these proteins, perhaps, they could be constituted within the substrate by surface modification for instance.

The amount of cell attachment increased with the use of the extracellular matrix proteins in the experiments. But with time, these differences were not significant. Morphological examinations by immuno-histochemistry also showed that there were no significant differences between the non-coated and coated surfaces. Furthermore, longer growing times were needed to control the proliferation rate and to allow for the formation of tight junctions. Another finding was, reducing the serum inhibited cell attachment and proliferation on all surfaces, even when they were pre-coated with the fibronection or laminin. Besides, the high serum was only used initially i.e. during first attachment until the cells reached fully confluence. After this, the serum was reduced down to 5% to maintain the monolayer. It was suggested that the introduction of the whole protein could cause the difficulties of adhered protein to adopt the correct orientation for cellular adhesion[155]. And so it was decided that the use of coating material would be abandoned. Moreover, it was better clinically, so as to prevent the introduction of more additives sub-retinally to reduce the risk of rejection.

4.4.5 The morphological changes of cultured cells

It was found that RPE and IPE primary cells might have changed in its morphology after passaging, even when they demonstrated a good morphology after first harvest. They tended to be more fibroblast-like with higher numbers of passages. They did however, still stain positive for cytokeratin, suggesting that they had not dedifferentiated. These findings were consistent with published reports[199, 200]. It is essential that the cells maintained their *in vivo* morphology even if they are still the same phenotype as these changes can be accompanied by a change in biologic activities[201]. It was suggested that the changes might have been due to loss of essential growth factors with divisions and passages *in vitro*. Growth factors such as pigment epithelium-derived factor (PEDF) are needed for development of actin cytoskeletal, absence of which would disrupt the assembly and stability of the cytoskeletal structure. The pigmentation was also reduced with number of passages. It was suggested that this was due to differentiation rather than dedifferentiation, as cells *in vitro*[202] did not produced melanosomes. As the cell divides, the melanin divides with the proliferating cultures. To reduce these problems after passaging, direct harvest on substrate was developed instead and this could be a better representation of the planned clinical practice. Cells obtained from patient/donor could be harvested directly on the substrate and expanded in

culture thus reducing the risk of changes in morphology after passaging and could have the potential to reduce time.

It was also proposed that the effect of trypsinisation might have had an effect on cell's migration[203] (as the chemo-attractants which guide the movement of cells were sensitive to trypsin) and retinoid metabolism[204] (because the cells lose their ability to form intermediates such as retinyl esters or 11-cis -retinoid isomers in the visual cycle). In our experiment, we have showed that there was little difference between the morphology of first harvest of BRPE cells using, two different enzymes (trypsin and collagenase type IV). The Collagenase type IV harvest was shown to produce higher initial yield number compared to trypsin, but when they reached confluence, the differences were insignificant. It was therefore concluded that the cells would produce a good morphology as long as the harvest technique was done correctly. This was in agreement with other study[205].

4.5 Evaluation of cell growth on the substrates

4.5.1 Morphologies of cells on PU

PU as films and as porous substrates (electrospun and formed by icing sugar) have been demonstrated to support attachment, growth and proliferations of an intact layer of cell lines and primary bovine and human RPE and IPE, with the correct method of harvest and culture conditions. They showed the correct morphologies; hexagonal 'cobble-stone' epithelial morphology, as illustrated by its F-actin phalloidin staining, uniform distributions of nuclei throughout the surface and the formation of occudens tight junctions. Cells also exhibited positive cytokeratin markers when attached on these surfaces, an evidence of the correct epithelial origin. However, there was some evidence of differences in distributions of cells between porous substrate and non-porous material (PU and control). Cells tended to be bigger and less dense when seeded onto a porous substrate. But they were still displaying similar markers, morphologies and functionalities. It was hypothesised that cells needed a bigger holding position on the porous material because of the surface condition. Surface topography was said to play an important role in shaping, orientating and adhesion of the cells[206]. Cytoskeletal functions, such

as microfilaments[207] and focal contact[208] were also said to play a part. In this case, due to the holes on the porous substrate, cells extended their microfilaments-containing filopodia (at the edge of the lamellipodia), surpassing the immediate hole to anchor a stronger 'foothold'. Although one could argue that probably it was the different origin of the cells that gave the difference in shapes and sizes (i.e. cells obtained from the macula area tended to be smaller and more closely packed than the cells originating from the periphery[8]) but all of the cells were equally mixed before seeding. These observations were seen repeatedly throughout the experiments and happened with both RPE and IPE (not recorded).

4.6 Functionality tests

4.6.1 Phagocytosis function

It is vital that the transplanted monolayer of cells can perform some if not all of the functions of the replaced damaged RPE cells. One of the important functions is phagocytosis of photoreceptor outer segment (POS). RPE cells phagocytose spent POS by binding, ingestion and digestion, forming a phagosome.

In order to test this, a proper way of isolating POS must be developed. We used a revised method from (Godchaux et. al[143] and Higgins et. al[144]). Although Higgins described that their distinctive orange band (containing POS) was found at an interface between the 0.8M and 1.0M, we on the other hand repeatedly found our distinctive orange band at the interface of between 1.2M and 1.0M (**Figure 4-2**). The isolated POS however, stained positive for the presence of Rhodopsin, a protein marker for the POS. Even though our derived POS was located at the different location of bands, the rhodopsin stain positively identified POS suggesting that our derived POS was the bigger particles of POS, as compared to Higgins study. In another study, Gaudchaux et al.[143] found that in a technique of isolating POS using isopycnic equilibrium on sucrose density, there were two distinct bands of where POS was found, band I of 1.127 g/ml sucrose density, and in band II of 1.142 g/ml sucrose density. Particles in Band II were larger than the particles in Band I and mostly rod-shaped. Band I had smaller particles and isolated groups of isolated disc membranes (**Figure 4-3**). Comparing the density of sucrose molarity[209], it can be deduced that our POS were the ones derived from Band II (1.142 g/ml), which was situated between the density of 1.1562 g/ml (1.2M sucrose) and 1.1318 g/ml (1.0M sucrose). This reinforced the hypothesis regarding our harvested POS, was actually the bigger-sized particles rather than the smaller-sized POS particles.

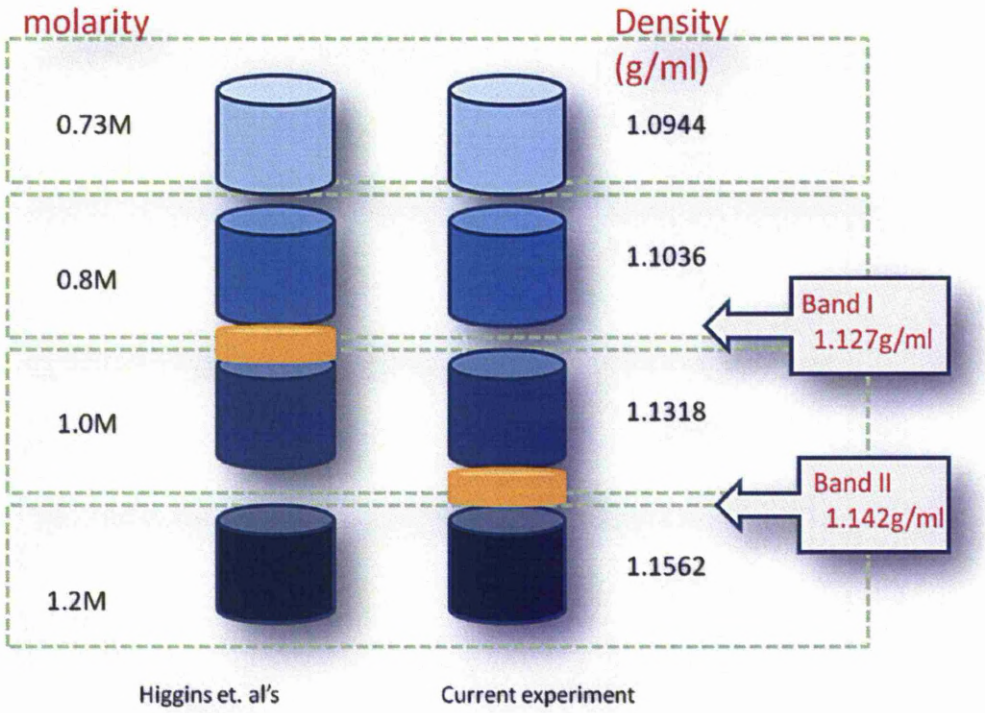

Figure 4-2: Diagram representing the POS harvest theory. The POS found by Higgins et al.[144] was derived at the 0.8M and 1.0M interface. Our POS was found forming between the 1.0M and 1.2M interface. Comparing the values of the molarity of sucrose and its density, it was suggested that our harvested POS corresponded to the POS found in band II as explained by Gaudchaux et al.[143].

Figure 4-3: The TEM images showing the difference between the POS derived from Band II (a) and Band I (b). Band II POS consists of bigger rod-shaped particles whereas the POS derived from Band I consists of smaller broken particles of isolated disc membranes. The images were obtained from Gaudchaux et al.[143].

The POS were labelled by two methods: labelling with SNARF-1® or with FITC-bound anti-Rhodopsin antibody for phagocytosis assay. SNARF-1®-labelled POS were used previously in the group and were reported in Thumann[93]. It would change the emission's wavelength upon changes in surrounding pH, red when attached to cell and yellow when it is internalised. But when it was tested in

different pH media buffers, pH 9 (basic) and pH 6 (acidic), the SNARF-1® labelled POS did not change its colour and so this labelling method was abandoned. FITC-bound anti-Rhodopsin was used instead and any bound but uningested POS were masked out with Tryphan blue[210]. However, the disadvantage of this procedure was the inability to compare the amount of bound and internalised POS.

From the results, it could be seen that the amount of phagocytosed POS increased over time with more internalisation with cells grown on the porous substrate compared to control. This could give the indication that the substrate not only supported growth and phagocytosis function of cells, but also enhanced this. Throughout the phagocytosis experiment, the POS was suspended in the same type of media i.e. supplemented with 5% serum and 5% sucrose. It has been suggested in a study that the content and culture conditions have an effect to the phagocytosis of cells *in vitro*[211], but in the current study, the rate of phagocytosis on all surfaces, using the same culture conditions were compared and so the effect of different culture conditions were eliminated.

As previously mentioned, the cells on the porous substrate tended to be bigger in sizes than the cells on non-porous substrate and control. Interestingly, cells on the porous PU, although less dense, phagocytosed more POS than the cells on control. A possible explanation for this was probably due to the fact that the cells were

smaller on the control surfaces, meaning that they were closely packed together and so had less receptor exposed, thus reduced phagocytosis. The cells on porous PU were less densely packed and so have more receptors exposed, therefore more phagocytosis (Figure 4-4).

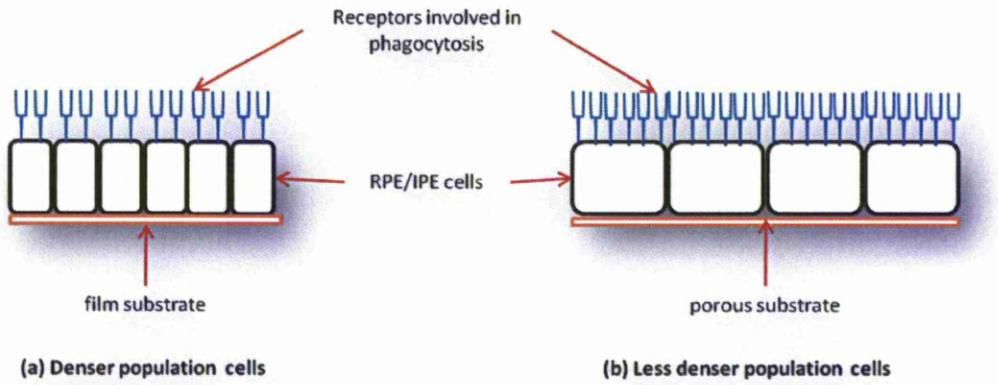

Figure 4-4: schematic drawing representing the theory regarding cells sizes/population density and the rate of phagocytosis. The smaller, closely packed and more dense cells (a) were thought to have less receptors exposed on their surface compared to the bigger, distantly packed and less cells (b), and so have a lower phagocytosis rate.

Another possible explanation was probably due to the different heterogeneity between RPE cells in a single primary culture. McLaren[212] mentioned in her studies that there were three types of cells: type 1, consisting of large heavily pigmented, bi-nucleated, undivided and least distributed cells, type 2, consisting of small mono-nucleated, low pigmentation and regularly distributed cells, and type 3, consisting

of small mono-nucleated, high pigmentation and regularly distributed cells. It was found that the rate of phagocytosis from the highest to the lowest were type 3, type 1 and type 2. And so, the smaller type 3 phagocytosed the quickest, bigger type 1 second, and smaller type 2 the least (see **Table 4-1**). This could be explained in the findings of the phagocytosis experiment that the cells on the porous material were mainly type 1 (bigger cells), whose rate of phagocytosis was higher than the cells on control mainly type 2 (smaller cells). If this was the case, then there was some kind of favouritism of the different kinds of cells growing on different surfaces. However, it came back to our original question of mixing all of the cells before seeding.

Table 4-1: Summary of findings modified from McLaren[212] compared to hypothetical current findings.

Cell type	shape		pigmentation	division	distribution	Rate of phagocytosis	My findings
I	Large binucleated	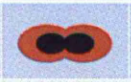	Heavily pigmented	undivided	Least distributed	medium	√ Faster phagocytosis
II	Small mononucleated		Non pigmented	divided	Regularly distributed	slowest	√ Slower phagocytosis
III	Small mononucleated		Heavily pigmented	divided	Regularly distributed	fastest	

Studies have shown that RPE cells *in vitro* bound to and consumed many substances such as red blood cells, algae, bacteria and yeast[213]. A normal RPE cell would use some specific binding sites to specifically phagocytose POS such, as αVβ5 integrin[214], CD36 trans-membrane glycoprotein[215], CD81 tetraspanin[216] and Mer Tyrosine Kinase (MERTK)[217]. The RCS (Royal college of Surgeon) rats with retinal degeneration MERTK defect have the inability to specifically phagocytose POS[218], but tests show that they will ingest polystyrene beads in-culture[219]. It was therefore hypothesised, that by blocking one of these integrins would reduce the uptake of POS but not other particles, and would demonstrate the selectivity of cells' phagocytosis function *in vitro* (**Figure 4-5**). The monolayers of cells grown on control and on our porous PU were tested on the selectivity of phagocytosis experiment. Some cells were challenged with anti-αVβ5 antibody, before being added with either POS or polystyrene beads (PB). Results showed that the numbers of POS and PB uptake increased over time on all surfaces, but there was a significant reduction of POS uptake when surface was challenged with the anti-αVβ5 antibody. The uptakes of PB were not affected. These suggest the selectivity of phagocytosis of our cells *in vitro*. It can also be observed from the results that the numbers of PB uptakes did not increase much between 3 hours and 24 hours on porous PU, suggesting that cells might have reached their maximum ingestion of the smaller particle size of PB compared to the bigger POS. This was not seen with

cells on control, as there was a possibility of the bigger numbers of cells per area on control. Further studies should be performed in the future to verify the observations.

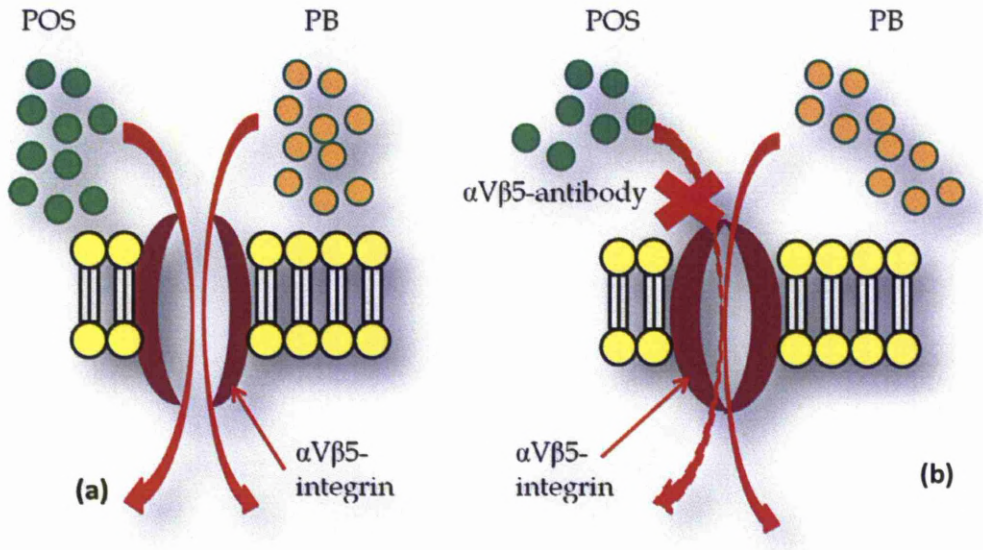

Figure 4-5: Schematic drawing of selectivity of phagocytosis experiment. αVβ5-integrins were required to phagocytose both POS and PB. When the integrins were blocked however, the phagocytosis of POS was reduced but the phagocytosis of PB was not affected.

4.6.2 Trans-epithelial transport

Another important role of the RPE cells is to permit trans-epithelial transport of nutrients and wastes in its blood retinal barrier function[220]. To experiment this, different sizes of fluorescently labelled dextrans were used. It was presumed that the fully confluent cells with their tight junctions would allow transport of smaller sizes dextran easier than the bigger ones. This experiment was tested on a layer of a fully confluent primary BIPE cells. In the experiment, dextran of 10kDa (blue), 70kDa (green) and 155kDa (red) were used. The sizes of dextrans were chosen to emulate the different biomolecules sizes: 10kDa dextran to represent retinol and vitamin A, the 70kDa dextran to represent albumin and some antibodies, and 155kDa to represent glycogens and some amino acids. The findings confirmed this theory. The results implied that the permeability of the fluorescently labelled probes through the RPE cells decreased considerably with the increasing sizes of the probe. The cumulative amounts of dextran collected were shown as a percentage of the initial concentration. It was found that the confluent monolayer of IPE cells on the porous substrate were 1.3 times more permeable to the smaller and medium sized dextrans, compared to the bigger size dextran over 4 and 24 hours. These findings do agree with previous findings[221]. However, it was reported in a study that permeability of the BM is not just dependent on the molecules's size but also on their ionic strengths and pH[222]. Further investigations are needed in the

future to study the permeability of the substrate-cells complex towards some biomolecules normally found between the BM and choroid.

4.7 *In vitro* injury model experiment

Another addition to the study was to perform an *in vitro* injury model to observe and to understand the cells behaviour, when the intact monolayers of cells on substrates were co-cultured with a confluent monolayer of RPE cells. Cells on each surface were labelled with different colour dyes to follow their migrations, if any. It was initially thought that prior to the addition of the substrate-cell complex, the area where they would be 'transplanted' onto should be injured first. This should emulate the injury site. After that, the substrate could be placed at the exact place. However, in the macula relocation surgery, the affected site was cut, rotated and located onto a different healthier area (usually supero-temporally) without previously injuring the new site[223]. Therefore, referring to this method, it was proposed that the similar method would be used, i.e. positioning the substrate-cells complex onto the monolayer of RPE in a culture dish, without previously injuring the site. Moreover, it was difficult to get to the precise location of the injury site, and would reduce the risk of disturbing the surrounding cells.

There were some problems and difficulties faced during the experiment. It was difficult to manipulate and handle the substrate-cells complex without a proper cutting tool; therefore, there were too many disruptions. Another problem was the difficulties of securing the borders of the substrate-cells complex inside the culture dish without any movements. Again, there was too much disturbance to the surrounding area. The third problem was the difficulties in maintaining the same height between the substrate-cells complex and the cells inside tissue culture dish. It was suggested that it might be difficult for cells to 'climb-up' for migration[224]. Using the pins to secure the substrate border did not solve this problem. It is thought that sub-retinal transplantation would also face this difference in height problem *in vivo*. The substrate-cells complex was secured in its place by heavy-oil tamponade normally used in eye surgery and it was suggested that this could be imitated *in vitro*.

There were different outcomes from the experiment. Some cells were seen to trans-migrated, some did not while there were signs of extra activities or growth at the implantation borders. It was not known if it was the results of 'migrated' cells or because of disturbing the sites. It was thought that RPE *in vivo* were usually un-dividing cells, therefore if the transplanted cells were already an intact confluent monolayer, there should be no effect on the recipient native RPE site. An

experiment has demonstrated that in the presence of a confluent intact monolayer, the time it takes to repopulate an area of the Bruch's membrane will be longer[123]. This emphasised the importance of transplanting a fully confluent monolayer of intact sheet of cells on a suitable substrate.

In a recent study by Julien et al.[225], it was found that implantation of a porous gelatine-coated polyimide membrane with 5µm thickness sub-retinally in rats produced complete retinal attachment up to four weeks after implantation. The thin membrane was successfully placed in nearly 67% of the rats, trialled without much implantation trauma, there were minimal disruptions to the surrounding implantation areas, but not to the overlying area. This provided us with a hypothesis that our porous PU with the similar thickness would not disturb the surrounding retinal area during and after the transplantation procedure. However, the transplanted polyimide was placed sub-retinally without any cells and it was found that there were some cells attaching to the implant as well as obstructions to the pores, which caused the blockages to the choroids supplying the area. It was not known if the cells were migrating RPE cells or macrophages. It was suggested that the effect of migratory cells (and thus blockages) might have been reduced if an intact autologous monolayer of RPE or IPE cells was transplanted instead. Another *in vivo* study involving transplantation of artificial substrates sub-retinally

with evidence that the transplant has minimal disturbance to the surrounding area, includes etched pore polyester membrane (PET) and a surface-modified expanded polytetrafluoroethylene (ePTFE) membrane[226].

Palanker et al.[227] found that cells migrate through perforated membranes when the pore sizes were more than 5μm. This was however, involving retinal cells and stimulating electrodes induced the migratory. The study demonstrated the ability of cells to migrate depending on the pore sizes. We have shown that it was possible to control the pore size of our substrate, and have managed to produce pore size of approximately 1μm in diameter.

This experiment with its limitation was just preliminary data and might not be the real representation of the cells response *in vivo*, but it may give us some indication and preparation of what will be needed before moving the trial into an animal model.

5 CHAPTER FIVE: CONCLUSION

In conclusion,

- This project has developed a porous PU with appropriate mechanical properties and porosities.
- This project has demonstrated that primary bovine RPE and IPE were successfully harvested and differentiated into a functional monolayer *in vitro.*
- Primary bovine and human RPE and IPE were shown to grow as a differentiated monolayer on non-porous and porous PU substrates.
- Differentiated monolayer of primary cells were functional in phagocytosing POS and transporting different seized dextran molecules

5.1 Future Research

- Majority of primary cultures used in the studies were BRPE and BIPE. It would be interesting to repeat the studies with aged human RPE and IPE. However, the availability of human tissue may limit this approach.
- The porous substrate developed showed a good cell response. Further optimisation and characterisation of the porous membrane will help to provide a more reproducible substrate, in particular in terms of mechanical properties.
- Functionality tests demonstrated cells to phagocytose POS. αVβ5 integrin have been demonstrated as having a role in selectively phagocytose POS. It is not known if other receptors are involved.
- There is a need to develop the surgical technique for transplantation procedure as demonstrated with the *in vitro* injury model studies. A wet lab facility has been set up and this can be utilised in perfecting the surgical technique for implantation.
- Collaborations with other groups such as Germany, Spanish and Hong Kong are underway for transition of trials in animals.

6 CHAPTER SIX: REFERENCES

[1] Cheng H, Govind N, Tiffany W et. al. Structural and functional MRI reveals multiple retinal layers. *Proceedings of the National Academy of Sciences* **103** (2006) 17525-17530.

[2] Maurice D. The structure and Transparency of the Cornea. *The Journal of Physiology* **136** (1957) 263-286.

[3] Chopdar A, Chakravarthy U, Verma D. Age-related macular degeneration. Clinical Review. *British Medical Journal* **326** (2003) 485-488.

[4] Moran D, Rowley J. Plate 20-3 of Chapter 20: The Senses. The Eye: Photoreceptors of the Retina. Histology Text Atlas Book. Lea & Febiger ,1988.

[5] Oyster CW. In Chapter 13 Retina I: Photoreceptors and Functional Organization. *The Human Eye: Structure and Function*. Sinauer Associates (1999) 545-575.

[6] Neuringer M. Infant vision and retinal function in studies of dietary long-chain polyunsaturated fatty acids: methods, results, and implications. *American Journal of Clinical Nutrition* **71** (2000) 256S-267S.

[7] Okubo A. The relationships of age changes in retinal pigment epithelium and Bruch's membrane. *Investigative Ophthalmology & Visual Science* **40** (1999) 443-449.

[8] Boulton M. Regional variation and age-related changes of lysosomal enzymes in the human retinal pigment epithelium. *British Journal of Ophthalmology* **78** (1994) 125-129.

[9] Frohlich E, Maier E, Klessen C. Isolation of Bovine Retinal Pigment Epithelial Cells Using Adhesion to Agarose: Demonstration of Cellular and Regional Heterogeneity. *Journal of Histochemistry and Cytochemistry* **51** (2003) 121-124.

[10] Altunay H. Fine structure of the Retinal Pigment Epithelum, Bruch's Membrane and Choriocapillaris in the Ostrich (Struthio camelus). *Anatomia, Histologia, Embryologia Journal* **33** (2004) 38-41.

[11] Geeraets W, Williams R, Chan G, et al. The relative absorption of thermal energy in retina and Choroid. *Investigative Ophthalmology & Visual Science* **1** (1962) 340-347.

[12] Tamai M. Current status of IPE transplantation and its potential as a cell-based therapy for age-related macular degeneration and retinal dystrophies. *Ophthalmology Research: Retinal Degenerations: Biology, Diagnostics and Therapeutics*. Chapter 18, 345-364.

[13] Strauss O. The Retinal pigment epithelium in visual function. *Physiological Reviews* **85** (2005) 845-881.

[14] Del Priore L, Kuo Y, Tezel T. Age-related changes in human RPE cell density and apoptosis proportion in situ. *Investigative Ophtahlmology & Visual Science* **43** (2002) 3312-3318.

[15] Imesch P, Wallow I, Albert D. The color of the human eye: A review of morphologic correlates and of some conditions that affect iridial pigmentation. *Survey of Ophthalmology* **41** (1997) S117–123.

[16] Forrester et al. The eye basic science in practice. 2nd Edition (2001) pp 28. Published by WB Saunders.

[17] Sumita R. The Fine Structure of Bruch's Membrane of the Human Choroid as Revealed by Electron Microscopy. *Journal of Electronmicroscopy* **10.2** (1961) 111-118.

[18] Chong V, Keonin J, Luthert P, et al. Decreased Thickness and Integrity of the Macular Elastic Layer of Bruch's Membrane Correspond to the Distribution of Lesions Associated with Age-related Macular Degeneration. *American Journal of Pathology* **166** (2005) 241-251.

[19] Booij J, Baas D, Beisekeeva J, et al. The dynamic nature of Bruch's membrane. *Progress in Retinal and Eye Research* **29** (2010) 1-18.

[20] Ugarte M, Hussain A, Marshall J. An experimental study of the elastic properties of the human Bruch's membrane-choroid complex: relevance to ageing. *British Journal of Ophthalmology* **90** (2006) 621-626.

[21] Huang J, Presley B, Chimento M, et al. Age-related changes in human macular Bruch's membrane as seen by quick-freeze/deep-etch. *Experimental Eye Research* **85** (2007) 202-218.

[22] Candiello J, Feola A, Elyaderani A, et al. Biomechanical Properties of the Bruch's Membrane: An Atomic Force Microscopy Study. *Investigative Ophthalmology & Visual Science* **46** (2005) e-abstract 1210.

[23] Candiello J, Balasubramani M, Schreiber E, et al. Biomechanical properties of native basement membranes. *The FEBS Journal* **274** (2007) 2897-2908.

[24] Moore DJ, Clover GM. The Effect of Age on the Macromolecular Permeability of Human Bruch's Membrane. *Invest Ophthalmol Vis Sci.* 2001 1 **42** (12):2970-5.

[25] Hussain AA, Starita C, Hodgetts A, Marshall J. Macromolecular diffusion characteristics of ageing human Bruch's membrane: Implications for age-related macular degeneration (AMD). *Experimental Eye Research* **90** (2010) 703-10.

[26] Harada T, Harada C, Parada L. Molecular regulation of visual system development: more than meets the eye. *Genes and Development* **21** (2007) 367-378.

[27] Moore K, Persaud T, Shiota K. *Color Atlas of Clinical Embryology*. WB Saunders (1994) Philadelphia.

[28] Thumann G. Development and Cellular Functions of the Iris Pigment Epithelium. *Survey of Ophthalmology* **45** (2001) 345-354.

[29] Schraermeyer U, Kociok N, Heimann K. Rescue effects of IPE transplants in RCS rats: short-term results. *Investigative Ophthalmology & Visual Science* **40** (1999) 1545-56.

[30] Rezai K, Lappas A, Kohen L, et al. Comparison of tight junction permeability for albumin in iris pigment epithelium and retinal pigment epithelium in vitro. *Graefes Archives of Clinical and Experimental Ophthalmology* **235** (1997) 48-55.

[31] Cai H, Sin M, Tezel T. Use of iris pigment epithelium to replace retinal pigment epithelium in age-related macular degeneration. A gene expression analysis. *Archives of Ophthalmology* **124** (2006) 1276-1285.

[32] WHO sites: Causes of blindness and Visual Impairment. Accessed from **http://www.who.int/blindness/causes/priority/en/index8.html** on 9th April 2007 at 16:00.

[33] Statistic from BBC health news, Age related macular degeneration. Accessed from http://news.bbc.co.uk/1/hi/health/medical_notes on the 23rd April 2007, 23:30 pm.

[34] Ambati J, Ambati B, Yoo S, Ianchulev S, Adamis A. Age-related Macular degeneration: Etiology, pathogenesis, and therapeutic strategies. *Survey of Ophthalmology* **48** (2003) 257-293.

[35] Priore L, Kuo Y, Tezel H. Age-Related Changes in Human RPE Cell Density and Apoptosis Proportion In Situ. *Investigative Ophthalmology and Visual Science* **43** (2002) 3312-3318.

[36] Holz F, Bellman C, Staudt S, Schiitt F, Volcker H. Fundus autofluorescence and development of geographic atrophy in age-related macular degeneration. *Investigative Ophthalmology and Visual Science* **42** (2001) 1051-1056.

[37] Sunness J, Gonzales-Baron J, Applegate C, Bressler N, Tian Y, Hawkin B, Barron Y, Bergman A. Enlargement of atrophy and visual acuity loss in the geographic atrophy form of age-related macular degeneration. *Ophthalmology* **106** (1999) 1768-1779.

[38] Schatz H, McDonald H. Atrophic macular degeneration. Rate of spread of geographic atrophy and visual loss. *Ophthalmology* **10** (1989) 1541-1551.

[39] Young R. Pathophysiology of age-related macular degeneration. *Survey of Ophthalmology* **31** (1987) 291-306.

[40] Zarbin M. Age-related macular degeneration: review of pathogenesis. *European Journal of Ophthalmology* **8** (1998) 199-206.

[41] Brody B, Gamst A, Williams R, et al. Depression, visual acuity, comorbidity, and disability associated with age-related macular degeneration. *Ophthalmology* **10** (2001) 1893-1900.

[42] Bird et al. from the International arm epidemiological study group. An international classification and Grading System for the Age-related Maculopathy and Age-related Macular Degeneration. *Survey of Ophthalmology* **39** (1995) 367-374.

[43] Mullins R, Russel S,Anderson D, Hageman G. Drusen associated with aging and age-related macular degeneration contain proteins common to extracellular deposits associated with atherosclerosis, elastosis, amyloidosis, and dense deposit disease. *Journal of the Federation of American Societies for Experimental Biology* **14** (2000) 835-846.

[44] Smith W, Mitchell P, Wang J. Gender, oestrogen, hormone replacement and age-related macular degeneration: results from the Blue Mountains Eye study. *Australian and New Zealand Journal of Ophthalmology* **25** (1997) S13-5.

[45] Schmidt S, Saunders A, LaPaz M, Postel E, et.al. Association of the Apolipoprotein E gene with age-related macular degeneration: Possible effect modification by family history, age, and gender. *Molecular Vision* **6** (2000) 287-293.

[46] Yates J, Moore A. Genetic susceptibility to age related macular degeneration. *Journal of Medical Genetics* **37** (2000) 83-87.

[47] Klaver C, Kliffen M, Duijn C, Hofman A, Cruts M, Grobbee D, Broeckhoven C, Jong P. Genetic association of apolipoprotein E with age-related macular degeneration. *American Journal of Human Genetics* **63** (1998) 200-206.

[48] Schachat A, Hyman L, Leske M, Connell A, Wu S. Features of Age-Related Macular Degeneration in a Black Population. *Archives of Ophthalmoogyl* **113** (1995)728-735.

[49] Klein R, Klein B, Linton K. Prevalence of Age-related Maculopathy, the Beaver Dam Eye study. *Ophthalmology* **99** (1992) 933-943.

[50] Smith W, Mitchell P, Leeder S. Smoking and age-related maculopathy. The Blue Mountains Eye Study. *Archives of Ophthalmology* **114** (1996) 1518-1523.

[51] Vingerling J, Dielemans I, Hofman A. The prevalence of age-related maculopathy in the Rotterdam Study. *Ophthalmology* **102** (1995) 205-10.

[52] Jampol L, Tielsch J. Race, macular degeneration, and the Macular Photocoagulation study. *Archives of Ophthalmology* **110** (1992) 1699-1700.

[53] Seddon J, Willett W, Speizer F, Hankinson S. A Prospective study of cigarette smoking and age-related macular degeneration in women. *The Journal of the American Medical Association* **276** (1996) no 14.

[54] Evans J, Fletcher A, Wormald R. 28000 cases of age-related macular degeneration causing visual loss in people aged 75 years and above in the United Kingdom may be attributable to smoking. *British Journal of Ophthalmology* **89** (2005) 550-553.

[55] McCarty C, Mukesh B, Fu C, Mitchell P, Wang J, Taylor H. Risk factors for age-related maculopathy: the visual impairment project. *Archives of Ophthalmoogy.* **119** (2001) 1455-1462.

[56] Xiaoyan D, Mrinali P, Chi-Chao C. Molecular pathology of age-related macular degeneration. *Progress in Retinal and Eye Research* **28** (2009) 1-18.

[57] Tomany S, Wang J, Leewen R, Klein R, Mitchell P, Vingerling J, Klein B, Smith W, Jong P. Risk factors for incident AMD pooled findings from 3 continents. *Ophthalmology* **111** (2004) 1280-1287.

[58] Seddon J, Ajani U, Sperduto R, Hiller R, Blair N, Burton T, Farber M, Gragoudas E, Haller J, Miller D. Dietary carotenoids, vitamins A, C, and E, and advanced age-related macular degeneration. Eye Disease Case-control study group. *The Journal of the American Medical Association* **272** (1994) no18.

[59] Seddon J, Cote J, Davis N, Rosner B. Progression of age-related macular degeneration: Association with body mass index, waist circumference, and waist-hip ratio. *Archive of Ophthalmology* **121** (2003) 785-792.

[60] Goldberg J, Flowerdew G, Smith E, Brody J, Tso M. Factors associated with age-related macular degeneration: an analysis from the first national health and nutrition examination survey. *American Journal of Epidemiology* **128** (1988) 700-710.

[61] Winkler B, Boulton M, Gottsch J, Sternberg P. Oxidative damage and age-related macular degeneration. *Molecular Vision* **5** (1999) 32.

[62] Darzin P, Mitchell P, Heller R. Sun exposure and age-related macular degeneration. An Australian case-control study. *Ophthalmology* **104** (1997) 770-776.

[63] Hyman L, Schachat A, He Q, Leske M. Hypertension, cardiovascular disease, and age-related macular degeneration. Age-Related macular degeneration risk factors study group. *Archive of Ophthalmology* **118** (2000) 351-358.

[64] Spraul C. Pathology of Choroidal atrophy and neovascularization. In abstracts from first workshop on cell transplantation in age-related macular degeneration. *Graefe's Archive of Clinical Experimental Ophthalmology* **242** (2004) 51-64.

[65] AREDS report no 8. A randomised, placebo-controlled clinical trial of high dose supplementation with vitamins C and E, beta carotene, and

zinc for age-related macular degeneration and vision loss. *Archives of Ophthalmology* **119** *(* 2001) 1417 -1436.

[66] Bone R, Landrum J, Guerra L, Ruiz C. Lutein and Zeaxanthin dietary supplements raise macular pigment density and serum concentrations of these carotenoids in humans. *The American Society for Nutritional Sciences Journal of Nutrition* **133** (2003) 992-998.

[67] Beatty S, Koh H, Phil M, Henson D, Boulton M. The role of oxidative stress in the pathogenesis of age-related macular degeneration. *Survey of Ophthalmology* **45** *(*2000) 115 -34.

[68] Kociok N, Joussen A. Varied expression of functionally important genes of RPE and choroid in the macula and in the periphery of normal human eyes. *Graefe's Archive for Clinical and Experimental Ophthalmology* **245** (2007) 101-113.

[69] Wadsworth S, Heier J. A Different Approach to Therapy for Wet AMD. *Review of Ophthalmology* **18** (2011) 60-62.

[70] Blaauwgeers H, Holtkamp G, Rutten H, Witmer A, Koolwijk P, Partanen T, Alitalo K, et al. Polarized Vascular Endothelial Growth Factor Secretion by Human Retinal Pigment Epithelium and Localization of Vascular Endothelial Growth Factor Receptors on the Inner Choriocapillaris: Evidence for a Trophic Paracrine Relation. *American Journal of Pathology 155 (*1999) 421-428.

[71] Gragoudas E, Adamis A, Cunningham E, Feinsod M, Guyer D. Pegatanib for neovascular Age-related macular degeneration. *The New England Journal of Medicine* **351** (2004) 2805-2816.

[72] Rosenfed P, Moshfeghi A, Puliafito C. Optical coherence tomography findings after an intravitreal injection of bevacizumab (avastin) for neovascular age-related macular degeneration. *Ophthalmic Surgery, Lasers and Imaging* **36** (2005) 331-335.

[73] Steinbrook R. The Price of Sight-Ranizumab, Bevacizumab, and the treatment of macular degeneration. *The New England Journal of Medicine* **355** (2006) 1409-1412.

[74] Humayun M, Juan E, Cerro M, Dagnelie G, Radner W, Sadda S, Cerro C. Human neural retinal transplantation. *Investigative Ophthalmology and Visual Science* **41** (2000) 3100-3106.

[75] Coupland S, Bechrakis N, Sehu W, Lee W. The pathology of drusen in abstracts of the first workshop on cell transplantation in age related macular degeneration. *Graefe's Archives of Clinical and Experimental Ophthalmology* **242** (2004) 51-64.

[76] Algvere P, Berglin L, Gouras P, Sheng Y, Kopp E. Transplantation of RPE in age-related macular degeneration: Observations in disciform lesions and dry RPE atrophy. *Graefe's Archive for Clinical and Experimental Ophthalmology* **235** (1997) 149-158.

[77] Algvere P, Gouras P, Dafgard K. Long-term outcome of RPE allografts in non-immunsuppressed patients with AMD. *European Journal of Ophthalmology* **9** (1999) 217-230.

[78] Wong D, Harding S, Grierson I. Foveal translocation with secondary confluent laser for subfoveal CNV in AMD: 12 month follow up. *British Journal of Ophthalmology* **84** (2000) 670-671.

[79] Eong K, Pieramici D, Fujii G, Ng E, Humayun M, Maia M, Harlan J, Schachat A. Macular translocation : unifying concepts, terminology and classification. *American Journal of Ophthalmology* **131** (2001) 244-253.

[80] Wong D, Stanga P, Briggs M, Lenfestey P, Lancaster E, Li K, Lim K, Groenewald C. Case selection in macular relocation surgery for age related macular degeneration. *British Journal of Ophthalmology* **88** (2004) 186-190.

[81] Aisenbrey S, Lafaut B, Szurman P, Grisanti S, Luke C. et.al. Macular translocation with 360° retinotomy for exudative age-related macular degeneration. *Archives of Ophthalmology* **120** (2002) 451-459.

[82] Wolf S, Lappas A, Weinberger A, Kirchhof B. Macular translocation for surgical management of subfoveal choroidal neovascularizations in

patients with AMD: first results. *Graefe's Archive for Clinical and Experimental Ophthalmology* **237** (1999) 51-57.

[83] Toth C, Freedman S. Macular translocation with 360-degree peripheral retinectomy impact of technique and surgical experience on visual outcomes. *Retina* **21** (2001) 293-303.

[84] Wong D, Charteris D, Cruz L. Letter: Age related macular degeneration: Macular relocation surgery was not taken into account .*British Medical Journal* **326** (2003) 1459.

[85] Crafoord S. Transplantation of IPE to the subretinal space in rabbit. Technique, morphology and photoreceptor survival, in abstract from first workshop on cell transplantation in age-related macular degeneration. *Graefe's Archives of Clinical and Experimental Ophthalmology* **242** (2004) 51-64.

[86] Meurs J, Biesen P. Autologous retinal pigment epithelium and choroid translocation in patients with exudative age-related macular degeneration: short-term follow-up. *American Journal of Ophthalmology* **136** (2003) 688-695.

[87] Thumann G, Aisenbrey S, Schraermever U, Lafaut B, Esser P, Walter P, Bartz-Schmidt K. Transplantation of autologous iris pigment epithelium after removal of choroidal neovascular membranes. *Archives of Ophthalmology* **118** (2000) 1350-1355.

[88] Abe T, Yoshida M, Tomita H, Kano T, Sato M, Wada Y, Fuse N, Yamada T, Tamai M. Auto iris pigment epithelial cell transplantation in patients with age-related macular degeneration: short-term results. *The Tohoku Journal of Experimantal Medicine* **191** (2000) 7-20.

[89] Crafoord S, Geng L, Seregard S, Algvere P. Experimental transplantation of autologous iris pigment epithelial cells to the subretinal space. *Acta Ophthalmologica Scandinavica* **79** (2001), 509–514.

[90] http://www.liv.ac.uk/researchintelligence/issue22/vision.htm

[91] Meurs J, Maaijwee K. Surgical approaches in patients with exudative age-related macular degeneration in abstracts: First workshop on cell transplantation in age-related macular degeneration. *Graefe's Archives of Clinical and Experimental Ophthalmology* **242** (2004) 51-64.

[92] Algvere P, Gouras P, Dafgård Kopp E. Long-term outcome of RPE allografts in non-immunosuppressed patients with AMD. *European Journal of Ophthalmology* **9** (1999) 217-230.

[93] Thumann G, Bartz-Schmidt K, Heimann K, et al. Phagocytosis of rod outer segments by human iris pigment epithelial cells in vitro. *Graefe's Archive for Clinical and Experimental Ophthalmology* **236** (1998) 753-757.

[94] Grierson I, Sheridan C, Rice D, Hiscott P, Wong D. Retinal pigment epithelial transplantation:the future in abstract of the First workshop on cell transplantation in age-related macular degeneration. *Graefe's Archives of Clinical and Experimental Ophthalmology* **242** (2004) 51-64.

[95] Ramrattan R, Van der Schaft T, Mooy C, de Bruijn W, Mulder P and de Jong P. Morphometric analysis of Bruch's membrane, the choriocapillaris, and the choroid in aging. *Investigative Ophthalmology & Visual Science* **35** (1994) 2857-2864.

[96] Streilein JW (ed): Immune Response and the Eye. *Chem Immunol. Basel, Karger* **73** (1999), 0.

[97] Enzmann V, Faude F, Wiedemann P, Kohen L. Immunological Problems of Transplantation into the subretinal space. *Acta Anatomica* **163** (1998) 178-183.

[98] Sheridan C, Williams R, Grierson I. Basement membrane and artificial substrates in cell transplantation. *Greafe's Archive of Clinical and Experimental Ophthalmology* **242** (2004) 68-75.

[99] Thomas M, Dickinson J, Melberg N et al. Visual results after surgical removal of subfoveal choroidal neovascular membranes. *Ophthalmology* **101** (1994) 1384-1396.

[100] Tezel T, Kaplan H, Priore L. Fate of human retinal pigment epithelial cells seeded onto layers of human Bruch's membrane. *Investigative Ophthalmology & Visual Science* **40** (1999) 467-476.

[101] Grierson I, Hiscott P, Hogg P, Robey H, Mazure A, Larkin G. Development, repair and regeneration of the retinal pigment epithelium. *Eye* **8** (1994) 255-62.

[102] Chong N, Keonin J, Luthert P, Frennesson C, et.al. Decreased Thickness and Integrity of the Macular Elastic Layer of Bruch's Membrane Correspond to the Distribution of Lesions Associated with Age-Related Macular Degeneration. *American Journal of Pathology 166 (*2005) 241-251.

[103] Stock U, Vacanti J. Tissue Engineering: Current state and prospects. *Annual Review of Medicine* **52** (2001) 443-451.

[104] Thumann G, et.al. Characteristics of Iris and Retinal Pigment Epithelial cells cultured on collagen type-1 membranes. *Current Eye Research* **31** (2006) 241-249.

[105] Thumann G, Schraermeyer U, Bartz-Schmidt K, et al. Descemet's membrane as membranous support in RPE/IPE transplantation. *Current Eye Research* **16** (1997) 1236-1238.

[106] Kiilgaard J, Wiencke A, Scherfig E, Prause J, Cour M. Transplantation of allogenic anterior lens capsule to the subretinal space in pigs. *Acta Ophthalmologica Scandinavica* **80** (2002), 76–81.

[107] Ichinose S, Nakahama K, Yoshida T, Kojima A, Mochizuki M, Morita I. The effects of amniotic membrane on retinal pigment epithelial cell differentiation. *Molecular Vision* **11** (2005) 1-10.

[108] Rabkin E, Schoen F. Cardiovascular Tissue Engineering. *Cardiovascular Pathology* **11** (2002) 305-317.

[109] Giordano G, Thomson R, Ishaug S, Mikos A, Comber S, Garcia C, Munir D. Retinal pigment epithelium cells cultured on synthetic biodegradable polymers. *Journal of Biomedical Material Research* **34** (1997) 87-93.

[110] Klee D, Dalton P, Berndt T, Vidovic E, Moeller M. Artificial membranes for cell transplantation in abstract from the first workshop on cell transplantation in age-related macular degeneration. *Greafe's Archives of Clinical and Experimental Ophthalmology* **242** (2004) 51-64.

[111] Rezai K, Farrokh-Siar L, Godowski K, Patel S, Ernest J. A model for xenogenic immune response. *Graefe's Archive for Clinical and Experimental Ophthalmology* **238** (2000) 352-358.

[112] Lu L, Garcia C, Mikos A. In vitro degradation of thin poly(DL-lactic-co-glycolic acid) films. *Journal of Biomedical Materials Research* **46** (1999) 236-244.

[113] Yamini Krishna, Carl M. Sheridan, David L. Kent, Ian Grierson, Rachel L. Williams. Polydimethylsiloxane as a substrate for retinal pigment epithelial cell growth. *Journal of Biomedical Materials Research (A)* **80A** (2007) 669-678.

[114] Krishna Y, Sheridan C, Kent D, Grierson I, Williams R. Growth and Function of Retinal Pigment Epithelial Cells on Surface Modified Expanded Polytetrafluoroethylene (ePTFE). Waiting to be published.

[115] Williams R, Krishna Y, Dixon S, Haridas A, Grierson I, Sheridan C. Polyurethane as potential substrates for sub-retinal pigment epithelial cell transplantation. *Journal of Materials Science: Materials in Medicine* **16** (2005) 1087-1092.

[116] KP Walluscheck, G Steinhoff, S Kelm, A Haverich. Improved endothelial cell attachment on ePTFE vascular grafts pretreated with synthetic RGD-containing peptides. *European Journal of Vascular and Endovascular Surgery* **12** (1996) 321-30.

[117] Tseng D, Edelman E. Effects of amide and amine plasma-treated ePTFE vascular grafts on endothelial cell lining in an artificial circulatory system. *Journal of Biomedical Materials Research* **42** (1998) 188–198.

[118] Joussen M, Heussen F, Joeres S, et al. Autologous Translocation of the Choroid and Retinal Pigment Epithelium in Age-related Macular Degeneration. *American Journal of Ophthalmology* **142** (2006) 17-30.e8.

[119] van Meurs J, Van Den Biesen P. Autologous retinal pigment epithelium and choroid translocation in patients with exudative age-related macular degeneration: short-term follow-up. *American Journal of Ophthalmology* **136** (2003) 688-695.

[120] MacLaren R, Uppal G, Balaggan K, et al. Autologous Transplantation of the Retinal Pigment Epithelium and Choroid in the Treatment of Neovascular Age-Related Macular Degeneration. *Ophthalmology* **114** (2007) 561-570.e2.

[121] Wong D, Stanga P, Briggs M, et al. Case selection in macular relocation surgery for age related macular degeneration. *British Journal of Ophthalmology* **88** (2004) 186-190.

[122] Tsukahara I, Ninomiya S, Castellarin A, et al. Early Attachment of Uncultured Retinal Pigment Epithelium from Aged Donors onto Bruch's Membrane Explants. *Experimental Eye Research* **74** (2002) 255-266.

[123] Algvere P, Berglin L, Gouras P, et al. Transplantation of fetal retinal pigment epithelium in age-related macular degeneration with subfoveal neovascularisation. *Graefe's Archive for Clinical and Experimental Ophthalmology* **232** (1994) 707-716.

[124] Del Priore L, Kaplan H, Tezel T, et al. Retinal pigment epithelial cell transplantation after subfoveal membranectomy in age-related macular degeneration: Clinicopathologic correlation. *American Journal of Ophthalmology* **131** (2001) 472-480.

[125] Ishida M, Lui GM, Yamani A, et al. Culture of human retinal pigment epithelial cells from peripheral scleral flap biopsies. *Current Eye Research* **17** (1998) 392-402.

[126] Shah S, Denham L, Elison J, et al. Drug delivery to the posterior segment of the eye for pharmacologic therapy. *Expert Review of Ophthalmolology* **5** (2010) 75–93.

[127] Binder S, Stanzel B, Krebs I, et al. Transplantation of the RPE in AMD. *Progress in Retinal & Eye Research* **26** (2007) 516-554.

[128] Gogolewiski S. Selected topics in biomedical polyurethanes. A Review. *Colloid and Polymer Science* **267** (1989) 757-785.

[129] Smith T. Tensile strength of polyurethane and other elastomeric block copolymers. *Journal of Polymer Science: Polymer Physics edition* **9** (1974) 1825-1848.

[130] Appliance for the Polyurethane Industry (API). The use of Polyurethanes in Medical Device applications. *Technical Bulletin* **2001** August; AX146.

[131] Zdrahala R, Zdrahala I. Biomedical Applications of Polyurethanes: A Review of Past Promises, Present Realities, and a Vibrant Future. *Journal of Biomaterials Applications* **14** (1999) 67-90.

[132] Lin H, Sun W, Mosher D, Garcia-Echeverria C, Schaufelberger K, Lelkes P, Cooper S. Synthesis, surface, and cell-adhesion properties of polyurethanes containing covalently grafted RGD-peptides. *Journal of Biomedical Material Research* **28** (1994) 329-42.

[133] Hsu S, Chen W. Improved cell adhesion by plasma-induced grafting of L-lactide onto polyurethane surface. *Biomaterials*.**21** (2000) 359-67.

[134] Mathur A, Collier T, Kao W, Wiggins M, Schubert M, Hiltner A, Anderson J. In vivo biocompatibility and biostability of modified polyurethanes. *Journal of Biomedical Materials Research* **36** (1997) 246–257.

[135] Barone FE, Perry L, Keller T, Maxwell GP. The biomechanical and histopathologic effects of surface texturing with silicone and polyurethane in tissue implantation and expansion. *Plastic and Reconstructive Surgery* **90** (1992) 77-86.

[136] B9 Polyurethanes Properties Guide: Biomer Technology Ltd.

[137]Zhu M, Provis JM, Penfold PL. Isolation, culture and characteristics of human foetal and adult retinal pigment epithelium. *Australian & New Zealand Journal of Ophthalmology* **26** supp (1998) S50-S52.

[138] Tezel TH, Del Priore LV, Kaplan HJ. Harvest and storage of adult human retinal pigment epithelial sheets. *Current Eye Research* **16** (1997) 802-809.

[139] Ho T, Del Priore LV, Kaplan HJ. Tissue culture of Retinal Pigment Epithelium following isolation with gelatine matrix technique. *Experimental Eye Research* **64** (1997) 133-139.

[140] Hu DN, Ritch R, McCormick SA, Pelton-Henrion K. Isolation and cultivation of human iris pigment epithelium. *Investigative Ophthalmology and Visual Science* **33** (1992) 2443-2453.

[141] Freshney R. Culture of Animal Cells: A Manual of Basic Technique page 117 Alan R. Liss Inc., New York.

[142] Carlsson R, Engvall E, Freeman A, et al. Laminin and Fibronectin in cell adhesion: Enhanced adhesion of cells from regenerating liver to laminin. *Proceedings of the National Academy of Science of the United States of America (PNAS)* **78** (1981) 2403-2406.

[143] Godchaux W, Zimmerman WF. Soluble proteins of intact bovine rod cell outer segments. *Experimental Eye Research* **28** (1979) 483-500.

[144] Higgins GT, *et al.* Induction of Angiogenic Cytokine Expression in Cultured RPE by ingestion of oxidized Photoreceptor Outer Segments. *Investigative Ophthalmology & Visual Science* **44** (2003) 1775-1782.

[145] Lowry *et al.* Protein Measurement with the Folin Phenol Reagent. *Journal of Biological Chemistry* **193** (1951) 265-275.

[146] Smith PK, *et al. Analitical. Biochemistry.* **150** (1985) 76-85.

[147] McLaren M, Inana G, Li C. Double Fluorescent Vital Assay of Phagocytosis by Cultured Retinal Pigment Epithelial Cells. *Investigative Ophthalmology & Visual Science* **34** (1993) 317-326.

[148] Bunce C, Xing W, Wormald R. Causes of blind and partial sight certifications in England and Wales: April 2007-March 2008. *Eye (London)* **24** (2010) 1692-1699.

[149] The Eye Diseases Prevalence Research Group. Prevalence of Age-Related Macular Degeneration in the United States. *Archives of Ophthalmology* **122** (2004) 564-572.

[150] Minassian D, Reidy A. Future sight loss UK (2): An epidemiological and economic model for sight loss in the decade 2010-2020. Epivision report for Royal National Institute of Blind People (RNIB) 2009.

[151] Chakravarthy U, Evans J, Rosenfeld P. Clinical Review: Age related macular degeneration. *British Medical Journal* **340** (2010) c981.

[152] Falkner-Radler C, Krebs I, Glittenberg, et al. Human retinal pigment epithelium (RPE) transplantation: outcome after autologous RPE-choroid sheet and RPE cell-suspension in a randomised clinical study. *British Journal of Ophthalmology* **95** (2011) 370-375.

[153] Itaya H, Gullapalli V, Sugino I, et al. Iris Pigment Epithelium Attachment to Aged Submacular Human Bruch's Membrane. *Investigative Ophthalmology & Visual Science* **45** (2004) 4520-4528.

[154] Sun K, Cai H, Tezel T, et al. Bruch's membrane aging decreases phagocytosis of outer segments by retinal pigment epithelium. *Molecular Vision* **13** (2007) 2310-2319.

[155] Treharne A, Grossel M, Lotery A, et al. The chemistry of retinal transplantation: the influence of polymer scaffold properties on retinal cell adhesion and control. *British Journal of Ophthalmology* (2010) e-publish doi:10.1136/bjo.2010.184002.

[156] Da Silva G, Junior A, Saliba J, et al. Polyurethanes as supports for human retinal pigment epithelium cell growth. *International Journal of Artificial Organs* **34** (2011) 198-209.

[157] Blair G, Dawe B, McEvoy J, et al. The Effect of Visible Light on the Variability of Flexible Foam Compression Sets". Orlando, Florida: Center for the Polyurethane Industry. 2007

[158] Bai C, Zhang X, Dai J, et al. A new UV curable waterborne polyurethane: Effect of CC content on the film properties. *Progress in Organic Coatings* **55** (2006) 291-295.

[159] Singh S, Woerly S, McLaughlin B. Natural and artificial substrates for retinal pigment epithelial monolayer transplantation. *Biomaterials* **22** (2001) 3337-3343.

[160] de Waard H, De Beer T, Hinrichs W, et al. Controlled Crystallization of the Lipophilic Drug Fenofibrate During Freeze-Drying: Elucidation of the Mechanism by In-Line Raman Spectroscopy. *The AAPS Journal* **12** (2010) 569–575.

[161] Jin C, Zhu B, Wang X, et al. Nanoscale surface topography enhances cell adhesion and gene expression of madine darby canine kidney cells. *Journal of Materials Science: Materials in Medicine* **19** (2008) 2215-2222.

[162] Data from British Sugar Pharmaceutical **http://www.bspharma.co.uk/RVEa12c90457ed44468b64253065a34b288,,.aspx**.

[163] Jiang P, Bertone J, Hwang K. Single-Crystal Colloidal Multilayers of Controlled Thickness. *Chemistry of Materials* **11** (1999) 2132-2140.

[164] Spaans C, de Groot J, Dekens F. High molecular weight polyurethanes and a polyurethane urea based on 1,4-butanediisocyanate. *Polymer Bulletin* **41** (1998) 131-138.

[165] Friberg T, Lace J. A Comparison of the elastic properties of human choroid and sclera. *Experimental Eye Research* **47** (1988) 429-436.

[166] Marmor M, Wolfensberger T. 1998. The retinal pigment epithelium. Oxford University Press, New York.

[167] Redenti S, Neeley W, Rompani S, et al. Engineering retinal progenitor cell and scrollable poly(glycerol-sebacate) composite for expansion and subretinal transplantation. *Biomaterials* **30** (2009) 3405-3414.

[168] Liao J, Yu J, Huang K, et al. Molecular signature of primary retinal pigment epithelium and stem-cell-derived RPE cells. *Human Molecular Genetics* **19** (2010) 4229-4238.

[169] Idelson M, Alper R, Obolensky A, et al. Directed differentiation of human embryonic stem cell into functional retinal pigment epithelium cells. *Cell Stem Cell* **5** (2009) 396-408.

[170] Altman S, Randers L, Rao G. Comparison of trypan blue dye exclusion and fluorometric assays for mammalian cell viability determinations. *Biotechnology Progress* **9** (1993) 671-674.

[171] Del Priore L, Kaplan H, Berger A. Retinal pigment epithelial transplantation in the management of subfoveal choroidal neovascularisation. *Seminars in Ophthalmology* **12** (1997) 45-55.

[172] Yamaguchi K, Gaur V, Turner J. Retinal pigment epithelial cell transplantation into aging retina: a possible approach to delay age-related cell death. *Japanese Journal of Ophthalmology* **37** (1993) 16-27.

[173] Algvere P. Transplantation of RPE in age-related macular degeneration: observations in discifrom lesions and dry RPE atrophy. *Graefe's Archive for Clinical and Experimental Ophthalmology* **235** (1997) 149-158.

[174] Chang Y, Finnemann S. Tetraspanin CD81 is required for the αvβ5-integrin dependent particle-binding step of RPE phagocytosis. *Journal of Cell Science* **120** (2007) 3053-3063.

[175] Aisenbrey S, Lafaut BA, Szurman P, et al. Iris pigment epithelial translocation in the treatment of exudative macular degeneration: a 3-year follow-up. *Archives of Ophthalmology* **124** (2006) 183-188.

[176] Streilein W, Ma N, Wenkel H, et al. Immunobiology and privilege of neuronal retina and pigment epithelium transplants. *Vision Research* **42** (2002) 487-495.

[177] Tezel T, Del Priore L, Kaplan H. Harvest and storage of adult human retinal pigment epithelial sheets. *Current Eye Research* **16** (1997) 802-809.

[178] Ho T, Del Priore L, Kaplan H. Tissue culture of retinal pigment epithelium following isolation with a gelatine matrix technique. *Experimental Eye Research* **64** (1997) 133-139.

[179] Frochlich E, Maier E, Klessen C. Isolation of Bovine retinal pigment epithelial cells using adhesion to agarose: Demonstration of Cellular and Regional Heterogeneity. *The Journal of Histochemistry & Cytochemistry* **51** (2003) 121-124.

[180] Shiosaka S, Kiyama H, Tohyama M. A simple method for the separation of retinal sublayers from the entire retina with special reference to application for cell culture. *Journal of Neuroscience Methods* **10** (1984) 229-235.

[181] Zhu M, Provis J, Penfold P. Isolation, culture and characteristics of human foetal and adult retinal pigment epithelium. *Australian and New Zealand Journal of Ophthalmology* **26** (1998) S50-S52.

[182] Aronson J. Human Retinal Pigment Cell Culture. *In-Vitro* **19** (1983) 642-650.

[183] Hu D, Ritch R, McCormick S, Pelton-Henrian K. Isolation and Cultivation of Human Iris Pigment Epithelium. *Investigative Ophthalmology & Visual Science* **33** (1992) 2443-2453.

[184] Tezel T, Del Priore L. Density-dependent growth regulation of pig retinal pigment epithelial cells in vitro. *Graefe's Archive for Clinical and Experimental Ophthalmology* **234** (1996) S89-S95.

[185] Hiscott P, Grierson I, McLeod D. Retinal pigment epithelial cells in epiretinal membranes: an immunohistochemical study. *British Journal of Ophthalmology* **68** (1984) 708–715.

[186] Tezcaner A, Bugra K, Haslrcl V. Retinal pigment epithelium cell culture on surface modified poly(hydroxybutyrate-co-hydroxyvalerate) thin films. *Biomaterials* **24** (2003) 4573-4583.

[187] Das S, Ghouras P. Retinoid Metabolism in cultured human pigment epithelium. *Biochem J* **250** (1988) 459-465.

[188] Chang W, Ye L, et al. Serum inhibits tight junction formation in cultured pigment epithelial cells. *Investigative Ophthalmology & Visual Science* **38** (1997) 1082-93.

[189] Yasunari T, Yanagihara N, et al. Effect of retinoic acid on proliferation and polyamine metabolism in cultured bovine retinal pigment epithelial cells. *Ophthalmic Research* **31** (1999) 24-32.

[190] Campochiaro P, Hackett A, et al. Retinoic acid promotes density-dependent growth arrest in human retinal pigment epithelial cells. *Investigative Ophthalmology & Visual Science* **32** (1991) 65-72.

[191] Clark R, Folkvord J, et al. Fibronectin, as well as other extracellular matrix proteins, mediate human keratinocyte adherence. *Journal of Investigative Dermatology* **84** (1985) 378-83.

[192] Varani J, Dixit V, et al. Thrombospondin-induced attachment and spreading of human squamous carcinoma cells. *Experimental Cell Research* **167**(1986) 376-90.

[193] Varani J, Nickoloff B, et al. Thrombospondin-induced adhesion of human keratinocytes. *Journal of Clinical Investigation* **81**(1988) 1537-44.

[194] Doyle J, Dowgiert R, Buzney S. Factors modulating the effect of retinoids on cultured retinal pigment epithelial cell proliferation. *Current Eye Research* **11** (1992) 753-765.

[195] Dong X, Chen N, Xie L, Wang S. Prevention of experimental proliferative vitreoretinopathy with a biodegradable intravitreal drug delivery system of all-trans retinoic acid. *Retina* **26** (2006) 210-213.

[196] Del Priore L, Geng L, Tezel T, Kaplan H. Extracellular matrix ligands promote RPE attachment to inner Bruch's membrane. *Current Eye Research* **25** (2002) 79-89.

[197] Heth C, Yankauckas M, Adamian M, Edwards R. Characterization of retinal pigment epithelial cells cultured on microporous filters. *Current Eye Research* **6** (1987) 1007-1019.

[198] Ho T, Del Priore L. Reattachment of Cultured Human Retinal Pigment Epithelium to Extracellular Matrix and Human Bruch's Membrane. *Investigative Ophthalmology & Visual Science* **38** (1997) 1110-1118.

[199] Song M, Lui G. Propagation of fetal human RPE cells: Preservation of original culture morphology after serial passage. *Journal of Cellular Physiology* **143** (1990) 196-203.

[200] Tomran-Tink J, Shivaram S, Chader G, et al. Expression, Secretion, and Age-Related Down regulation of Pigment Epithelium-Derived Factor, a Serpin with Neurotrophic Activity. *The Journal of Neuroscience* **15** (1995) 4992-5003.

[201] Grisanti S, Guidry C. Transdifferentiation of Retinal Pigment Epithelial Cells from Epithelial to Mesenchymal Phenotype. *Investigative Ophthalmology & Visual Science* **36** (1995) 391-405.

[202] Flood M, Gouras P. The Organization of Human Retinal Pigment Epithelium in vivo. *Vision Research* **21** (1981) 119-126.

[203] Campochiaro P, Glaser B. Endothelial Cells Release a Chemoattractant for Retinal Pigment Epithelial Cells In Vitro. *Archives of Ophthalmology* **103** (1985) 1876-1880.

[204] Von Recum H, Okano T, Kim S, Bernstein P. Maintenance of Retinoid Metabolism in Human Retinal Pigment Epithelium Cell Culture. *Experimental Eye Research* **69** (1999) 97-107.

[205] Brown R, Middleton C. Morphology and locomotion of individual epithelial cells in culture. *Journal of Cell Science* **78** (1985) 105-15.

[206] Clark P, Connolly P, Curtis S, et al. Cell guidance by ultrafine topography in vitro. *Journal of Cell Science* **99** (1991) 73-77.

[207] Iwig M, Glaesser D. On the role of microfilaments in cell-shape-mediated growth control of lens epithelial cells. *Cell & Tissue Kinetics* **18** (1985) 169-82.

[208] Ohara P, Buck R. Contact guidance in vitro: A light, transmission, and scanning electron microscopic study. *Experimental Cell Research* **121** (1979) 235-249.

[209] Heidcamp W. Density and refractive indexes of sucrose (table 3.2) in Cell Biology Laboratory Manual. Accessed from **http://homepages.gac.edu/~cellab/chpts/chpt3/table3-2.html** on the 27th September 2010.

[210] McLaren M, Inana G, Li C. Double Fluorescent Vital Assay of Phagocytosis by Cultured Retinal Pigment Epithelial Cells. *Investigative Ophthalmology & Visual Science* **34** (1993) 317-326.

[211] Karl M, Valtink M, Bednarz J, Engelmann K. Cell culture conditions affect RPE phagocytic function. *Graefe's Archive for Clinical and Experimental Ophthalmology* **245** (2006) 981-991.

[212] McLaren M. Kinetics of Rod Outer Segment Phagocytosis by Cultured Retinal Pigment Epithelial Cells: Relationship to Cell Morphology. *Investigative Ophthalmology & Visual Science* **37** (1996) 1213-1224.

[213] Mayerson P, Hall M. Rat retinal pigment epithelial cells show specificity of phagocytosis in vitro. *Journal of Cell Biology* **103** (1986) 299-308.

[214] Nandrot E, Kim Y, Brodie S, et al. Loss of synchronized retinal phagocytosis and age-related blindness in mice lacking alphavbeta5 integrin. *The Journal of Experimental Medicine* **200** (2004) 1539-1545.

[215] Ryeom S, Sparrow J, Silverstein R. CD36 participates in the phagocytosis of rod outer segments by retinal pigment epithelium. *Journal of Cell Science* **109** (1996) 387-395.

[216] Takeda Y, Tachibana I, Miyado K. Tetraspanins CD9 and CD81 function to prevent the fusion of mononuclear phagocytes. *The Journal of General Physiology* **161** (2003) 945-956.

[217] Feng W, Yasumura D, Matthes M, et al. Mertk Triggers Uptake of Photoreceptor Outer Segments during Phagocytosis by Cultured Retinal Pigment Epithelial Cells. *The Journal of Biological Chemistry* **277** (2002) 17016-17022.

[218] Chaitin M, Hall M. Defective ingestion of rod outer segments by cultured dystrophic rat pigment epithelial cells. *Investigative Ophthalmology & Visual Science* **24** (1983) 812-820.

[219] Vollrath D, Feng W, Duncan JL, et al. Correction of the retinal dystrophy phenotype of the RCS rat by viral gene transfer of Mertk. *Proceedings of the National Academy of Sciences of the United States of America* **98** (2001) 12584-12589.

[220] Strauss O. The Retinal Pigment Epithelium in Visual Function *Physiological Reviews* **85** (2005) 845-881.

[221] Krishna Y. (2006) PhD Thesis University of Liverpool. Use of artificial substrate for retinal pigment epithelial cell growth and transplantation.

[222] Lyda W, Eriksen N, Krishna N. Studies of Bruch's membrane; flow and permeability studies in a Bruch's membrane-choroid preparation. *American Journal of Ophthalmology* **44** (1957) 362-9; discussion 369-70.

[223] D Wong, P Stanga, M Briggs, et al. Case selection in macular relocation surgery for age related macular degeneration. *British Journal of Ophthalmology* **88** (2004) 186–190.

[224] Sadava D, Remer T, Petersen K. Hyperplasia, hyperproliferation and decreased migration rate of colonic epithelial cells in mice fed a diet deficient in vitamin D. *Biology of the Cell* **87** (1996) 113-116.

[225] Julien S, Peters T, Ziemssen F, et al. Implantation of ultrathin, biofunctionalized polyimide membranes into the subretinal space of rats. *Biomaterials* **32** (2011) 3890-3898.

[226] Stanzel B, Clemens C, Sanislo S, et al. SD-OCT Complements Histology in Evaluation of Potential Bruch's Membrane Prosthetics. *ARVO Meeting Abstracts* **51** (2010) 5241.

[227] Palanker D, Huie P, Vankov A. Migration of Retinal Cells through a Perforated Membrane: Implications for a High-Resolution Prosthesis. *Investigative Ophthalmology & Visual Science* **45** (2004) 3266-3270.